Experimental investigations and non-linear numerical analyses of skewed one-way prestressed concrete bridge decks

Volume 1 : Experimental Investigations

Thesis submitted in accordance with the requirements of the University of Liverpool for the degree of

Doctor in Philosophy

by

Michael D Cope

September 1987

SUMMARY

This thesis is primarily concerned with the design and analysis of composite concrete bridge decks, although some of the analytical procedures developed herein have a wider applicability. In the current study composite construction refers to precast, pretensioned concrete beams acting compositely with insitu concrete.

The work is broadly divided into two sections, experimental and analytical. For the experimental programme two 1:3.5 scale models of skewed bridge decks were designed to current standards and meticulously constructed. Comprehensive data acquisition facilities were installed and the testing programme for each model deck was based on current design loading. Detailed test results are presented and the full range structural response investigated and explained. The analytical investigation programme ran concurrently with the experimental programme and involved the development of material and structural modelling schemes and appropriate numerical modelling techniques. These were incorporated in an analytical package which involved the design and implementation of a sophisticated finite element program named SNAP.

Composite concrete bridge decks are the solutions chosen for many crossings in the UK. However, the literature survey revealed that the previous experimental research was very limited and had been conducted during the 1950's. This position is reflected in the limited and ambiguous guidance that is currently available to designers. No analytical research on composite construction could be found.

The experimental programme revealed several interesting features, such as; the inherently large factor of safety that results from current design practices; the unusual crack patterns that indicate limited breakdown of composite action; the complete breakdown of composite action along the supported edges at high load levels. The implications of the observed structural behaviour for analysts and designers are explored.

The heterosis plate bending element was selected for the finite element analyses. Sophisticated non-linear solution procedures, including the arc-length method and the BFGS quasi-Newton method, were also developed and incorporated into the SNAP program. A decisive feature in the success of the analyses described herein was the inclusion in the program of a wide range of solution procedures, which were available for selection based on the current structural behaviour. The program was endowed with limited intelligence so that it could automatically switch between solution methods as numerical difficulties were encountered during an analysis. The program was subjected to testing and verification against the results of other published investigations. The SNAP program design philosophy resulted in a simple to use, comprehensive and effective tool for the analyst. Several new analytical concepts and methods, such as; a hybrid element for analyses of composite construction; scaled space and new convergence criteria and; statistically varied material properties were developed during the present study.

Finally, conclusions are drawn from the reported investigations and recommendations for further work are given.

CONTENTS

ACKNOWLEDGEMENTS

The author thanks the Department of Civil Engineering of the University of Liverpool for giving him the opportunity to carry out the research described herein. He wishes to express his sincere gratitude and appreciation to his supervisor Professor R J Cope, for his help and guidance throughout the course of the project. The supervision by Dr A B Templeman during the final stages of the research is appreciated.

The author wishes to express his appreciation to the Bridges Division of the Transport and Road Research Laboratory under the supervision of Dr Tilly, for funding the majority of the work described herein. In particular the author wishes to thank Dr M A Crisfield for his constructive criticism, constant encouragement and helpful advice.

Also the author wishes to thank Mr D C Monaghan, the Departmental Superintendent, for many helpful suggestions; Mr A Cowan, without whose skill and conscientiousness, the high standard of construction and testing would not have been achieved; Miss J Marshall, for her conscientious typing of the thesis including the numerous complex tables; Mrs B Cotgreave and Mr S Glass for the willingness and high standard of care that they have shown during the preparation of the figures and plates.

The computational aspects of this research would not have been as sophisticated or comprehensive without the outstanding computing service that has been made available through the many staff of the Liverpool University Computer Laboratory. The author wishes to thank these staff for their assistance, willingness and helpful suggestions during the course of the work. Thanks are also due to Mr J Wilkinson for his assistance in implementing the data logging systems used for the model tests.

Special thanks are due to the author's wife for her constant understanding and support.

1. COMPOSITE CONCRETE SLAB BRIDGES

1.1 Introduction

In this thesis, "composite construction" refers to precast, pretensioned concrete beams acting compositely with in-situ concrete. The inclusion of voids in the in-situ concrete is not considered. Prestressed precast beams are available for spans of 4 m - 18 m.

In cross-section, the beams have the shape of an inverted T and the dimensions of the bottom flange are fixed. To cater for different spans, the overall depth, size of top flange, and quantity of prestress are varied.

Standard holes through the bottoms of the webs allow transverse steel to be threaded through the assembled beams. The standard spacing of these holes is 610 mm and a number of bars can be threaded through each hole. Top steel can be placed in the in-situ concrete above the tops of the beams.

The cross-section of the bridge deck used for model 1 is shown in Figure 1.1, to illustrate the form of construction under consideration.

In a survey of eighty bridges in Kent, Bergg[1] found that, in 1973, the deck costs of simply supported decks, with spans of up to about 18 m and incorporating precast beams, were cheapest when composite construction was selected. Unfortunately, no information on the skew of the decks was included. Although the costs quoted in the paper are now out of date, it is thought that the relative values are not likely to have changed significantly.

Composite construction was included as an option in the range of Standard Bridges prepared by the Department of Transport[2]. Designs are for overbridges supporting a D2APR (Dual carriageway, two lane, all purpose road) and for underbridges supporting a D3M (Dual carriageway, three lane rural motorway) or a D2APR, over a 1 x S5.5 or S7.3 (Single carriageway roads with 2m verges and either 5.5m or 7.3m carriageways).

For the standard bridge decks, the reinforcement is positioned parallel to the sides of the deck. An orthogonal arrangement of reinforcement is preferable from stiffness and strength considerations, but the arrangement selected is probably more economic. As the maximum skew angle of the standard decks is 25°, the lack of structural efficiency is unlikely to be severe.

The first model tested was based on a Standard Underbridge Deck with 25° of skew. A geometric scale of 1:3.5 was selected. Details of the model are given in Chapter 4 and relate to the data given for a bridge carrying a D2APR over an S5.5 on Standard Bridge Drawings D2/APR/2/7.3/UB/SC5.5/ /T/1 and /2/ /UB/ SC5.5/ /T/1.

To examine the influence of greater skew angles on the structural behaviour of composite construction, bridge design offices were approached for examples of recent designs. There was little response to the request, but a suitable design was kindly made available by Cheshire County Council, and the author would like to express his thanks for the considerable help provided.

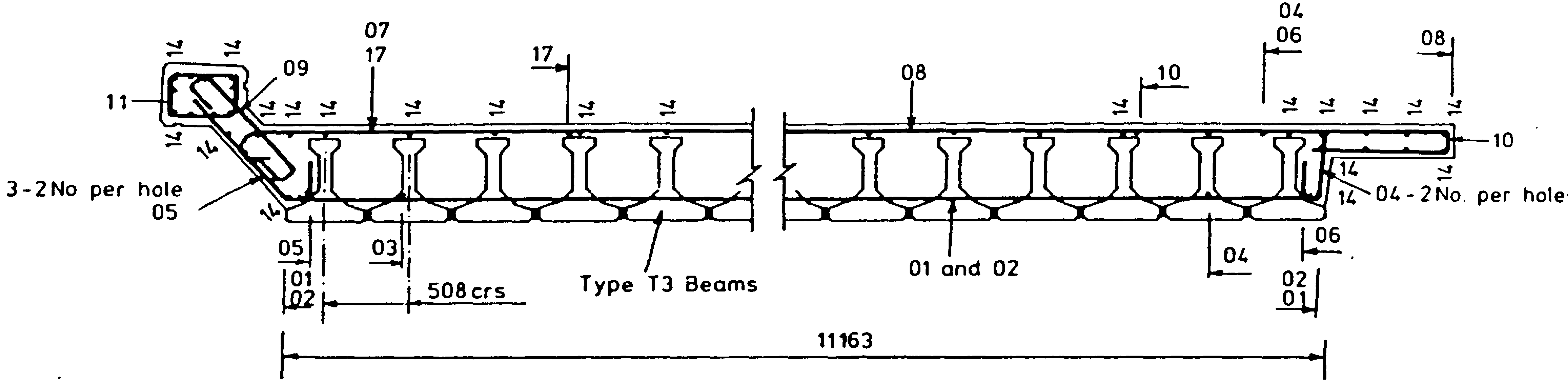

FIG. 1.1 FULL SIZE DECK SECTION

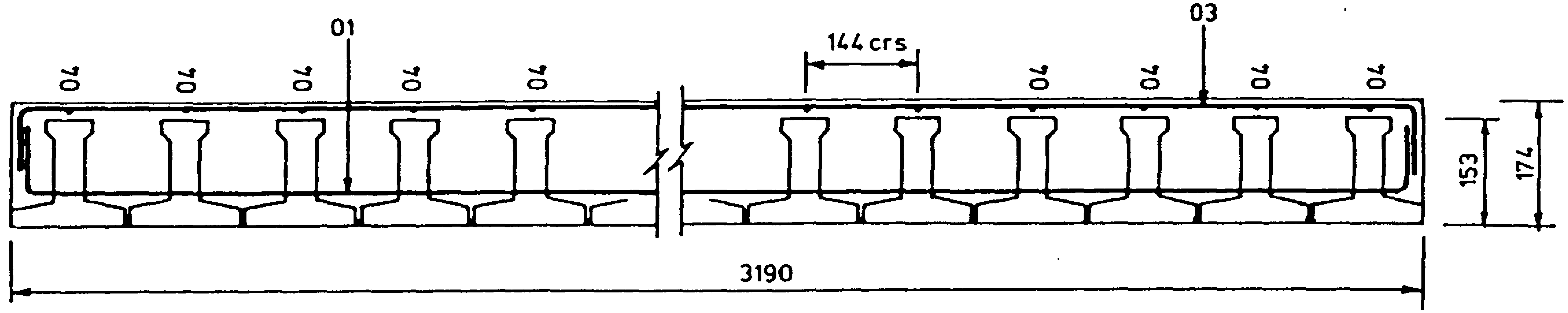

FIG. 1.1 MODEL DECK SECTION

The second model tested was based on an idealisation of the central span of a three span simply supported bridge deck with a 5.5 m carriageway and two 1.5 m verges. The idealised bridge had a skew of 40° (internal acute corner 50°). The deck had a width of 8.9 m. The beams were the largest from the range of standard C&CA inverted T sections, and had a span of 16.45 m. The right span was, thus, about 12.6 m. The transverse soffit steel had a skew of -18° (i.e. a 72° inclination to the free edge). The top steel was placed parallel and perpendicular to the beams. The hogging principal moments in the obtuse corner were, thus, at a considerable inclination to the bar directions. A geometric scale of 1:3.5 was selected. Details of the model are given in Chapter 6.

1.2 Design philosophy

The British Standards and Codes of Practice that relate to concrete bridge design have been the subject to a good deal of radical change and almost continued development and amendment over many years. The most recent change resulted from the adoption of a limit state design philosophy in BS5400. Prior to this, design had been carried out to a working load and elastic stress philosophy such as that contained in the earlier British Standards relating to bridge design, such as BS153. BS5400, which appeared in 1978, was arranged so that the values chosen for the various safety factors resulted in similar structures to those designed to the existing design documents. Thus, even though there was a radical change in design concept and method, the resulting structures were largely the same.

With BS5400 the critical design criteria for a reinforced concrete structure are those at the Ultimate Limit State (ULS) (conceptually failure of the structure) and thus the design concepts in BS5400 differ fundamentally from those of the earlier working stress codes. Conversely, with prestressed concrete, the critical design criteria are generally those of the Serviceability Limit State (SLS). Thus the design criteria for prestressed concrete are similar under BS5400 and the previous design documents.

Unfortunately the difference in the critical design criteria between reinforced and prestressed concrete has resulted in confusion over the design method for composite construction. There are a number of areas where the code is unable to give adequate guidance, such as the treatment of transverse shear and the cracking and stress limitations at the Serviceability Limit State. In these areas it is debatable whether composite structures should be treated as reinforced, prestressed or a hybrid of the two.

A multitude of committees were formed for the purpose of drafting BS5400 and this is apparent in the British Standard that appeared. While the technical basis for the design clauses is sound the way in which it is specified and presented is not conducive to efficient and error free design. In some cases, the code has been described as 'a mine field waiting to catch out the unwary'. While it may be argued that the unwary should not be designing bridges, the object of the exercise is the efficient design of effective, safe and durable bridge structures.

The Department of Transport, for whom the majority of bridge are constructed, initially refused to allow the adoption of BS5400 for the design of its structures, unless amended by its own implementation documents. After the incorporation, in the 1984 edition, of the majority of the amendments contained within the latter document, the DTp did allow the use of BS5400 in principle. However, the DTp still required the use of its own implementation documents in conjunction with the revised code.

BS5400 does not cater for some features which are specific to composite construction, such as integral action of the precast beams and the insitu concrete. Implicit in current design is the assumption of fully composite action for all states. Current design philosophy dictates that, generally, the design of composite bridge decks is governed by the prestressed concrete and steel stress limitation of the Serviceability Limit State. The deck is sized and the prestress selected to comply with these criteria. However, the prestressed concrete stress limitation clauses are not particularly appropriate to composite construction since the prestress force is uni-directional and, generally, at a considerable angle to the principle moments. This is particularly true for a skewed deck. Thus, while the prestressed concrete stress limitation clauses are satisfied there may be significant cracking in the insitu concrete. In cases of high skew the amount of prestressing required to prevent cracking, even in the beams, may be prohibitive.

With current design generally only one beam type is specified for all the beams contained within the structure (that is all beams have the same profile and prestressing configuration). This beam type is configured to comply with the worst SLS requirements of any part of the deck.

Following 'compliance' with the SLS requirements the design is checked at the Ultimate Limit State. In the majority of cases the flexural component of this check is a mere formality since the members sized for SLS compliance result in a significant overprovision of ultimate strength. This is further compounded by the uniform provision of beams sized for the occurrence of the worst SLS effects.

The methods of design against shear failure are significantly different for reinforced and prestressed concrete. Thus the design of a composite deck to resist shear can be particularly troublesome. For a skew slab the principal shears can be at a significant angle to the direction of the prestressed beams thus making the selection of criteria difficult. In the simpler case where the principal shears are coincident with the beams the amount of shear resistance that can be expected from the insitu concrete complicates the calculations. Furthermore, for end zones, one must consider the amount of prestress that has been transmitted to the concrete.

Generally, the design of bridge decks at the Ultimate Limit State will be carried out using an elastic analysis. The use of an elastic analysis would appear to be an anomaly in a Limit State environment where a non-linear or plastic method would seem more appropriate. While the adoption of cracked stiffnesses for the ULS analysis will result in a more realistic approach, it will still not resemble the failure condition in the majority of cases.

The advantages of composite construction can be seen as two fold. Firstly, the use of precast members results in more accurate factory construction and also site costs are reduced since little formwork is required for the construction of the insitu slab. Secondly, the presence of prestressed concrete should enhance the structures durability. For BS5400 the differences between the treatment of reinforced and prestressed concrete are very distinct and this is clearly apparent in serviceability cracking and stress limitations. This distinction is not inherent since there are a multitude of structural states between reinforced and prestressed concrete. Therefore the adoption of continuous criteria spanning the range from reinforced to prestressed concrete may be more appropriate, especially for composite construction. A continuous approach would no doubt be beneficial as more sophisticated and complex computer systems become available, at realistic prices, for use in design.

1.3 References

1. Bergg, J.A. "Eighty highway bridges in Kent," Proc. Instn. Civ. Engrs., Pt. 1, Vol. 54, p. 571-603 (1973) and discussion, Vol. 55, p. 339-347, (1974).

2. Department of Transport, "BD 5/80. Standard Bridges", (1980).

PAGE

NUMBERING

AS ORIGINAL

2. LITERATURE SURVEY

2.1 Previous Experimental Research

2.1.1 Previous Tests on Models of Composite Construction Slab Bridges

Manual and computer based literature searches revealed little evidence of data from model tests of composite bridges. Enquiries to the Cement and Concrete Association and the libraries of the Professional Institutions revealed no further material. The only reports of tests that were found were from the Cement and Concrete Association, and these were conducted in the late 1950's.

Tests on three models of right bridge decks of composite construction have been reported by Best and Rowe[1]. The models were 11'-4" wide x 6" deep and had a span of 10'-0". Thirteen, post-tensioned, grouted, inverted T beams, with 1/2" gaps between bottom flanges, were incorporated in each model. The designs were carried out for longitudinal moments only (live load of 220 lb/ft^2, together with a knife edge load of 900 lb/ft) x 125%. Four 0.2" diameter wires in the bottom flange were prestressed to ensure a small compressive stress on the soffit under the design loading. Each composite beam was calculated to be capable of withstanding about twice the design moment.

No transverse reinforcement was placed in the first model. The second and third models had 1/4" diameter mild steel bars, hooked at one end, placed through 5/8" diameter holes in the webs of the precast beams. As the maximum aggregate size was 3/8", it seems likely that bonding would be poor over the web widths. In models 2 and 3, transverse bars were at 8" centres over the central 4' and at 12" centres elsewhere.

Model 3 differed from model 2, only in the use of a lower strength in-situ concrete.

No mention is made in the report of any reinforcement having been placed above the precast beams.

As the precast beams were post-tensioned, the prestressing wires were provided with external anchorages. The tops of the bottom flanges and the sides of the webs of the precast beams were wire brushed to remove any surface laitance. This was done to enhance bond between the precast and insitu concretes.

At the time of the tests, understanding of bridge deck behaviour under concentrated loading was in its infancy. The researchers, therefore, concentrated their attention on studying the responses of the models to applications of a single bogie of the HB vehicle. No dead weight compensation or other loadings were applied. The bogie was positioned symmetrically about the transverse centre line in two locations. One, with a set of inner wheels on the longitudinal centre line (central loading), see Fig. 2.1(a) and the other with an outer set of wheels 1'-10.5" from a free edge (eccentric loading). Each bridge was loaded first by central loading, then by eccentric loading, and, finally, to failure by central loading. The equivalent working load on a single HB bogie model was 10 tons, and the load levels studied before the final test to failure were up to 15 tons.

Transverse cracking of the precast beams occurred at a load between 23 and 24 tons during the test to failure of model 1. Transverse cracking in models 2 and 3 were first noted at 23 tons. Failure of model 1 occurred at a total load of 27 tons. Yield lines ran from the

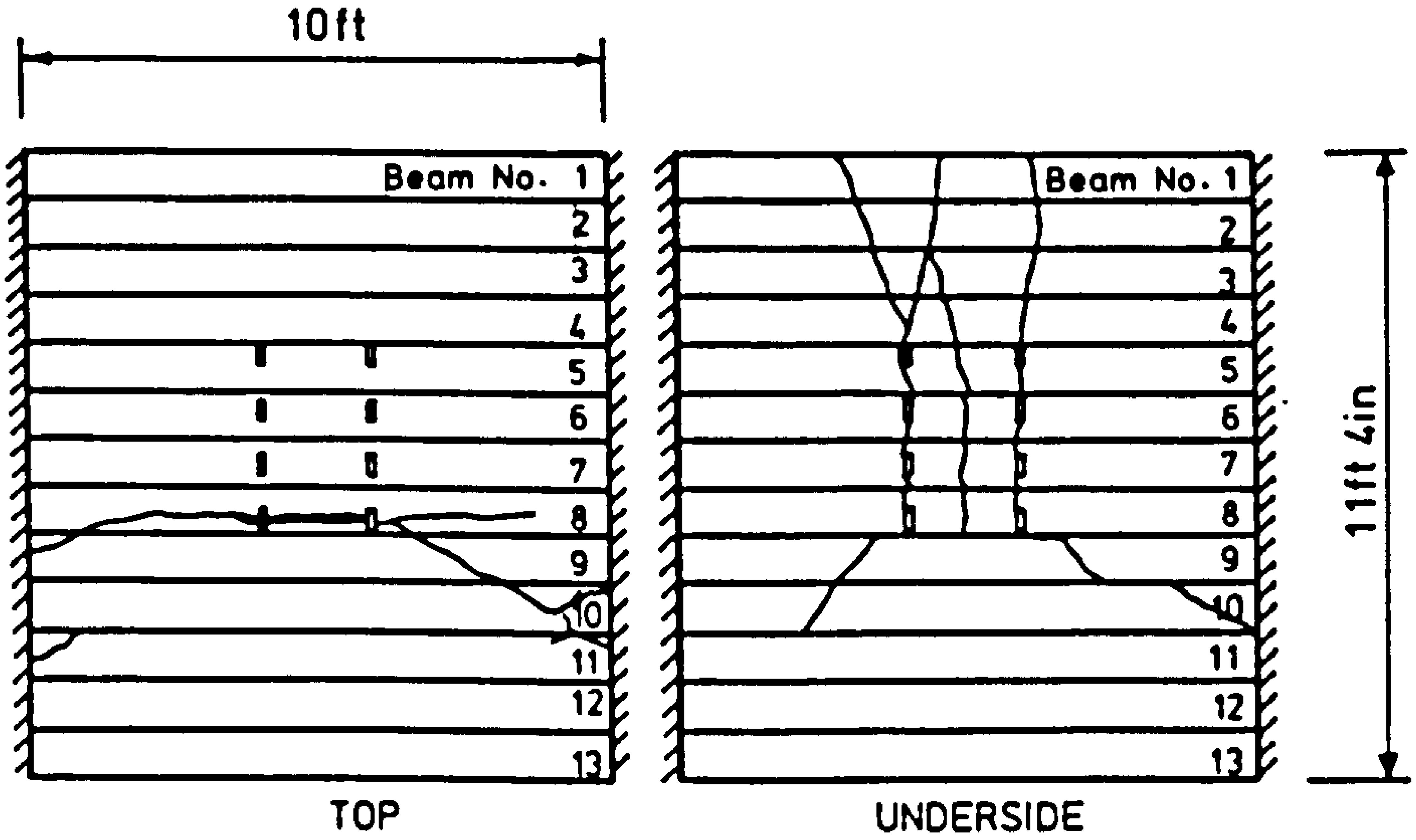

a) Crack patterns on Bridge 1 at failure.

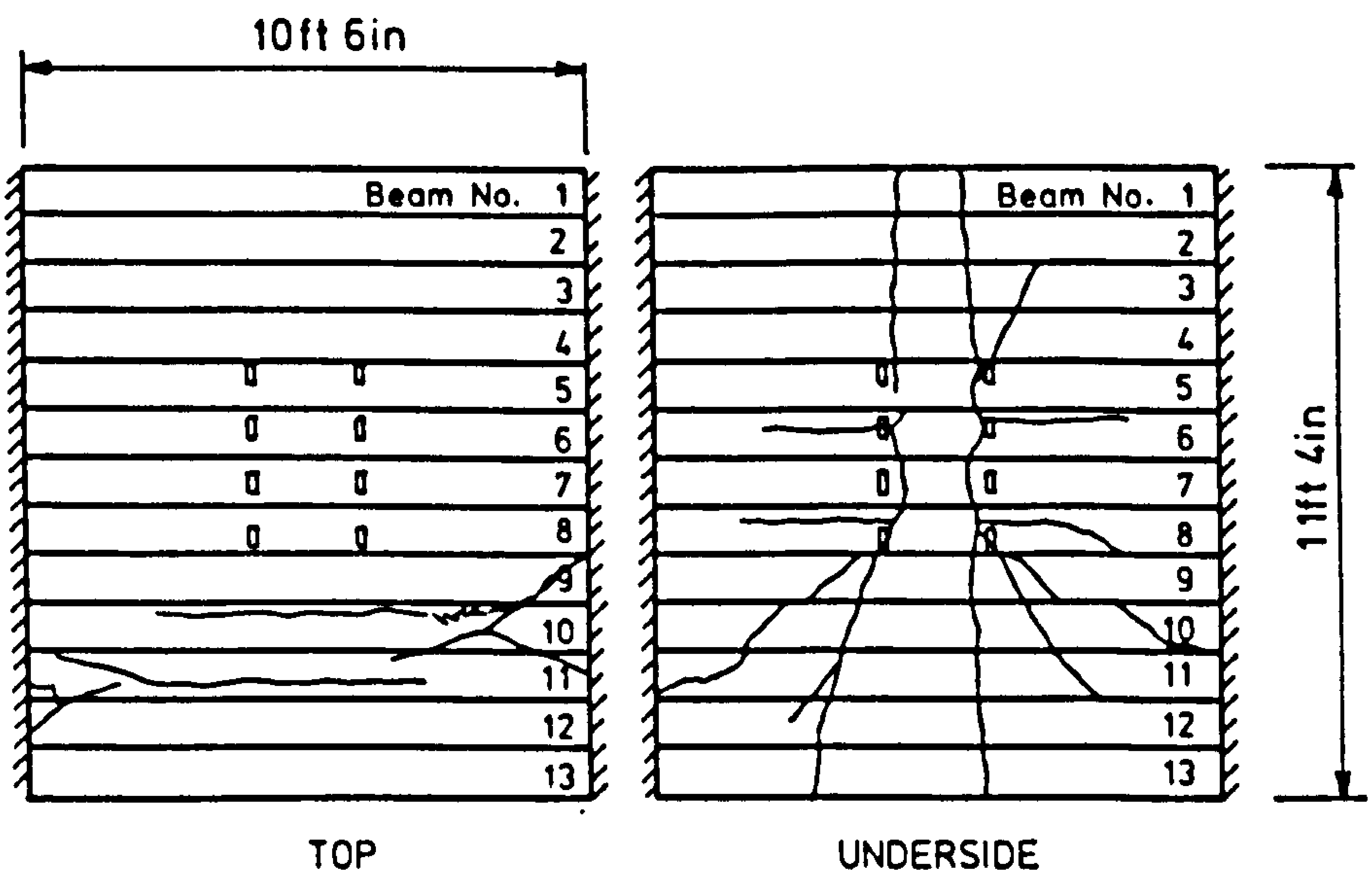

b) Crack patterns on Bridge 2 at failure

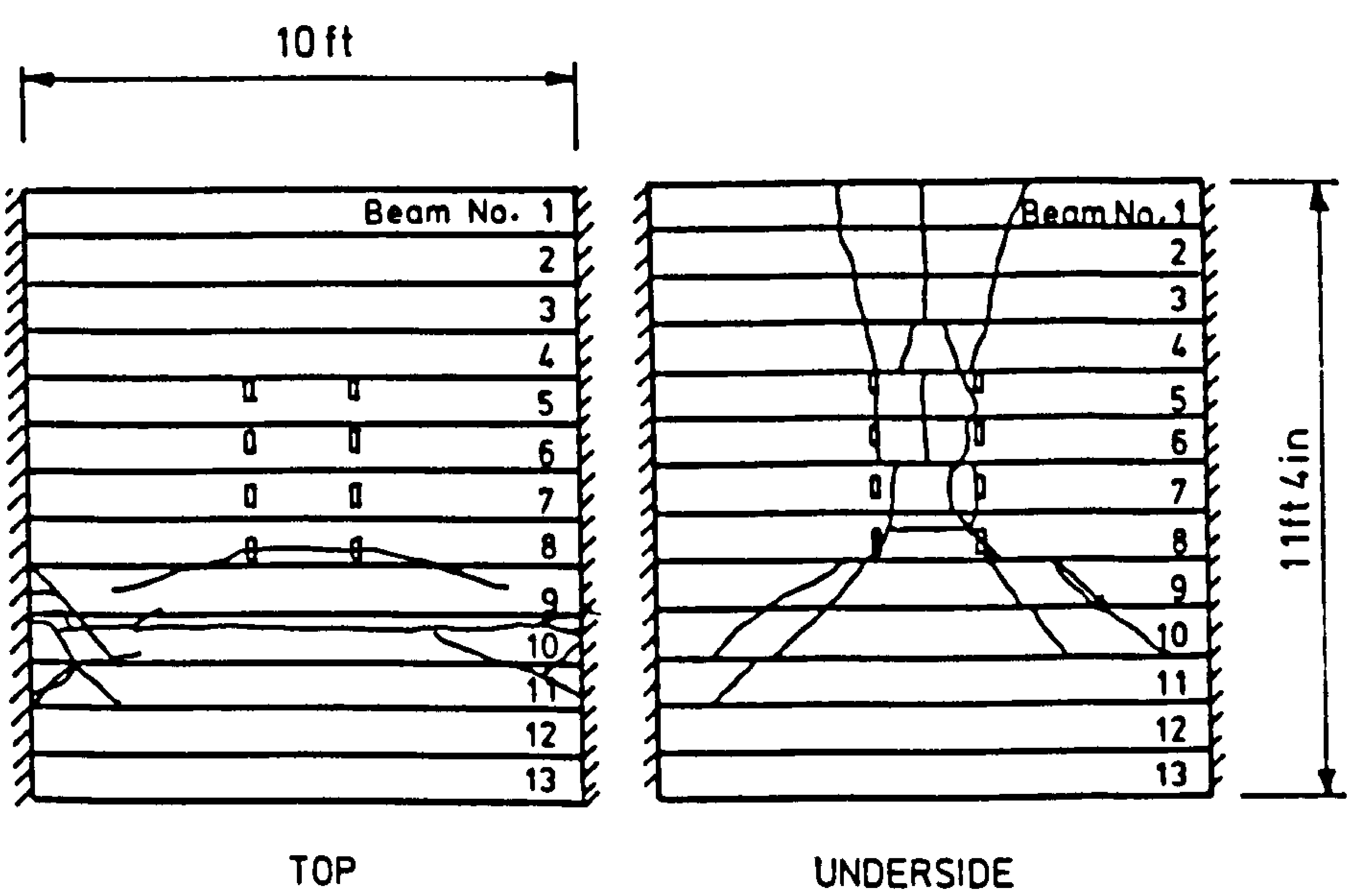

c) Crack patterns on Bridge 3 at failure

FIG. 2.1. CRACK PATTERNS FROM BEST AND ROWE MODEL BRIDGE TESTS

innermost edge of the HB bogie to the free edge and back at a shallow angle to the supported edges. There were few, distinct cracks, see Figure 2.1(a).

Transverse cracking extended over the entire width of the soffit of model 2 at a load of 24 tons. At 25 tons, diagonal cracks formed, starting from approximately the centre of the bridge. These cracks increased in width with increasing load, whereas the transverse cracks in the same region did not. The crack pattern at failure, which occurred at 29 tons, is shown in Figure 2.1(b).

Model 3 failed at 27 tons, with the crack pattern shown in Figure 2.1(c).

Of particular interest in the cracking of Bridge 2 is the short length of shear or tearing cracks at the 'loaded edge' of beam 10. Unfortunately, no mention is made of this cracking in the reports and it is impossible to deduce at what load level it occurred. The sparsity of soffit cracking in all of the models suggests that bond failure occurred in the precast beams. The sparsity of cracking on the top surfaces is due to the lack of reinforcement. However, due to the concentrated nature of the loading, part of the deck lifted off the supports.

2.1.2 Tests on end diaphragms with precast units and insitu concrete

Clark and West[2] have reported the results of tests to determine the torsional stiffness of support diaphragms in beam and slab bridges. Their report describes the results of torsion tests on eight quarter scale models of end diaphragms of bridge decks formed of precast, pretensioned, inverted T beams connected only by a top slab and end diaphragms. It is of interest in connection with the present work because the models tested could be viewed as a transverse slice of a deck formed of composite construction. The analogy is not exact, as the torsional shear flows in these models are around the small rectangular cross-sections, whereas the shear flows in the interior of a slab from the twisting moments would be mainly horizontal. However, the analogy is more reasonable near the supported ends of a slab, where the twisting moments may be large, and the shear flow is around three sides of a section.

Diaphragms D1R and D2R, see Figure 2.2, represented conditions closest to those in the composite slab models, although the diaphragm models were amply provided with links. The results obtained are mainly of interest up to cracking of the concrete. To exaggerate the tendancy for the insitu concrete to shrink away from the precast beams, a high shrinkage insitu mix was provided. The torque-twist relationships reported were linear up to the predicted torque level to cause cracking, and the torsional inertias of the specimens were similar to the values calculated for homogeneous sections.

Cracking initiated in the added concrete and extended to the insitu/precast interface. With further loading, the cracks propagated through the precast concrete. This suggests that no significant slip was taking place between the precast beams and added concrete prior to failure. Failures were caused by slip between one of the precast beams and the neighbouring insitu concrete.

The tests did not attempt to investigate the interaction between bending and torsion. It is likely that transverse bending would assist in causing slip at the interface of the two concretes. However, the tests do indicate full composite action under torsion until cracking, providing the transverse bending effects are negligible.

2.1.3 Tests of tensile strength across composite concrete interfaces

A study of the tensile strength of concrete across construction joints has been reported by Waters[3]. The ratio of the strength at the joint to the strength of the parent concrete, for no surface treatment and with laitance remaining on the surface of the first cast concrete, was 0.45. This ratio was found to increase to 0.78 when the first cast concrete was allowed to dry out before casting the remaining concrete. Two reasons were given for this. Firstly, the absorption of mixing water into the dry surface decreases the water/cement ratio of the new concrete against the joint; and, as the water is being absorbed into the old concrete, the finer granules of cement in the fresh concrete are absorbed into the interstices.

2.1.4 Tests of shear strength across composite concrete interfaces

Shear can be transmitted across a smooth construction joint by both cohesion and friction. Tests conducted by Johansen[4] indicate a reduction of 60% cohesion compared with the monolithic concrete[5], provided the angle of friction is assumed to be that of the monolithic concrete.

Plasticity theory[5] theory gives the normal failing stress by:-

$$\sigma = \frac{c \cos \theta}{\cos \beta \sin(\beta - \theta)} ,$$

where β is the angle of the failure plane; θ is the angle of friction, which is assumed to be 37°; and c is the cohesion.

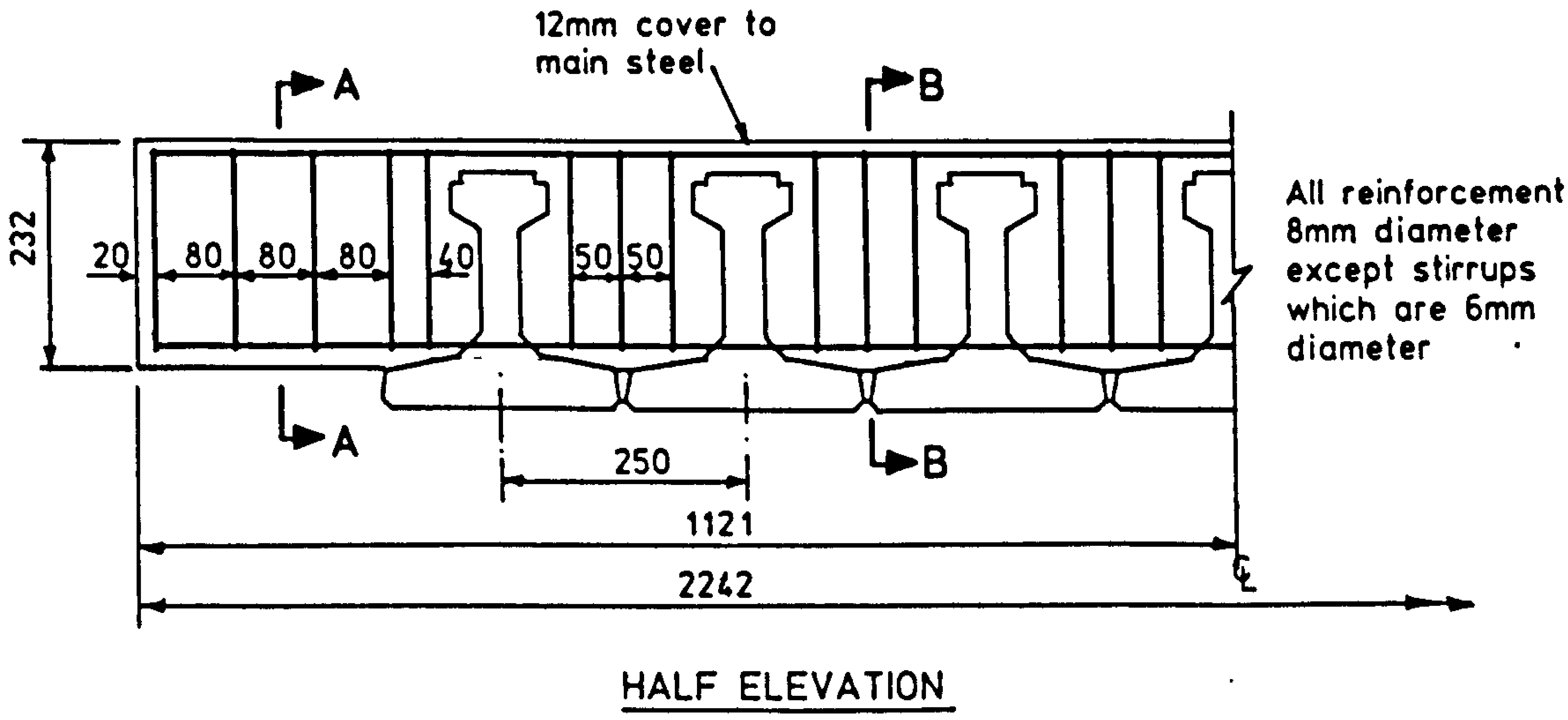

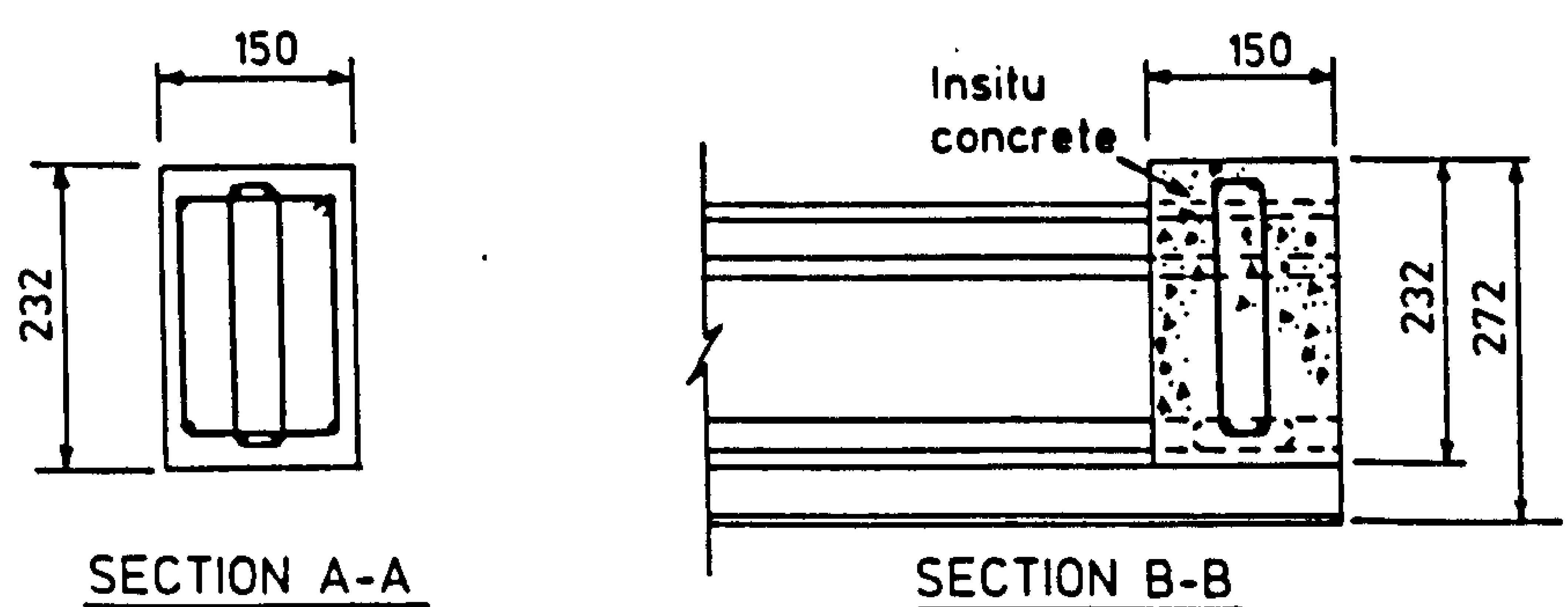

a) Diaphragm D1R

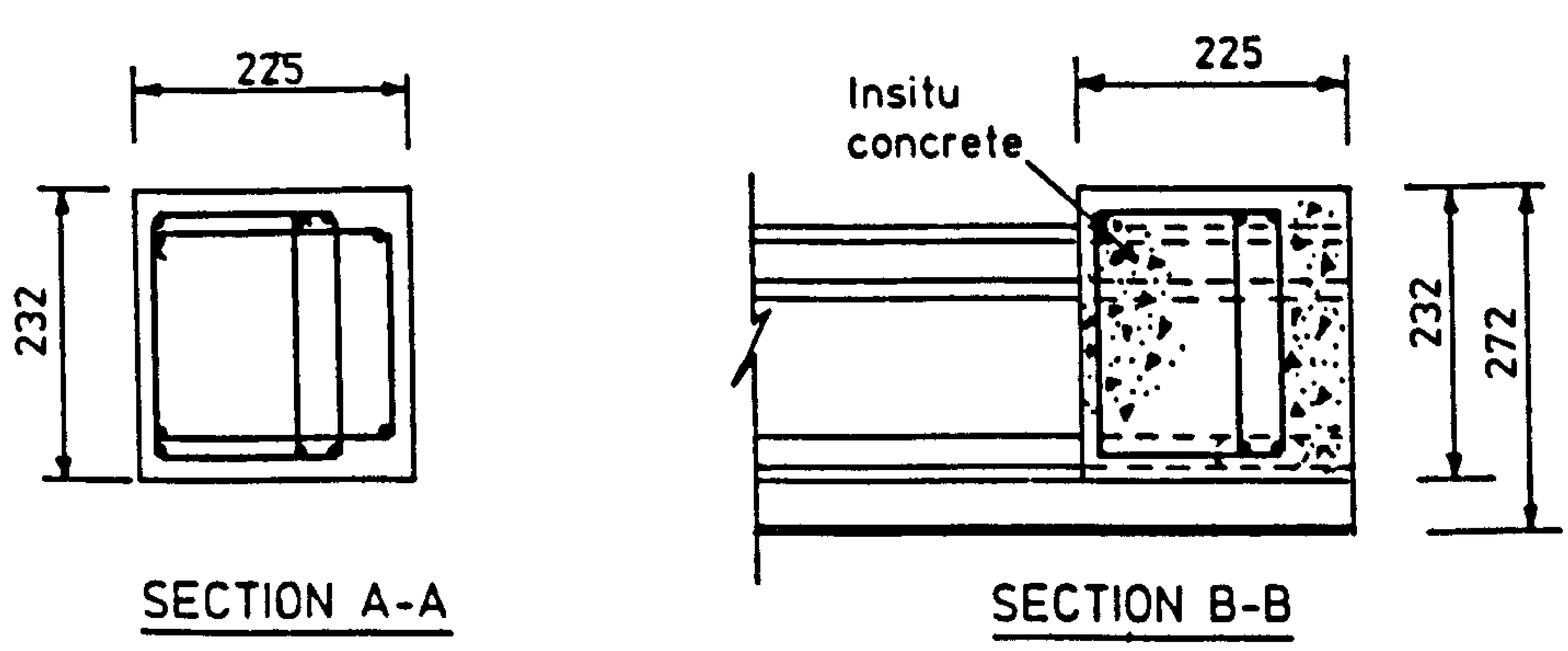

b) Diaphragm D2R

FIG. 2.2. DETAILS OF TEST DIAPHRAGM UNITS, D1R AND D2R.

Clark and Gill[6] have reported the results of tests on smooth construction joints subjected to axial compression and shear. The face of each construction joint was cast against an oiled plywood former, and no attempt to improve the bond by degreasing or roughening was made. They found that the cohesion decreased with the age of the first half of the specimen at the time the joint was formed. The reason given for this trend was that the amount of moisture available at the interface to aid hydration of the cement at the joint reduces with time as the first half dries. This result and reasoning contradict that of Waters[3]. However, all but 2 of Clark's series of tests used a considerably lower water/cement ratio than did Waters, and the importance of a dry surface may be dependent on the amount of free water present in the mix. A further possible cause of the different results may be due to changes in cement over the 30 year time interval between the two series of tests. Because of the large scatter of data points, Clark recommends that no dependence of strength upon age should be considered in design.

Using his own test data, and that of Johansen, Clark proposed the following characteristic joint strengths:-

sigma

$\tau = 2.56\ \cancel{N/mm^2}$	$0 < \sigma \leqslant 0.04\,f_{cu}$	(2.1)
$\tau = 0.07\ f_{cu} + 0.75\ \sigma,$	$0.04\ f_{cu} < \sigma \leqslant 0.263\ f_{cu}$	(2.2)
$\tau = 0.267\ f_{cu},$	$0.263\ f_{cu} < \sigma$	(2.3)

Comparison of Equation 2.1 with the sliding criterion $|\tau| = c - \sigma \tan \theta$, ($\sigma$ compression -ve) indicates that the sliding formula is not applicable, or that the angle of friction has increased to about 68°, which is not likely. Equation 2.2 indicates that the cohesion at the joint is 0.07 $f_{cu} \approx 0.09 f_c$, compared with the typical value $c = 0.25 f_c$ for monolithic concrete.

2.2 Previous Analytical Research

An extensive manual and computer based literature search did not reveal any previous analytical investigations pertaining to composite construction. For the development of the SNAP (Slab Nonlinear Analysis Program) program a survey of relevant finite element methods was conducted. This survey encompassed both traditional approaches and more recent innovations which are now gaining widespread popularity. From the results of this review the SNAP program was developed using the features most appropriate to composite construction. Details of this review have been included in Chapter 8 on the development of the SNAP program and are, therefore, not included here.

2.3 References

1. Best, B.C. and Rowe, R.E. "Abnormal loading on Composite Slab Bridges", Research Report No 7, Cement and Concrete Association, (1959).

2. Clark, L.A. and West, R. "The torsional stiffness of support diaphragms in beam and slab bridges", Technical Report 42.510, Cement and Concrete Association, (1975).

3. Waters, T. "A study of the tensile strength of concrete across construction joints", Mag. of Conc. Res. Vol. 5, No. 18, p. 151-153, (1954).

4. Johansen, K.W. "The strength of joints in concrete", Bygnings-statiske Meddelelser, Vol. 2, p. 67-68, (1930).

5. Jensen, B.C. "Lines of discontinuity for displacements in the theory of plasticity of plain and reinforced concrete", Mag. of Conc. Res. Vol. 27, No. 92, p. 143-150, (1975).

6. Clark, L.A. and Gill, B.S. "Shear strength of smooth unreinforced construction joints", Mag. of Conc. Res. Vol. 37, No. 131, p. 95-100, (1985).

3. MODEL CONSTRUCTION AND DATA ACQUISITION

3.1 Construction of the Models

The pretensioned beams were constructed in groups, see Plate 3.1, and assembled on the bearings. Transverse reinforcement was then threaded through the holes in the webs and fixed in position, see Plate 3.3. Vertical side shutters with their top surfaces following the precambered beam profiles to ensure a constant deck thickness were then positioned. Top reinforcement was fixed and the in-situ concrete poured. All of the concrete was cured under wet sacking covered by polythene sheeting.

3.1.1 Model Pretensioned Beam Construction

Model 1

A table was constructed to which vibrators were attached. The top of the table was made of a high grade ply to ensure a flat soffit and good durability. Five strips of ply with widths equal to those of the soffit flanges were secured to the table top to facilitate the accurate assembly of the side shutters for each of the five beams in a group.

For the first set of beams cast (those used for the studies described in Appendix 2.5*) each side shutter was constructed from 3 lengths of 16 SWG steel plate with a continuous box sections welded to its outer face to provide stiffness. The dimensional accuracy achieved was not satisfactory, and the beams used in the model were constructed using commercially formed side shutters manufactured from a single strip of 8 SWG steel plate. The dimensional accuracy obtained from these shutters was of a high order.

* Appendix 2.5 of Research Report No. TRR 842/368 produced for the Transport and Road Research Laboratory.

A pretensioning frame was constructed from hollow box sections and holes for the pretensioning wires were carefully drilled, see Plate 3.1.

The effects of different tendon stressing sequences were studied in order to ensure a uniform, accurate prestress in all the precast beams. Unlike the method normally used commercially, where a number of beams are cast as a long line around the same set of continuous wires, the model beams were cast side by side. Thus the losses in the anchorages had a larger effect than normal for the model beam prestressing. This problem coupled with the elastic shortening of the prestressing frame, dictated that a two pass system had to be adopted for prestressing.

The two pass system consisted of starting with the centre beam and then moving to the outer beams in a systematic and symmetric manner, stressing the wires to approximately 80% of the required prestress. The beams then underwent a second stressing pass taking the prestress up to 100% of that required. Because of the two pass system, an alternative to extension monitoring had to be found for applying the prestress. The procedure adopted used a load cell to indicate the stressing load, and extension monitoring to check anchorage losses. After stressing, an extensometer was fastened to a wire so that the effects of stressing the other wires could be monitored.

After the tendons had been stressed, the stirrups, transverse hole formers, and side shutters were positioned, see Plate 3.2. The side shutters were braced transversely across the top of the casting bed using a jig which ensured accurate location, see Plate 3.1.

After the concrete had gained sufficient strength, the side shutters were removed. This operation took place one or two days after casting. The side shutters were treated with a demoulding fluid, and no attempt was made to remove any of this from the side faces of the concrete beams. Commercial beam manufacturers indicated that this would be normal practice.

The tendon force was transferred to the concrete beams when the concrete had reached a cube strength of 40 N/mm^2, generally after about five days. The cube strengths at the time of transfer were recorded. For the first set of beams cast (those used for the studies described in Appendix 2.5*) the tendon force was transferred using the prestressing jack. This operation released tendon forces one at a time. It required each wire to be re-strained so that the force on the anchorage could be removed and the anchorage could be released After the anchorage had been freed, the tendon force was transferred to the concrete over a period of about one minute, by reducing the hydraulic pressure to the jack.

This procedure was felt to be suspect due to the high level of the jacking force needed to release the anchorage. The poor bond behaviour of these beams may have been due, at least in part, to partial bond break down due to this procedure. It was also felt to be desirable to achieve a more uniform transfer of prestress.

For the beams in the deck and those studied in Appendix 5.1, the following procedure was, therefore, followed. A second steel box beam was placed at the jacking end of the prestressing frame and separated from it by hydraulic jacks with screw collars, as shown in Plate 3.1.

* Appendix 2.5 of Research Report No. TRR 842/368 produced for the Transport and Road Research Laboratory.

After stressing, the tendons were anchored to the second box beam. When the concrete had matured, the two jacks between the prestressing frame and the second box beam were loaded just sufficiently to enable the screw collars to be untightened. The prestress force was then transferred from all of the tendons together, over a period of about a minute, by releasing the force in the two jacks.

Model 2

Essentially, the same procedure was followed to construct the beams for the second model as had been used for the beams of model 1. The prestressing table had to be lengthened, a stiffer pretensioning frame of similar design was constructed, and new side shutters were purchased.

The design for model 2 was practically complete before the reasons for the poor behaviour observed in the beam tests described in Appendix 2.5* had been firmly identified. Therefore, the decisions taken during the first part of the design reflected this position. In order to provide a greater transmission/bond length the beams were cast 1040 mm longer than the scale length. The desire to increase the bond, and the availability of various prestressing tendons, led to 7.9 mm diameter 7 wire strand being selected for the precast beams of model 2.

3.1.2 Model Slab In-situ Construction

After the model beams had been cast, they were lifted onto the already positioned bearings in the testing frame. This method allows the self weight of the deck to be borne by an assemblage of beams and not by the slab. Thus applying the same load to each bearing, see Plate 3.3.

* Appendix 2.5 of Research Report No. TRR 842/368 produced for the Transport and Road Research Laboratory

Model 1

Once all of model 1's 22 beams had been positioned in the testing frame, the placement of the ancillary reinforcement was carried out. The bottom transverse bars were threaded through the holes in the beam webs. Anchorage for these bars was provided by 100 mm bend-ups at each end. These were held in the vertical position by wire ties to the tops of the shear links. The bundles of three bars through each hole were spread as far apart as possible to increase bond. The top longitudinal reinforcement was threaded below the tops of and clipped to the shear links. The top transverse steel was placed on top of and clipped to the top longitudinal steel. End anchorage was provided by 100 mm bend-downs at each end of the top transverse steel.

The relatively small size of the model deck allowed all the reinforcing bars to be continuous. With no need for the lapping of bars. The reinforcing bar system was uniform over the whole area of the model deck.

Model 2

The reinforcement arrangement for model 2, although similar in nature to model 1, was more complicated. The complexity arose from the fact that the lower transverse reinforcement did not run parallel to the supported edges, as it had done in model 1. The direction of the lower transverse reinforcement in the full size deck is dictated by the beam spacing, transverse hole spacing and the angle of skew. Because the transverse hole spacing could not be scaled, a system using two slightly different beam types with different longitudinal offsets for each of the 17 beams, had to be used. Thus, the scaled amount of reinforcement at the required angle was provided.

Anchorage for these bars was provided by 110 mm bend-ups at each end, see Plate 3.4. Again, no lapping was required. The top longitudinal reinforcement was placed in a similar way to that of model 1, with the top transverse reinforcement placed on top of the longitudinal bars and clipped to them. The top transverse reinforcement was placed in a direction perpendicular to the free edge and was anchored by 150 mm bend-downs at each end, see Plate 3.4.

To avoid the extra length of the precast beams acting as a slab, the in-situ concrete was cast just longer than the scaled deck length, leaving the extra beam lengths as overhangs, see Plate 3.4.

The reinforcement arrangement of model 2 caused difficulties in the placement of the lower transverse steel in the end zones. The bend-up at a bar end could not be applied before the bar was threaded through the transverse holes in the webs. This limited the bend-up to the distance between adjacent webs, a distance of 110 mm.

3.1.3 General Considerations:

The initial concrete mix design followed the procedure suggested by the Department of the Environment[1,2,3]. The mix design was verified and modified in the light of test mix results. Even though many trial concrete mixes had been carried out during the development of the model concrete for the precast beams of model 1, it was necessary to make small amendments to the mix design during the casting of the early batches of beams for model 1.

Because of the small size of the laboratory mixer, 3 mixer loads were required for each set of 5 beams for model 1, and 4 mixer loads for the 4 beams in each set for model 2. The surface area to volume of both the concrete mixer and the beams resulted in significant loss of fluid in the mix. It was observed from the casting of the first set of beams for model 1 that the mix was too harsh, and did not possess the required workability.

Initially, the water/cement ratio was 0.535 and the aggregate/cement ratio was 4.97. The original mix included the addition of plasticiser (Cormix P2) at the rate of 80 ml per 50 kg of cement, to increase workability. It was not considered satisfactory to increase the plasticiser content of the mix to obtain the desired increase in workability. The reduction in harshness and the increase in workability was, therefore, obtained by varying the water/cement ratio and the aggregate/cement ratio. The mix that proved to be most satisfactory possessed a water/cement ratio of 0.545 and an aggregate cement ratio of 4.69. This final mix gave good compaction around the small congested section and, of particular importance, around the transverse hole formers in the lower part of the section.

The formwork for both of the model decks was constructed so that its support structure was completely separate from that of each model. This was intended to ensure that the same load was applied to each of the support load-cells under self weight.

During the construction of model 1, the importance of maintaining a clear gap between the flanges of adjacent beams was not fully appreciated. During the curing of the in-situ concrete, the model deck was observed to bend upwards at the free edges and load was transferred from the end load cells to the central cells. This is believed to have been caused by shrinkage in the in-situ concrete. As the concrete at the bottom of the section began to shrink, movement was prevented either by the lack of a gap between adjacent beams, or by the gap having been filled with cement paste. However, there was little restraint to movement at the top of the section, hence the transverse sagging curvature observed in the model deck.

The most obvious indication of what had occurred came from the load cells along the supported edge, some of which were completely free, with no applied load. The gaps between the load cells and the deck were measured and a plot is shown in Figure 3.1. Before testing, the load cells were adjusted to ensure a relatively uniform distribution of load along the supported edge.

Great care was taken while positioning and sealing the beams of model 2. A minimum gap of 3 mm was left between adjacent beams. This gap was sealed by applying a bead of sealant from above to the gaps, along the tops of the bottom flanges. This method ensured that there was a gap between adjacent beam flanges filled with soft sealant and no cement paste. After the in-situ concrete of model 2 had been cast, the situation was monitored. There was no recurrence of the transverse curvature problem, and the distribution of the load on the support load cells was reasonably uniform.

When the covering material was removed from the top surface of model 2, after the in-situ concrete had been curing for approximately 2 weeks, some cracking was noticed. The cracking was confined to relatively small zones, and the cracks were aligned either along the top transverse steel or along the top corner of the web of an inverted 'T' beam. The cracks aligned along the transverse reinforcement were approximately 75 mm long and the crack width was generally in the range 0.0 → 0.3 mm. The cracks were positioned between some of the webs of adjacent beams.

The Concrete Society Technical Report 224[4] 'Non-Structural Cracks in Concrete' refers to plastic settlement and plastic shrinkage cracks. These types of cracks form when the concrete is in a plastic state a few hours after placing the concrete. Plastic settlement cracks tend to form when the new concrete sets and shrinks and the shrinkage is restrained in some way. The restraint can be provided by fixed top steel. In effect, the concrete hangs from this top steel. Thus, with small cover, the top bars "pull through", producing a crack between the top steel and top surface, together with a small void below the top bars. Plastic shrinkage cracks are primarily formed by rapid drying out and generally extend deep into the structure. This type of cracking occurs when the rate of evaporation exceeds the rate of bleeding.

In full size structures, plastic settlement cracks are typically found in deep beams, whereas shrinkage cracking is generally found in flat slabs. Even though the model is a deck slab, it has been concluded that the cracking visible on the top surface of model 2 is due to plastic settlement. This deduction is based on two features. Firstly, with regard to ambient conditions, the concrete was placed inside a laboratory with no wind and with a controlled ambient temperature of approximately 10-15°C, and the slab was cured under wet sacking and polythene sheets. Therefore, the evaporation rate would have been low. Secondly, with regard to the structure, the model section of the new concrete was effectively an assemblage of relatively deep lengths of concrete separated by the precast beam webs and the top reinforcement was incapable of downward movement, being restrained by the tops of the inverted 'T' beam webs.

The effect of the cracks on the behaviour of model 2 was likely to be small, considering their shallow nature. However, as a precaution, all visible cracks were filled with a very low viscosity epoxy resin.

After the testing of model 2, which is fully described in Chapter 7, had been completed, six 150 mm diameter cores were removed from the model. These full depth cores allowed the extent of the early age cracking to be investigated whilst also allowing the effectiveness of the resin injection to be evaluated. These investigations confirmed the suspicion that the early age cracking was a result of settlement rather than shrinkage. The cracks were observed to progress no further down the section that the top reinforcement. It was concluded that early age cracking should not have a significant effect upon the structural response since it had been shown that the cracks were due to settlement and also that the resin injection had been successful in filling these cracks.

3.2 Data Acquisition

3.2.1 Model 1 : Data Collection

It was envisaged, at an early stage, that the data collection system for the model tests would have to incorporate computer processing if it was to be effective. Therefore, after assessing the available data acquisition systems, it was decided to use an Intercole Ms Logger unit driven from the departmental Data General Eclipse mini computer. Data was stored on the Eclipse computer during the test and subsequently transferred to the central IBM 3083 mainframe computer for in-depth analysis and manipulation for presentation.

A program was written for the Eclipse computer to drive the Logger unit. This program was highly interactive and possessed many useful features to allow significant local processing of the data, detection of gross errors and monitoring of the events in engineering units. All readings were written to a printer locally, as a safeguard against failure of the magnetic storage media used to hold the results on the Eclipse computer.

Five different types of transducer were used for data collection: load cells; electrical strain gauges; platinum resistance thermometers; linear voltage displacement gauges; and electro-mechanical strain gauges.

Load cells were used for the supports with an accuracy of ± 0.25 kN and also on the HB Bogie jack with an accuracy of ± 1 kN.

Three types of electrical strain gauges were used on model 1, 60 mm linear gauges on the beam soffits aligned along the beams, 20 mm rosettes on the top surface and 20 mm weldable strain gauges attached to the prestressing wire and reinforcement.

All of the electrical strain gauges were connected in a half bridge configuration with a dummy gauge mounted on a similar material to the active gauge. This system coupled with the stable constant current sources gave results which were very stable over time, with a resolution of 0.48 $\mu\epsilon$ and were temperature compensated. However PRT's (Platinum Resistance Thermometers) were also positioned around the slab, some on the surface and some cast inside the in-situ concrete.

These monitored the instantaneous temperature distribution around the slab whenever readings were taken from the strain gauges.

Regions of concrete in tension generally pose difficult problems for the capture of strain data. Strain gauges are not generally satisfactory, because of their low tensile strength and their subsequent inability to survive cracking of concrete. However, in this case, the majority of the concrete subjected to tensile strains from the applied loading was in fact prestressed. The prestress delays the onset of cracking, thereby allowing strain gauges to produce reasonable results for heavier loads.

Linear strain gauges 60 mm long were attached to the soffit of the precast beams while they were assembled in the frame, before the casting of the in-situ concrete. To cater for the post cracking phase and to obtain strain information from more points than could be realistically strain gauged, de-mec points were also used.

The de-mec points, with a gauge length of 100 mm, were positioned at systematic locations on the soffit of model 1, see Figure 6 of Appendix 5.3. Their locations, forming continuous lines transversely, were selected to provide information on transverse strains across sections parallel to the supported edges. Other de-mec points were positioned across the 60 mm strain gauges on the soffit for two reasons. Firstly, they enabled data on the correlation between strain gauge and de-mec points to be obtained, see Figure 3.2 and secondly they gave strain information in the post cracking range. However, readings from these isolated de-mec points needed careful interpretation, due to the possibility of cracks passing close to, but not through the gauge length between de-mec points.

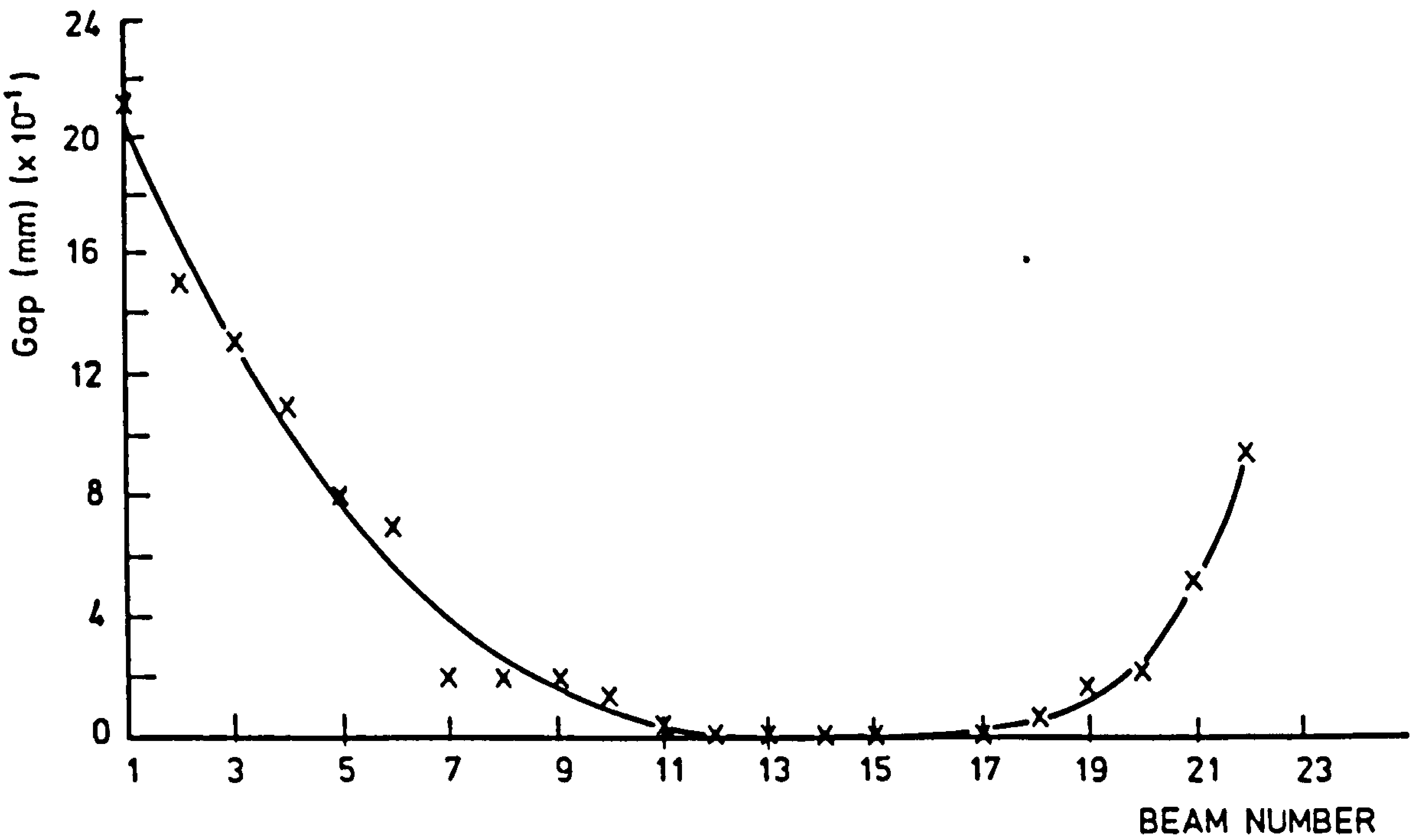

FIG. 3.1 DIAGRAM SHOWING THE GAPS THAT WERE MEASURED ALONG SUPPORT LINE 1 OF MODEL 1 AFTER CURING OF THE IN-SITU CONCRETE

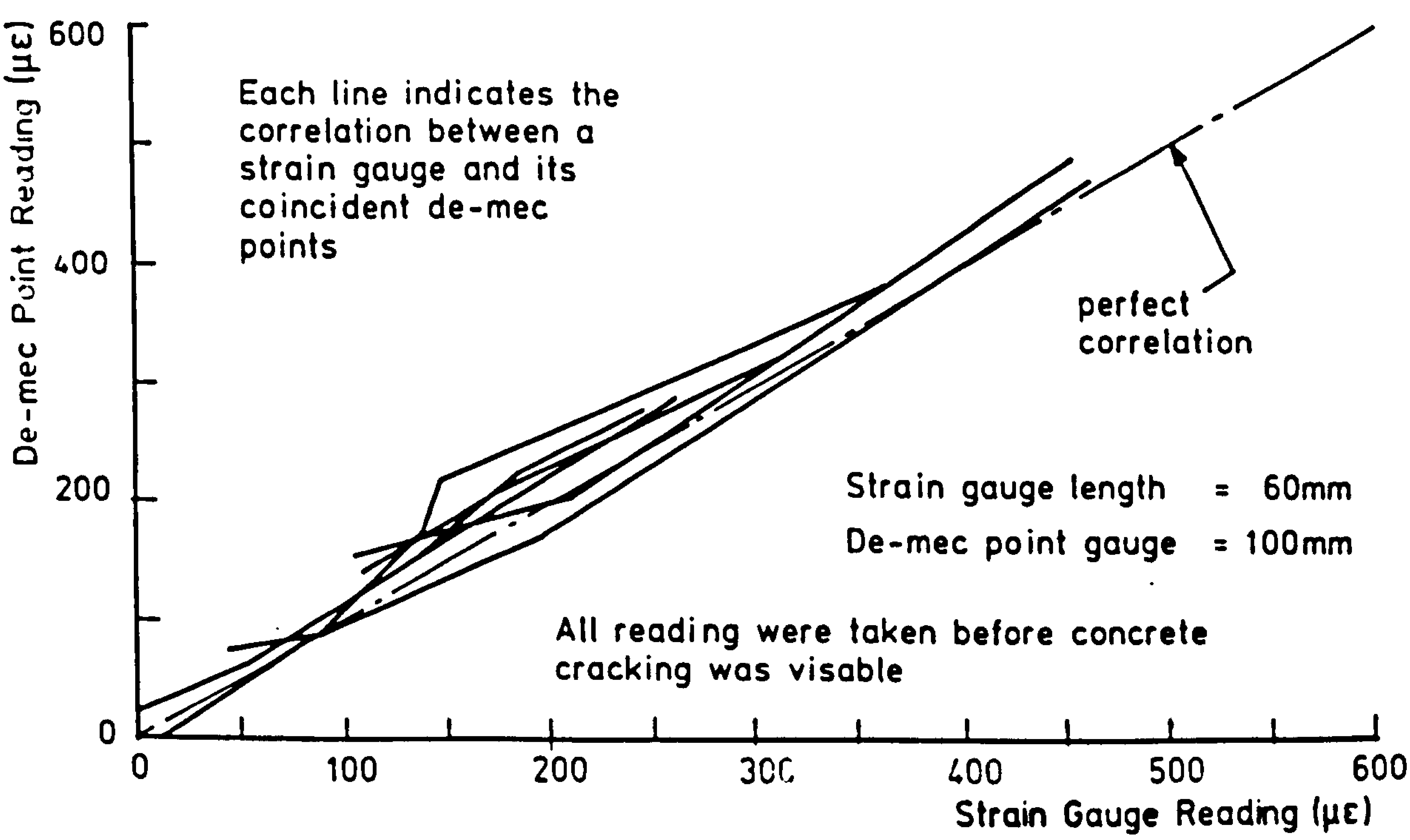

FIG. 3.2 DIAGRAM SHOWING THE CORRELATION BETWEEN STRAIN GAUGES AND COINCIDENT DE-MEC POINTS ON THE SOFFIT OF MODEL 1 DURING TESTING.

The normal method of measuring de-mec strains is to use a de-mec body onto which is mounted a calibrated dial gauge. Recording the readings manually from the dial gauge and then manually processing them would have severely limited the analysis of the results. Therefore, methods of electrically measuring the de-mec strain were investigated. The solution arrived at for model 1 used the only electrical de-mec unit that was commercially available. The unit, which is shown in Plate 3.5, works on the principle of a strain gauged cantilever being displaced by the moving de-mec points. Besides having electronically readable output, the unit, with a range of ± 30000 $\mu\epsilon$, could be used across cracks. The accuracy displayed by this unit was satisfactory, as can be seen from Figure 3.2, which shows the correlation obtained between de-mec and strain gauge readings.

The displacement of model 1 was monitored by 12 LVDT's mounted on a frame which was independent of the testing rig. A few of the LVDT's had a range of, 30 mm whereas most had a range of 50 mm. They all displayed a good resolution of ± 0.05 mm.

During the test on model 1, there were 99 transducers and 47 sets of de-mec points attached to the model.

3.2.2 Model 2 : Data Collection

The systems used for the collection of data from model 2 were similar to those used for model 1 . There were, however, areas where improvements were made and these are described below.

20 mm rosettes were again attached to the top surface, however, for model 2, similar rosettes were also used on the beam soffits. This

change from linear gauges to rosettes was for the investigation of the greater torsional shear anticipated in the beam flanges.

Weldable strain gauges were attached to the prestressing wires used for model 1. However, attaching these gauges to the prestressing strand used for model 2 posed a more difficult problem. After an investigation, weldable gauges were rejected in preference to normal foil strain gauges, which were attached to the strand after it had been coated with a ductile plastic epoxy resin to give it a smooth surface. After the gauges were attached, they were liberally coated with waterproofing, for protection in the harsh concrete environment. Weldable strain gauges were used for the non-prestressed reinforcement in a similar way to model 1. Successful tests for accuracy and repeatability were carried out to validate the use of foil gauges on the strands.

Although the electrical de-mec unit had given satisfactory results for model 1, it was felt that the instrument was the weak link in the data collection facilities. Therefore, a number of steps were taken to improve the accuracy and reliability of the de-mec strain readings. Most noticeable of these was the development of a new electrical de-mec unit. The final design used a standard C & CA de-mec's body, onto which was mounted a very accurate LVDT, see Plate 3.6. The new de-mec unit provided a range of $\pm$ 15000 $\mu\epsilon$ to a precision of $\pm$ 8 $\mu\epsilon$.

The computer program that had been written to drive the logging system was improved, so that it sampled the de-mec unit four times over a period of 7 seconds. The maximum variation of any of the four incremental readings from the average of the incremental readings (ϵ_{av}) was compared to a preset figure (10 $\mu\epsilon$ for $\epsilon_{av} < 1000$ $\mu\epsilon$, 1% for

ϵ_{av} > 1000 $\mu\epsilon$). If any reading was outside the appropriate range, more readings were taken until a steady signal was obtained. After a group of de-mec readings had been recorded, a repeat reading of a few randomly chosen points in the group was carried out. The new readings were compared with the criterion given above. If any of the repeat readings did meet the criterion, the group was re-read and the same process carried out.

Before the de-mec unit was used for a scan, it was calibrated against an invar calibration bar. The calibration bar was accurate to 50 $\mu\epsilon$ in 10000 $\mu\epsilon$.

3.2.3 Model Bearings

Both models had one supported edge resting upon bearing units similar to the one shown in Plate 3.7. The top part of the unit incorporated a load cell with a low profile design, this ensured that the units were very stable. The load was transferred from the 'elastomeric' type bearing through a 20 mm thick steel plate to the hardened steel load button that can be seen on the top of the load cell. The spherical surface of the load button allowed rotation about the three axes, while the lower half of the unit incorporated ball bearings to allow ± 10 mm of translational movement in plan.

The second supported edge, known as the 'dead end' rested upon the same number of 'elastomeric' type bearings, however the supports under these did not incorporate load cells or ball bearings. Therefore the 'dead end' bearing units still allowed rotation about the three axes but translation in plan was restricted. The units were not fastened down in any way therefore translation was possible if the side force overcame the friction of steel upon steel.

3.3 References

1. Design of normal concrete mixes, Department of The Environment, 1975.

2. Concrete Practice, Cement and Concrete Association, 1975.

3. Concrete Mix Design, F.D. Lyndon, Applied Science Publishers Limited, 1972.

4. Non-Structural Cracks in Concrete, The Concrete Society Technical Report 22, December 1982.

BLANK IN ORIGINAL

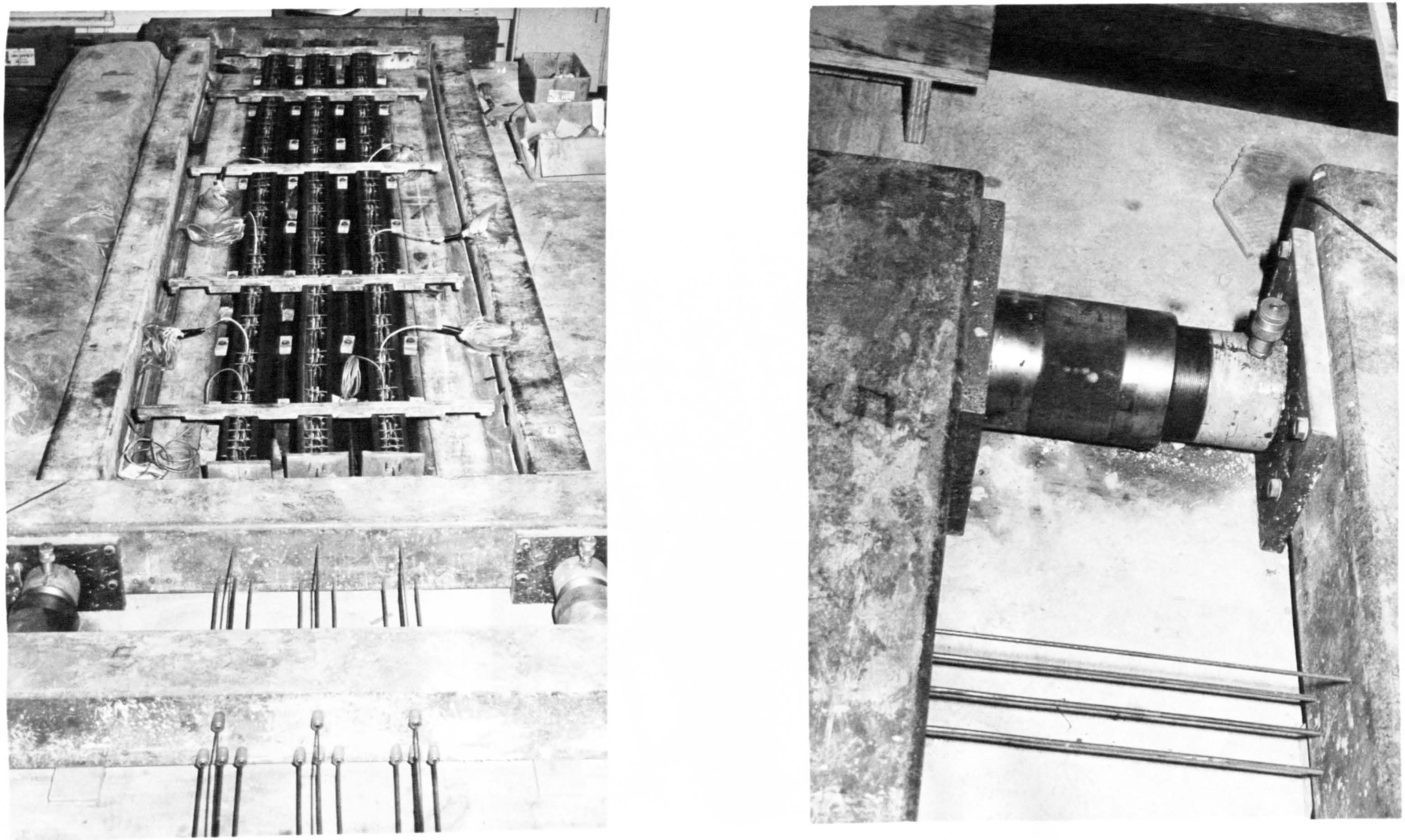

PLATE 3.1 THE PRETENSIONING FRAME THAT WAS USED FOR THE PRODUCTION OF MODEL 1 BEAMS.

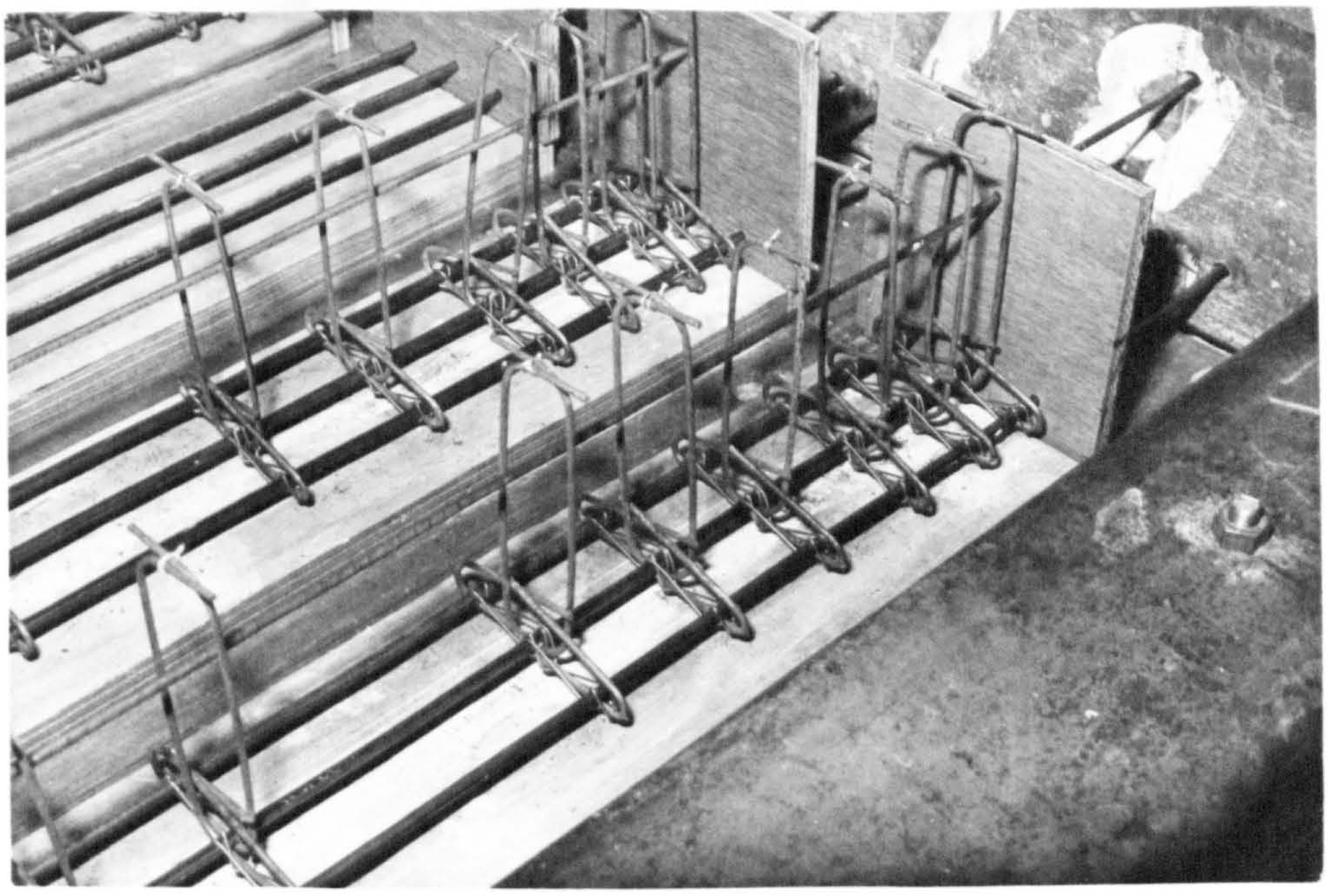

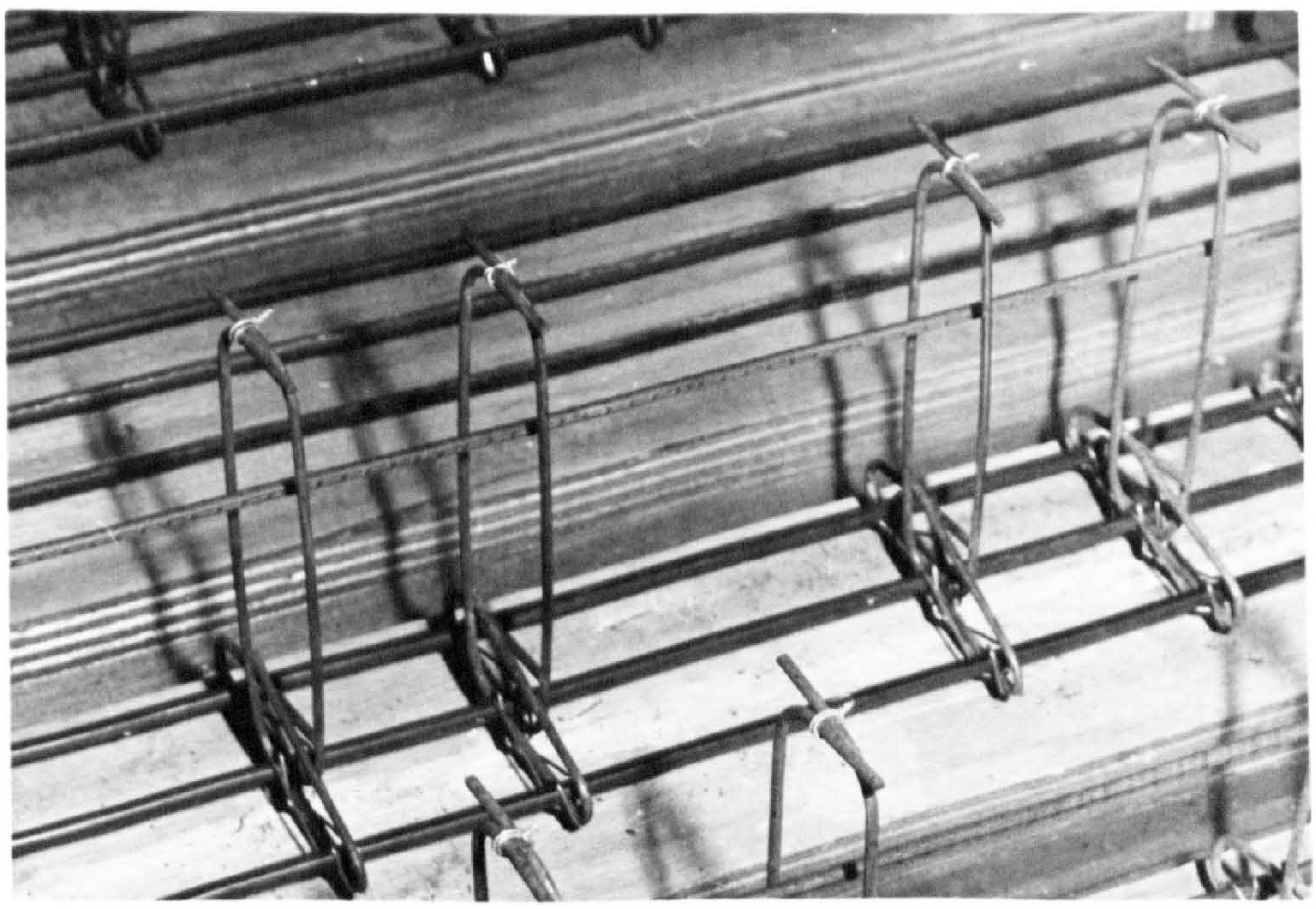

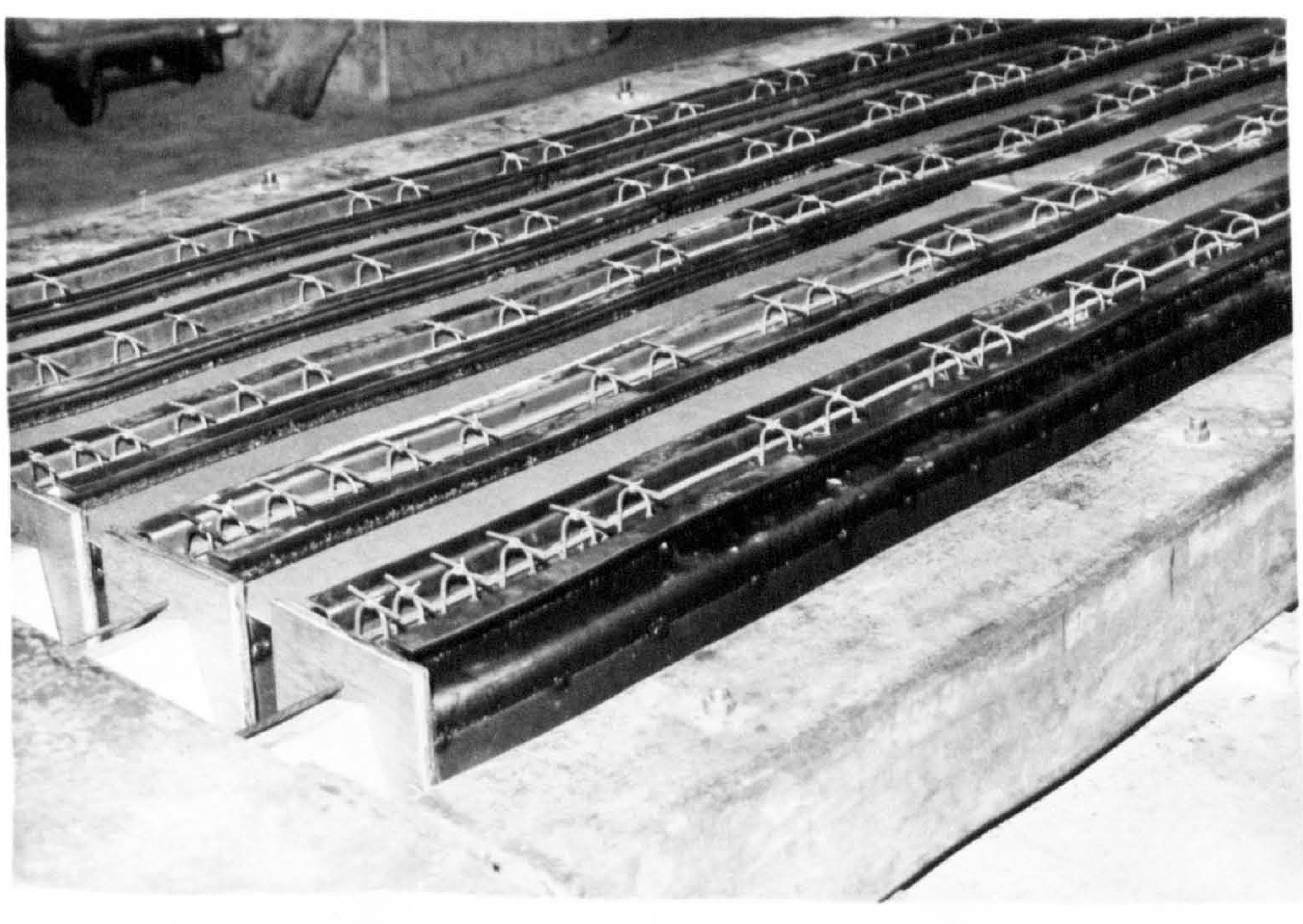

PLATE 3.2 DETAILS OF THE STIRRUP AND SHUTTER ASSEMBLIES USED FOR THE BEAMS OF MODEL 1

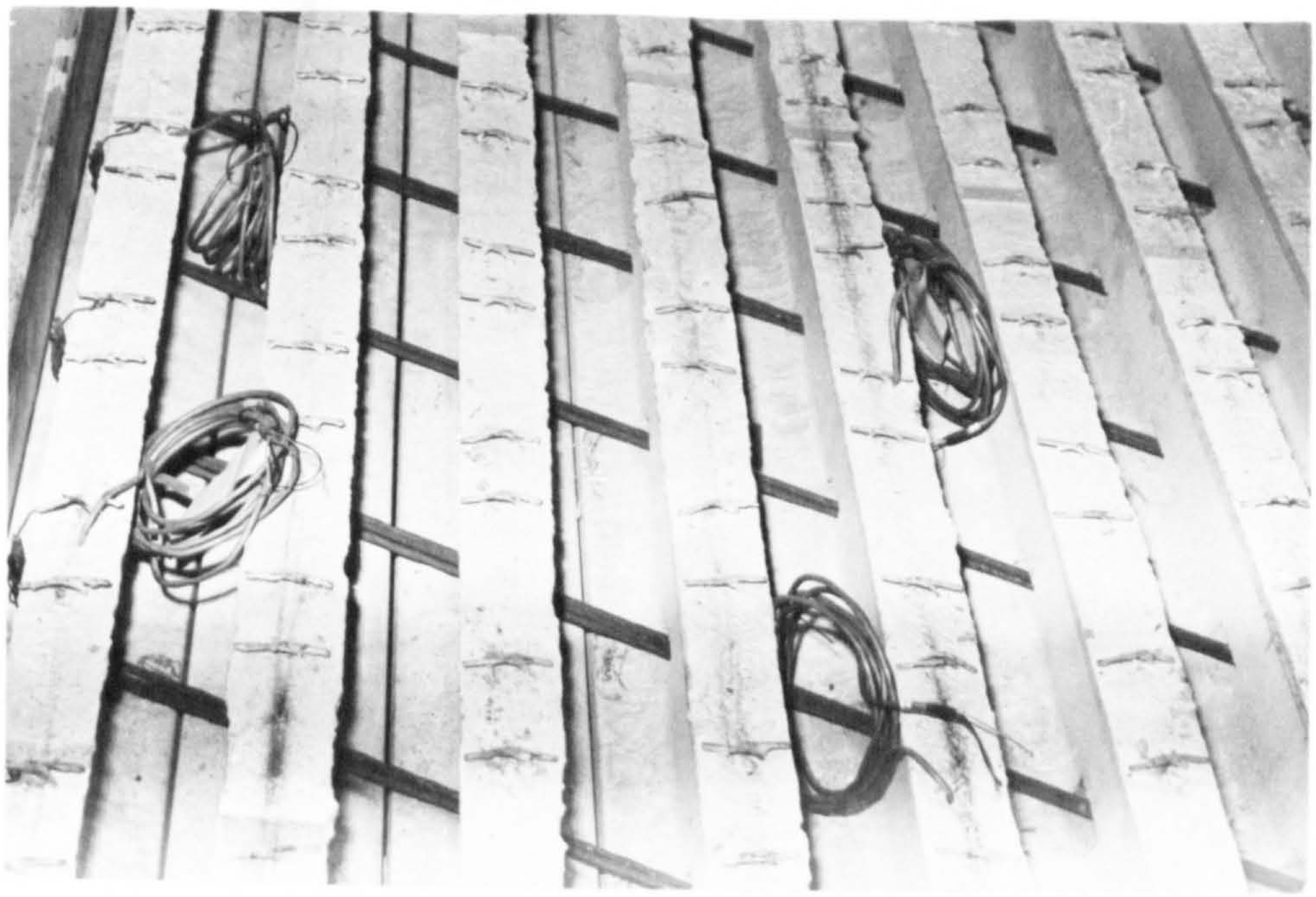

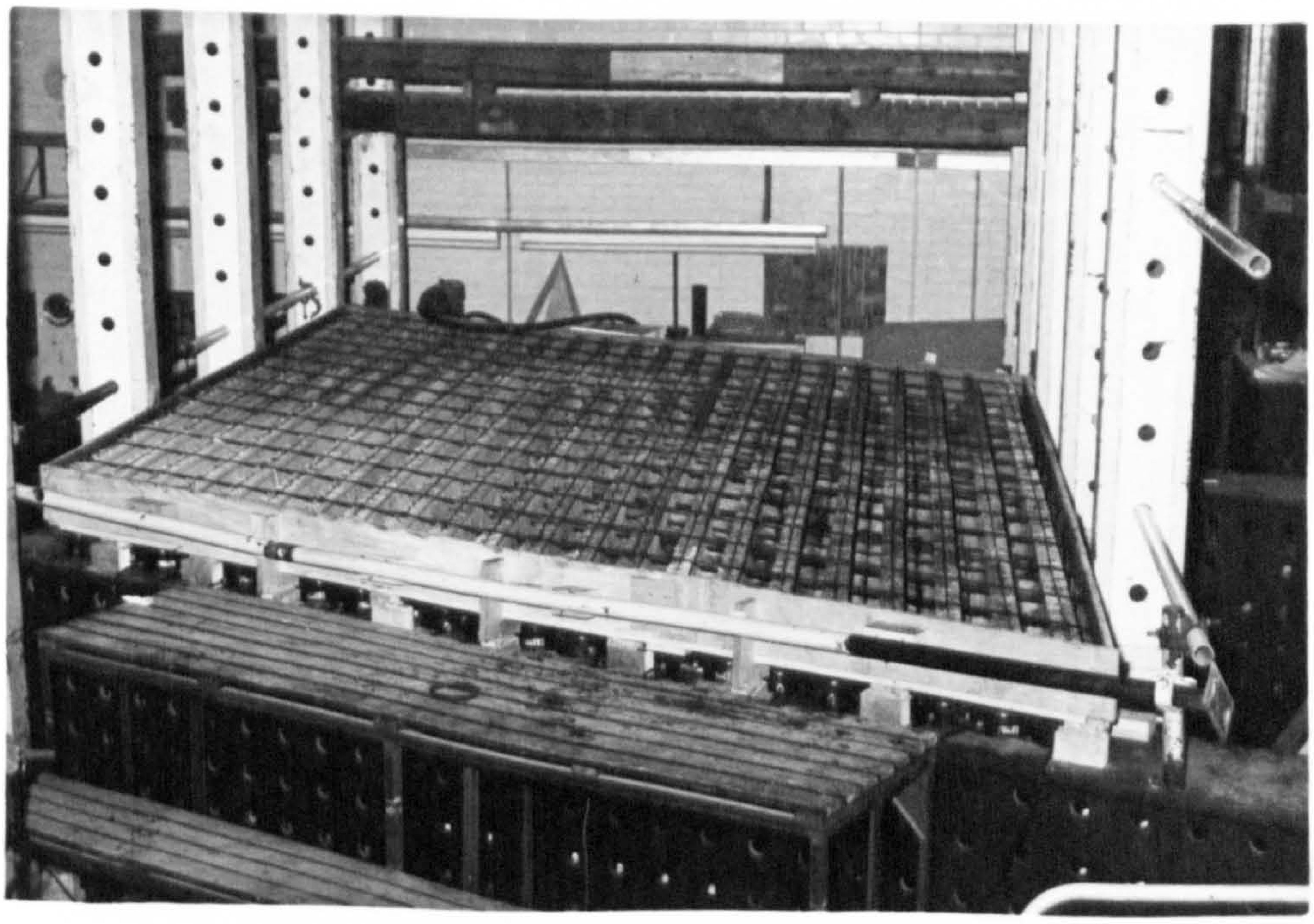

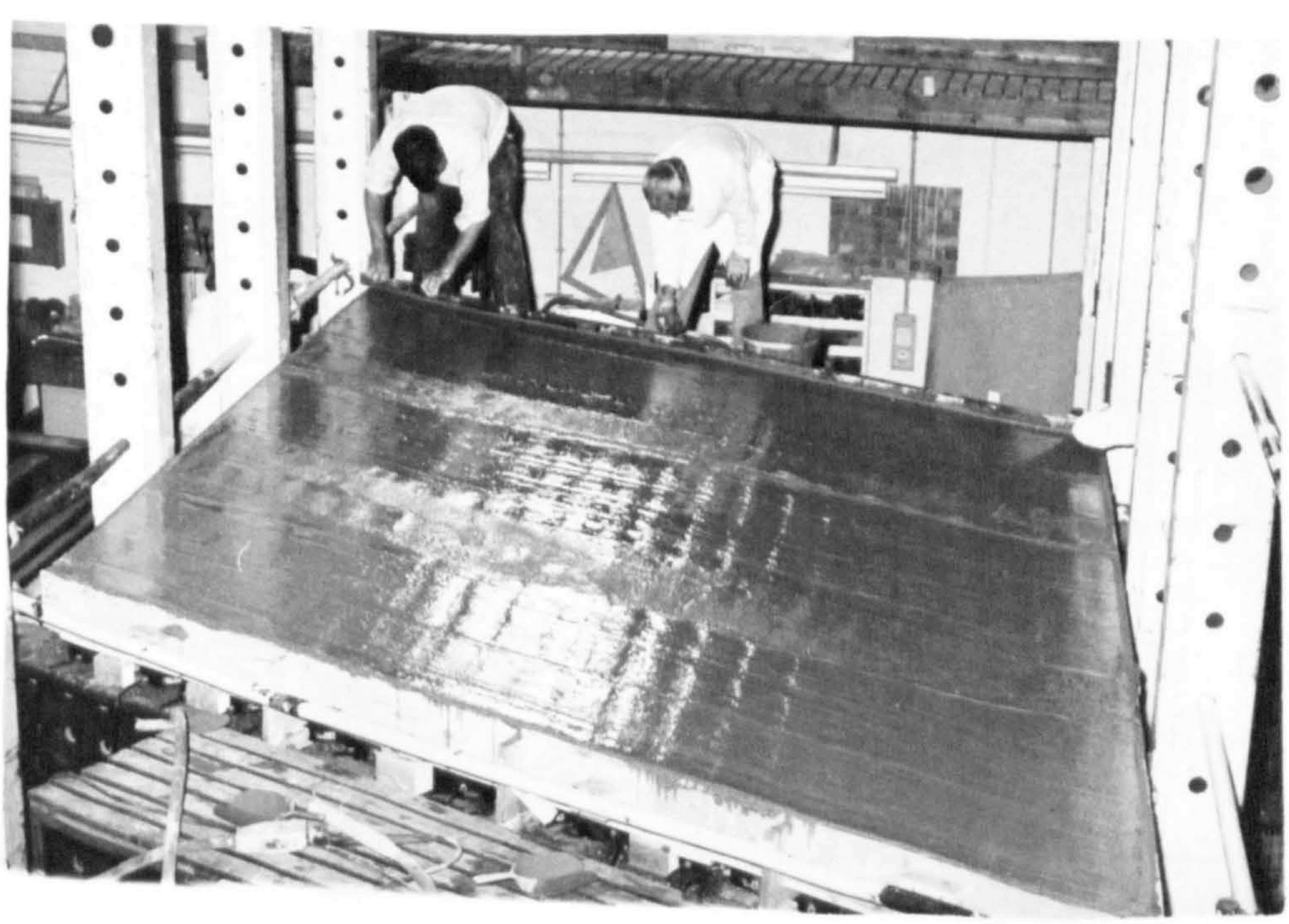

PLATE 3.3 NON-PRESTRESSED REINFORCEMENT AND IN-SITU CASTING DETAILS FOR MODEL 1

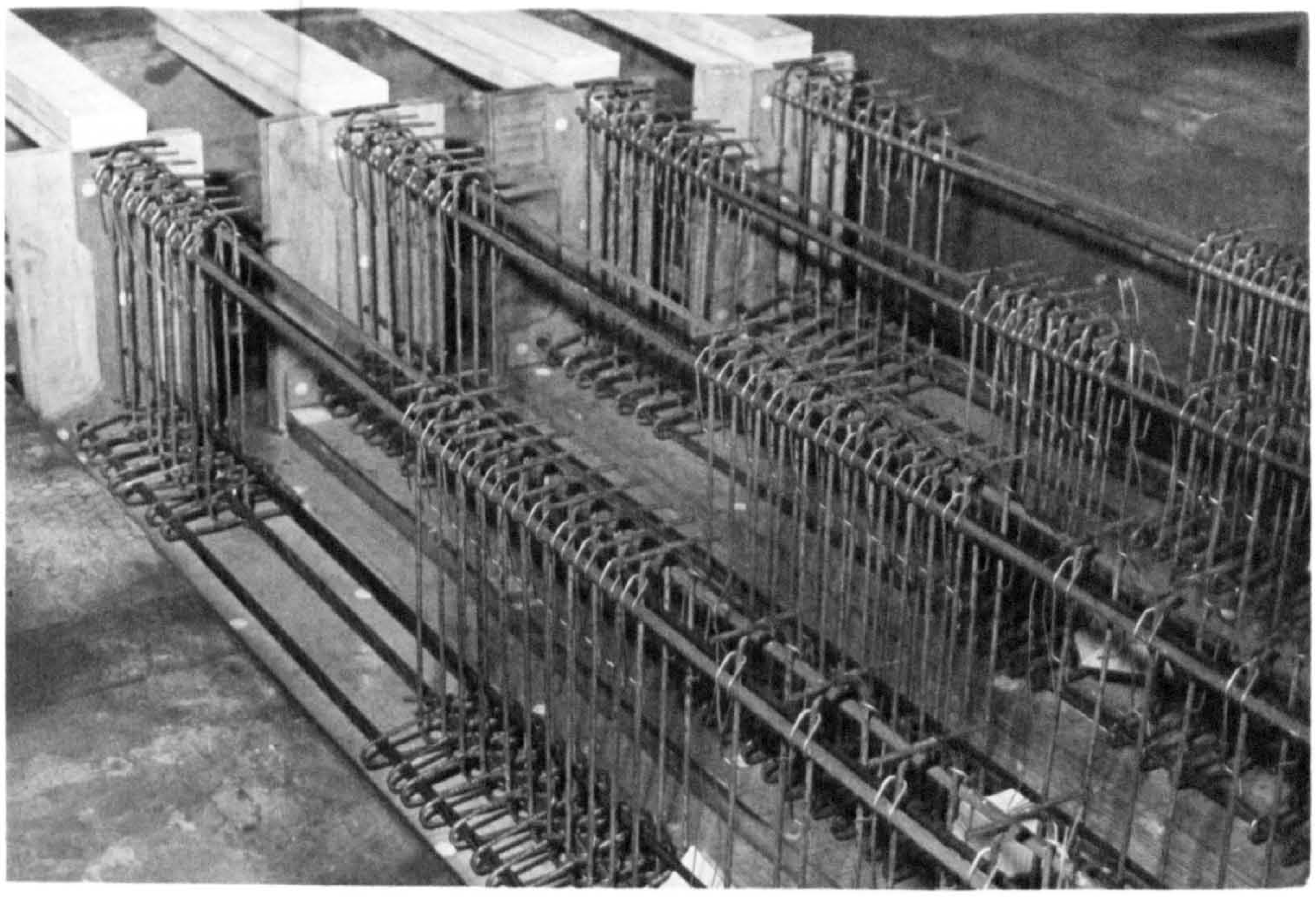

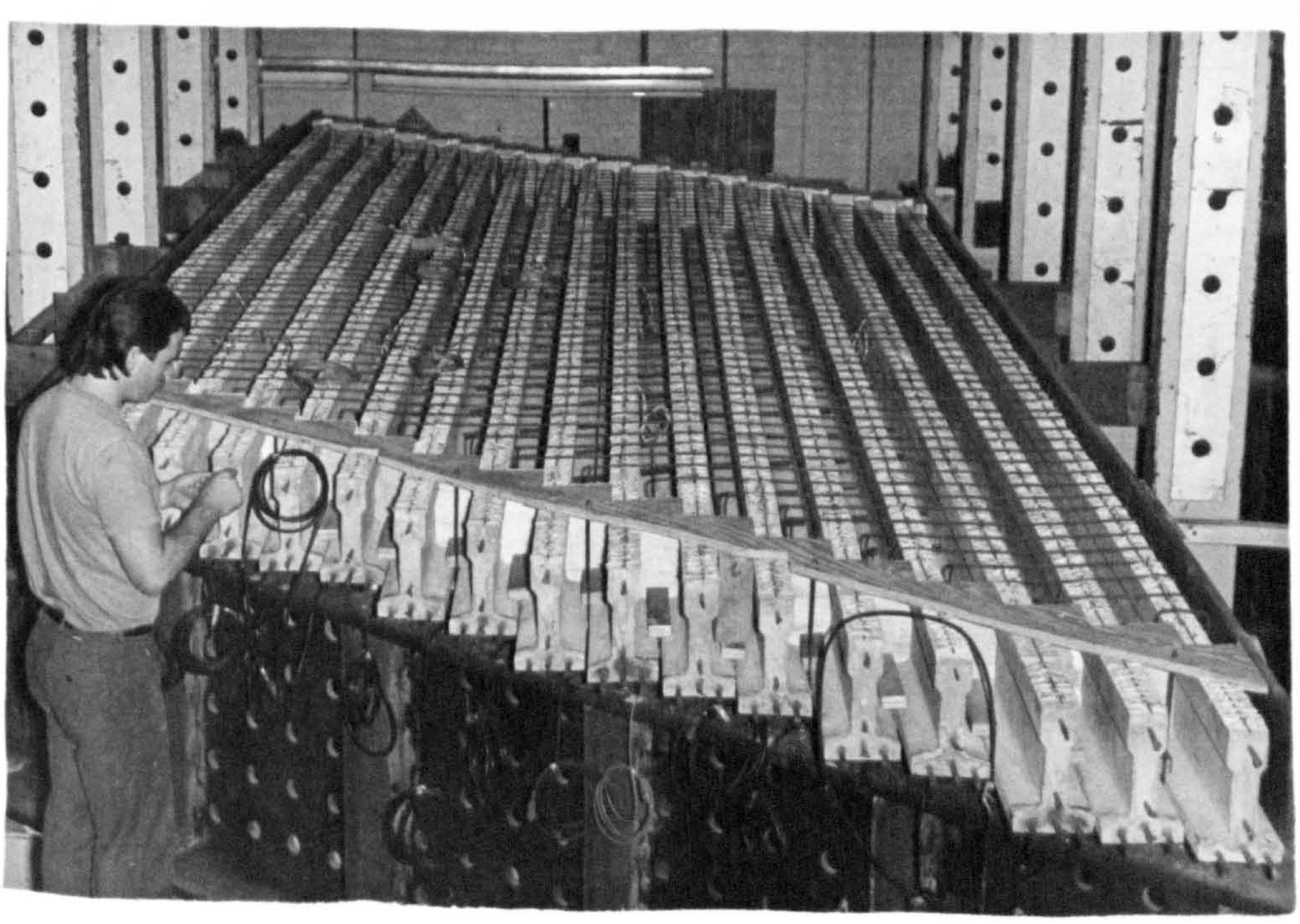

PLATE 3.4 MODEL 2 CONSTRUCTION DETAILS

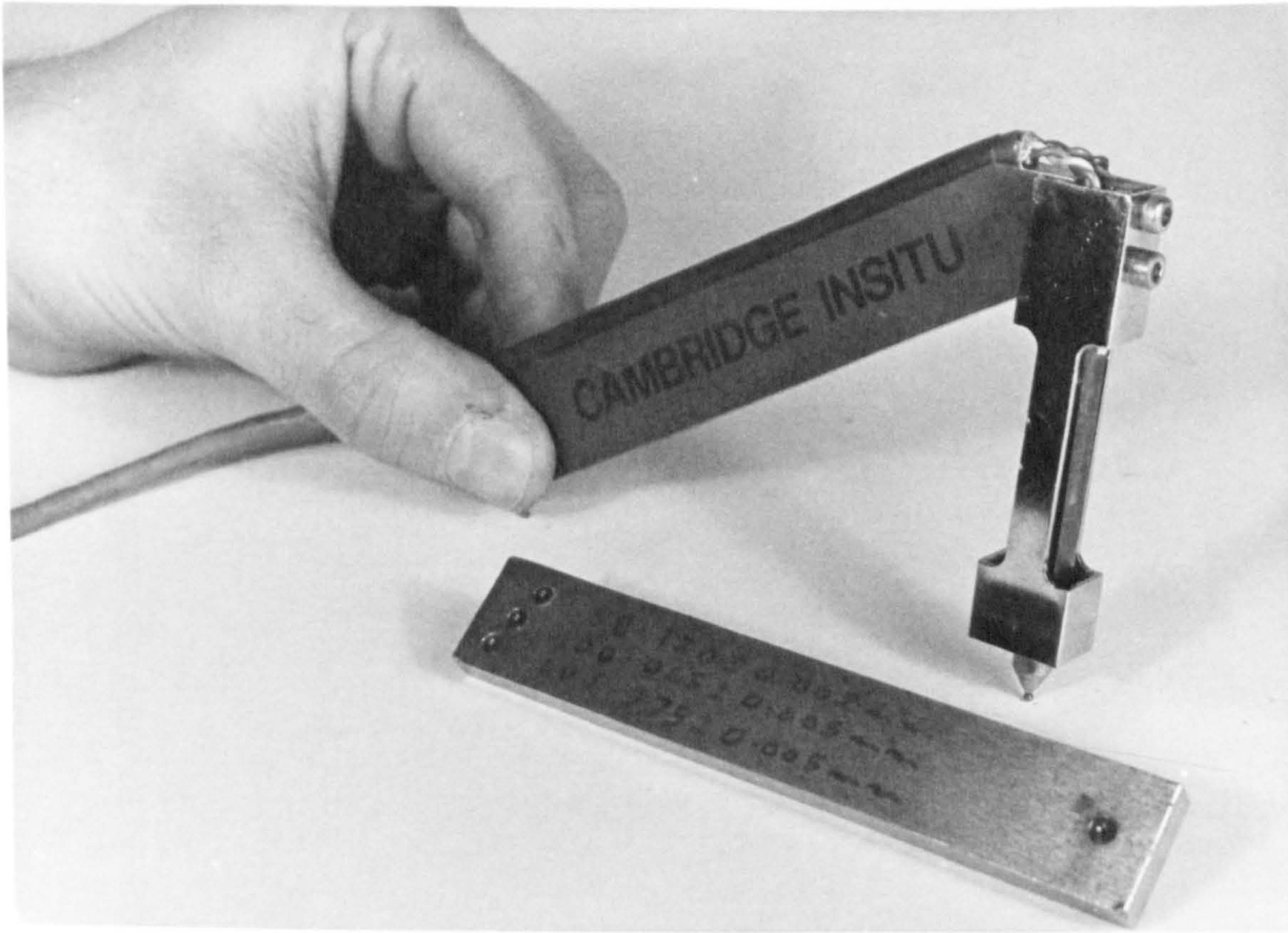

PLATE 3.5 ELECTRICAL DE-MEC UNIT THAT WAS USED DURING THE TEST ON MODEL 1

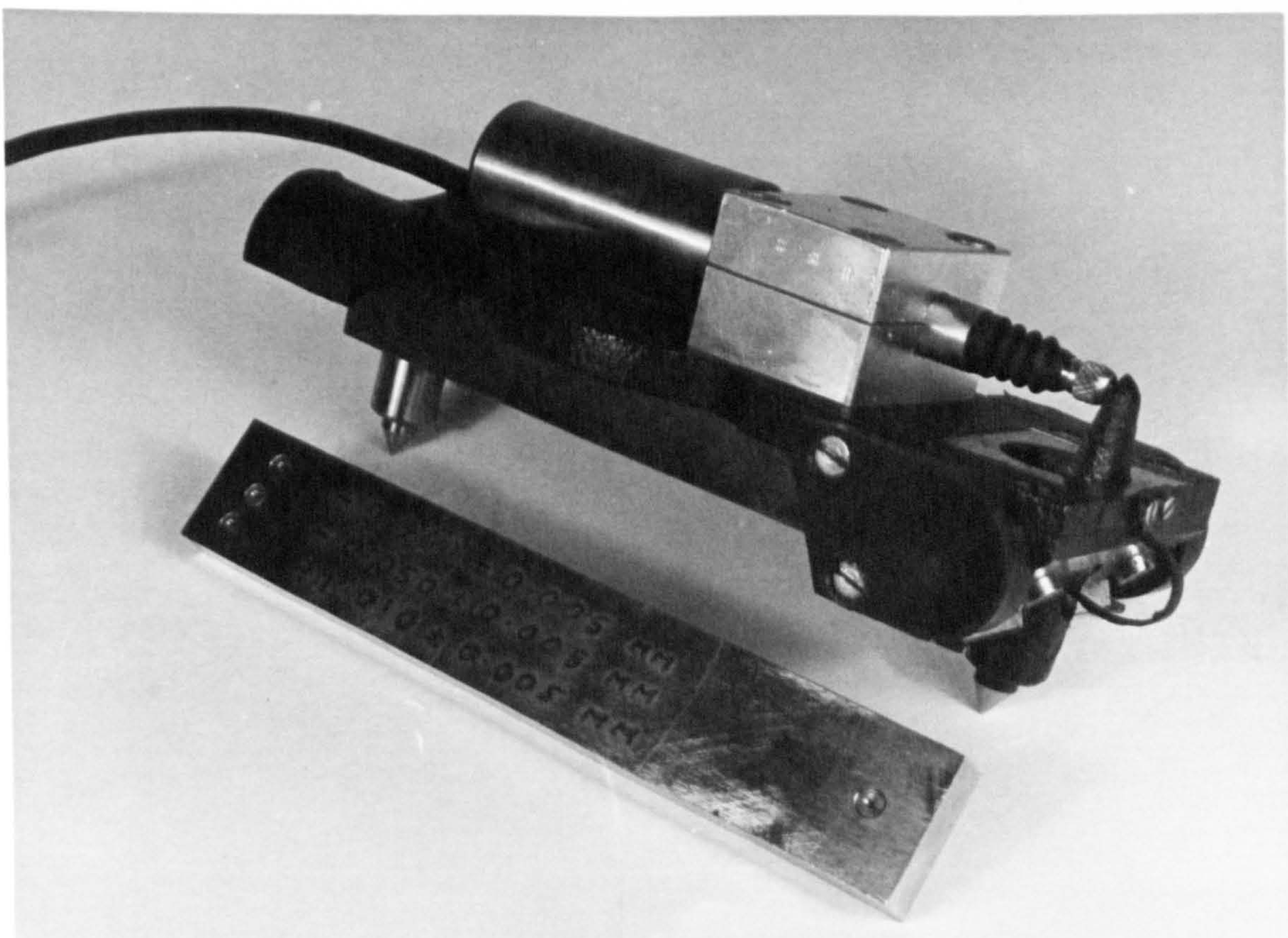

PLATE 3.6 ELECTRICAL DE-MEC UNIT THAT WAS USED DURING THE TEST ON MODEL 2

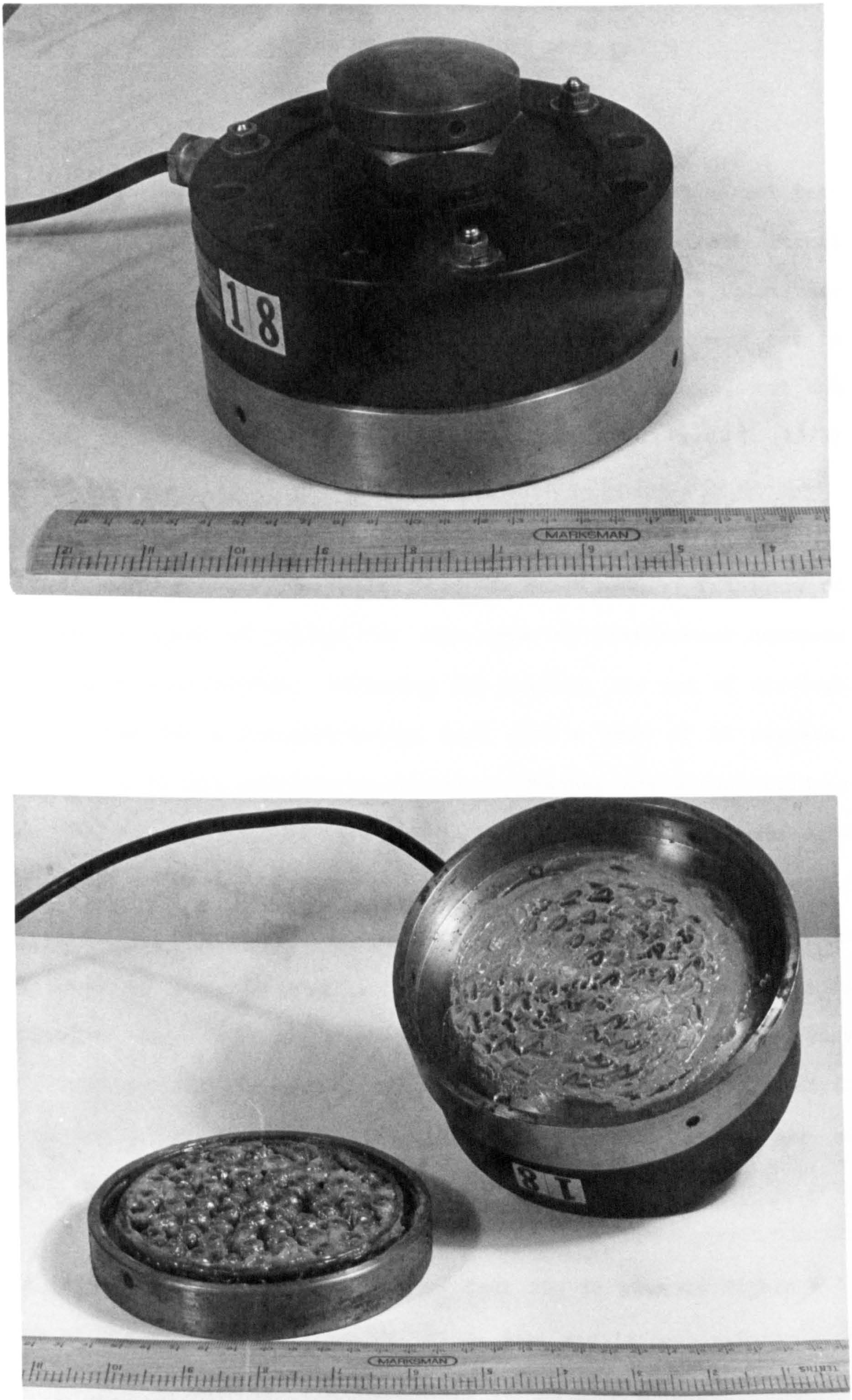

PLATE 3.7 MODEL DECK SUPPORT, WHICH INCORPORATED A LOAD CELL AND A BALL BEARING UNIT, AND ALLOWED MOVEMENT IN THE X-Y PLANE.

4. DESIGN OF MODEL BRIDGE DECK 1

4.1 Introduction

The literature survey revealed an almost complete lack of useful test data for composite concrete slab bridges. To simulate actual conditions as closely as possible in the laboratory, the relatively large scale of 1:3.5 was selected. Loading intensities were set to provide equal strains in the model and prototype bridges, and the loading patterns studied were modelled on BS 5400 Part 2 (1978) highway loadings.

Initially, information was sought from The Department of Transport on the current state of design for this type of prestressed concrete bridge deck construction. Following the enquiry, one set of drawings was received for a standard bridge deck with a skew of 25 degrees. However, it is not possible to ascertain whether any actual bridges have been constructed from this standard design. Further designs were requested from The Department of Transport, although no further information was received. Enquiries were also made of consultants, in the hope of obtaining more drawings. Although the consultants approached were very willing to discuss design, they were very reluctant to supply drawings and detailed information. The first model bridge deck design was therefore based on the one set of drawings supplied.

The general layout of the full size deck can be seen in Figure 4.1. Each of the prestressed beams is 535 mm deep and is pretensioned with 13 No. 12.5 mm diameter 7 strand prestressing tendons each loaded to 116 kN. The position of the tendons can be seen in Figure 4.2. Twenty two of these beams laid side by side at 504 mm centres carry one dual carriageway, two lane, all purpose road (D2 APR) over a 5.5 m single carriageway road with 2 m verges.

4.2 Overall model concept

Initially, the implications of model construction were considered. In particular, the question of how close to scale the model would have to be in order for the results to be meaningful, bearing in mind the constraints of time, feasibility and finance, had to be resolved. It was decided that discrete beams would have to be used to take account of the different natures of prestressed and non-prestressed concrete, the different concrete grades and the effect of bond between the pre-cast and in-situ concretes. These factors give this type of construction a complex set of properties which could not be satisfactorily modelled in any other way.

The maximum skew given on the drawings for standard bridges is 25 degrees and the maximum beam span is 11.5 m. It was decided to base the model on these parameters, to obtain the most interesting and useful results.

Once the type of model construction and full scale dimensions had been decided, it was necessary to calculate the smallest practical scale factor that could be employed, considering the facilities available for testing and the smallest feasible size for construction of the prestressed beams. A compromise was arrived at, whereby the capacity of the available testing facilities was doubled; and the precast beams were reduced to the smallest feasible size at which dimensional inaccuracies would have an acceptably small effect on behaviour and

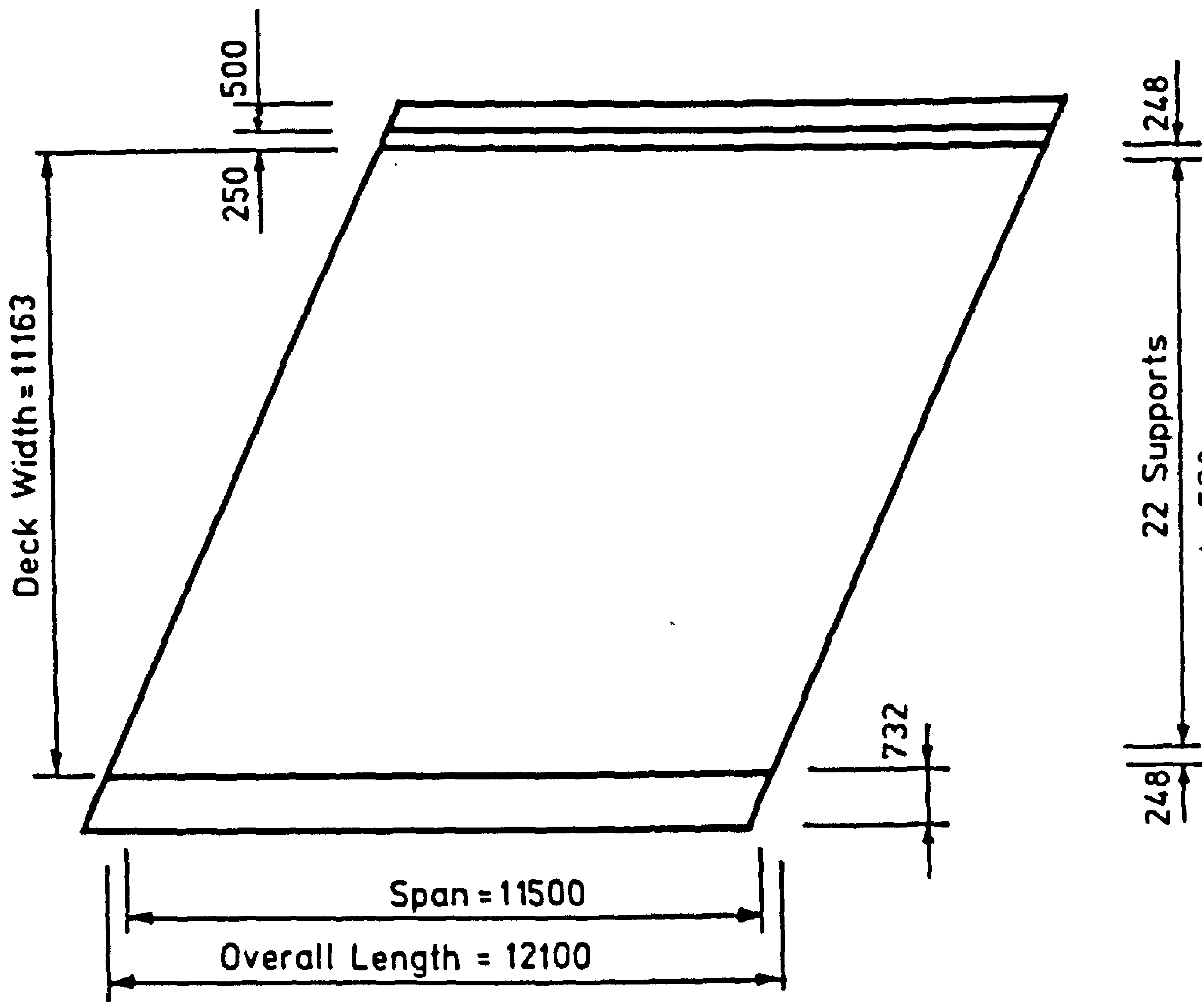

FULL SIZE DECK

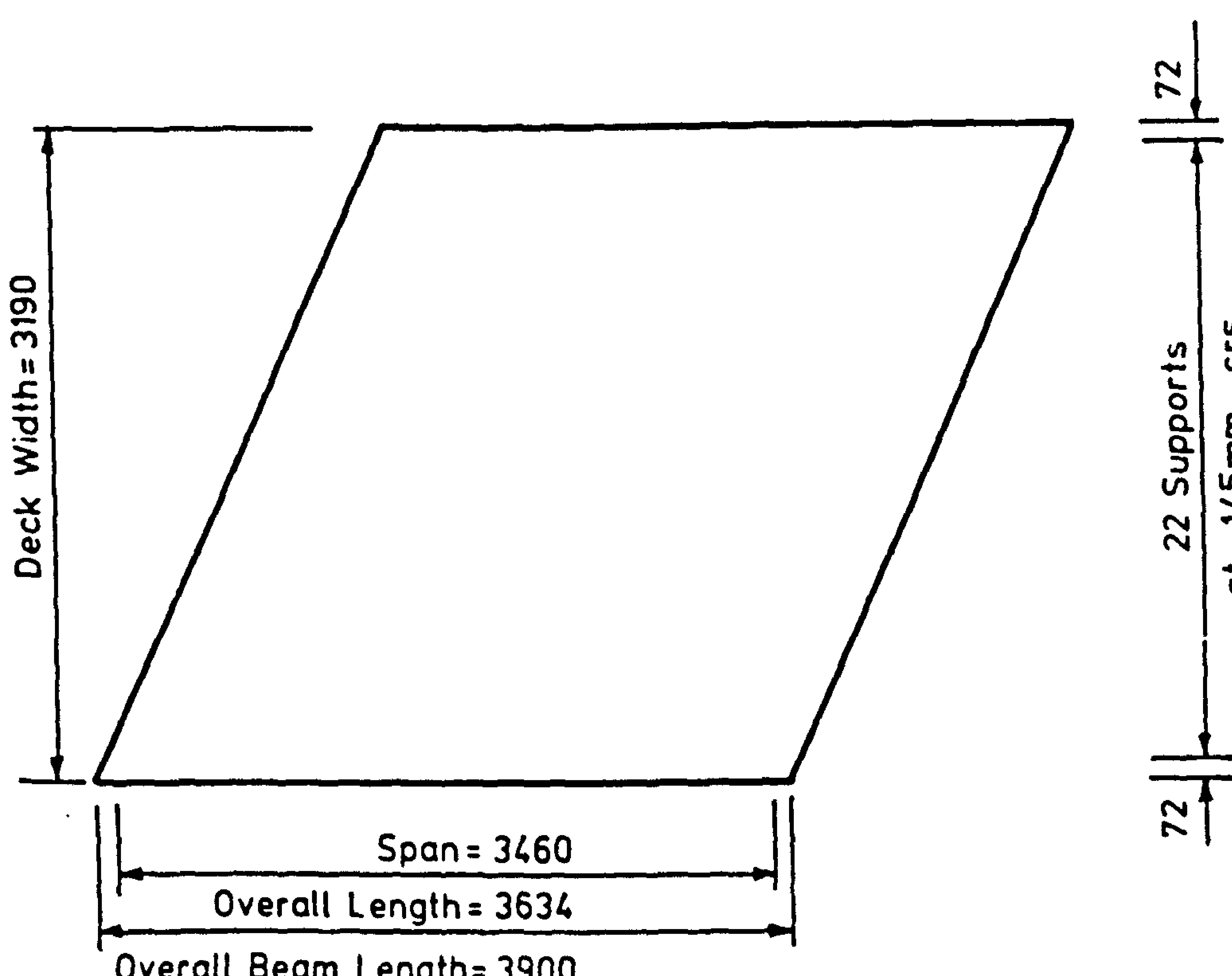

ALL DIMENSIONS IN mm.

MODEL DECK

FIG. 4.1. GENERAL DETAILS OF FULL SIZE & MODEL DECKS

safety. This allowed the model to be designed at a scale factor of 3.5. The dimensions of the resulting model deck and a comparison with the full size structure can be seen in Figures 4.1-4.4.

4.3 Loading

For the purposes of the analysis, the model deck was considered to have three notional lanes (BS 5400 Pt 2 (1978) cl 3.2.9.3) each of width 997 mm. The Department of Transport's finite element package STRAND2 was used to provide data to assess the compliance of the model bridge deck with BS 5440 (1978). The finite element mesh used for these analyses is shown in Figure 4.5.

Initially, a set of 16 basic load components was devised:

1. Dead weight and density correction of 0.0144 N/mm^2
2. Superimposed dead load of 0.00196 N/mm^2
3. Full HA uniformly distributed load in the upper edge lane of 0.00812 N/mm^2
4. Full HA knife edge load at centre span of upper edge lane of 8.41 N/mm
5. Full HA uniformly distributed load in the middle lane of 0.00812 N/mm^2
6. Full HA knife edge load at centre span of middle lane of 8.41 N/mm
7. Full HA uniformly distributed load in lower edge lane of 0.00812 N/mm^2
8. Full HA knife edge load at centre span of lower edge lane of 8.41 N/mm.
9. 45 units of one HB bogie at centre span of middle lane of 9184 N per wheel

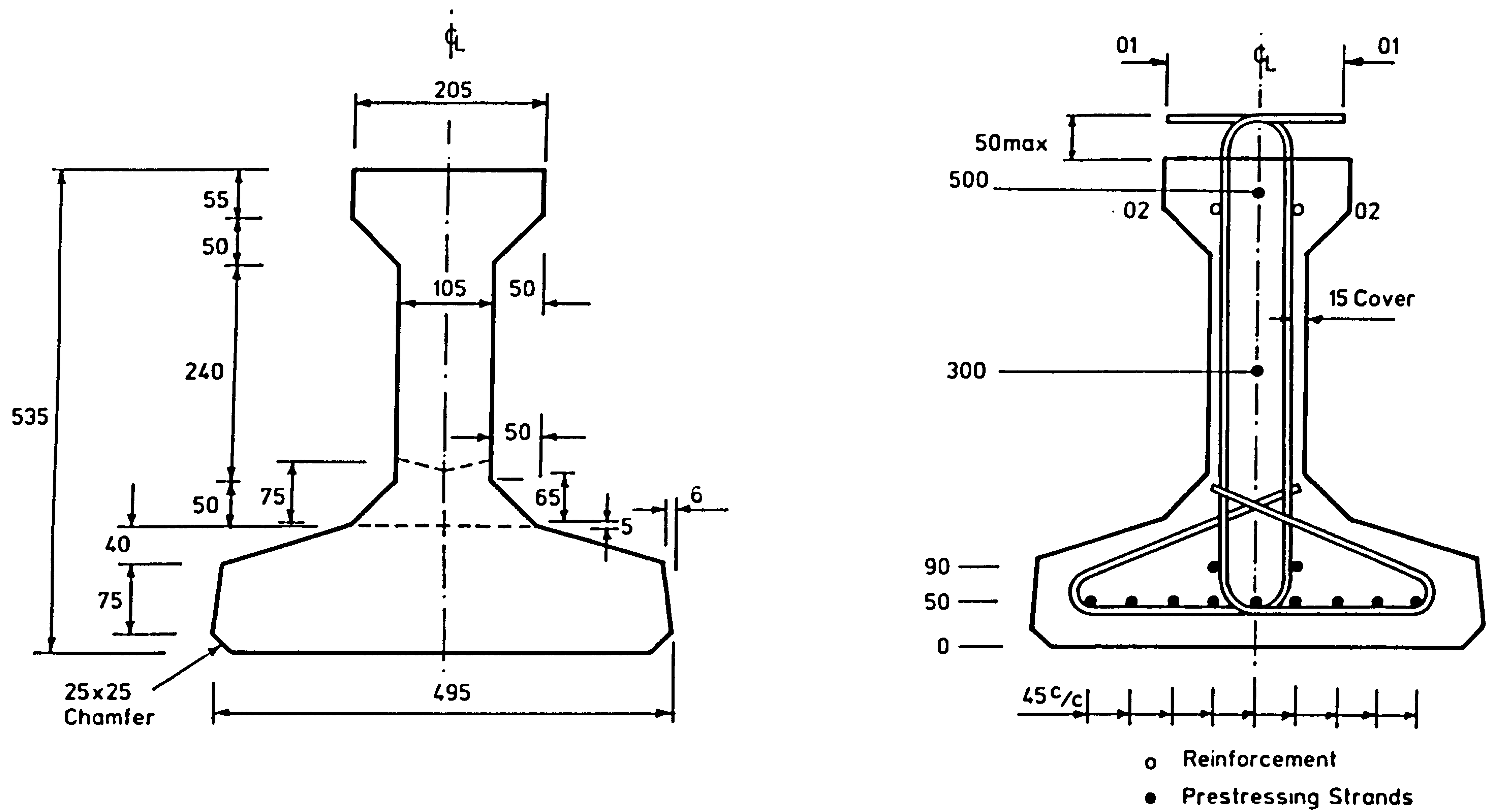

FIG. 4.2a. DETAILS OF FULL SIZE PROFILE AND PRESTRESSING LAYOUT

10. 45 units of one HB bogie at centre span of lower edge lane of 9184 N per wheel
11. Full HA knife edge load adjacent to acute corner in upper edge lane of 8.41 N/mm
12. Full HA knife edge load adjacent to right support in middle lane of 8.41 N/mm
13. Full HA knife edge load adjacent to obtuse corner in lower edge lane of 8.41 N/mm
14. 45 units of one HB bogie at 1/3 span in lower edge lane adjacent to obtuse corner.
15. 45 units of two HB bogies in lower edge lane, one at 1/6 span adjacent to obtuse corner and the other adjacent to the acute corner
16. Temperature loading

In all except load case 15, the span of the deck is too small for a second HB bogie to have a significant effect.

Load case components 1 to 10 are concerned mainly with the analysis for assessing the flexural design, whereas load case components 11 to 15 are concerned with the analysis for assessing the design against shear failure. After the load case components had been processed, their effects were combined, using the appropriate load partial safety factors (γ_{f1}), to obtain the main analytical load combinations. These combinations are described below and illustrated in Figure 4.6. Wind, and collision loadings were not considered.

Load combination 1:- This load combination consisted of the superimposed dead load in addition to the self weight and density

BAR LOCATING TABLE					
			BENDING SCHEDULE No.		
BAR REF.	TYPE SIZE	GROUPING	SHAPE CODE	CRS.	TOTAL No.
01	R10	2x2x2	99		8
	R10	2x3x2	99	50	12
	R10	2x2x2	99	75	8
	R10	2x2x2	99		
	R10	2x4x2	99	135	16
	R10	1x2x2	99	610	
02	R12	1x2x2	20		4

Notes

1. Concrete — Class 50/20

2. Concrete Finishes

   Formed Surfaces
   non exposed surfaces — Class F1
   precast beam exposed surfaces — Class F5

   Unformed Surfaces — Class U4
   beams top — (see Note 18)

3. Cover
   general — 30 min

4. Reinforcement lap lengths — 40d min

5 Bending schedule No. given at head of Bar Locating Table

6 Supports for vertically stacked beams to be in a vertical line and between 0.30m and 0.60m from each end.

7. Excepting links framing web holes one set of links may be displaced to touch adjacent to provide wider stacking area between stacked beams.

Prestressing Notes

8. Strand to be 12.5mm dia. 7 wire low relaxation

9. Each strand to be tensioned to 116kN

10 Beam concrete to achieve min cube strength of $40 N/mm^2$ at transfer

FIG. 4.2b. FULL SIZE BEAM BAR LOCATING TABLE AND NOTES.

correction. All other load combinations, unless otherwise stated, included this load combination.

Load combination 2:- It was assumed that the superimposed dead load had been removed, so as to produce the worst effect for transverse sagging moments.

Load combination 3:- 45 units of one HB bogie, was placed at mid span in an edge lane with HA in the far lane, to check the resistance to longitudinal sagging moments.

Load combination 4:- The superimposed dead load was removed for this combination and 45 units of one HB bogie was placed as close to the edge as possible to consider the worst case of transverse hogging moments.

Load combination 5:- This load combination is similar to load combination 3, except that the knife edge loads and the HB bogie were moved closer to a supported edge. The centre of the HB bogie was at 1/3 of the span for the worst shear effect. With the bogie in this position, the second bogie was partly on and partly off the deck at the far support. For this reason, and considering the relative distances involved, the second bogie was neglected. The knife edge loads were positioned approximately 2.5 slab depths from the supported edge.

Load combination 6:- This combination is similar to 5 except that the HB bogie was moved so that the nearest point of the bogie axle was at 2 slab depths from the support. The KEL's were placed in a similar position to those in combination 5.

Load combination 7:- This load combination consisted of the maximum HA loading without the presence of HB loading to check the longitudinal sagging moments.

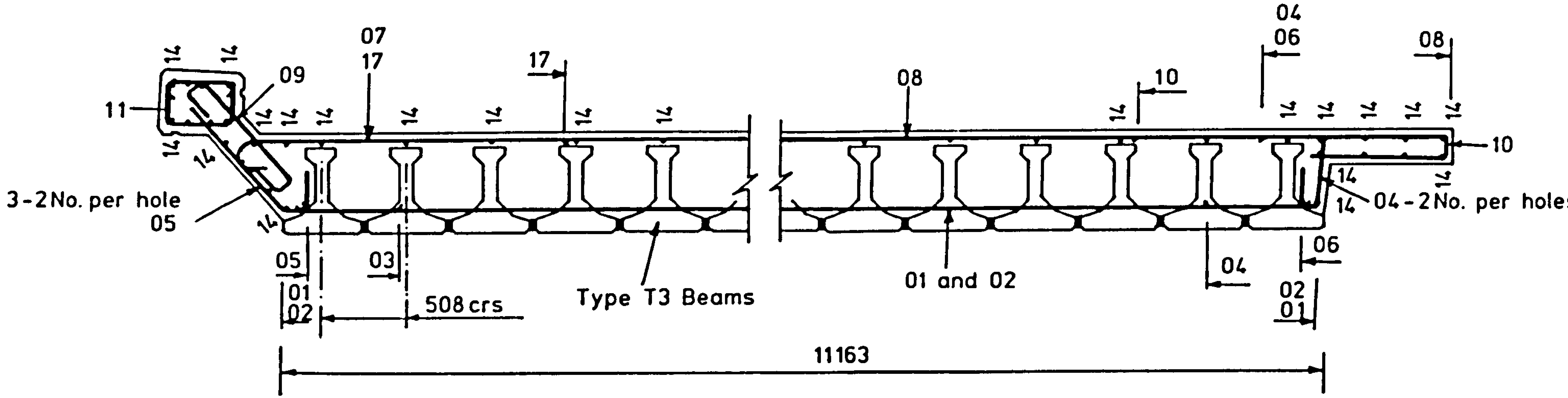

FIG. 4.3a. FULL SIZE DECK SECTION

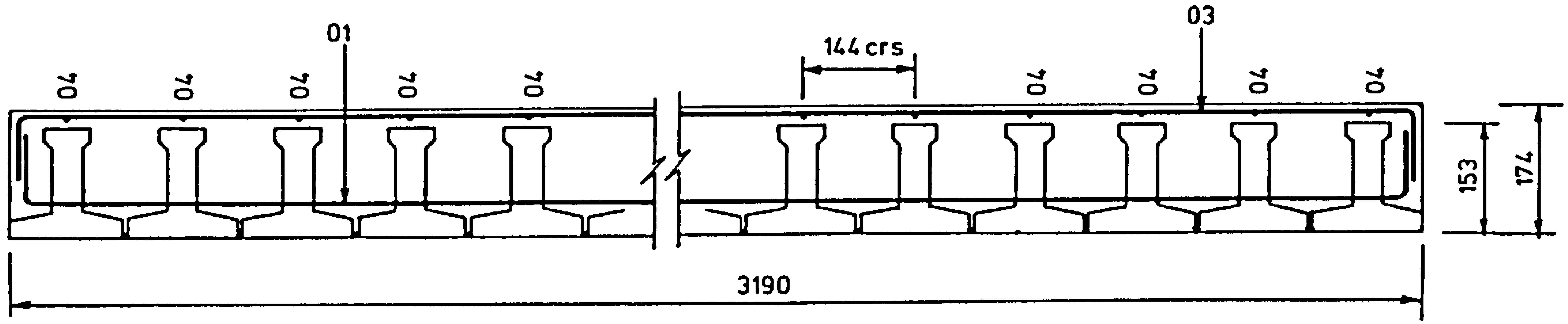

FIG. 4.3b. MODEL DECK SECTION

All 7 load combinations were utilised for both the Serviceability and Ultimate Limit State checks. The analyses were repeated for both uncracked and cracked transverse bending stiffnesses.

The relative importance of knife edge loads was considered, for the combinations concerned with bending strength. After an investigation, it was discovered that, for the critical cases, the knife edge loads had an effect of less than approximately 4% on the maximum moments. Therefore, considering the scale of their effects and the difficulty of application, it was decided to ignore the knife edge loads during the physical testing of the model bridge decks.

4.4 Bearings

The bending moment and shear force distributions in a slab bridge are dependent on the spacings and stiffnesses of the bearings. No details of the nature of the support bearings for the standard bridge deck were provided on the drawings supplied. After discussions with consultants and bridge bearing manufacturers, it was concluded that elastometric bearings were typical for this form of construction. From the information provided, a typical stiffness of 71 kN/mm for a full size bearing was determined.

The stiffness of a model bearing was set at 1/3.5 times a prototype bearing stiffness to give scale displacements under scaled loads. For the purposes of analysis, when there are fewer support points than there are bearings, the stiffnesses of the analytical bearings were determined so as to maintain the total support stiffness along an edge.

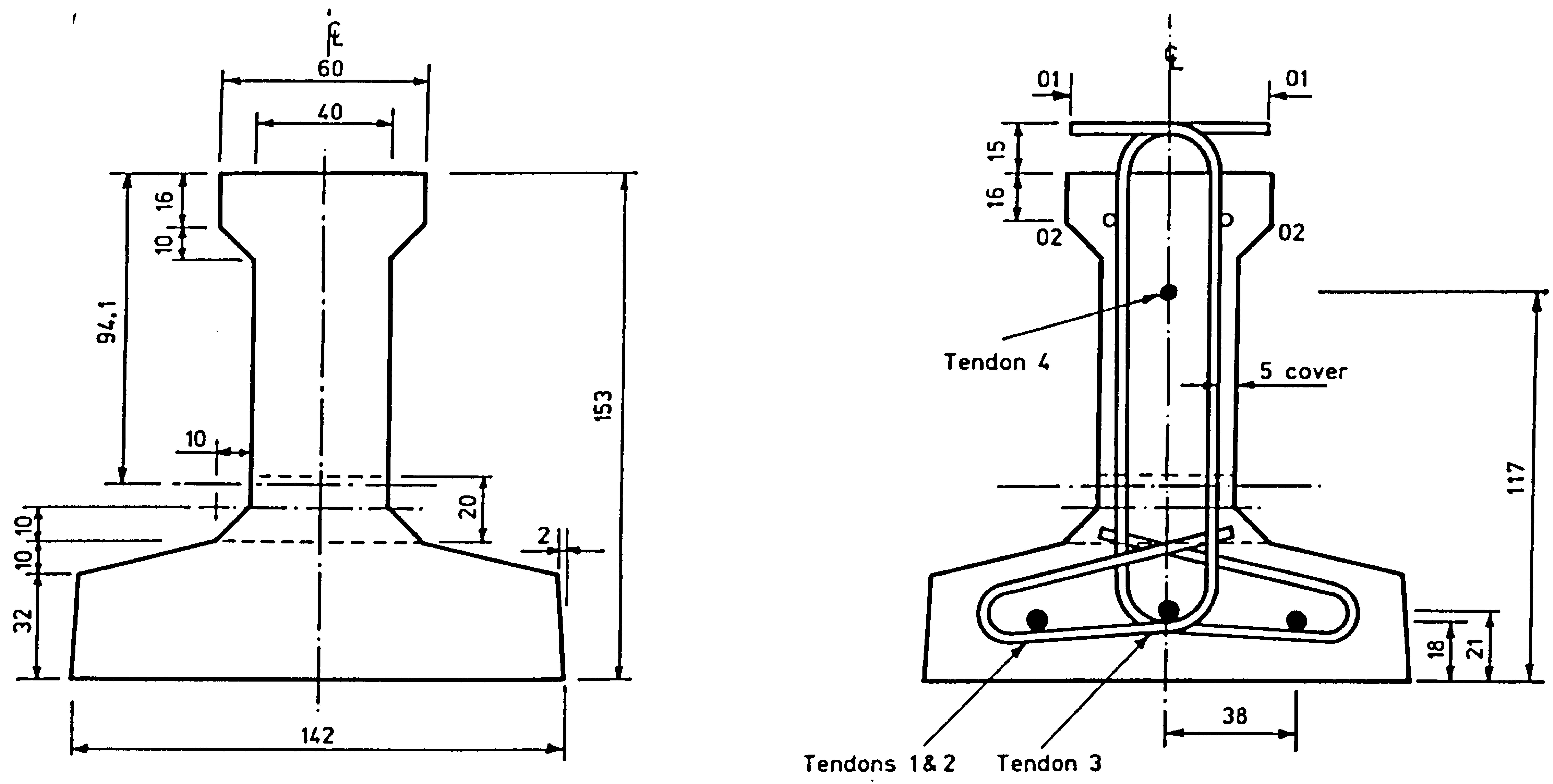

FIG. 4.4a. DETAILS OF MODEL BEAM PROFILE AND PRESTRESSING LAYOUT

4.5 Model Bridge Deck 1 Design

Only a brief summary is included here, detailed calculations can be seen in the Appendices of Research Report no TRR 842/368, produced for the Transport and Road Research Laboratory (hereafter referred to as the Report).

4.5.1 Model Beam Design

The first consideration in the design was the model beam section profile. The shape chosen is as close as possible to an exact scale, taking into account that fine detail could be lost without detriment. Some thicknesses were increased to enable satisfactory manufacture. At all times, the values for the overall geometrical properties: area; second moment of area; and neutral axis depth were kept as close to the scale values as practical. A comparison of these properties is given in Tables 4.1-4.2. It was considered important to retain some form of top flange as well as a bottom flange. At the time, the importance of these top flanges on the behaviour of the deck was unknown. However, to assist in "containing" the in-situ concrete and to enhance interface bond and shear transfer between beams, it was decided to incorporate a top flange, even though the geometrical properties of the section were then not quite as close to the scaled quantities.

Prestressing of the full size beams was provided by numerous 12.5 mm diameter 7 wire tendons. For the model, only prestressing wire was available, and then only in a limited range of sizes. The model prestressing system was chosen so that:-

	Steel Details				Moment Details	
	Area		Centroid Ecc. From NA.		Decomp. Moment	Ultimate Moment
	Pres. (mm^2.)	Rein. (mm^2.)	Pres. (mm)	Rein. (mm)	(Nmm.)	(Nmm.)
Prototype	1209	226	425	55	131.2×10^6	323.2×10^6
Model	101	36	119	14	3.06×10^6	7.343×10^6
Error	2.3%	-	2%	10%	0.002%	2.6%

Table 4.1 Comparison between Prototype and Model Beam Section Properties.

	Geometry			Prestress		
	A (mm^2)	x (mm.)	I (mm^4)	Average (N/mm^2)	Top (N/mm^2)	Soffit (N/mm^2)
Prototype	113230.	338.	3.285×10^9	13.318	-0.181	21.19
Model	10414.	94.1	23.36×10^6	12.4	-0.48	19.53
Error	12%	2.6%	6.7%	6.9%	-	7.8%

Table 4.2 Comparison between Prototype and Model Beam Section Properties.

1. The area of steel was as close to scale as possible;
2. The net lever-arms, both from the slab neutral axis and the beam neutral axis were as close, as possible, to scale;
3. The prestress in the top and bottom fibres was similar to that in the full size beam;
4. The prestress was at approximately the same proportion of the characteristic strength of the steel as in the full size beams, taking into account the different stress-strain relationships for strand and wire.

As the diameter of the model wires was greater than the scale size and the wires were plain, their bond properties were not truly-scaled quantities. The beams were, therefore, cast longer than scale to provide a greater anchorage bond length. In the full size beams, there are sufficient wires to allow a gradual debonding, whereas in the model there are only a few wires, so a fully-bonded design was adopted.

In addition to the prestressing wires, there was also a quantity of non-prestressed reinforcement in the top flange. This was larger than the scale amount due to available bar sizes and the desire to have two separate bars at each edge of the top flange. This accounts for the large error in the scale reinforcement area. However, this increased area of steel should not affect the model behaviour significantly, as no appreciable hogging moments were predicted, and the bars were positioned close to the neutral axis of the composite slab.

The beam profile design and prestress arrangement were checked at transfer to ensure that the limiting stress clauses of BS 5400 (1978)

BAR LOCATING TABLE					
			BENDING SCHEDULE No		
BAR REF	TYPE SIZE	GROUPING	SHAPE CODE	CRS	TOTAL No
01	R3	2*1*2	99	--	4
01	R3	2*1*2	99	--	4
01	R3	2*3*2	99	--	12
01	R3	2*1*2	99	--	4
01	R3	2*2*2	99	153	8
01	R3	2*4*1	99	225	48
02	R4	2*1	20	--	2

Notes

1 Concrete 50/6

2 Cover - General 8 min

PRESTRESSING NOTES

1. All Wire to BS5896-1980
2. Tensioning Forces:-
   Tendons 1, 2 & 3 34.7kN
   Tendon 4 18.9kN
3. Minimum Cube Strength at Transfer $40 N/mm^2$
4. Tendon Sizes:-
   Tendons 1, 2 & 3 6.0mm ϕ
   Tendon 4 4.5mm ϕ

FIG. 4.4b. BAR LOCATING TABLE AND NOTES FOR MODEL BEAMS were complied with. For this calculation, the self-weight of the beams was neglected, because of the scale effect and the fully bonded design that had been adopted.

The drawings of Figure 4.4 shown the final section and prestressing arrangement.

4.5.2 Initial Serviceability Assessment

Once the model beam design had been decided, it was checked for compliance with serviceability requirements. This was achieved using the STRAND program to analyse the deck using the appropriate long term material properties and safety factors for the Serviceability Limit States. The total moments along the beam of the idealised isotropic and homogeneous deck were used for these checks. Details of stress limit calculations are given in Appendix 2.1 of the Report.

However, with this form of construction, some tensile stresses will be present in the soffit flanges of the beams when torsional moments also act upon the beams, albeit at a relatively large angle to the line of the beams.

That this is so can be seen by considering stress resolution. If the Cartesian x direction is placed along the beam axis, and the normal stress σ_n of a soffit fibre inclined at α degrees to the x axis (clockwise positive), then

$$\sigma_n = \sigma_x \cos^2\alpha + \sigma_y \sin^2\alpha - \sigma_{xy} \sin 2\alpha \qquad (4.1)$$

Due to prestress $\sigma_x = -\sigma_c$, $\sigma_y = 0$, $\sigma_{xy} = 0$

Due to bending and torsion $\sigma_x = \sigma_t$, $\sigma_y = 0$, $\sigma_{xy} = \tau$

The nett stress $\sigma_n = (\sigma_t - \sigma_c) \cos^2\alpha - \tau \sin 2\alpha$

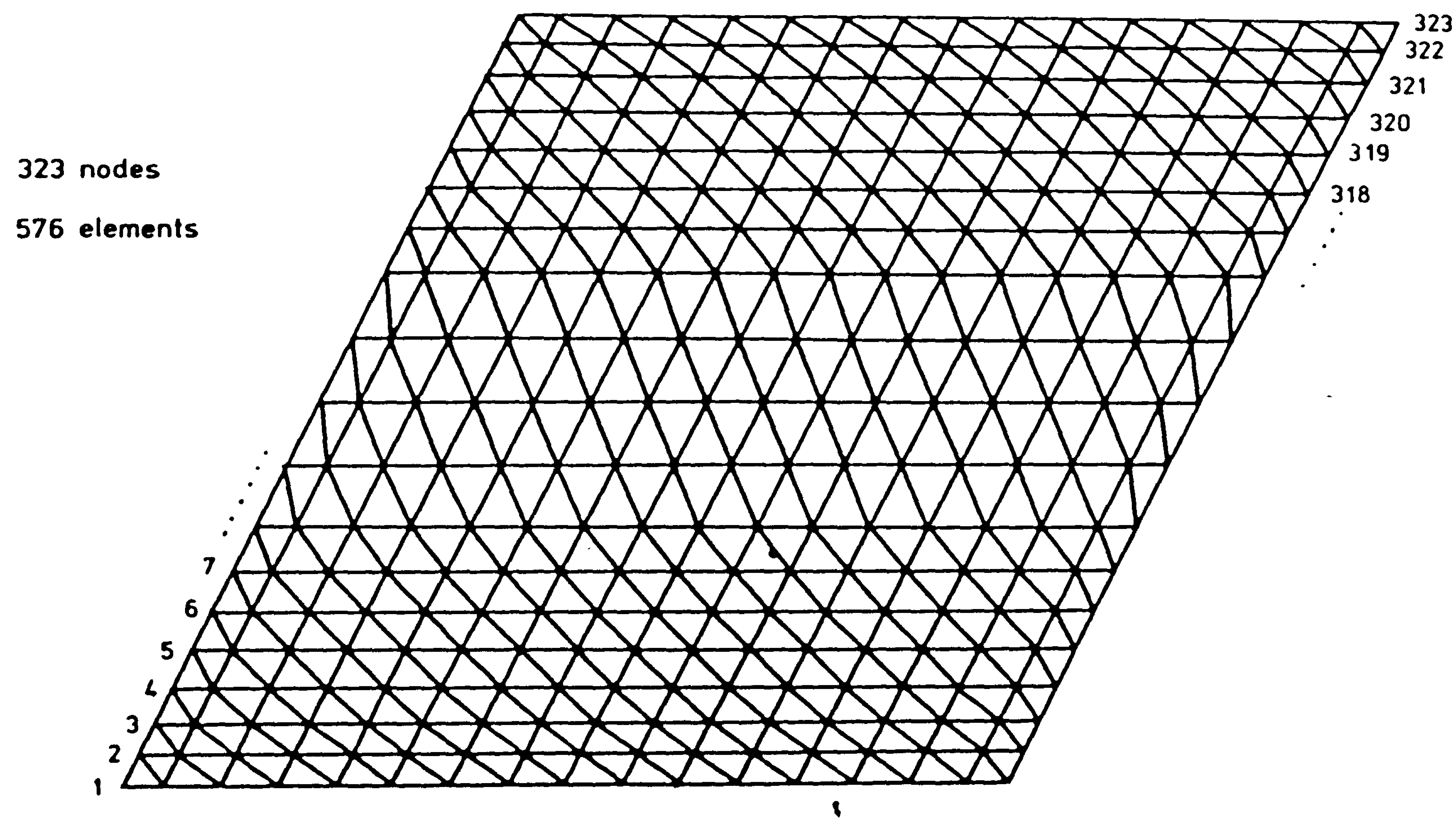

FIG. 4.5. FINITE ELEMENT MESH USED FOR THE STRAND ANALYSIS OF MODEL 1

For no tensile stress $\sigma_n < 0$ for all values of α. Dividing by $\cos^2\alpha$ and neglecting to consider $\alpha = 90°$; since for that case $\sigma_n = 0$, gives the requirement that $|\sigma_c| > \sigma_t + |2\tau \tan\alpha|$, for no tensile stress in any direction. Thus, in the presence of torsion, there must be some tension in the material at an angle approaching 90° to the beam axis.

4.5.3 Ancillary Deck Reinforcement

For the lower transverse reinforcement, the exact scaled distance between beam holes could not be used for two reasons. Firstly, there were no suitable bars of the correct size available for the transverse reinforcement and also the provision of scaled shear links would not have been possible. Therefore, the spacing was increased so that the area, position and type of transverse reinforcement could be modelled as accurately as possible, while also considering the reinforcement spacing clauses of BS 5400 (1978). Finally, 6 mm Torbar in bundles of three and placed through each hole was chosen. The holes were spaced at 225 mm centres, see Figure 4.8. The corresponding details for a full size deck are shown in Figure 4.7.

A similar philosophy was adopted for the modelling of the top transverse steel. Nominal top longitudinal reinforcement was included in the design for crack control considerations, even though the small, required ultimate moment of resistance was catered for by the additional top beam reinforcement and the fact that negligible longitudinal hogging moments were expected.

Essentially, the full size deck contains uniformly distributed non-prestressed reinforcement over its whole plan area, see Figure 4.9. However, there are additions to this reinforcement in zones

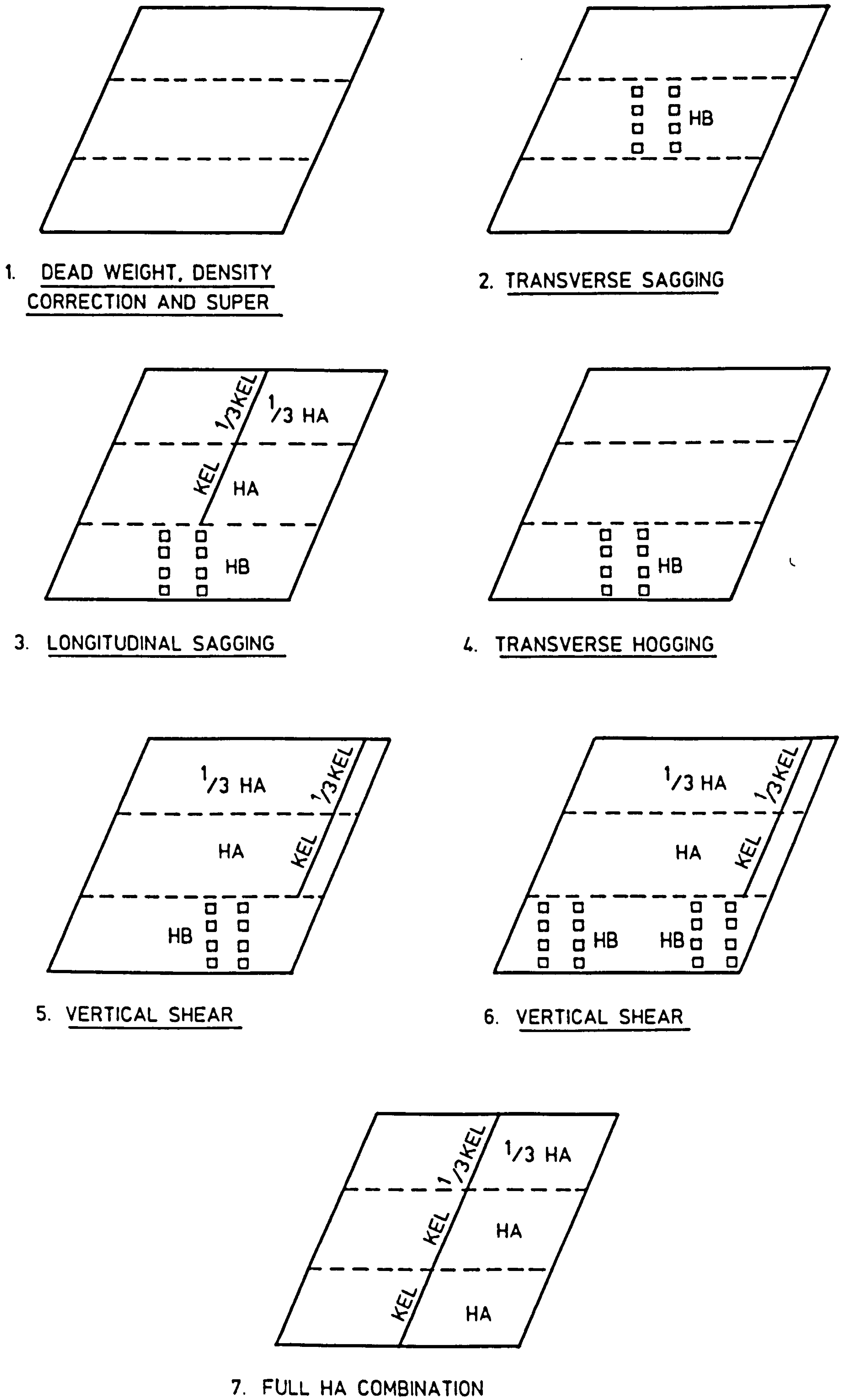

FIG. 4.6. LOAD COMBINATIONS.

adjacent to the parapet along the free edge. The parapet and transverse section details can be seen in Figure 4.3a. It was felt that this parapet could be neglected in the model idealisation. This was because the parapet would be designed and constructed in such a manner that its effect upon the behaviour of the overall slab would be small. Otherwise, because the parapet has a high eccentricity from the NA of the slab, it would fail early in an overloading situation, subsequently having little effect upon structural behaviour. The ancillary reinforcement designed for the model is shown in Figure 4.10.

4.5.4 Ultimate Limit State for Bending

After tentative designs for both the prestressed beams and the ancillary reinforcement had been decided, the overall structure was checked at the Ultimate Limit State. The STRAND program was utilised to produce the required Moments of Resistance using the Wood-Armer equations. The directions and intensities of the principal moments at the ULS for load combination 3 can be seen in Figure 4.11. The Moments of Resistance of the sections perpendicular to the reinforcement were calculated using the simplified stress block of BS 5400 (1978), while taking into account the different concretes used for the beams and in-situ material. This analysis revealed that, with the moment fields produced by STRAND, the strength of the transverse sagging section was significantly less than that required, by a factor of about 2.

A yield line analysis was, therefore, carried out. The details are given in Appendix 2.2 of the Report and they show that the deck, including the transverse section, possesses sufficient strength to resist the moments at the ULS condition. Subsequently, the STRAND

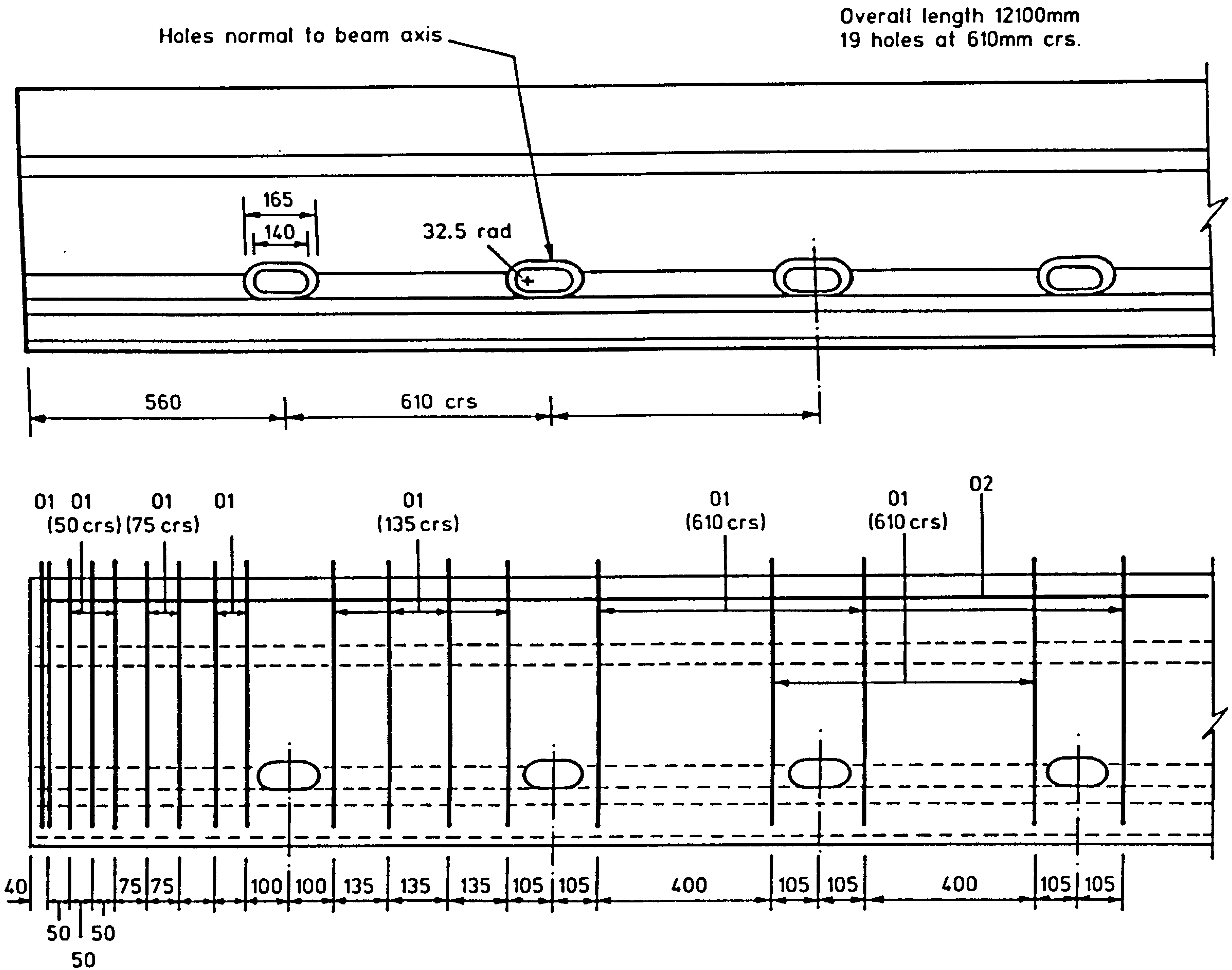

FIG. 4.7. DETAILS OF FULL SIZE BEAM TRANSVERSE HOLE AND SHEAR REINFORCEMENT LAYOUT

program was run using a calculated cracked stiffness for the transverse direction, and the results from this analysis showed that the reinforcement provided was then sufficient to satisfy the Wood-Armer conditions. The details can be seen in Appendix 2.3 of the Report.

4.5.5 Final Flexural Serviceability Limit State Analysis

From the results of the Serviceability Limit State analysis by STRAND, the limiting stress and crack control clauses of BS 5400 (1978) were shown to be complied with for the reinforced concrete in the transverse direction. However, it is debatable how appropriate the crack control clauses are to construction of this type. In which all but the top surface is encased in prestressed concrete.

4.5.6 Shear Design

When the flexural analysis had been concluded, the shear resistance of the slab was assessed. All shear design and calculations were carried out at the Ultimate Limit State, as interface shear design, which is checked at the Serviceability Limit State, need not be considered with this form of composite construction (BS 5400 Pt 4 (1978) cl 7.4.2.3).

Shear Reinforcement Design: All vertical shear reinforcement for this mode of construction is provided by shear links in the prestressed beams. Two, R10 shear links at 610 mm centres, each with two legs, are specified for the full size deck, see Figures 4.2 and 4.7. The smallest practicable size for the model shear links was 3.0 mm diameter, which was adopted. Thus, the spacing of the transverse holes through the beams was modified to ensure a scaled quantity of shear reinforcement. The distance was changed from 174 mm to 225 mm, an increase of approximately 29%.

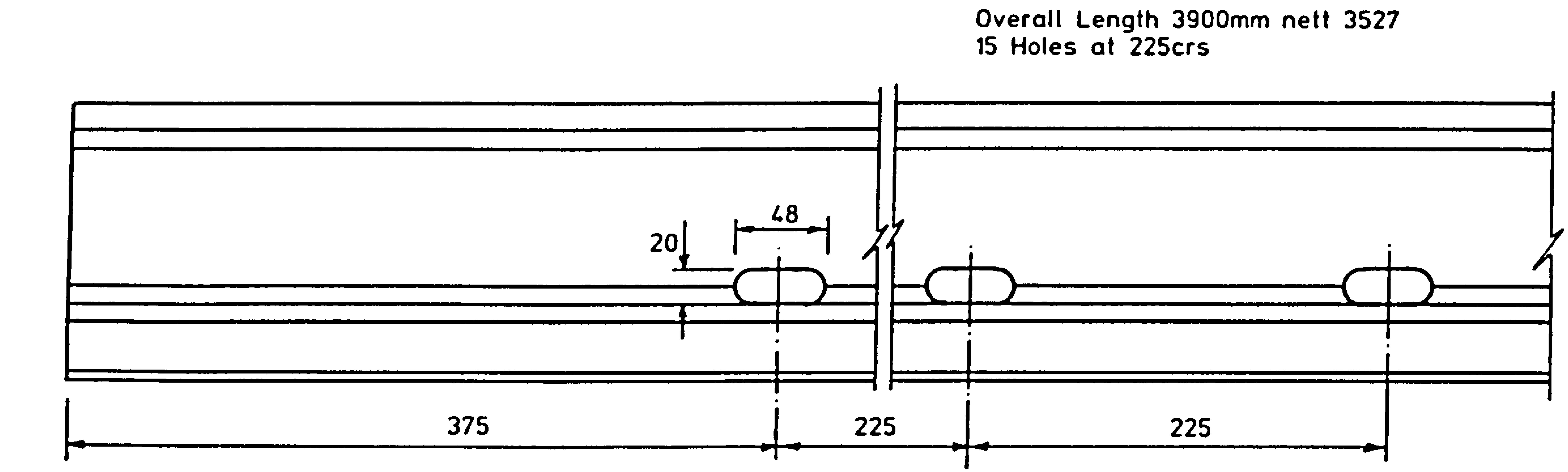

TRANSVERSE HOLE LOCATION

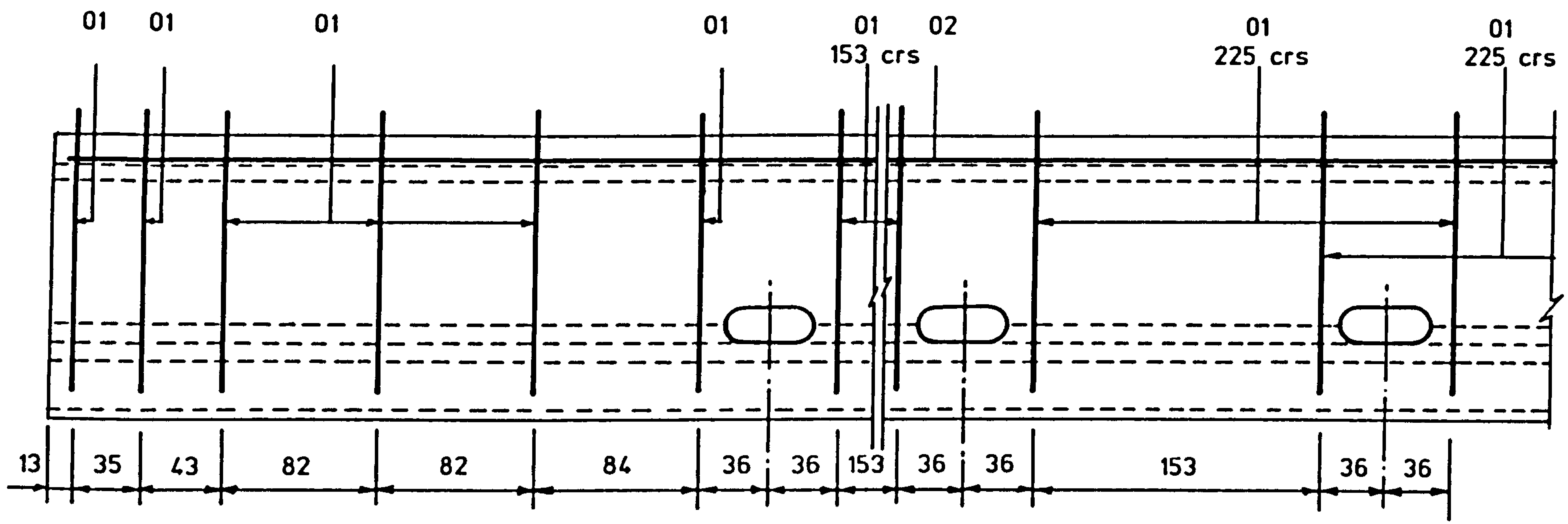

REINFORCEMENT DETAIL

FIG. 4.8. DETAILS OF MODEL BEAM TRANSVERSE HOLE AND SHEAR REINFORCEMENT LAYOUT

The quantity of shear reinforcement in the full size structure is increased at the ends of the beams to resist the splitting action of the prestressing wires and the shear near the supports. Reproducing the details of the shear reinforcement design was considered too complicated for realistic production of the model beams, and they were therefore modified. Also, the model beams are longer than the scaled size, and overhang the bearings, to provide the longer bond length required by the round wires. Thus, the most severe effects of splitting and vertical shear occur at different sections.

The profile of the model shear links can be seen in Figure 4.4. It can be seen that the model link shape agrees closely with that of the full size beam, as shown in Figure 4.2.

Shear Analysis: The STRAND program was used to obtain the shear forces present in the model deck at the Ultimate Limit State. The directions and intensities of the principal shear forces for load combination 5 can be seen in Figure 4.12.

The shear reinforcement along the model beams is divided into three sections. Two sections at opposite ends reaching approximately 2 slab depths from the supports, and the third section in the middle where the reinforcement is uniform. Thus, load combinations 5 and 6 were used for the analyses of the strengths of the middle and end sections respectively.

The design of a composite slab of this type is complex and open to debate. This is due to the interlaced nature of the reinforced and prestressed concretes, neither of which is generally in the direction

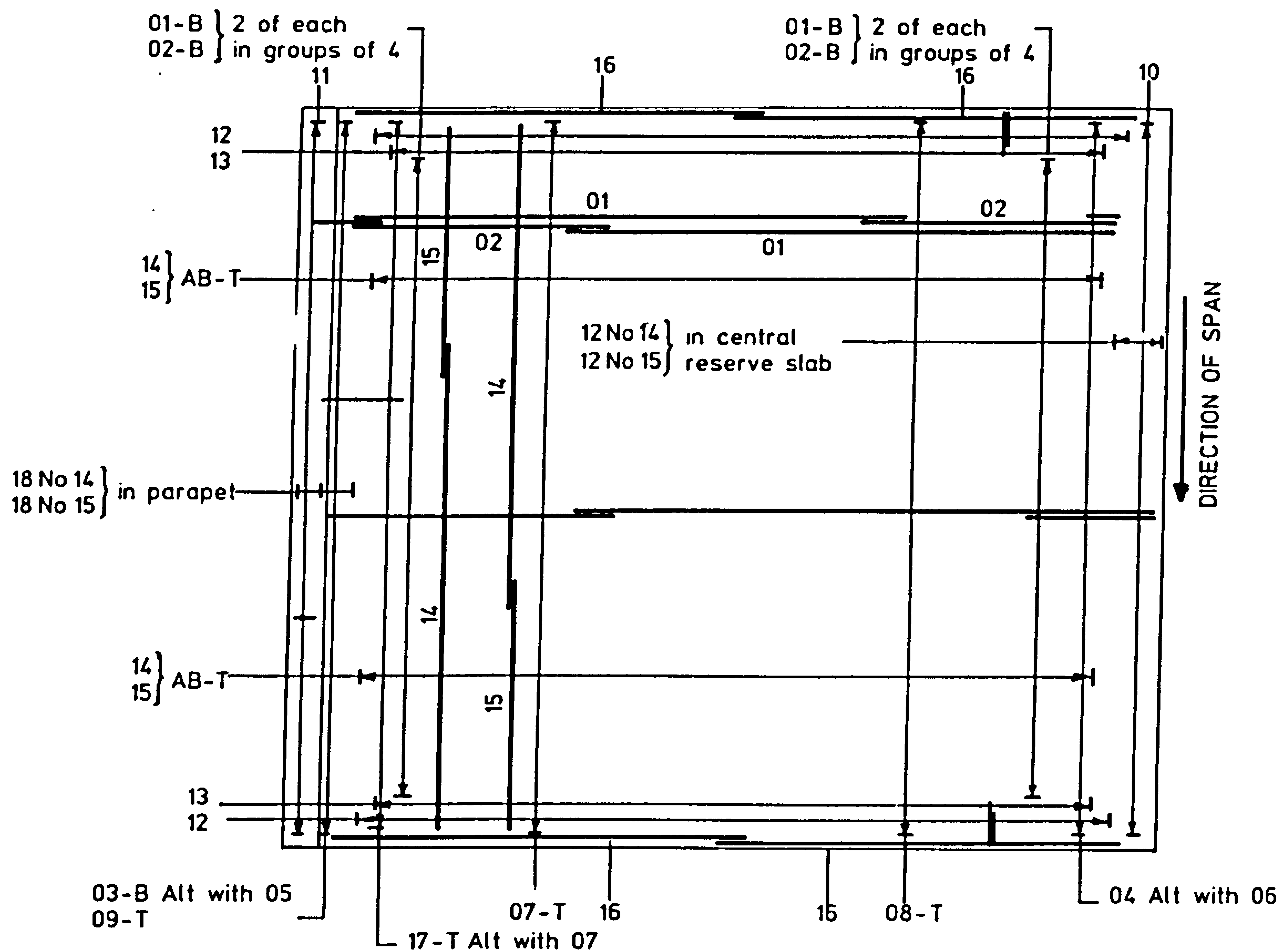

FIG. 4.9 a. REINFORCEMENT LAYOUT FOR FULL SIZE DECK

of principal shear forces. After the required shear strengths for the longitudinal and transverse directions had been obtained from the analysis, for two critical sections, a number of different approaches was used to assess the strengths of the sections. Details of the calculations are given in Appendix 2.3 of the Report.

4.5.7 Bond of the round wire tendons

As mentioned above, the model beams were constructed longer than the scaled size to provide a longer length for bond action to develop. The scaled distance from the centre of a bearing to the beam end is 85.7 mm, whereas 307 mm was actually provided.

In Appendix 2.5 of the Report, the results of strain measurements on a number of model beam tendons are recorded. These show that the prestress losses are close to those calculated (see Appendix 2.6 of the Report), at both the centre and quarter points, 60 days after release.

One of the beams that had been rejected for inclusion into the model bridge deck, because of lateral bowing and the presence of surface voids was tested to failure in bending. The first crack detected by the naked eye was at a calculated concrete tensile stress in excess of that expected and the beam failed by crushing at a higher load than calculated. There was evidence of bond slip. Details of the test are given in Appendix 2.5 of the Report.

Some of the remaining rejected beams were formed into composite beams and tested in bending. Failure of these beams was initiated by a flexural crack and was due to bond failure. The reasons for this are described in Appendix 2.5 of the Report.

BAR LOCATING TABLE

			BENDING SCHEDULE No.		
Bar Ref.	Type Size	Grouping	Shape Code	Crs.	Total No.
01	Y16	2x2x(2x)	20	610	
02	Y16	2x2x(2x)	20	610	
03	Y16	2x2x	62	610	
04	Y16	2x2x	38	610	
05	Y12	2x1x(3+)	45	610	
06	Y12	2x1x(3+)	52	610	
07	Y12	2x1x	39	300	
08	Y12	2x1x	20	300	
09	Y12	2x1x	55	100	
10	Y12	2x1x	38	100	
11	Y12	2x1x	74	100	
12	Y12	2x2x23	37	508	92
13	Y12	2x2x22	37	508	88
14	Y12	2(18+12+22)	20		104
15	Y12	2(18+12+22)	20		104
16	Y12	2x4x3	20		24
17	Y16	2x1x(-1)	39	300	

NOTES

1 In-situ concrete — Class 40/20

2 Concrete Finishes
Formed Surfaces
- non exposed surfaces — Class F1
- precast beam exposed surfaces — Class F5
- string course and facia — Class F3

Unformed Surfaces
- beams top — Class U4
- deck top — Class U1
- parapet beam — Class U3

3 Construction joints shall be to the approval of the Engineer

4 Cover
- deck slab — 25 min
- faces at expansion joints — 40 min

5 Reinforcement lap lengths — 40d min

6 Bar spacing to be measured at right angles or parallel to bridge ℄

7 Bending schedule No.(s) given at head of Bar Locating Table

8 Abbreviations
- T - top
- B - bottom
- AB - alternative bars
- ABR - alternative bars reversed
- NCS - normal crossfall slabs only
- SES - super elevated slabs only

FIG. 4.9b. FULL SIZE DECK BAR LOCATING TABLE AND NOTES.

Although an improved concrete mix was used for the beams in the bridge deck, and they were of a better quality, and the prestress release technique was improved, a number of measures were studied to improve the anchorage of the prestressing tendons. These are discussed in Appendix 2.5 of the Report.

Tests on two composite members incorporating prestressed beams similar in quality to those used for the model deck are described in Appendix 3.1 of the Report. One of the beams had end plates welded to the prestressing tendons. The load deflection graphs for the two members were similar, as were the ultimate moments and the crack patterns. Cracking was well distributed and indicated good bond until the tendon stresses approached yield. It was concluded that bond failure in the beams of the model deck was unlikely, until the tendon stress approached yield. However, as the behaviour of the two beams was so similar, as a precaution, mild steel plates were welded to the ends of the prestressing tendons in the beams of the model deck.

As cracking of the soffit of the model bridge deck was well distributed, and the extent of the cracking was increasing until failure, see Chapter 5 Figure 5.8, it was concluded that bond action was satisfactory.

4.5.8 Bursting Stresses

Due to the bursting action of the prestressing tendons in the end zone of the beams, extra shear reinforcement is provided to resist this cracking. Green[4] suggests that the required area of vertical

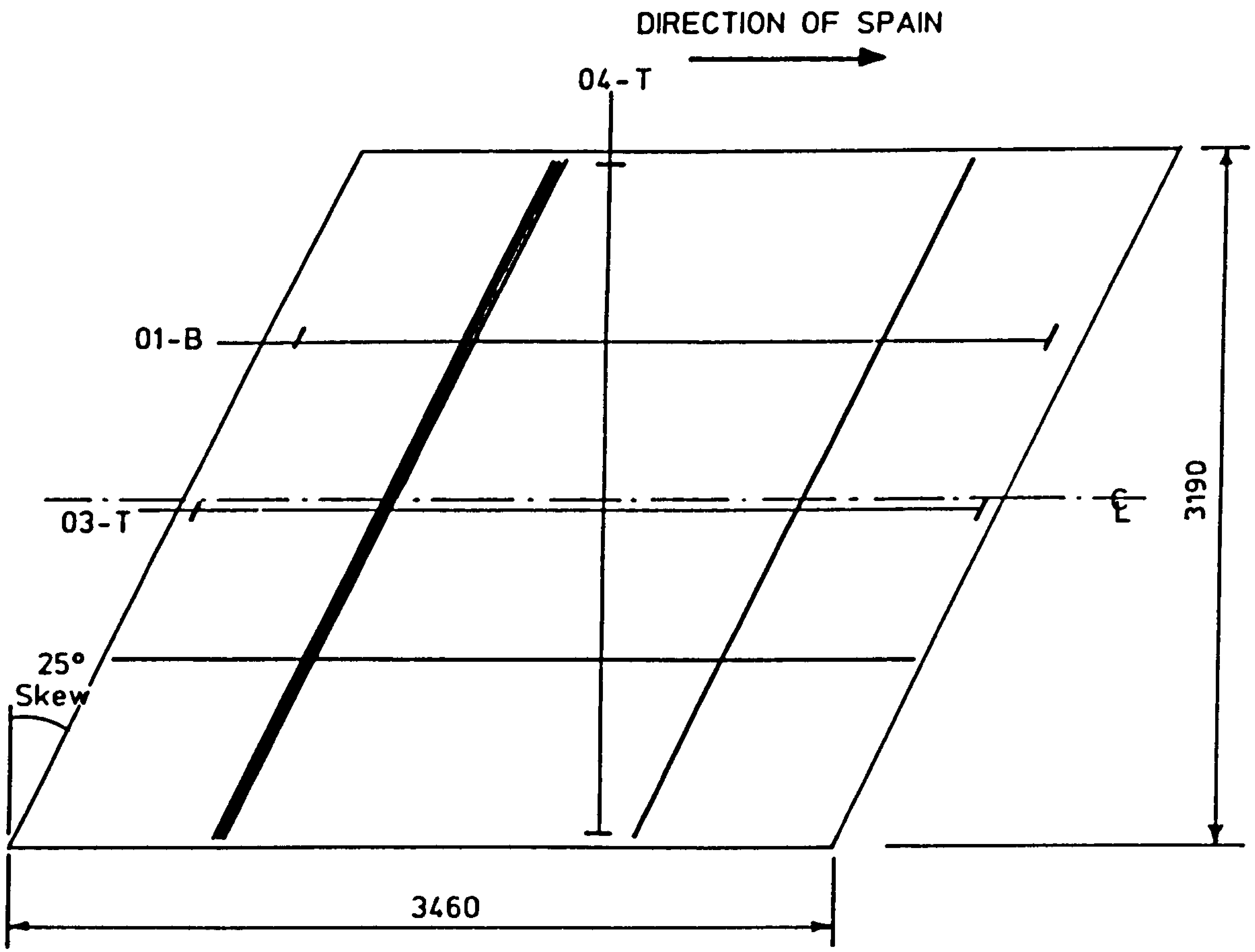

FIG. 4.10. MODEL DECK AND REINFORCEMENT DETAILS

BAR LOCATING TABLE

			BENDING SCHEDULE No.		
BAR REF.	TYPE SIZE	GROUPING	SHAPE CODE	CRS.	TOTAL No.
01	Y6	1(3 * 15)	20	225	45
03	Y6	1(1 * 14)	20	260	14
04	Y3	1(1 * 22)	20	144	22

Notes

1. In-situ Concrete 40/6
2. Cover 7mm. min
3. Bar spacing measured at right angles or parallel to deck centreline
4. Abbreviations
   T - Top
   B - Bottom
5. Sealing joints between beams to be agreed

reinforcement can be calculated from an analogy with a deep beam. In this case, it was found that 3 extra shear links in the end zone would provide sufficient restraint.

4.5.9 Detailing

Transverse holes:- The transverse holes are slightly larger than scale, so that they can accommodate the larger than scale transverse reinforcement bars and also to allow adequate concrete flow through the holes. This is necessary to ensure good bond to the transverse reinforcement along its entire length. As has been mentioned earlier, these holes, which are spaced at 610 mm in the full size deck have a spacing of 225 mm in the model deck. This represents a relative increase in spacing of 29%.

Cover:- Generally, the cover to the reinforcement in the model beams is 8 mm. However, cover to the vertical legs of the shear links is reduced to 5 mm, although these are later encased in concrete by the insitu slab. Cover to the main reinforcement of the composite slab has been standardised at 7 mm, which is approximately 18% less than scale to accommodate the larger than scale reinforcing bars.

Cracking:- Cracking considerations are satisfied by compliance with BS5400 Pt 4 (1978) cl 6.8.8.2.2. The spacing of the top transverse bars is 260 mm and of the bottom transverse bar is 225 mm, with the top longitudinal bars at 174 mm centres.

4.5.10 Concrete

Every attempt was made to ensure that the properties of the model concrete simulate as closely as possible those of the full size concrete.

FIG. 4.11. MODEL DECK 1 PRINCIPAL MOMENTS AT ULS.

Beams:- A 50/20 concrete was specified for these units, which is represented in the model by 50/6 concrete. From this specification, it can be seen that the aggregate size is only slightly above scale. Several leading prestressed beam manufacturers were consulted concerning detailed of mixes and moulds used by themselves. From these discussions, it was decided to use a rapid hardening cement with a moderate amount of plasticizer and to aim at a 7 day cycle time. Although this mix design would give a strength of 40 N/mm^2 at 5 days, the 28 day cube strength would be greater than 50 N/mm^2, approximately 58-60 N/mm^2. I was assured that this was representative of normal practice. The mix design for the beams can be seen in Appendix 1.2 of the Report.

In-situ composite slab:- A 40/20 concrete was specified, which was represented in the model by a 40/6 model concrete. The mix design can be seen in Appendix 1.2 of the Report.

4.5.11 General Considerations

During construction of a full size deck, the precast beams are layed side by side on their bearings, all additional reinforcing steel is then placed in position. Subsequently, wet concrete is poured on the deck to form the composite slab. Hence, all dead weight is carried by the precast beams in the longitudinal direction while none of the auxiliary reinforcement is stressed.

In the model slab, the actual dead weight of the model forms only part of the scaled self weight to be applied to the structure. The remainder consists of the scale factor density correction. Therefore strictly, the density correction loading should be applied to the

STRAND ANALYSIS OF MODEL PRESTRESSED DECK (REINFORCED ANALYSIS, 25 DEG).

UNCRACKED STIFFNESS WITH SKEWED REINFORCEMENT. PLOT OF PRINCIPAL SHEARS FOR ULS. LOAD COMBINATION WITH HB AT 1/6.

Stage : 1/ 3 Date : 11/10/85 at 20:53:53 Geometrical Scale Factor = 22.32 Z Shear Scale, .750E 2 = ⟷

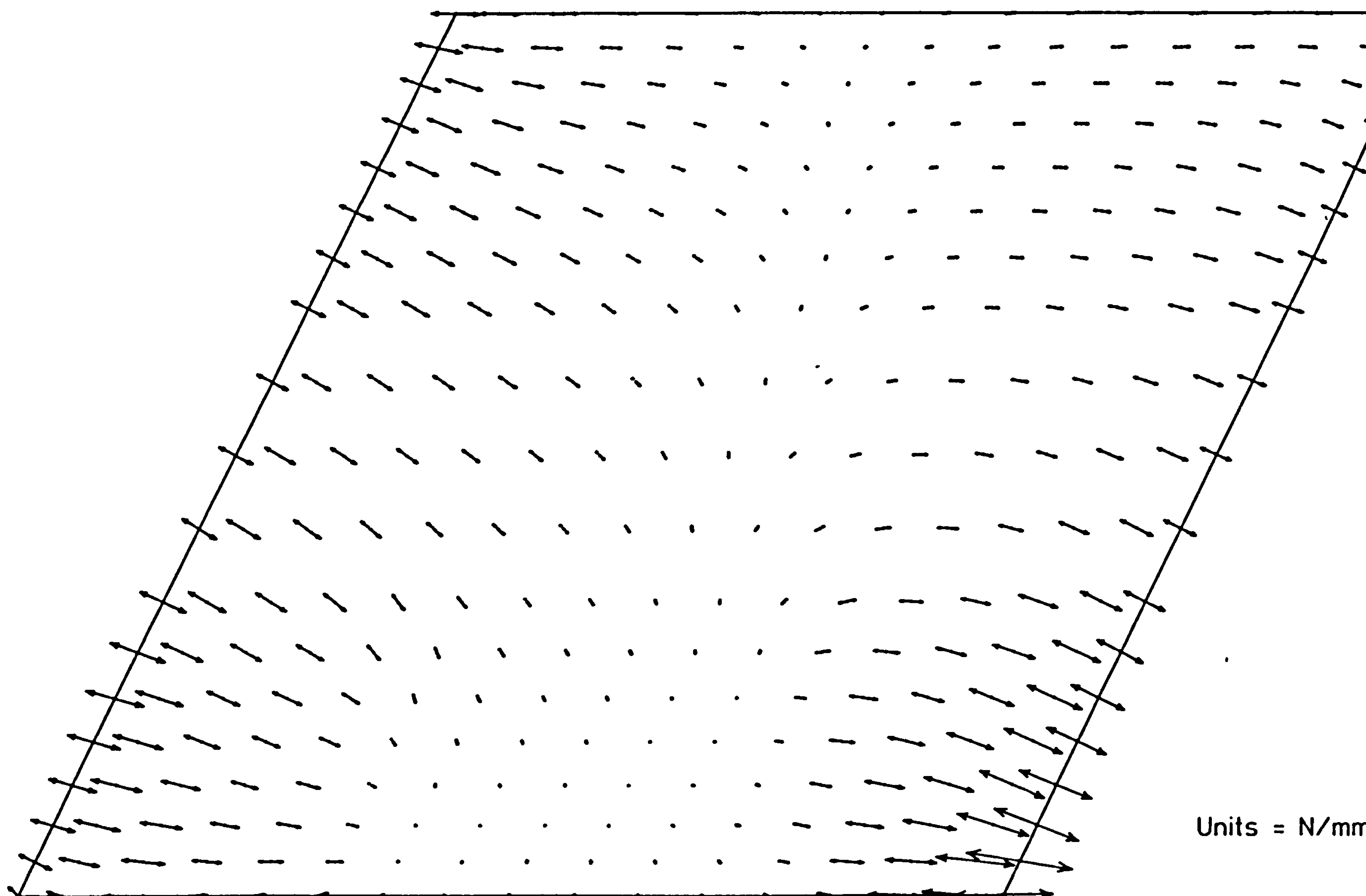

FIG. 4.12. MODEL DECK 1 PRINCIPAL SHEARS AT ULS.

beams before the in-situ composite slab is cast. For the model, the density correction was applied after the in-situ concrete had been cast and allowed to harden. Thus, the model acted as a slab for the application of the density correction and transverse moments were then present in the composite slab under simulated self weight loading alone.

The maximum moments present in the slab from the density correction loading represent approximately 19% of the moment present at the serviceability limit state in the critical zone. These moments are unlikely to effect the ultimate strength of the slab, as the redistribution that occurs when the reinforcing steel yields should ensure that there will be little difference between the moment fields in the model and in the full size bridge deck.

If the alternative course of action of applying the density correction for the model slab to the beams by hanging or other such mechanism using 10 kg weights, 60% of the model plan area would have been covered, thus preventing access to the underside of the model slab for strain readings and crack propogation plotting.

4.6 REFERENCES

1. Department of Transport, "BD 5/80. Standard Bridges", (1980).

2. British Standards Institution, "BS5400 - Steel, Concrete and Composite Bridges", Parts 1, 2 and 4, (1978).

3. Clark, L.A. "Concrete Bridge Design to BS5400", Construction Press, (1983).

4. Green, J.K. "Detailing for standard prestressed concrete bridge beams", Cement and Concrete Association, publication 48.018, (1973).

PAGE

NUMBERING

AS ORIGINAL

5. TESTING OF MODEL DECK 1

5.1 Main testing programme

The initial part of the main testing programme was designed to reproduce, as closely as possible, the effects of traffic loading on a full-size bridge deck. Three load patterns were applied. The HB bogie was placed in the centre of each of the three nominal lanes in turn and the load on it increased to give 45 units at the serviceability limit state intensity. This level of loading was applied twenty times to facilitate any incipient crack growth. When the bogie was in an outer lane, one third SLS intensity HA loading was applied in the other two lanes. However, when the bogie occupied the centre lane there was no SLS HA loading applied in the outer lanes to give the worst transverse moments.

Loading of ULS intensity was then applied with the HB bogie in the centre of an outer lane. The bogie load was then doubled and removed. For the final test, the bogie load was gradually increased until the load carrying capacity of the bridge deck began to reduce.

A timetable of the construction and testing events is presented in Table 5.1.

General views of the model under loading can be seen in Plate 5.1. The load-deflection history close to the centre of the free edge can be seen in Figure 5.1. The vertical axis of this figure shows the load on the jack connected to the HB bogie. The recorded load includes an allowance for the density correction and superimposed dead loading that could not be applied by steel weights in the vicinity of the HB bogie. This accounts for the 'false-zero' of the plot. The effects of working loads plotted were for the HB bogie in the same position as for the ultimate limit state and failure loadings.

5.1.1 Material specimen tests

Numerous standard specimens were taken from the concrete mixes used to construct the model. These specimens, when tested under standard conditions, were used to gauge the strength of the material at various stages. The most significant of these were at release of prestress in the pretensioned beams (generally at about 5 days); at 28 days; and at the time of testing. A summary of the results obtained from specimens tested at release and at 28 days is given in Tables 5.2 and 5.3. Results from the specimens tested when the model deck was loaded to failure can be seen in Tables 5.4 and 5.5 and a statistical analysis of these properties is given in Table 5.6.

A number of the standard 150 mm Ø x 300 mm concrete cylinders were used to obtain stress-strain curves. Each cylinder had three sets of de-mec points equally spaced around its periphery at mid-length. After each test specimen had been capped with plaster the applied load was increased in increments. Strain readings were taken after each increment for the three sets of De-mec points and averaged. It was difficult to keep good control of the tests at high strain levels with the load control arrangement that was employed. Hence, probably, the stress-strain plots shown in Figure 5.2 do not show the full extent of the concrete's ductility.

It will be noticed from Figure 5.2 and Table 5.6 that the mean precast and in-situ concrete cube crushing strengths are 64.9 N/mm^2 and 38.3 N/mm^2 respectively, while the cylinder crushing strengths observed

FIG. 5.1. PLOT OF THE LOAD DEFLECTION HISTORY OF MODEL 1

from the stress-strain tests are 43 N/mm^2 and 29.5 N/mm^2 respectively. Thus the ratios of the cylinder to the cube strengths for the precast and in-situ concretes are therefore 0.66 and 0.77. For the precast concrete, there is a large deviation from the generally accepted value of about 0.8. It is difficult to define precisely why this occurred. However, from Figure 5.2(i) the cylinder strengths of the four specimens tested varied from approximately 42 N/mm^2 to 45 N/mm^2, while the cube strengths from 29 specimens had a standard deviation of 7.1 N/mm^2 and a range of 76.6 N/mm^2 to 49.4 N/mm^2. Also, when it is recalled that the specimens came from 6 separate mixes cast over a period of approximately 2.5 months it can be seen that there was sufficient scope for a large deviation to occur. As the value of initial modulus is relatively insensitive to the concrete strength over the strength range observed, the measured modulus will be used with the average cube strengths for calculation purposes.

Event Dates	Description of Event
22-3-84 to 4-6-84	Precast Beams Cast
8-8-84	In-situ Concrete Cast
22-2-85	Start of Testing
25-2-85 to 12-4-85	Serviceability Limit State Testing
23-4-85 to 27-4-85	Ultimate Limit State Testing
3-5-85 to 7-5-85	Test to Failure
8-5-85	End of Testing

Table 5.1 Timetable of Events for Model 1

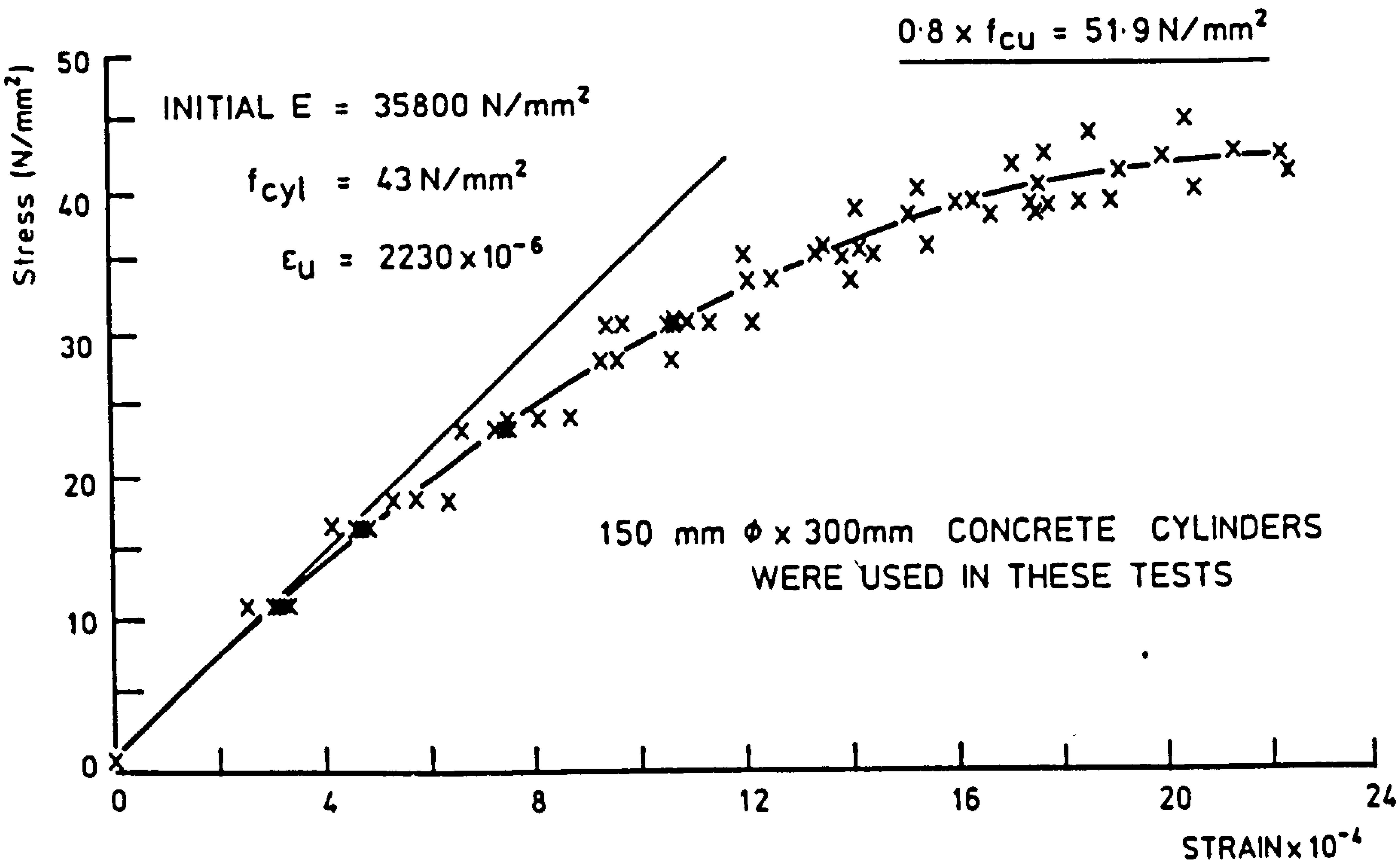

(i) Precast Concrete

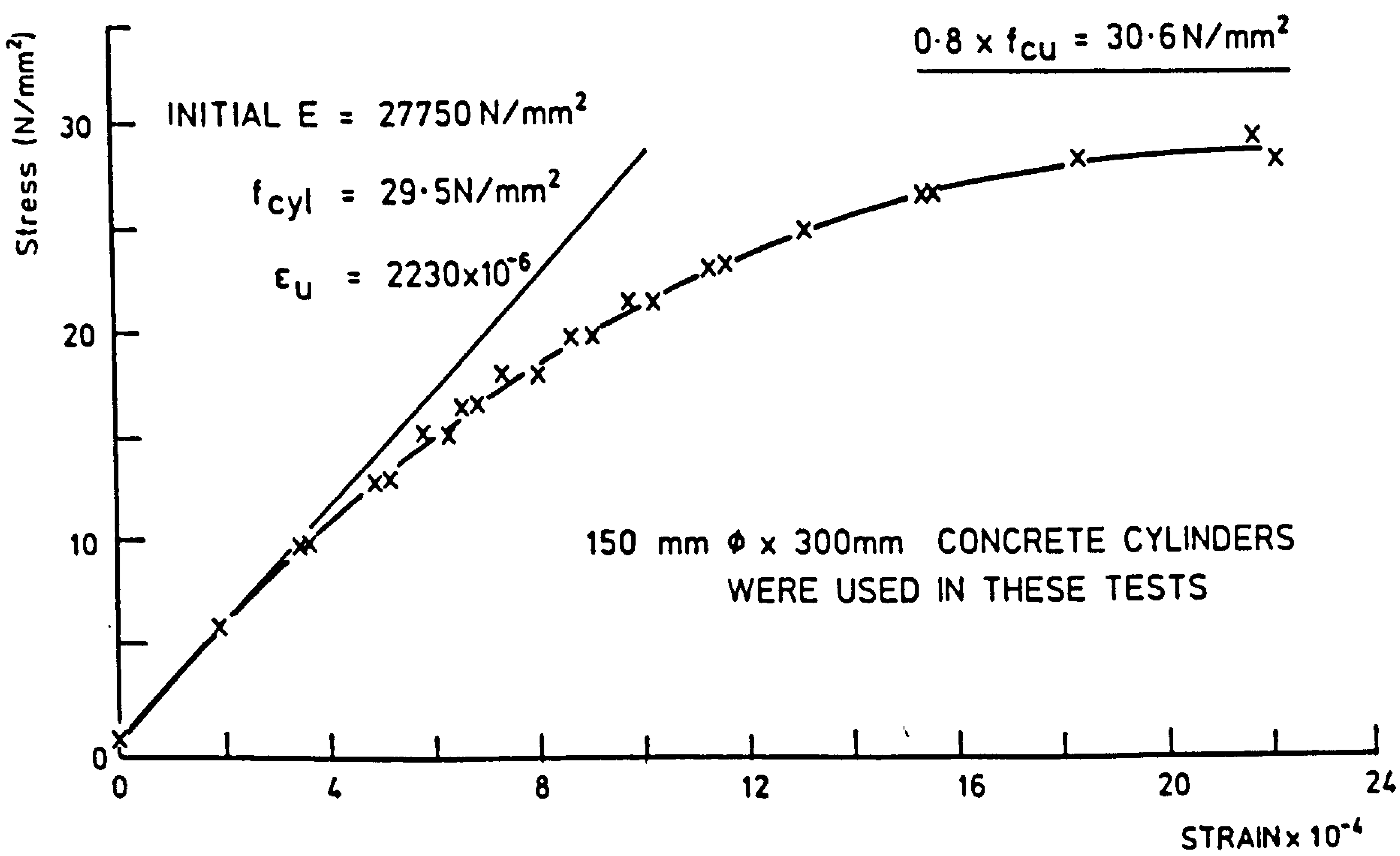

(ii) In-situ Concrete

FIG. 5.2. STRESS-STRAIN CURVES FOR THE CONCRETE THAT WAS USED IN MODEL 1

Precast Concrete				
Mix No	Cast Date	Average Cube strength at release	Average strength at 28 days	
		N/mm^2	100mm cubes (crushed) N/mm^2	150mm x 300mm cylinders (split) N/mm^2
1	21-3-84	48.3	61.7	3.8
2	4-4-84	44.5	54.2	3.5
3	16-4-84	50.4	61.5	3.6
4	27-4-84	39.7	57.9	3.6
5	15-5-84	49.6	66.5	3.8
6	4-6-84	43.8	56.7	-

Table 5.2 Summary of concrete test results: tests carried out at release and 28 days.

In-situ Concrete				
Mix No	Cast Date	Average strength at 7 days	Average strength at 28 days	
		N/mm^2	100mm cubes (crushed) N/mm^2	150mm x 300mm cylinders (split) N/mm^2
-	8-8-84	27.0	40.7	3.1

Table 5.3 Summary of concrete test results: tests carried out at 7 days and 28 days

Precast Concrete		
Mix No	Details	Results N/mm^2
1	100mm cubes (crushed) 150mm cylinders (split) 50mm cubes (crushed) 50mm cylinders (split)	66.4, 74.4, 72.3 3.3 73.8, 78.1, 77.8, 65.0, 80.4 4.8, 4.6, 3.6, 4.0, 5.4, 5.0
2	100mm cubes (crushed)	53.1, 49.4
3	100mm cubes (crushed)	68.3, 66.2, 63.1, 66.9, 66.7 63.6, 68.6, 71.6, 59.5
4	100mm cubes (crushed) 150mm cylinders (split)	61.1, 62.5, 63.0 4.1
5	100mm cubes (crushed) 150mm cylinders (split)	69.8, 77.2, 71.5, 72.7, 76.6, 67.4 4.2
6	100mm cubes (crushed) 150mm cylinders (split)	58.9, 62.8, 60.1, 53.6, 55.7, 57.8 4.2, 3.4

Table 5.4 Precast Concrete Material Properties for Model Deck 1

In-Situ Concrete		
Mix No	Details	Results N/mm^2
1	100mm cubes (crushed) 150mm cylinders (split) 50mm cubes (crushed) 50mm cylinders (split)	39.6, 36.3, 37.9, 39.0, 38.0,37.7 40.6, 38.5, 37.0, 38.2, 38.5, 38.3 3.1, 3.0 38.4, 36.0, 37.5, 37.6, 37.7, 37.6 3.3, 2.7, 2.7, 3.2, 2.9, 2.7

Table 5.5 In-Situ Concrete Material Properties for Model Deck 1

Precast Concrete			
Test	Sample	Mean	S.D.
100mm cubes (crushed)	29	64.9	7.1
150mm cylinders (split)	5	3.9	0.5
50mm cubes (crushed)	5	75.0	6.1
50mm cylinders (split)	6	4.6	0.7

In-Situ Concrete			
Test	Sample	Mean	S.D.
100mm cubes (crushed)	12	38.3	1.1
150mm cylinders (split)	2	3.0	0.1
50mm cubes (crushed)	6	37.5	0.8
50mm cylinders (split)	6	2.9	0.3

Table 5.6 Statistical Analysis of Concrete Material Properties for Model Deck 1

Tests were also carried out upon samples of the prestressing wire and reinforcing steel that was used in model 1. The four types of material employed were, 6mm diameter prestressing wire, 4.5mm diameter prestressing wire, 6mm diameter 'Torbar' high yield reinforcement and 3mm diameter 'Mild' steel reinforcement. Numerous samples of the 6mm and 4.5mm wire were tested during the manufacture of the 6 sets of precast beams. Four samples of each of the reinforcement types were also tested.

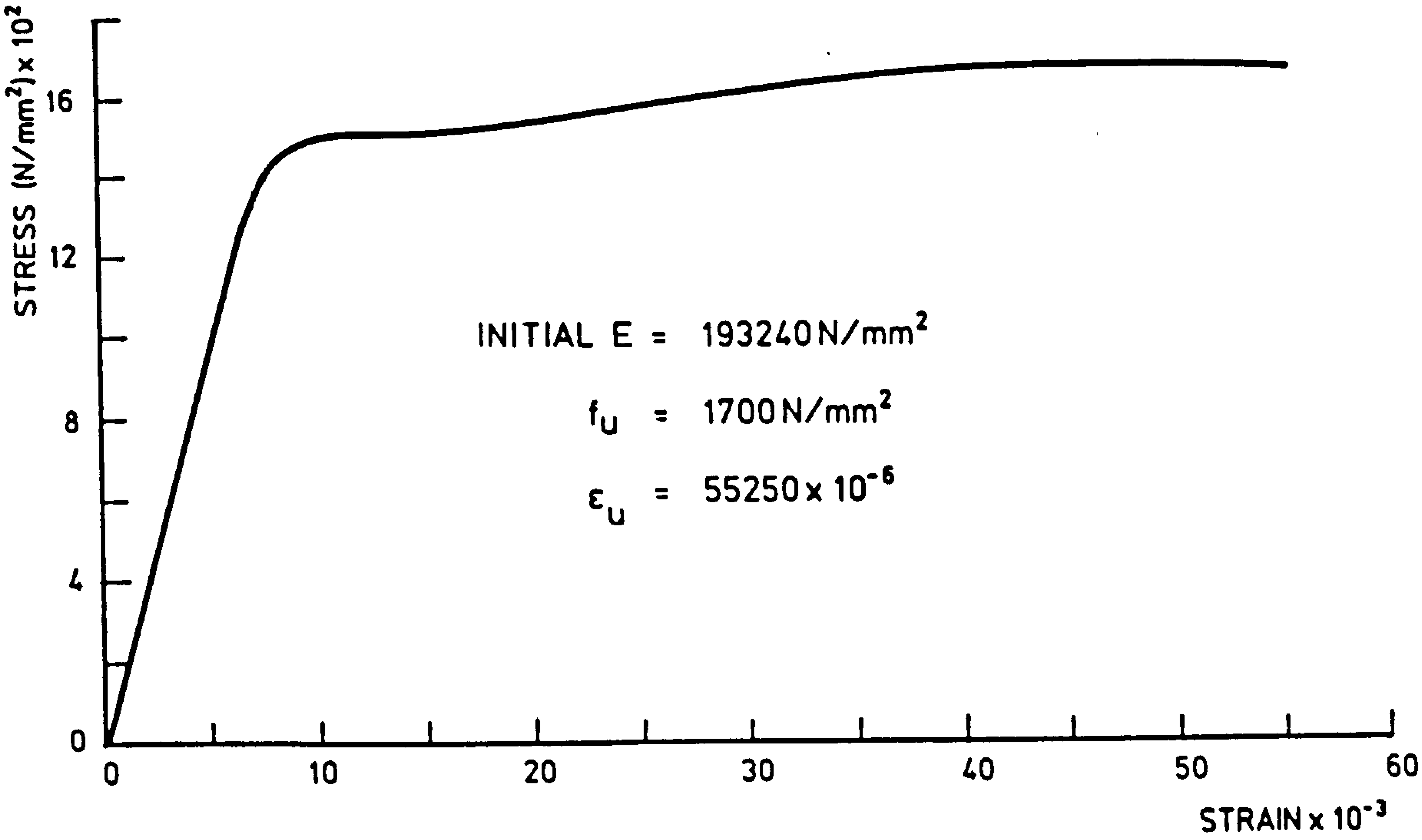

(i) 6mm Φ Plain Prestressing Wire

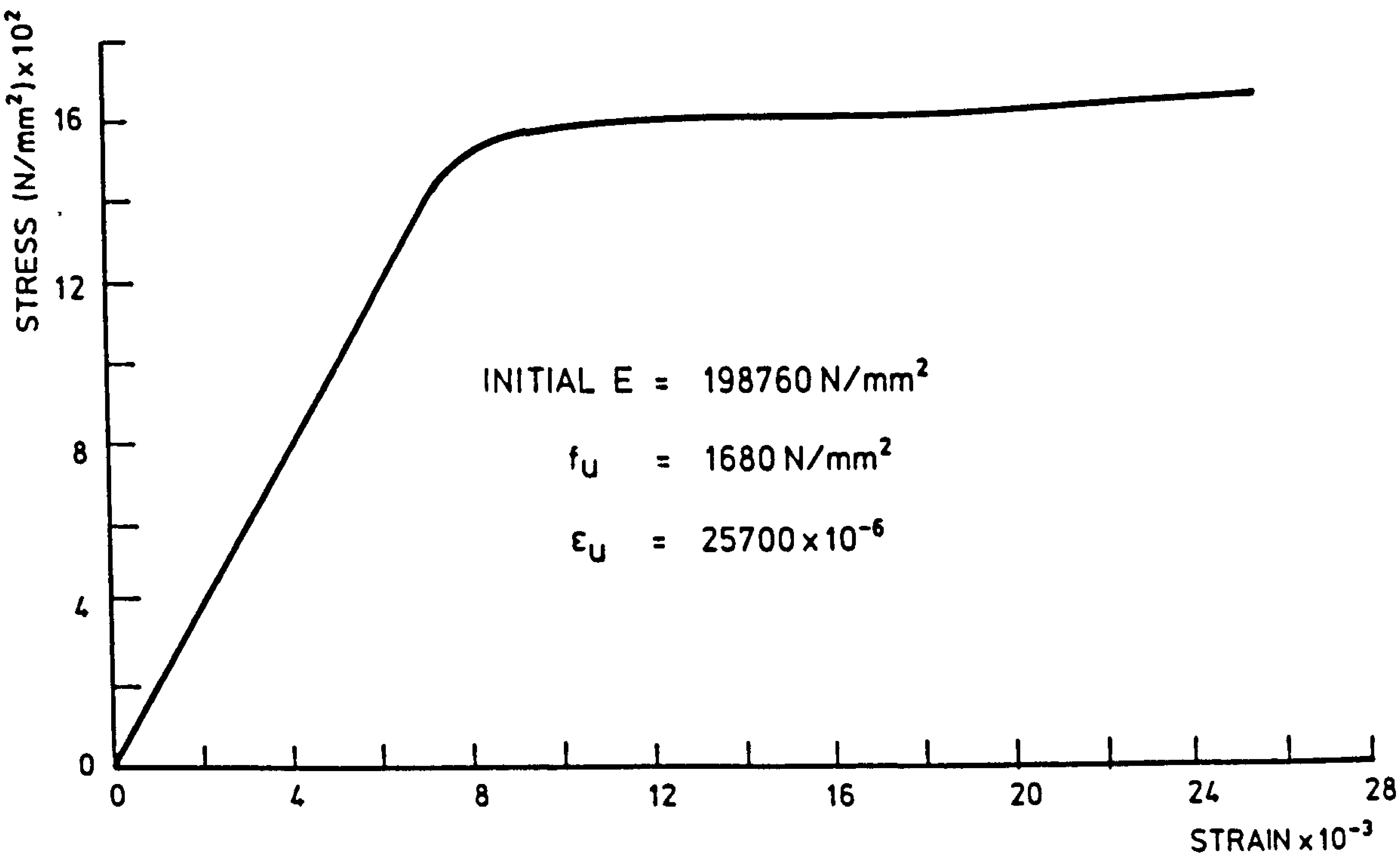

(ii) 4·5mm Φ Triple Indented Prestressing Wire

FIG. 5.3. STRESS-STRAIN CURVES FOR THE PRESTRESSING STEEL USED IN MODEL 1

Each test was carried out on a specimen approximately 300mm long in an Avery tensile test machine under displacement control. The initial part of the curve, including the whole elastic and half of the plastic region, was monitored using an electrical extensometer. Thereafter, the displacement of the machine cross-head was used to obtain strains. The results of the tests indicated that the 4.5mm diameter prestressing wire, 6mm diameter 'Torbar' reinforcement and the 3mm diameter 'Mild' steel exhibited good property consistency over their lengths. However, the 6mm diameter prestressing wire tests revealed a variation of approximately ± 4% in the material properties over its length. The stress-strain plots for all 4 materials can be seen in Figures 5.3 and 5.4.

5.1.2 Bearing stiffness test

The model deck was supported upon 44 'elastomeric' type supports. The 22 of these that were situated along support line 1 also incorporated load cells. Each support consisted of two layers of 6mm rubber, with a sheet of steel sandwiched between, and each possessed a stiffness of approximately 20.1 kN/mm. This corresponds to a full size stiffness of 70.5 kN/mm, which is representative of commercially available bearings.

5.1.3 Model Deck test

Initially, the deck was loaded with 9.4 tonnes (1 tonne = 1000 kg mass, which under gravity exerts a force of 9810 N) of density correction and 2.64 tonnes of superimposed dead loading. This was evenly distributed across the width of the deck and along the length as far as one slab depth from the support lines. The imposed loading was only continued as far as one slab depth from the support lines for two reasons. Most importantly, this arrangement would allow visual

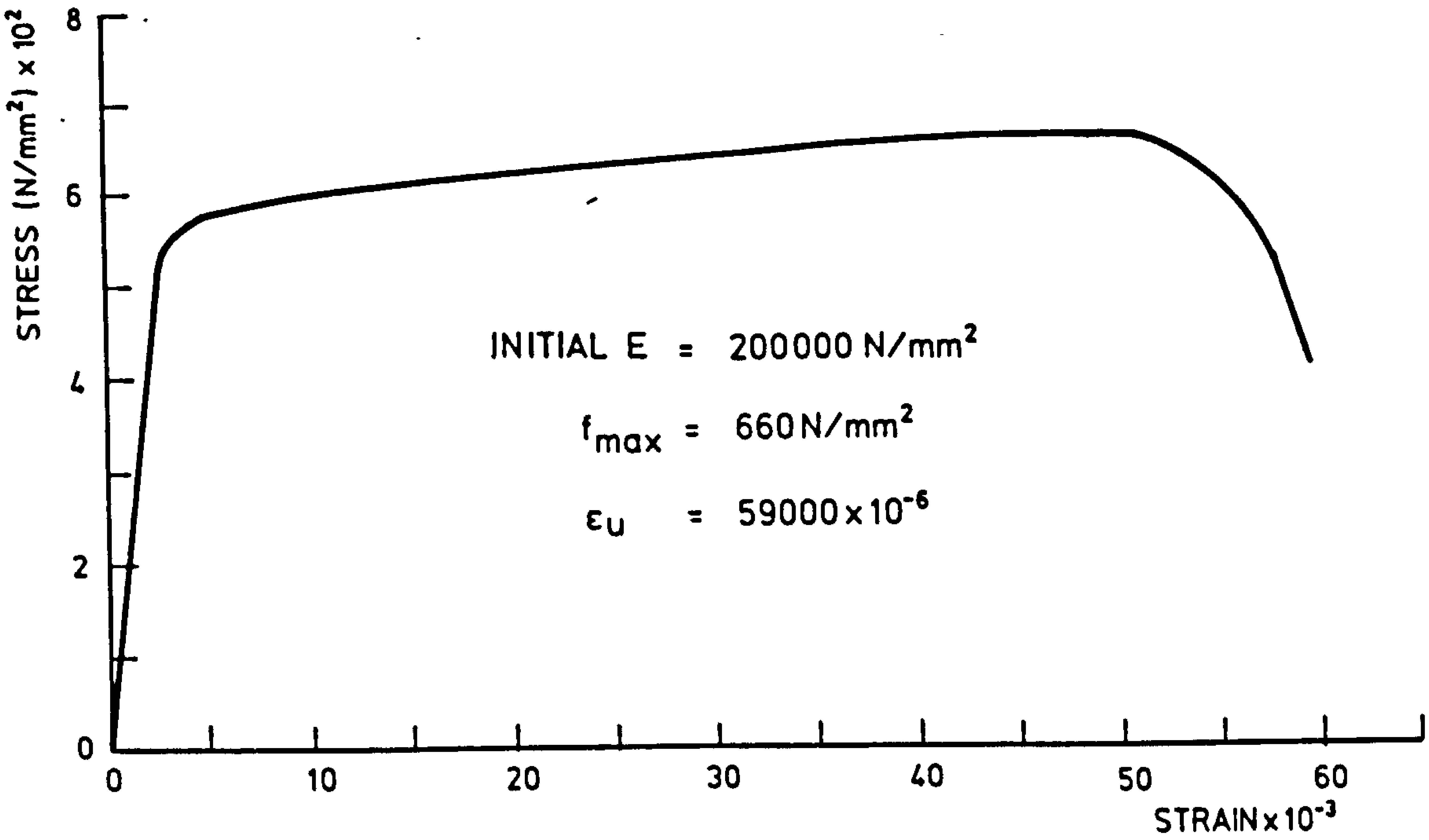

(i) 6mm Φ 'Torbar' High Yield Reinforcement

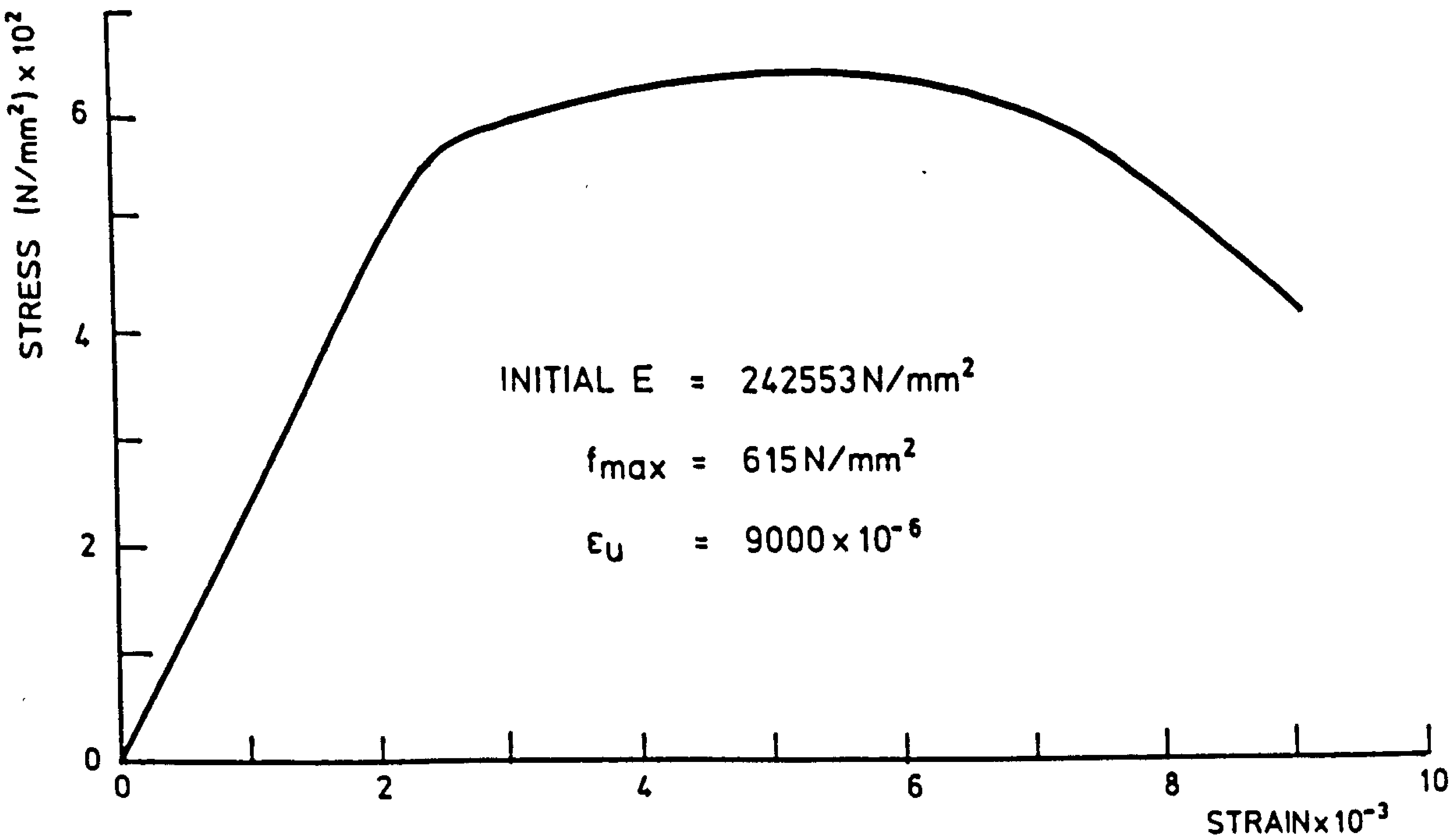

(ii) 3mm Φ 'Mild' Steel Reinforcement

FIG. 5.4. STRESS-STRAIN CURVES FOR THE REINFORCING STEEL USED IN MODEL 1

access to the top surface around the supports and secondly because loading closer to the bearings would have only limited influence on the structural response and there was a limited number of steel weights available. With all the dead load applied, readings were taken and the model inspected. There was no indication of cracking and the deflection measurements showed that the model was behaving in a reasonably linear fashion, considering the low load level and the consequent experimental errors associated with small values.

One third HA SLS level loading of 0.99 tonnes per lane was then applied to the complete model area using dead weights. This loading was intended to produce the same effects as "average" traffic loading. From the readings taken, it was deduced that the structural behaviour was essentially linear.

A model HB bogie was then placed at the centre of each lane in turn, and loaded up to the model serviceability limit state 45 unit loading of 80.0 kN and then unloaded a number of times. 20 cycles were carried out for each lane, with readings taken and inspections carried out before, during and after each set of 20 cycles. During these tests, the uniformly distributed loading representing 0.33 HA serviceability level loading was retained. The deflection measurements showed that during the first application of the HB bogie load, with the bogie placed in an outside lane, the structural response became non-linear, with non-recoverable deflections of 0.3-0.4 mm being recorded near the centre of the free edge. Average deflections along the centre line at mid-span were 2.3 mm without the HB loading and 3.7 mm with the HB loading. However, no cracks were visible to inspection with the naked eye on either the soffit, sides or top of the model.

When cycled serviceability loading tests had been finished, the HB bogie was placed in bogie position 1, see Figure 5.5. The uniformly distributed live loading was rearranged and factored for the ULS condition so that there was 1/3 HA in lane 3, full HA in lane 2 and just the HB bogie in lane 1. However, in addition to the factored live loading, there was also 4.6 tonnes of self-weight, 10.82 tonnes of factored density correction and 3.86 tonnes of factored superimposed dead loading. The density correction, superimposed dead loading and uniformly distributed live loading were provided in the form of 20 kg black steel weights. These were evenly distributed over the width of the deck and along the deck as far as one slab depth from the support lines.

0.5 x 45 units of ULS HB bogie loading was then applied to the structure, readings were taken and the slab surfaces examined. 1.0 x ULS HB bogie loading was then applied. No cracking was noticed using the naked eye at either of these two load levels. The HB bogie load was then increased to 1.5 x ULS intensity, and cracking was noticed at this load level in the in-situ concrete that was visible along the free edge of the deck. These cracks were very narrow and well-distributed along the edge adjacent to the HB bogie. However, no cracking was visible on the soffit of the model deck.

After the cracks had been marked and a set of readings taken, the HB bogie load was increased to 2.0 x ULS (90 units at ULS). This caused relatively extensive cracking on the soffit of the model, and a number of small cracks were also noticed on the top surface around the obtuse corner, in the same lane as the HB bogie. These top surface cracks appeared to run in a direction perpendicular to the supports. The soffit cracking was spread over an area one lane wide and a third of the span long, under the HB bogie. The crack spacing was approximately 200 mm while the widths were in the range 0.05 - 0.1 mm. The direction tended to be parallel to the supports, see Figure 5.6.

After the model state at 2.0 x ULS HB bogie loading had been noted, the HB loading intensity was increased to 2.5 x ULS. The soffit cracks propagated and additional cracks formed closer to the support lines. The maximum crack width was approximately 0.23 mm. There was increased cracking on the top surface of the obtuse corner. The full extent of top surface cracking could not be ascertained, however, due to the applied UDL loading, which was in the form of black steel weights. New cracking was noticed at this stage in area C which is shown in Figure 5.5. The maximum deflection had increased to 17.7 mm, the maximum concrete compressive strain on the top surface adjacent to the HB bogie was 1440 μ-strain. The maximum tendon strain of 6680 μ-strain also occurred in the same area and this strain would correspond to a tendon stress of 1336 N/mm^2. From Figure 5.3(i) it can be seen that a stress of 1336 N/mm^2 is approximately equal to 93% of the yield stress for the material.

An attempt was then made to increase the load to 3.0 x ULS HB intensity. However, the displacements were increasing at such a rate that it was decided to switch control of the testing programme to displacement. Therefore, subsequently, the displacement transducer under the HB bogie was used to control load increments.

For the next increment, the displacement was increased to 29.1 mm, while the load was equal to 2.7 x ULS HB. At this stage, the cracking was further intensified while the loading on the load cells at the

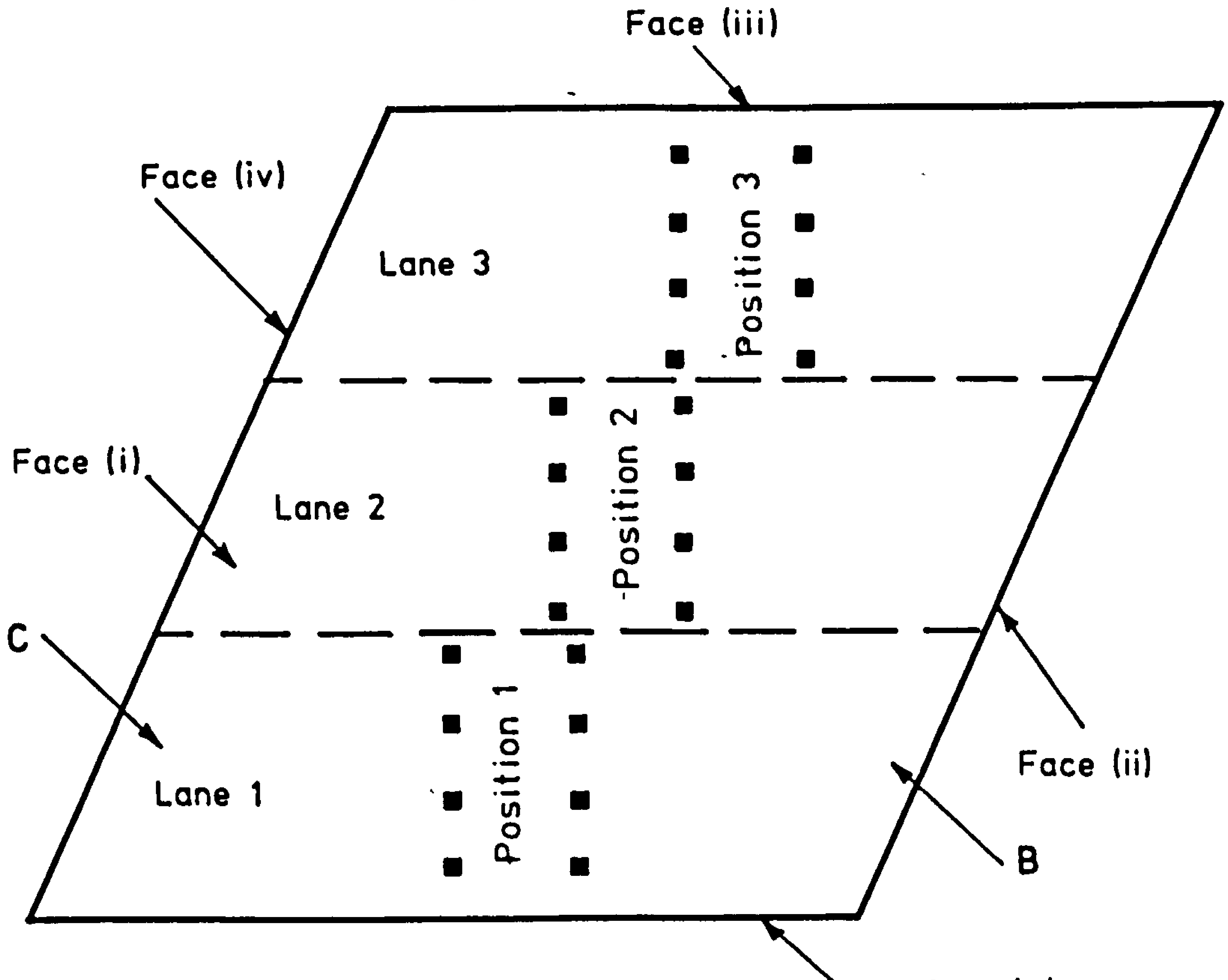

Top Surface

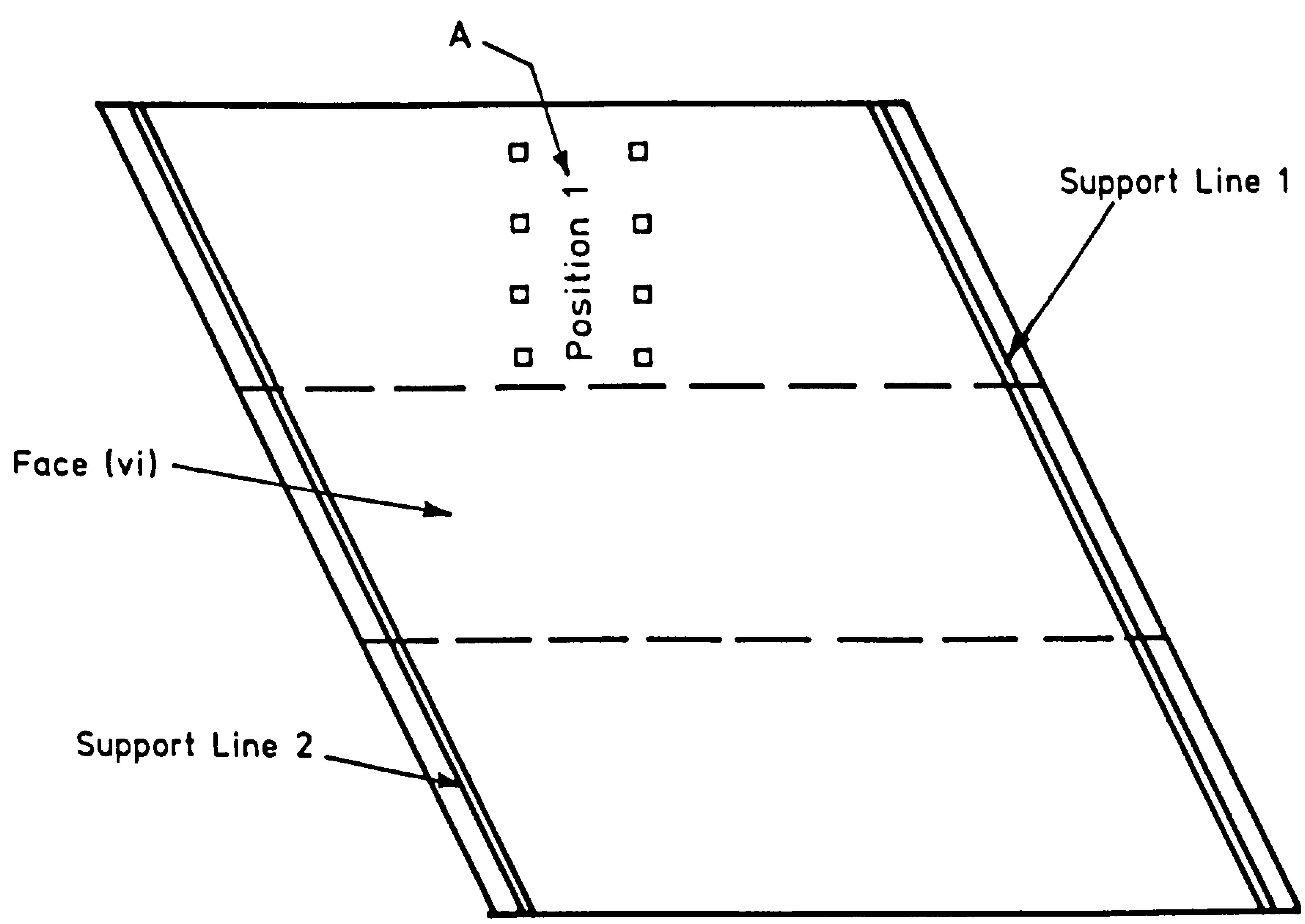

Soffit Surface

FIG. 5.5. PLAN OF MODEL 1 SHOWING THE DETAILS REFERRED TO IN THE TEXT.

acute end of support line 1 began to decrease. After a set of readings had been taken and the state of the model noted, the displacement was then increased to 32.5 mm, while the load reached 2.93 x ULS HB. By this time, the cracking on the soffit of the model had developed to such an extent that distributed cracking covered approximately 60% of the plan area. The concrete also began crushing along the top surface under the HB bogie load pads.

It is unfortunate that most of the top surface of the model was covered with steel weights which would not allow inspection of possible top surface cracking. The appearance of the top surface after the test with the weights removed suggests that there may have been extensive top cracking at this stage. At 2.93 x ULS HB bogie loading, a shear crack began forming at approximately quarter span, between the HB vehicle bogie and the obtuse corner.

The displacement was increased to 40.4 mm, at which stage the acute corner end of support line 1 lifted off the bearings. Lift off extended as far as the fourth beam in. A second shear crack began forming just to the side of the HB bogie pad nearest the obtuse corner. The cracking along the top surface of both support lines was very intense. The load at this level was 3.04 x ULS HB. The crushing under the axles of the HB bogie developed further. However, it was difficult to judge the exact extent of this because of the platform that was used for the operation of the screw jack.

The displacement was then increased to 55.9 mm with a load of 3.22 x ULS HB, followed by an increase to 65.8 mm with a load of 3.26 x ULS HB. By this stage, there was significant lateral movement at the base

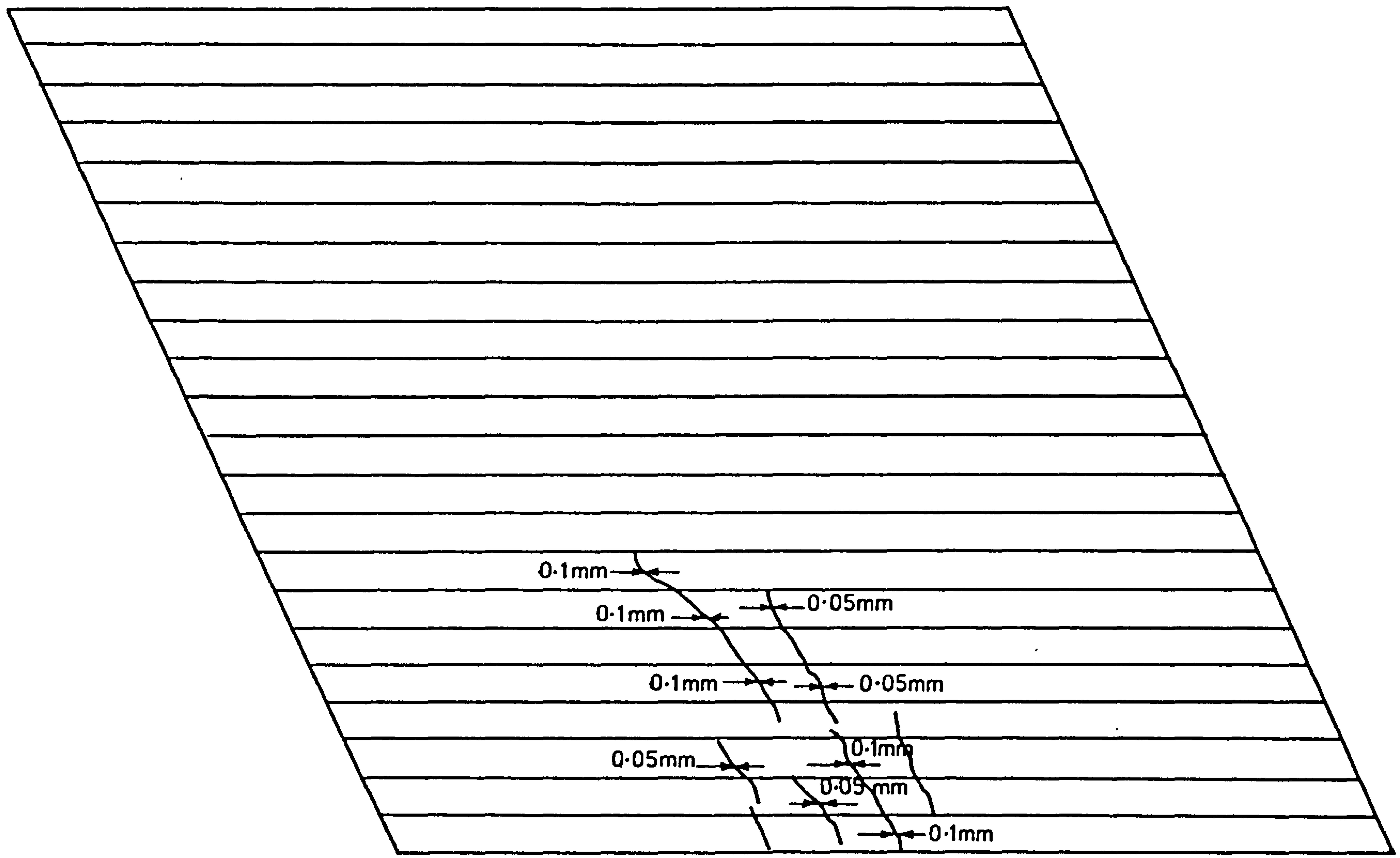

FIG. 5. 6. CRACK PATTERN ON THE SOFFIT OF MODEL DECK 1 AT 2.0 x ULS. HB BOGIE.

of the shear crack at quarter span, while there was none at the top, suggesting that the obtuse corner end of the edge beam 1 was parting company with the rest of the deck.

An increase in displacement to 78.9 mm was then made with no increase in load. Further displacement was applied while the load remained constant. When the displacement had reached 117 mm, it was noticed that the in-situ concrete was parting company with the top of the bottom flange of beam 2 in the obtuse corner. The gap between the two concretes was approximately 3 mm; this can be seen in Figure 5.7.

The displacement was finally increased to 137 mm by which time the load had dropped off to 3.09 x ULS HB. By this stage the deflections were so large that it was felt the testing rig was becoming unstable. Therefore, bearing in mind the significant reduction in load, the test was stopped.

During the test, the maximum recorded strain in the prestressing tendons was 16500 μ-strain while the maximum recorded surface concrete compressive strain was 4340 μ-strain. At the end of the test, the acute corner of support line 1 had lifted off its bearing by approximately 12 mm.

The crack patterns on the top and soffit surfaces of the deck at failure are shown in Figures 5.8 and 5.9 and Plates 5.2 to 5.3. Cracking on the side and end of the deck are shown in Plate 5.4.

During the final stages of the test on model 1, crack width measurements were taken at the 14 points shown in Figure 5.8.

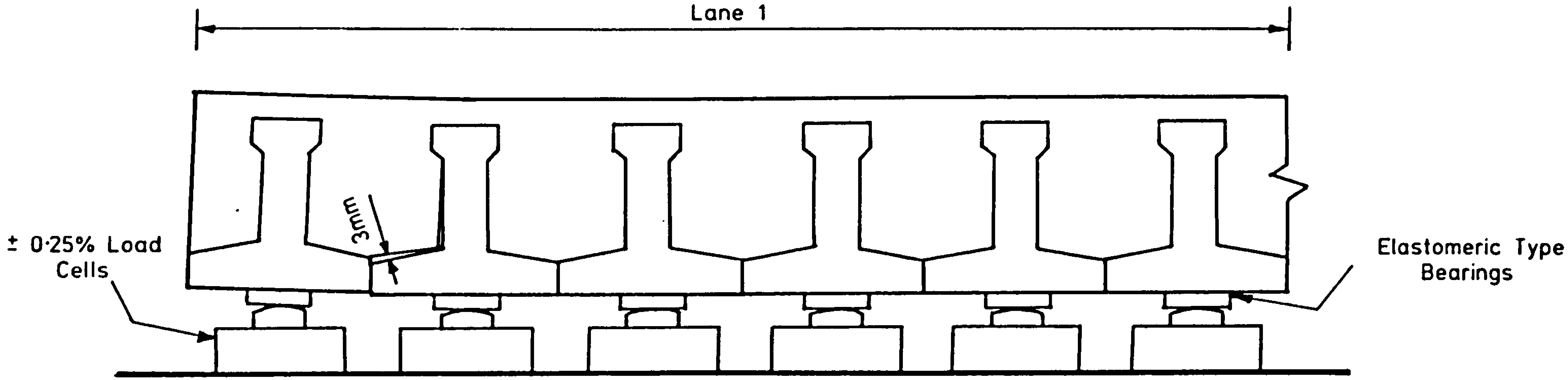

End Elevation of Support Line 1

FIG. 5.7. SEPARATION OF THE IN-SITU CONCRETE AND BEAM CONCRETE AT THE OBTUSE CORNER

Table 5.7 gives the crack width measurements together with the load and displacement levels at which they were taken. The displacement measurements refer to a point at mid-span of the second beam in from the free edge under the HB bogie.

Load Level x ULS HB	3.27	3.27	3.21	3.22	3.19	3.04
Displacement level (mm)	65.8	78.9	92.3	103.0	117.0	137.0
Station	Crack Widths (mm)					
1	1.0	1.2	1.7	1.6	2.0	2.0
2	0.8	1.2	0.7	1.0	1.0	1.0
3	0.6	0.7	0.9	0.8	0.9	0.7
4	0.5	0.6	0.7	0.7	0.7	0.6
5	0.3	0.4	0.5	0.6	0.6	0.7
6	0.2	0.7	0.6	1.0	1.0	1.5
7	0.4	1.2	0.8	0.8	1.0	1.3
8	0.4	0.6	0.5	0.6	0.7	0.8
9	2.0	2.3	3.0	3.8	5.0	6.0
10	2.0	2.1	2.0	2.2	2.0	2.3
11	0.3	0.7	1.0	1.2	1.0	1.3
12	1.2	1.3	1.4	2.0	3.0	2.1
13	1.2	1.2	1.1	1.4	1.5	1.2
14	1.2	1.1	1.5	1.7	1.5	1.8

Table 5.7 Crack Widths that were Measured close to Failure for Model Deck 1

5.1.4 Cores

After the surfaces of the failed model had been comprehensively photographed, 6" and 3" cores were removed from locations where the

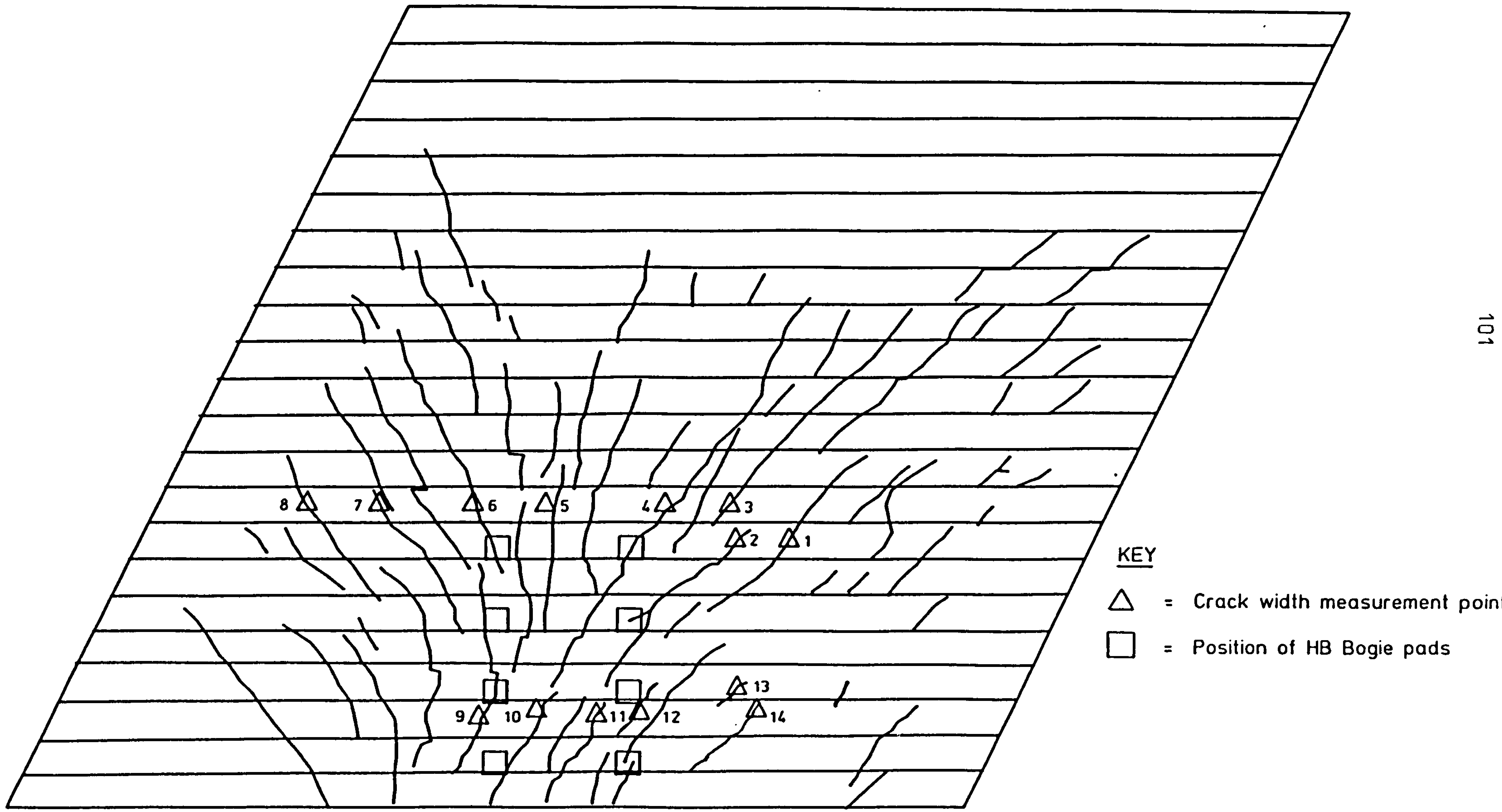

FIG. 5.8. PLOT OF THE CRACK PATTERN ON THE SOFFIT OF MODEL 1 AT FAILURE

model had behaved in an unusual way during the test to failure. Plate 5.5 illustrates the features revealed by one of these cores. This core was taken from near support line 2 at the junction between lanes 2 and 3, see Figure 5.5.

These cores showed that the 'tearing' type of cracking, that was visible on the top surface after removal of the dead weights was generally aligned above one side of a precast web. In most cases these cracks formed above the side of a web closest to the HB Bogie, although it was observed that in some instances these cracks 'crossed over' the tops of the webs and then aligned themselves above the opposite side of the web. From one of the cores it was observed that a cross over had occurred where the top transverse steel passed across a beam.

Inspection of the core shown in Plate 5.5 revealed that there was separation of the insitu and precast concretes below the cracks on the top. This separation tapered from 0.3mm at the top where one could see light through the core, to 0.07mm at the bottom. It was also noted that on one side of the core the separation continued vertically down through the lower flange as a crack, while there was no separation around the lower flange. The crack however was not visible with a 0.01mm microscope on the base of the core. On the opposite side of the core the separation followed the profile of the lower flange and was visible on the base. Even though a large separation was present, the core unit was still rigid due to the reinforcement which passed through it. In most cases, it was very difficult to locate the other interfaces that were present around the periphery of the core, such was the integrity of the other composite interfaces.

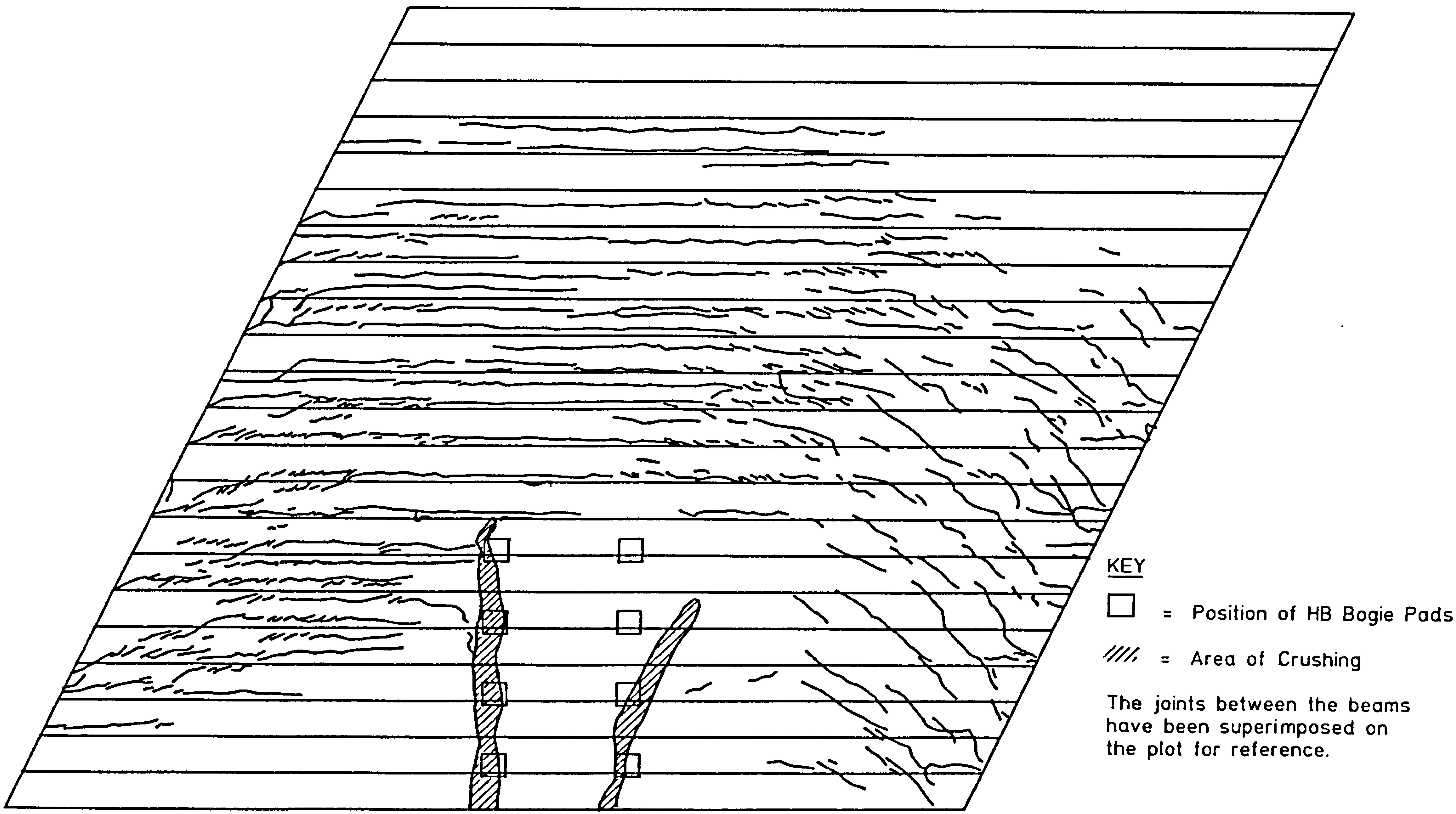

FIG. 5. 9. PLOT OF THE CRACK PATTERN ON THE TOP OF MODEL 1 AT FAILURE.

Besides the inspection of the separation the cores also allowed the standard of construction to be analysed. The precast concrete was well compacted with very little air entrainment. The coarse aggregate was densely packed throughout the depth of the section. The insitu concrete was also well compacted although there was slightly more air entrained than in the precast concrete. Again the coarse aggregate was densely packed. The overall depth of the core was measured at 173mm giving an error of 0.6% when compared with the depth specified in the design. It was also possible to assess the accuracy with which the prestressing and reinforcement had been placed. It was found that the prestressing placement error was less than 1mm while the reinforcing it was approximately 1.5mm at the particular locations where cores had been taken.

5.2 Results Processing

At the completion of the testing programme for model 1, an initial analysis of the transducer readings was carried out. The purpose of this analysis was to check consistency and to select readings from those stages of the programme that would be most useful for assessing the structural response. The test readings selected are presented in the Tables of Appendix 5.3, which also contains Figures showing the locations of the transducers. The test results are assessed and compared with analytical predictions in Chapter 11.

5.3 Tests on Longitudinal and Transverse Strips

In addition to the tests on model deck 1, separate tests were performed on 1 to 3.5 models of transverse and longitudinal strips of a prototype deck.

5.3.1 Tests on transverse strips

A beam representing a transverse strip of model 1 was formed by sawing reject beams into 440 mm lengths; assembling twenty of them side by side, with transverse reinforcement threaded through the web slots; and then casting in-situ concrete. The two beams so formed were each 440 mm wide x 174 mm deep x 2900 mm long. Details of the beams and of the test results are given in Appendix 5.2.

The beams were tested with a constant sagging moment zone of 1200 mm. Cracks on the elevation started at the precast flange junctions, but showed no distinct preference on their subsequent courses. Some followed the precast concrete profiles, others were nearly vertical. This indicated excellent bond between the insitu and precast concretes under short term, monotonic loadings. There were cracks at all precast flange junctions in the constant moment zone, from which it was deduced that the insitu concrete provided good bond for the transverse reinforcement.

The moment-central deflection curves for the tests showed an excellent degree of agreement see Figure 3 in Appendix 5.2. The effects of tension stiffening were small and calculations for the post-cracking phase based on zero tensile strength gave acceptable predictions of the neutral axis depth.

5.3.2 Tests on longitudinal strips

Tests on composite beams incorporating 1, 2 and 3 rejected prestressed beams, respectively, are described in Appendix 2.5 of Research Report No TRR842/368, produced for the Transport and Road Research Laboratory. However, the results obtained are only of value up to the formation of the first crack in the prestressed beams. These data show that the specimens with more than one precast member have a higher stiffness than do specimens incorporating only one precast member, also see Appendix 5.1.

The reason for this is not completely clear. It is reasonable to suppose that cracking of the confined concretes due to bending stresses would be delayed, however, micro-cracking due to restraint of early thermal contraction is more likely in the confined concretes. The calculated stiffness using specimen moduli is close to the value obtained for the specimens with more than one precast member. This suggests that the stiffening effects of confinement and the effects of greater restraint to thermal contraction approximately cancelled out in those specimens. However, in the specimens with a single precast member, the micro-cracking in the in-situ concrete was, presumably, the dominant effect.

In Appendix 5.1, tests on two composite beams incorporating single precast members of good quality are described. One of these had end plates welded to the tendons to simulate as closely as possible conditions in the model deck. The test results for these specimens provide useful data up to flexural failure.

For loads up to the load levels at which tendons started to yield, the behaviour of the two specimens were similar. The degree of similarity is reflected in the moment-curvature diagrams shown in Figure 5 of Appendix 5.1. It was concluded that the end plates would not affect the model test results until the tendons in a beam started to yield. For greater curvatures, bond failure was possible, but in that eventuality, the end plates would enable a beam to sustain its ultimate moment.

The tests showed that there was no separation of in-situ and precast concretes. Visible cracks did not appear until the prestressed flanges of the precast beams cracked. Cracking was well distributed. From the concrete strain measurements (Table 4, Appendix 5.1) it can be seen that all of the cracks started in the same load increment and continued opening, but that one crack became dominant, with a width about twice that of its neighbours.

5.3.3 Comment

The tests on the longitudinal and transverse strips provided useful information on the flexural behaviour of the deck. The data will be used to assess the capabilities of the material models in the non-linear analytical method to cope with the flexural behaviour of composite construction.

BLANK IN ORIGINAL

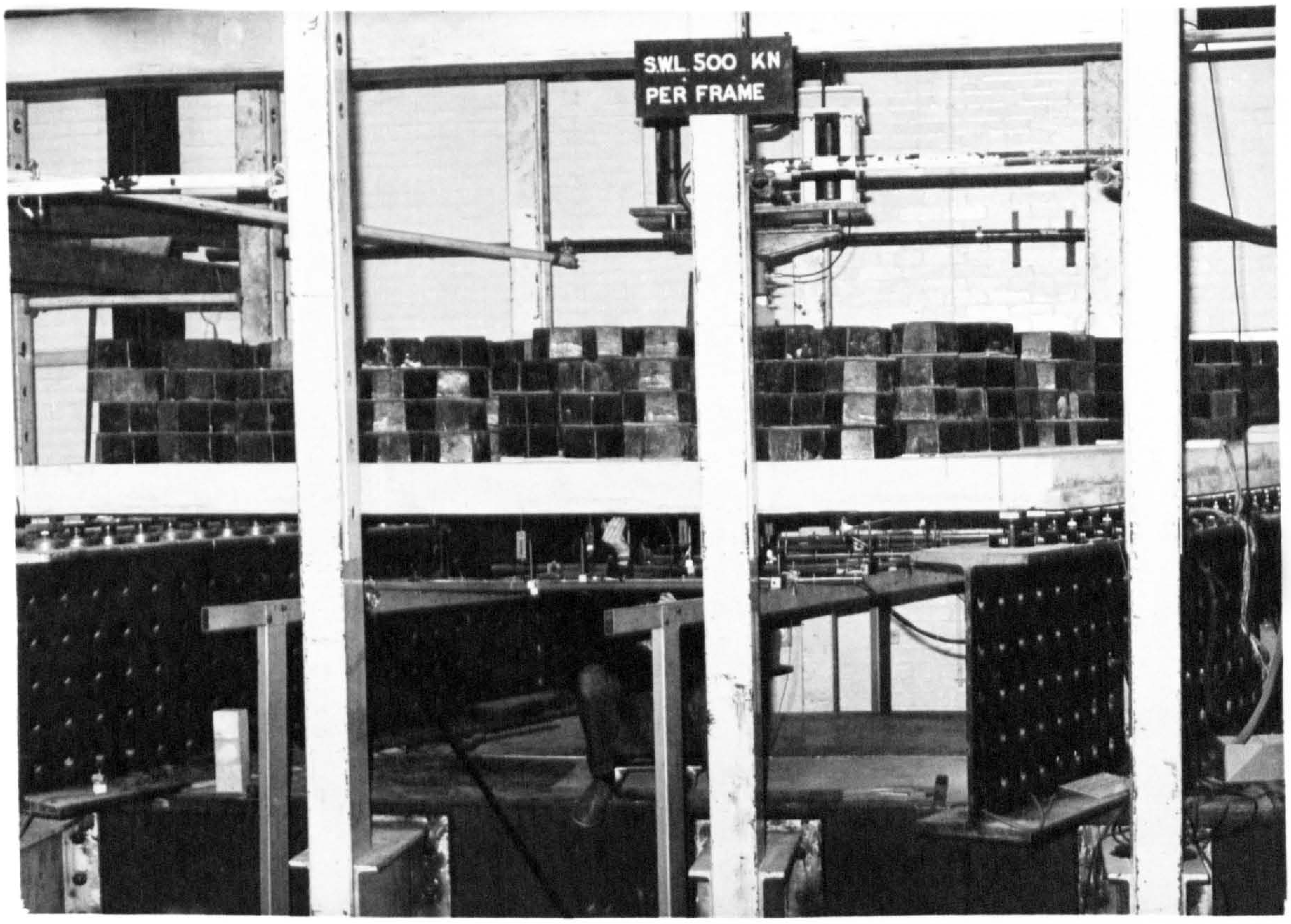

PLATE 5.1 MODEL DECK 1 UNDER TEST

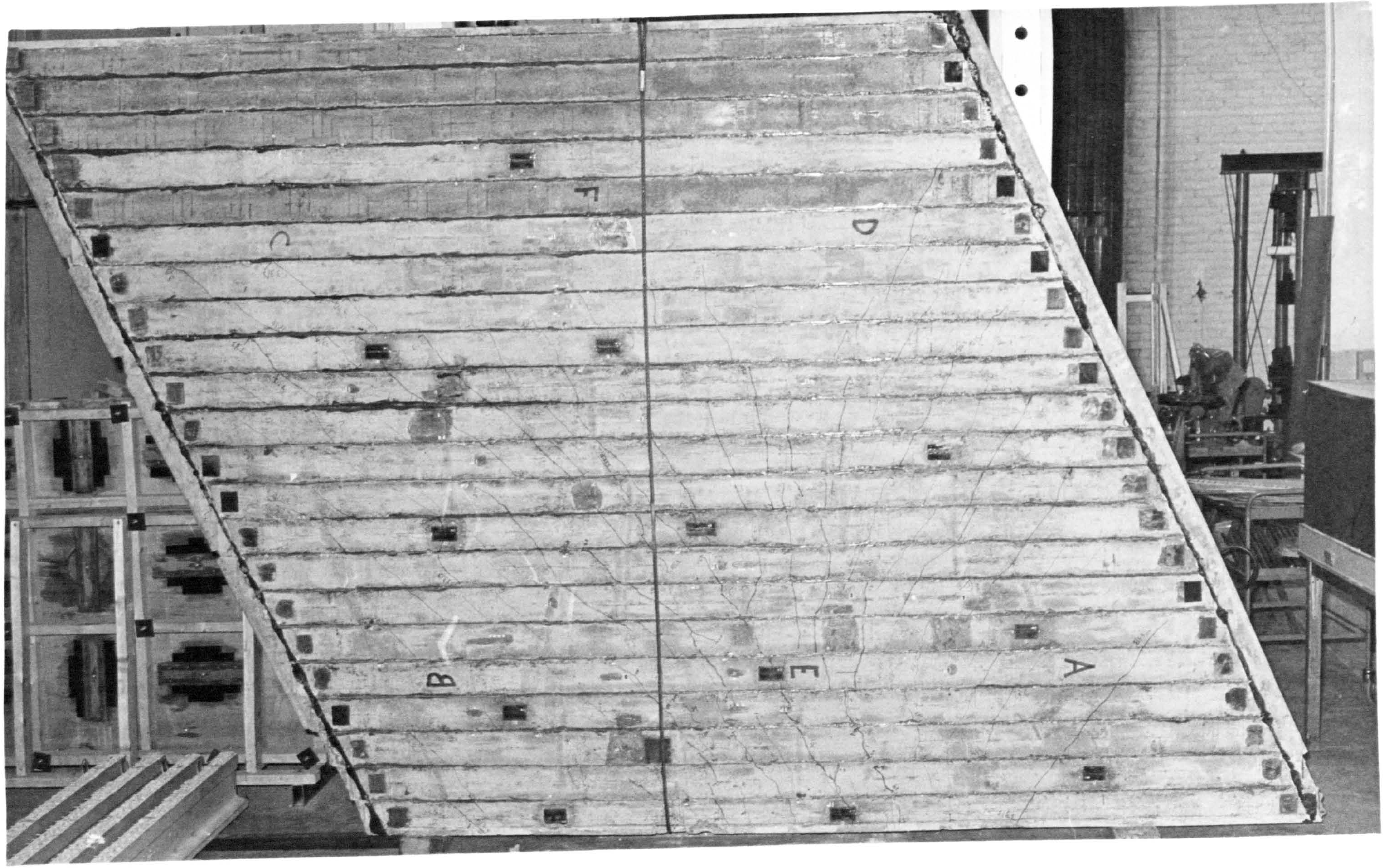

PLATE 5.2 MODEL 1 SOFFIT CRACKING

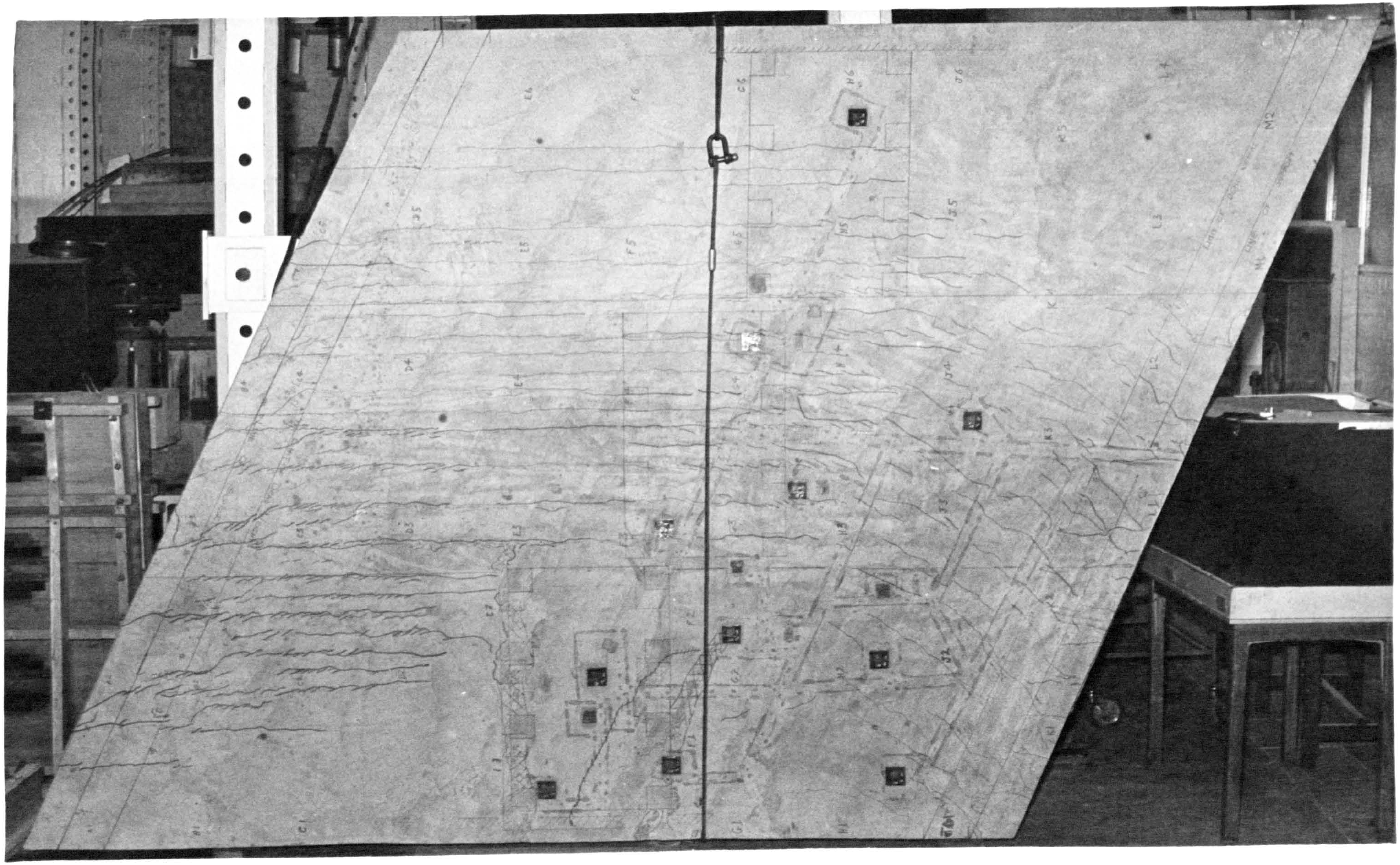

PLATE 5.3 MODEL 1 TOP SURFACE CRACKING

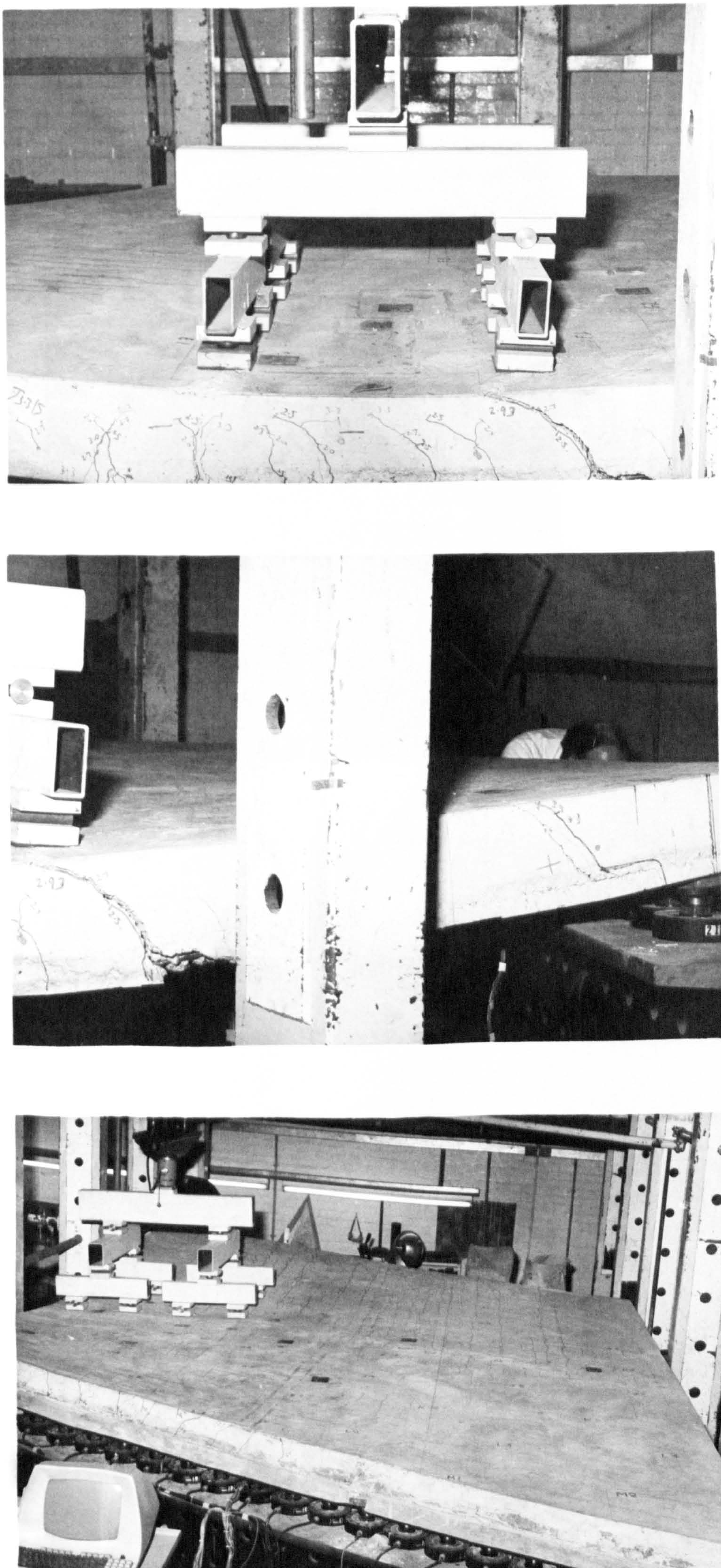

PLATE 5.4 CRACKING ON THE SIDE FACES OF MODEL 1

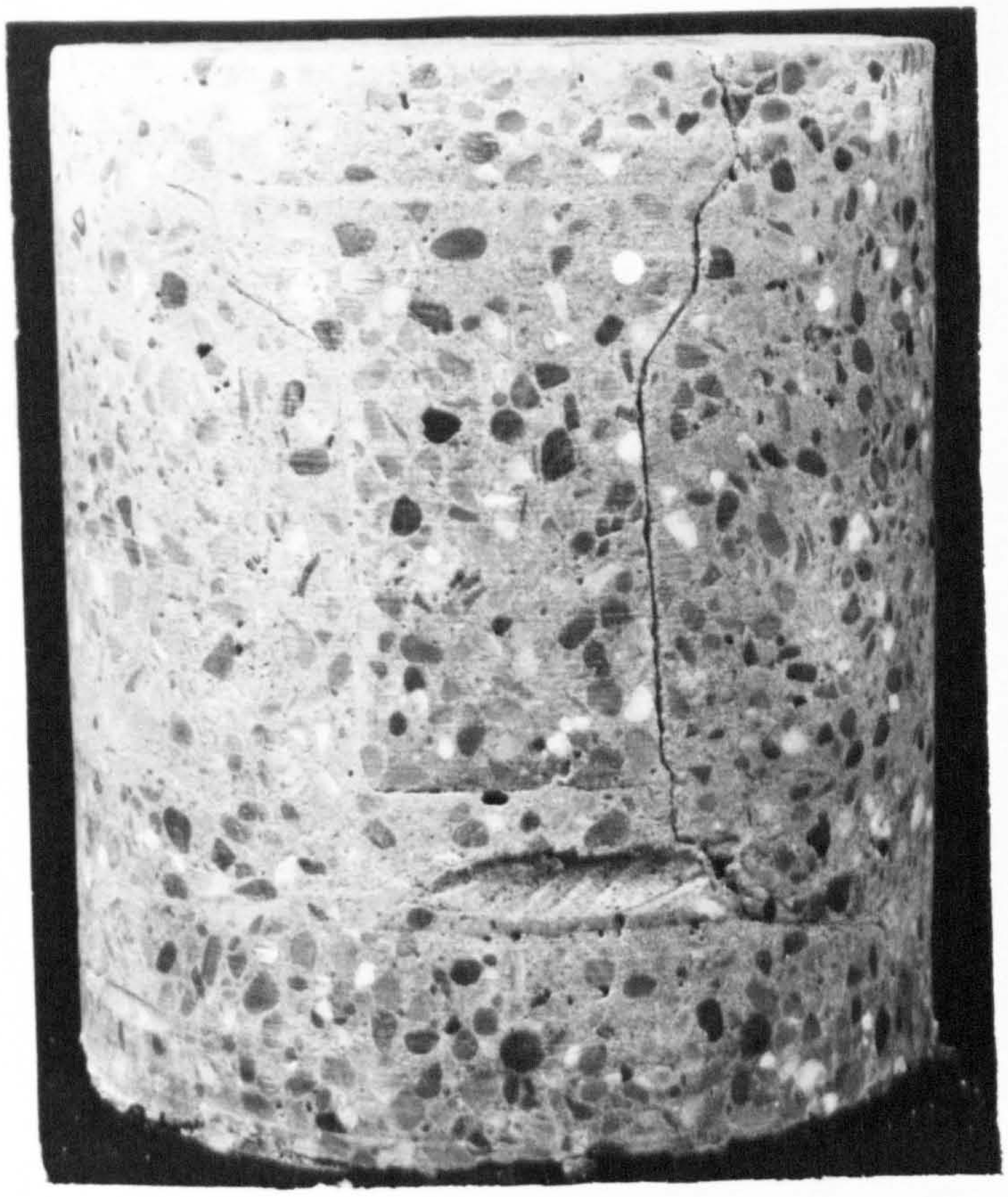

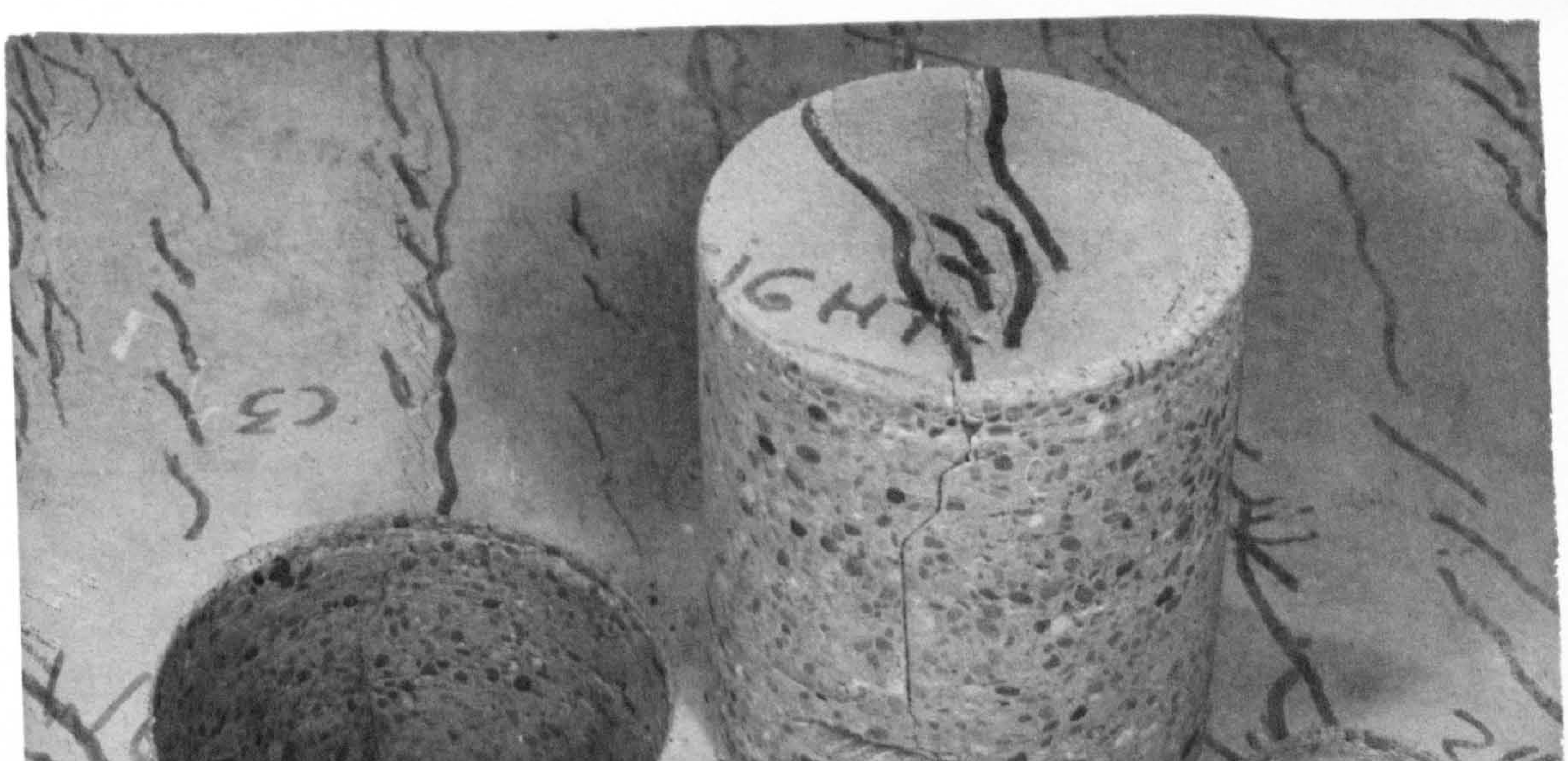

PLATE 5.5 150 MM DIA. CORE THAT WAS REMOVED FROM MODEL 1

6. DESIGN OF MODEL BRIDGE DECK 2

6.1 Introduction

In order that realistic and reliable results could be obtained, model 2, like model 1, was designed at a scale of 1:3.5. This scale factor was the optimum choice considering the constraints of time, finance, experimental errors and testing system resources.

The considerable difficulty that had been experienced during the search for a suitable prototype for model 1 was again experienced with model 2, even though enquiries had been initiated well in advance of the design period. Several different types of organisations were contacted including consultants and County Councils. However, Cheshire County Council kindly made available a design and summary calculations for a structure that was under construction, hence the structure reflected design practice at that time.

The full size structure consists of a three span bridge carrying a 2 lane 5.5 m general purpose road with 1.5 m verges over a 7.3 m two lane carriageway with 3.5 m verges. The skew of the deck is 40° 10' 50". Figures 6.1 and 6.3 show the general layout of the full size section. The deck consists of 17 T10 inverted T beams laid side by side at 525 mm centres. Each beam is prestressed with 19 No 12.5 mm Ø standard 7 strand prestressing tendons, each conforming to BS 5896 1980 and stressed to 115.5 kN. Details of the full size beam section can be seen in Figure 6.4.

The model loading was arranged to provide strain similitude between the full size structure and the model. The loading patterns were modelled on BS 5400 Pt 2 (1978) highway loadings.

6.2 Model Concept

The constraints upon the modelling concept for model 1 in Chapter 4 were also valid for model 2. Therefore, essentially the design concept for model 2 was the same as for model 1. Thus, model 2 incorporated discrete prestressed beams and a weaker concrete for the in-situ slab.

The general details of the model are given in Figure 6.2. The span was set at 4700 mm, the width at 2542 mm and the skew at 40°.

A scale of 1:3.5 was used for model 2. At this scale factor it had been shown with model 1 that the model beams could be accurately constructed and pre-stressed. However, even though the testing frame capacity had been doubled for model 1 the jacking capacity would not be sufficient to ensure failure of model 2 at a scale of 1:3.5. This problem was resolved through the use of a tension jacking system which is more fully described in Chapter 7.

The design calculations for model 2 are not as extensive or detailed as those carried out for model 1 in Chapter 4. It was felt that detailed checking of the Cheshire County Council design was not necessary since the design was modern and hence reflected current design practice. Model section strengths were checked against scaled prototype section strengths, and a check at the Ultimate Limit State was carried out using the yield line method.

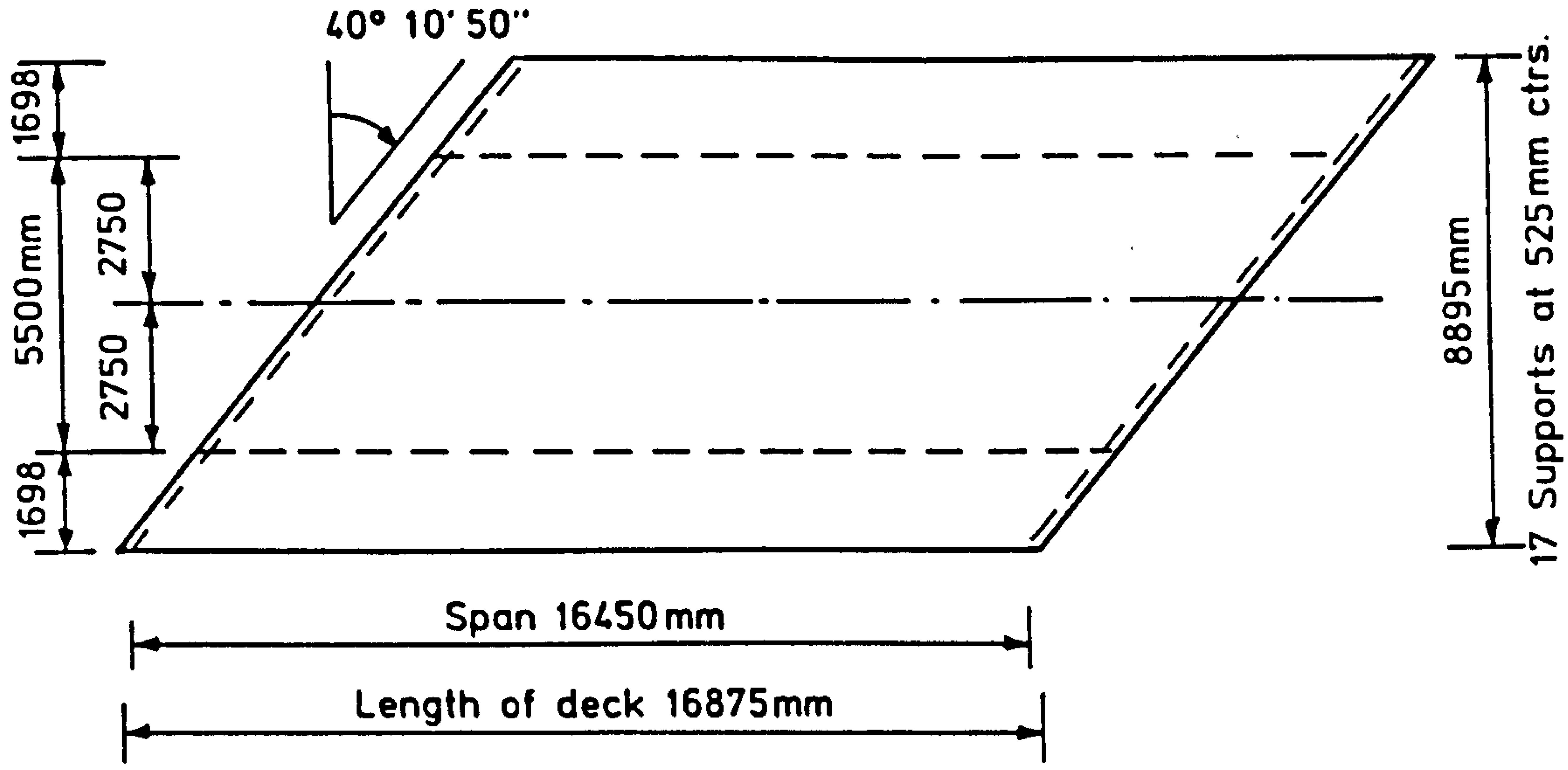

FIG. 6. 1. GENERAL DETAILS OF FULL SIZE DECK 2

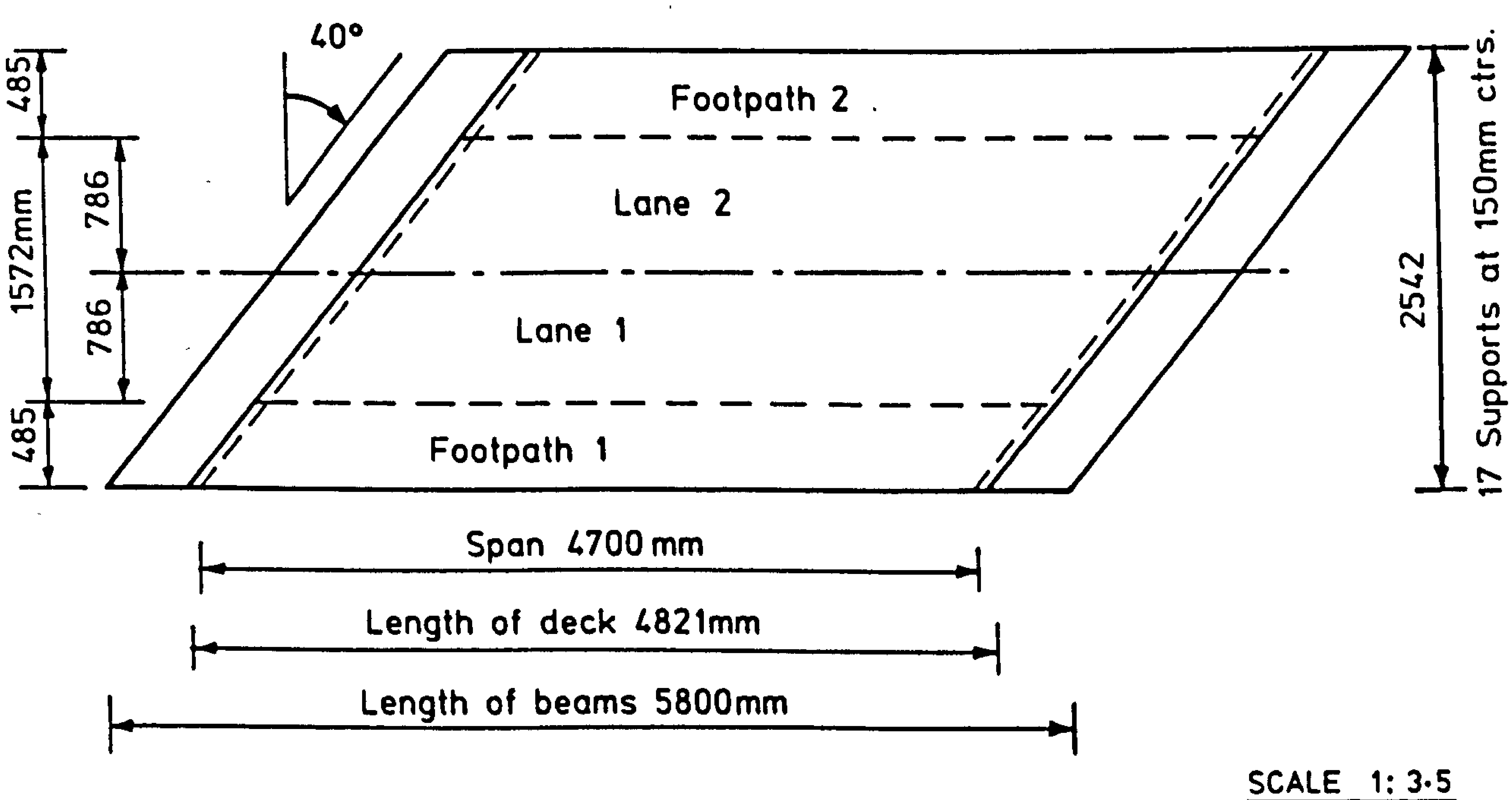

FIG. 6. 2. GENERAL DETAILS OF MODEL DECK 2

Summary calculations, including the data file for the STRAND2 finite element program were provided by Cheshire County Council. These indicated that isotropic properties had been employed for the STRAND2 analyses. Also, it appeared that the parapets were modelled in the STRAND2 analyses as equivalent stiffness concentric edge beams. At failure it was assumed that the parapets could not be considered to act as structural elements. Therefore, the high moments that the parapets attracted due to the eccentricity of the upstanding concrete were allocated to the three adjacent beams in the ratios 5/9, 3/9 and 1/9, respectively. As all of the beams were made the same as the edge beam, this resulted in a bridge deck having a high factor of safety against overall collapse.

6.3 Loading

The scaled 5.5 m carriage way of the model was considered to have two notional lanes (BS 5400 Pt 2 (1978) cl 3.2.9.3) each 786 mm wide. All loading was modelled on BS 5400 Pt 2 (1978), however, the BS 5400 HB bogie was too wide to fit into one lane of the 5.5 m carriageway (BS 5400 Pt 2 (1978) cl 6.4.2). The bogie dimensions given in BS 153 are smaller than those stated in BS 5400 and allowed the wheels of a bogie to fit into one lane. Therefore, considering the design of the prototype; the possibility of widening the carriageway through the removal of the verges; and the spirit of the code, the model was analysed with a HB bogie in lane 1 and co-existant HA loading in lane 2.

Seven nominal load components were considered:-

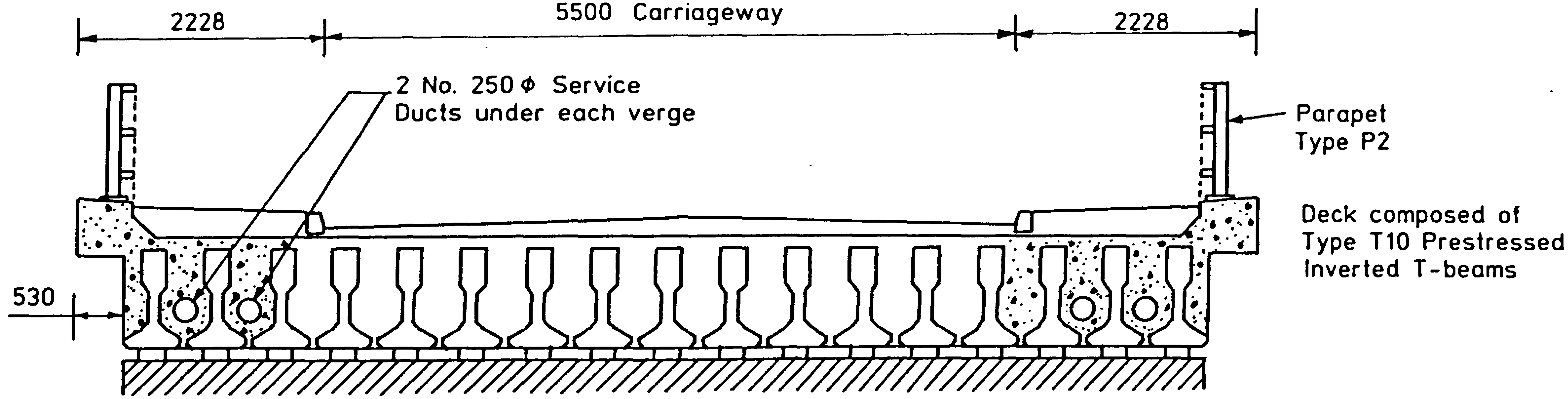

FULL SIZE DECK 2 SECTIONS

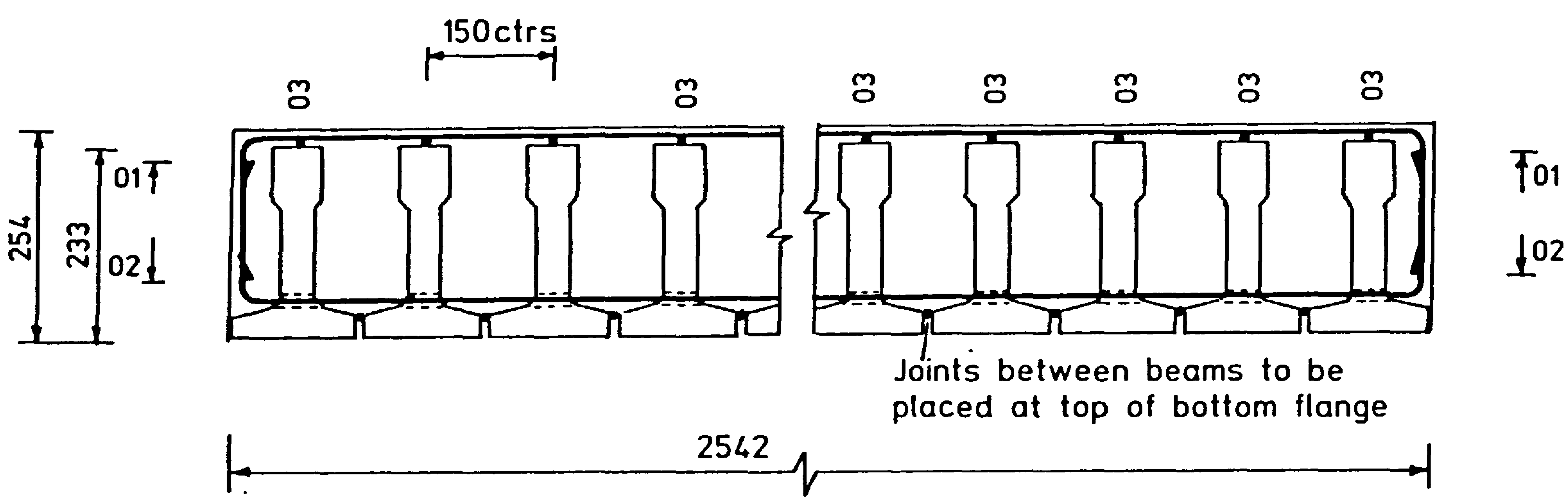

MODEL DECK 2 SECTION

FIG. 6.3. SECTIONAL END ELEVATIONS OF FULL SIZE AND MODEL DECK 2

1. Model self-weight over the complete slab area of 5.98 x 10^{-3} N/mm^2
2. Density correction loading over the complete slab area of 14.95 x 10^{-3} N/mm^2
3. Superimposed dead loading over the complete slab area of 2.4 x 10^{-3} N/mm^2
4. Footpath live loading along both footpaths of 2.31 x 10^{-3} N/mm^2
5. HA UDL in lane 2 of 10.91 x 10^{-3} N/mm^2
6. HA KEL at mid-span in lane 2 of 9796 N
7. 45 units of one HB bogie in lane 1 at mid-span of 73470 N.

Values for γ_{f1} (load partial safety factor) obtained from BS 5400 Pt 2 (1978) Table 1 were applied to the load component values when they were combined into load cases for the yield line analysis.

6.4 Bearings

It is recognised that the bending moment and shear force distribution in the support region are highly dependent upon the spacing and stiffness of the supports. Great care was taken to produce model bearings that exhibited similar properties to those used in the full size design. To this end tests were carried out on many rubber types to obtain their physical property parameters. In its final form, the model bearing consisted on a rubber and steel sandwich in an elastomeric format. The model bearing had a stiffness of 40.4 kN/mm, which corresponds to a full size stiffness of 141 kN/mm. The design of the bearings is more fully described in Chapter 3.

6.5 Model Bridge Deck 2 Design

A descriptive account of the design of model 2 is given here, and criteria and significant results are included. Detailed calculations,

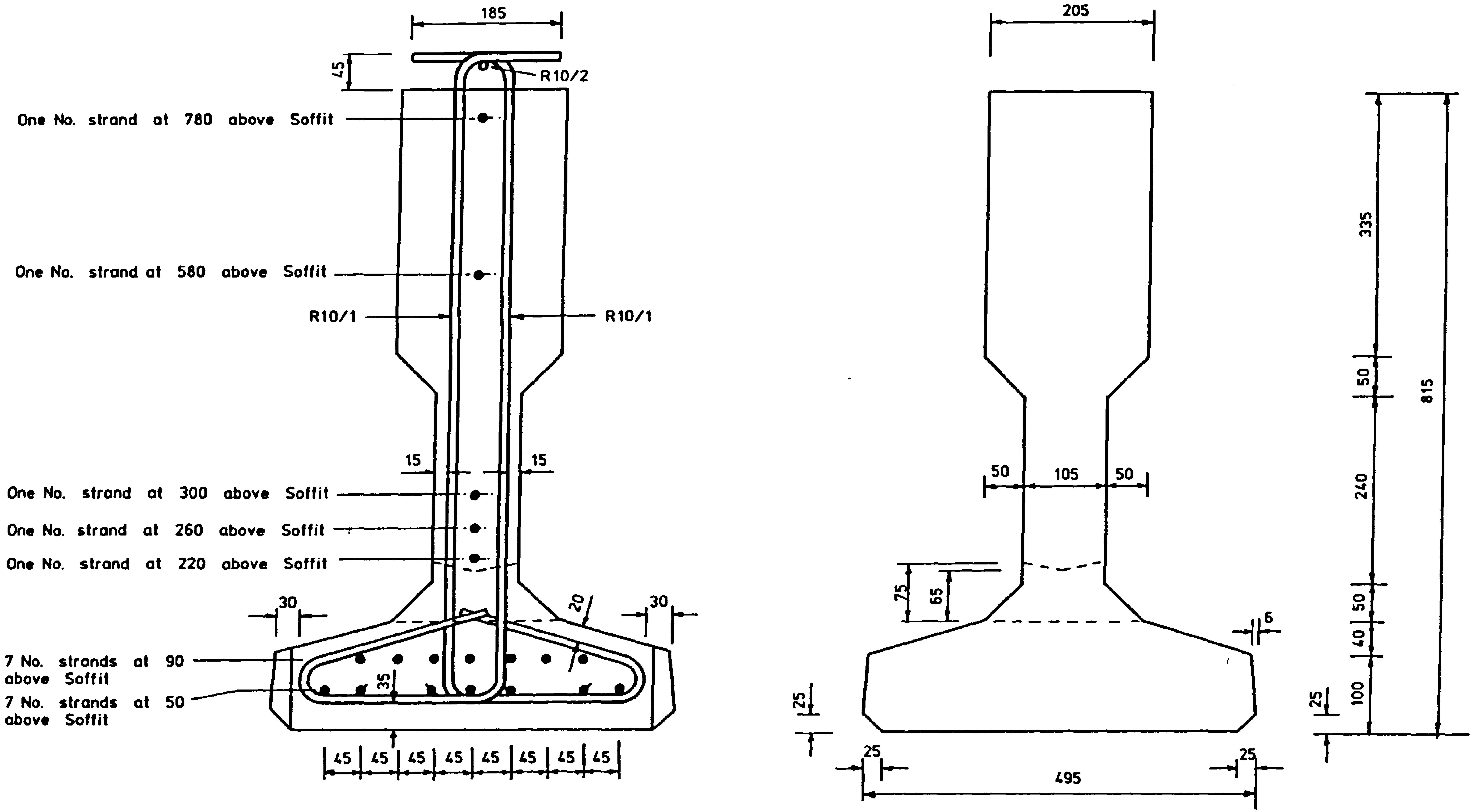

FIG. 6.4. END ELEVATION OF FULL SIZE DECK 2 PRECAST BEAMS SHOWING GEOMETRICAL AND REINFORCEMENT LAYOUT

where appropriate, are given in the Appendices of Research Report No TRR 842/368, produced for the Transport and Road Research Laboratory (hereafter referred to as the Report).

6.5.1 Model Beam Design

The dimensional details of different members of the standard T beam family are identical, except for the overall height and the depth of the top flange. Therefore, the model 2 beam profile is similar to that of model 1. As with model 1, the model 2 beam profile and its properties were kept as close to scale as possible. For model 2, the web thickness was maintained at 40 mm to facilitate successful manufacture. The overall height was fixed at the scale value of 233 mm. It was necessary to enlarge the top flange to allow the geometric properties of the T10 beam to be modelled accurately. The bottom flange detail of the section was also amended to increase the accuracy of the geometric properties. A comparison of these properties is given in Tables 6.1 and 6.2. It can be seen from these tables, that the errors are generally less than 3.5% for the principal geometrical properties.

	Geometry			Prestress		
	A (mm^2)	X (mm)	I (mm^4)	Average (N/mm^2)	Top (N/mm^2)	Soffit (N/mm^2)
Prototype	171560	356	12.39×10^9	-12.79	2.82	-24.89
Scaled Prototype	14005	102	82.56×10^6	-12.79	2.82	-24.89
Model	14470	101	85.47×10^6	-13.42	1.56	-24.89
Percentage Difference	3.3%	0.7%	3.5%	4.9%	44.7%	0%

TABLE 6.1 Comparison between Prototype and Model Beam Section Geometrical Properties

	Steel Details				Moment Details	
	Area		Centroid Ecc. From NA		Decomp. Moment	Ultimate Moment
	Pres. (mm^2)	Rein. (mm^2)	Pres. (mm)	Rein. (mm)	(Nmm)	(Nmm)
Prototype	1767	78.5	-164.2	489	866.7×10^6	1.63×10^9
Scaled Prototype	144.2	6.4	-46.9	140	20.21×10^6	38.0×10^6
Model	153.2	56.5	-49.3	119	21.06×10^6	40.2×10^6
Percentage Difference	6.2%	-	5.1%	14.8%	4.2%	5.3%

TABLE 6.2 Comparison between Prototype and Model Beam Steel and Moment Properties

The prestress in the full size beams is provided by 19 No 12.5 mm Ø prestressing strands. For model 2, only a limited range of strands and wires were available, all with different material properties, bond behaviour, and diameters. The majority of material and physical properties for these products are the subjects of standard tests and, therefore, reasonably accurate guides can be obtained from manufacturers literature. However, the bond performance of the available products is not well documented.

After considering the critical nature of the bond properties, a comprehensive series of tests was initiated to obtain definitive data on the available products. Appendix 4.5 of the Report deals with these tests in detail, however, in summary, the bond properties of the strand were found to be far superior to those of wire, whether the wire was plain; physically roughened or crimped.

The criteria for selecting the model prestressing system were:-

1. The area of steel to be as close to scale as possible.
2. The lever-arm for the composite slab and the eccentricity from the beam neutral axis, to be as close to scale as possible.
3. The prestress in the top and bottom fibres to be similar to that in the full size beam.
4. The prestress in the tendons to be at approximately the same proportion of the characteristic strength of the steel as in the full size beams, taking into account the different stress-strain relationships when appropriate.
5. The bond properties to ensure similar behaviour in the model and the full size beams.
6. The ultimate moment of the model longitudinal section to be as close to scale as possible.

The chosen prestressing arrangement, which is shown in Figure 6.7, incorporated the smallest diameter strand that was available. Even so, there was an over provision in the steel area of 6%. However, the excellent bond properties of the strand, compared to the wire, outweighed this small error. Consequently, the ultimate moment of resistance was in error by 5%. However, the important soffit prestress level was modelled exactly. Sufficient tendons were provided in the full size beams to allow gradual debonding towards the ends of the beams. However, in the model, the reduced number of tendons dictated that a fully bonded design had to be adopted.

In addition to the prestressing, a nominal amount of reinforcement was added to the top flange. The relatively low self-weight of the beams (no density correction could be applied at this stage), and the fully bonded design combined with the prestress to produce small tensile stresses in the beam top fibre. The reinforcement was, therefore,

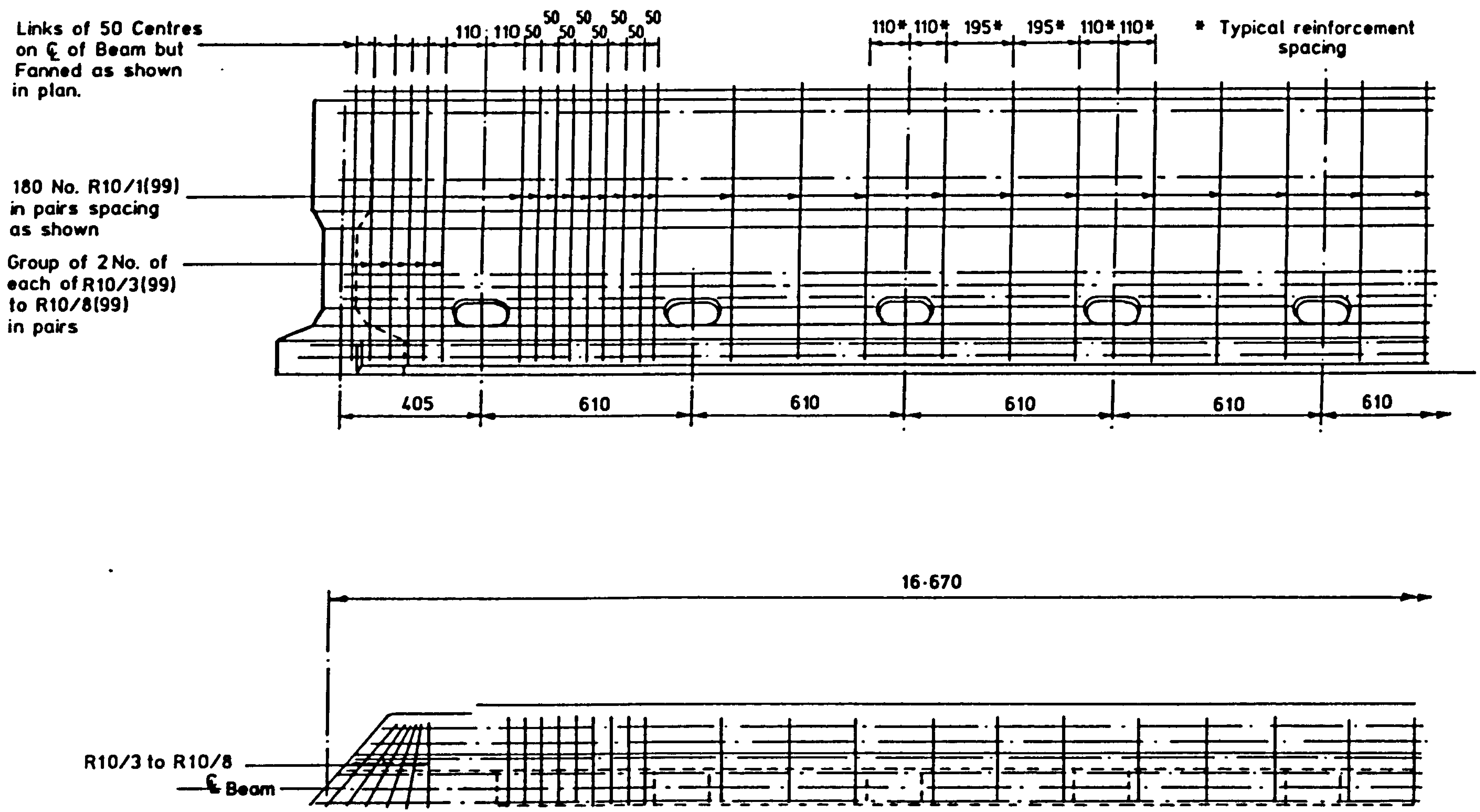

FIG. 6. 5. DETAILS OF FULL SIZE DECK 2 PRECAST BEAM TRANSVERSE HOLE AND SHEAR REINFORCEMENT LAYOUT

included to ensure that a stable condition with small crack widths would result if cracking occurred. This reinforcement accounts for the large difference in Table 6.2 for the area of reinforcement. However, it was considered that this would not have a significant effect upon the model behaviour, as its position close to the composite slab neutral axis would result in little change to the section properties. The drawings in Figure 6.7 give the final section profile and prestressing details.

6.5.2 Ancillary Deck Reinforcement

The lower transverse steel was threaded through preformed holes in the beam webs. Unlike model 1, where the lower transverse reinforcement was parallel to the supports, model 2's reinforcement was aligned at 108° to the beam axis, see Figure 6.6.

Initially a feasibility study was carried out to investigate the options that were available to model this reinforcement arrangement. Exact scaling was not a practical option, considering the limited range of small reinforcing bars that were available and the complexity of manufacture. Unless an exact multiple of the scaled hole spacing was employed, a number of different types of beam would be required. The optimum configuration, from all of the options that were considered, incorporated a hole spacing of 261 mm which is 1.5 times the scale value. The reinforcement was arranged in alternate bundles of 3 and 4 bars of 6 mm Ø Torbar through the web holes. The resulting area of steel per unit length was only 0.5% greater than the required scale value. Theoretically three different beam types are required for this arrangement. However, with a ragged edge to the slab, two beam types suffice. Thus, the two beam types of Figures 6.8 and 6.9

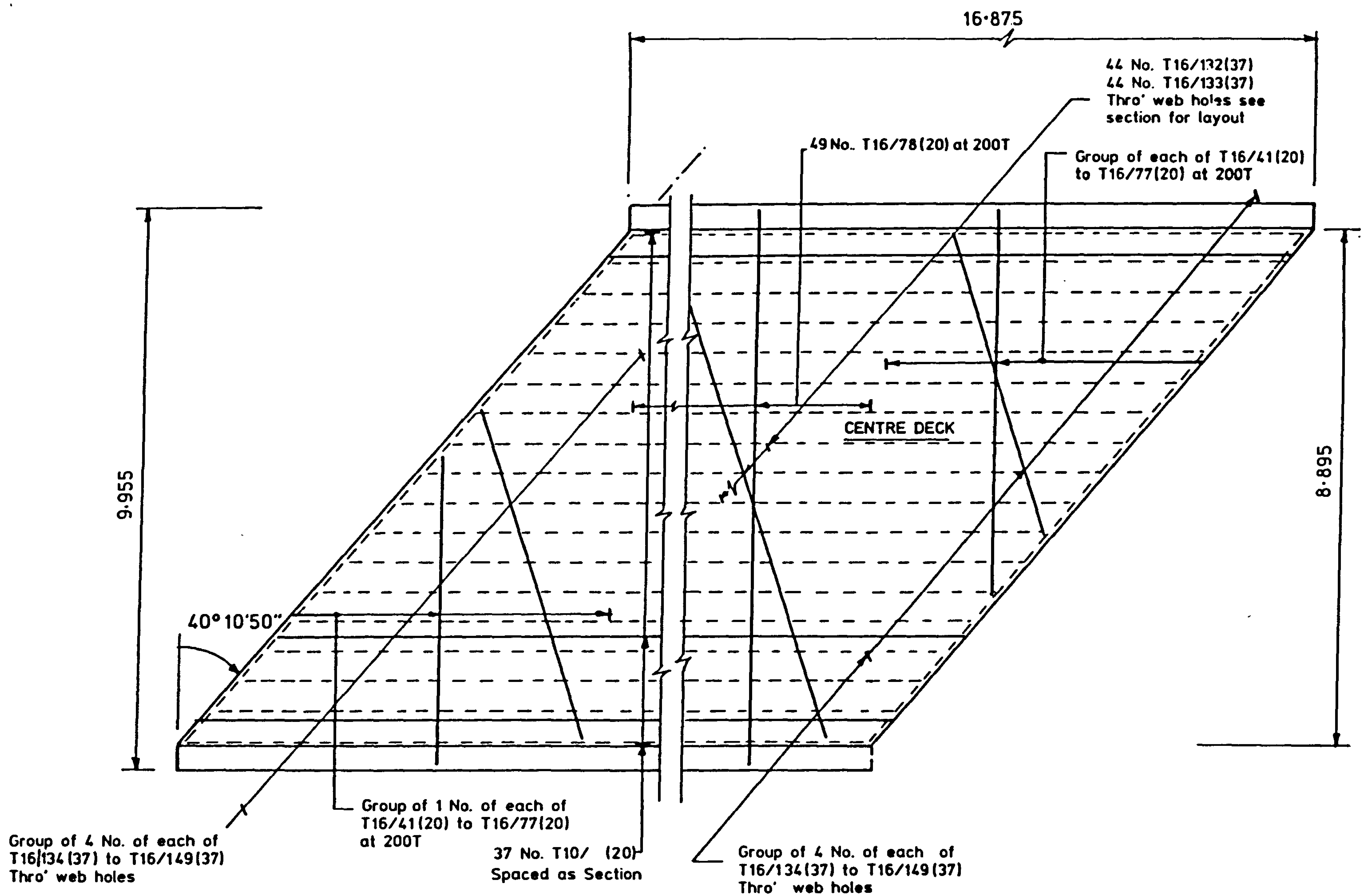

FIG. 6.6. REINFORCEMENT LAYOUT FOR FULL SIZE DECK 2

were specified. Details of the full size lower transverse reinforcement layout are shown in Figures 6.5 and 6.6.

A similar philosophy was adopted for the top transverse reinforcement, however, a complex arrangement was not required in this case. Details of the chosen arrangement, consisting of 6 mm Ø Torbar at 97 mm centres, can be seen in Figure 6.10.

Nominal longitudinal top reinforcement, in the form of one 3 mm Ø mild steel bar above each beam, was included for crack control and to allow easier placement of the top transverse steel. Negligible longitudinal hogging moments were expected. Moreover, the small required ultimate moment of resistance was provided by the extra beam reinforcement.

The full size deck included parapets along each free edge, see Figure 6.3. However, for the model, it was felt that these details were not necessary, considering their small effect on behaviour and also the unnecessarily increased complexities in construction and interpretation of results for the free edge regions that would otherwise be necessary. One would not expect the parapets to increase the ultimate capacity of the slab due to their early failure in an overload situation.

Essentially, the reinforcement layout in the full size deck is uniform, see Figure 6.6, except for the regions adjacent to the parapets. As the parapets were not being modelled, a uniform reinforcement arrangement was specified for the model.

6.5.3 Ultimate Limit State Check

For the Ultimate Limit State check, design moments of resistance were

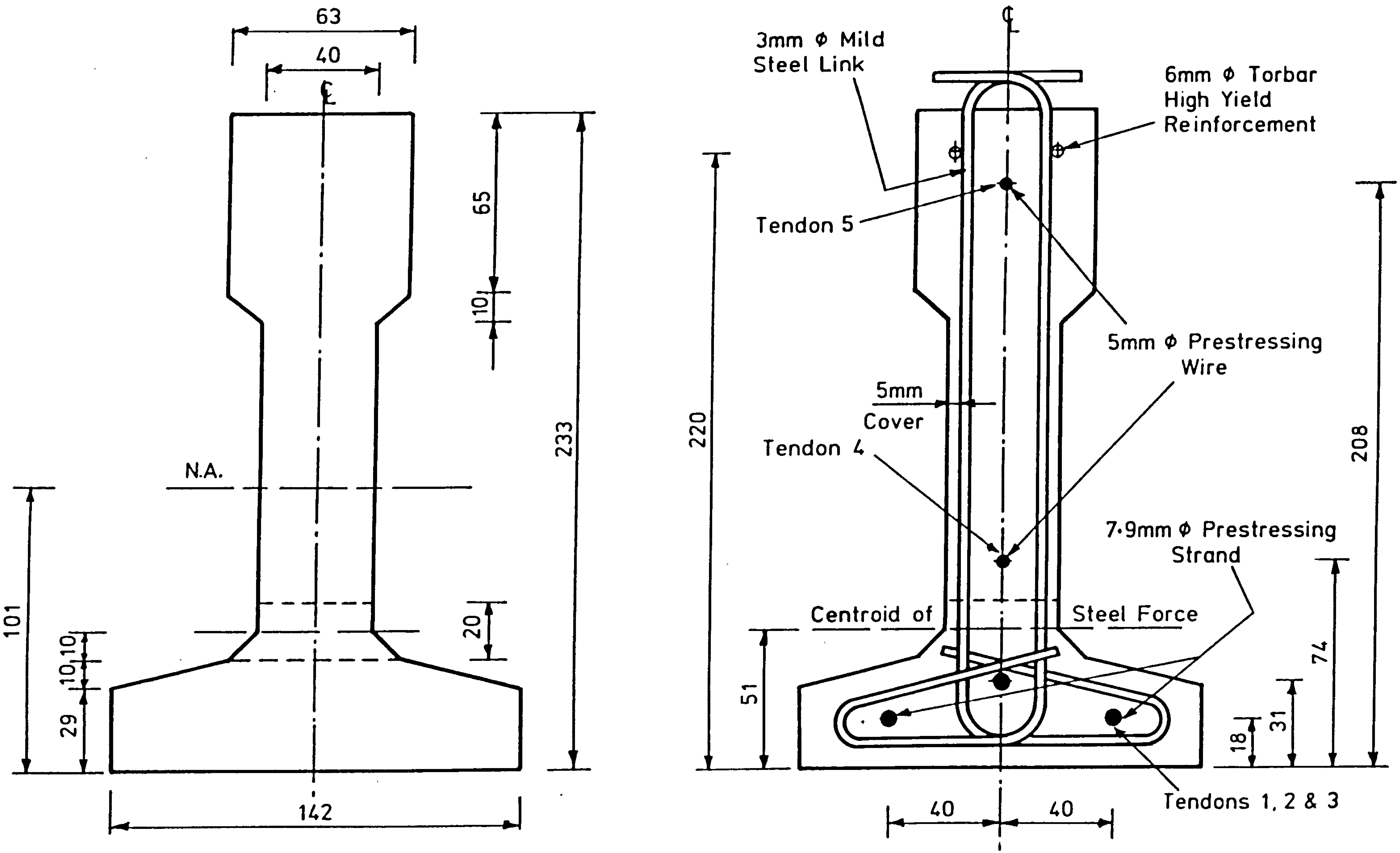

FIG. 6.7. DETAILS OF MODEL 2 BEAM PROFILE AND PRESTRESSING LAYOUT.

calculated in accordance with BS 5400 Pt 4 (1978) and the details of these calculations are given in Appendix 4.1 of the Report.

These moments of resistance were required in the yield line analysis[1,2] that were used to assess the model's safety factor against global failure. The details of these calculations are given in Appendix 4.3 of the Report. In summary, this investigation revealed that the model possessed a high factor of safety against global failure. For the prestressed inverted T beam, with in-situ fill form of construction, the prestressing and reinforcement arrangements is designed for the critical location. Subsequent provision of these arrangements in a uniform manner results in an inherently high factor of safety against global failure. Many different yield line patterns were investigated, and it was shown that the simplest pattern involving a single sagging yield line at mid-span was the most critical. The provided moment of resistance was 268 kNmm/mm, while the moment required by the most critical yield line mechanism with design ultimate loading was 145 kNmm/mm.

6.5.4 Shear Design

Shear reinforcement design:- All the shear reinforcement in the full size slab is provided by shear links contained within the prestressed beams, see Figure 6.4. The full size shear reinforcement layout is uniform along the central region of the span, becoming denser towards each support. For the central region, three R10 shear links, each with two legs are provided at 610 mm centres, see Figure 6.5. The smallest practicable size mild steel rod that could be used for the model shear links was 3 mm Ø. Therefore, with the modified beam transverse hole spacing, an accurately scaled shear resistance was obtained by providing four R3 shear links, each with two legs at 261

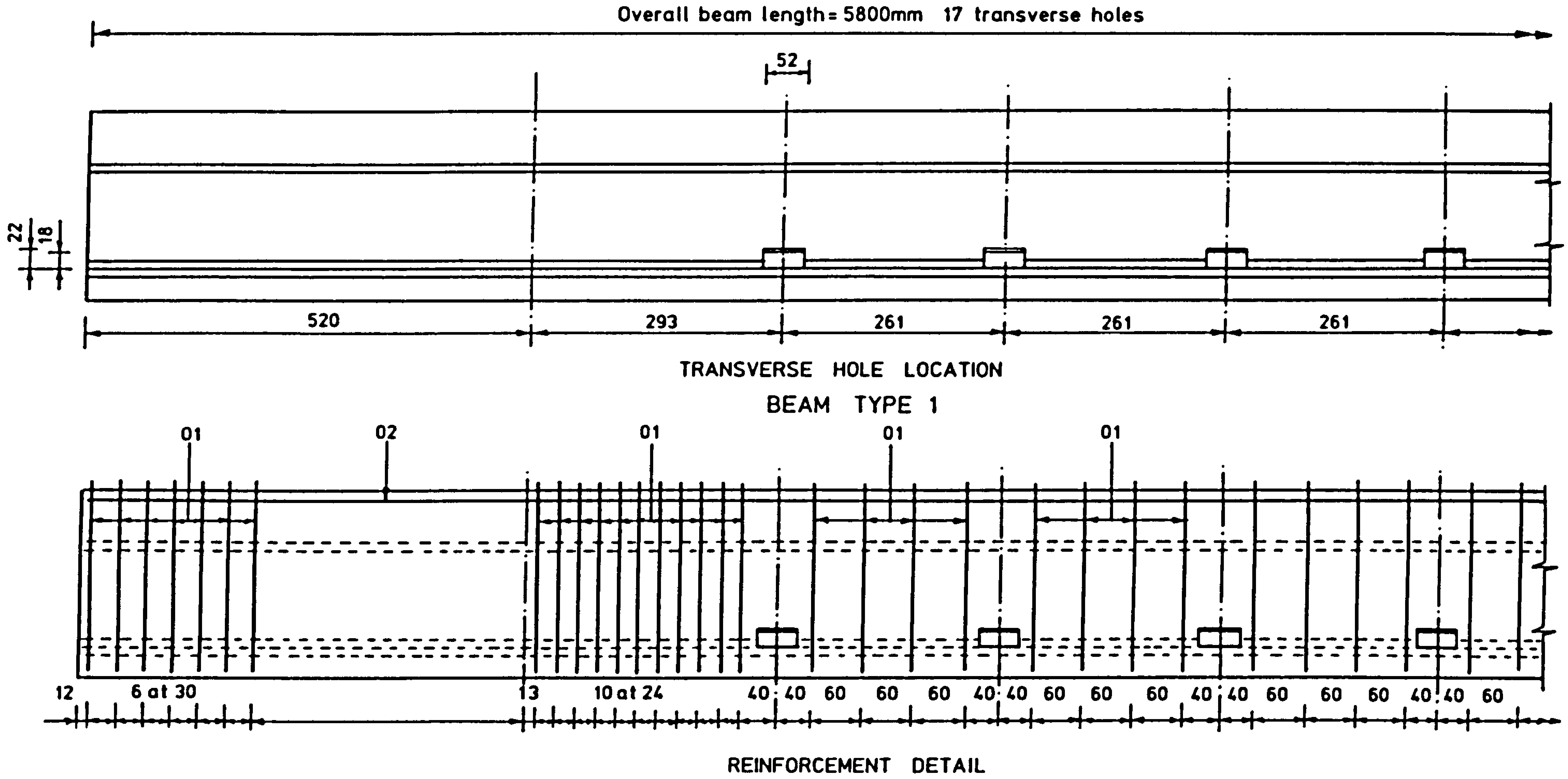

FIG. 6.8. DETAILS OF MODEL DECK 2, PRECAST BEAM TYPE 1 TRANSVERSE HOLE AND SHEAR REINFORCEMENT LAYOUT.

mm centres for the central region. At all times, the shear reinforcement design criteria of BS5400 Pt 4 (1978) were applied to the model shear link design.

In the full size beams, the density of the shear reinforcement is increased towards the ends of the beam to resist vertical shear and coexistant splitting actions. The length of the model beams was greater than the scale length and hence the most severe effects of vertical shear and splitting occurred at different sections. Therefore, the shear reinforcement at the end of the model beams was detailed to resist splitting only, using a method suggested by Green[3]. This method, which is conservative, applies a deep beam analogy to the problem. The resulting arrangement extended as far as one effective depth from the end of the beam and is shown in Figure 6.8. The shear reinforcement adjacent to the supports was redesigned in accordance with BS 5400 Pt 4 (1978) using shear intensities obtained from the calculations provided by the prototype designers. Along the end region of the full size beam, the area of shear reinforcement per unit length was calculated at various sections. These values were scaled down and mapped onto the relevant part of the model beam. From these values, the number of links for each section were calculated. The links were spaced to give good distribution while also ensuring adequate clearance to the transverse holes.

The shear link profile was designed to give adequate protrusion from the tops of the beams to provide a good connection with the in-situ concrete, while also allowing 5 mm cover to the sides of the beam webs. The shear links were designed to encircle all of the longitudinal steel, while also encompassing the majority of the bottom flange area and allowing simple manufacture. The chosen shear link

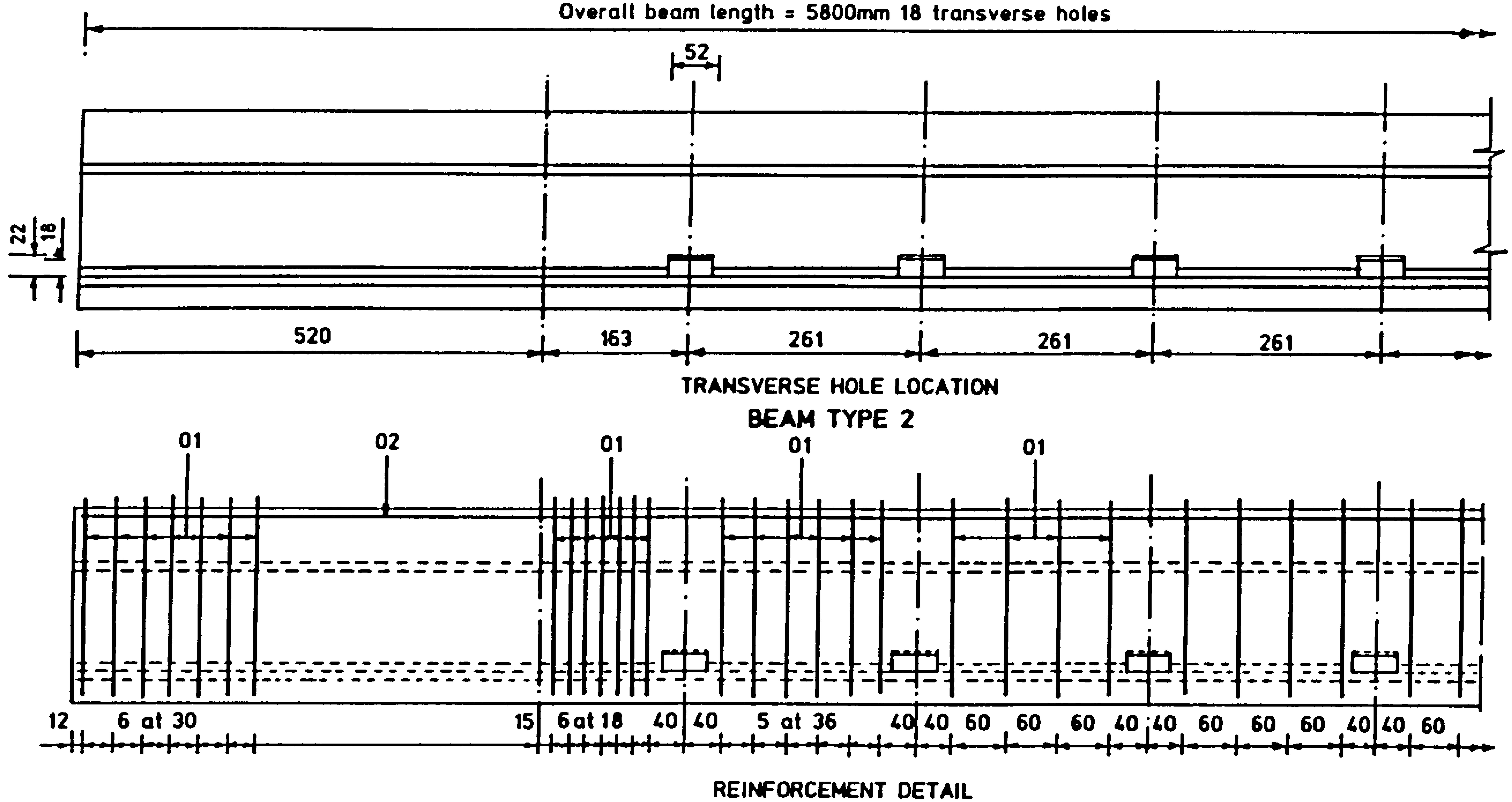

FIG. 6.9. DETAILS OF MODEL DECK 2 PRECAST BEAM TYPE 2 TRANSVERSE HOLE AND SHEAR REINFORCEMENT LAYOUT.

profile can be seen in Figure 6.7. It will be noticed that the model profile agrees closely with that of the full size beam shown in Figure 6.4.

6.5.5 Detailing

Transverse holes:- The shape of the model 2 transverse beam holes were similar to those in the full size beams, see Figures 6.4 and 6.7 However, the size of the model holes were increased over the scale size to accommodate the larger amount of scaled transverse reinforcement that passed through each model hole. The walls of each model hole were square to facilitate simpler manufacture while the hole axis was aligned along the lower transverse steel, at 108° to the beam axis, to allow optimum use of the hole. To cater for the larger than scale web thickness, the invert of each hole was inclined to allow the insitu concrete to flow freely resulting in well compacted concrete around the reinforcing bars.

Cover:- The model cover was standardised at 7 mm, although the cover between the shear links and web sides was reduced to 5 mm. However, this surface is subsequently encased in in-situ concrete. At 7 mm, the standard cover is approximately 18% less than scale so that the larger than scale reinforcing bars could be accommodated.

Concrete:- Every attempt was made to ensure a high level similitude between the model and full size concretes.

Precast Concrete:- A 52.5/20 concrete is specified for the prototype deck which was represented by a 52.5/6 concrete in the model. Generally for precast prestressed concrete, the cube strength at transfer is the major criterion upon the mix design. For model 2, a

FIG. 6.10. REINFORCEMENT LAYOUT FOR MODEL DECK 2

transfer strength of 40 N/mm^2 was specified, which is identical to that specified for model 1 and, therefore, the same mix design was used. It was known that this mix would achieve a 28 day cube strength in the range 58-65 N/mm^2 and would, therefore, meet the specification. A cycle time of 7 days was planned for the precast beam casting. This allowed a 5 day curing period with 2 days for preparation and casting of the subsequent set of beams. Details of the mix for the precast beams and the aggregate grading curve, can be seen in Appendix 1.2 of the Report.

In-situ Concrete:- A 45/20 concrete is specified for the full size in-situ and therefore a 45/6 concrete was specified for the model. A 40/6 concrete had been used for model 1 and this mix was modified to produce the 45/6 concrete that was required for model 2. Details of this in-situ concrete mix, and the aggregate grading curve can be seen in Appendix 1.2 of the Report.

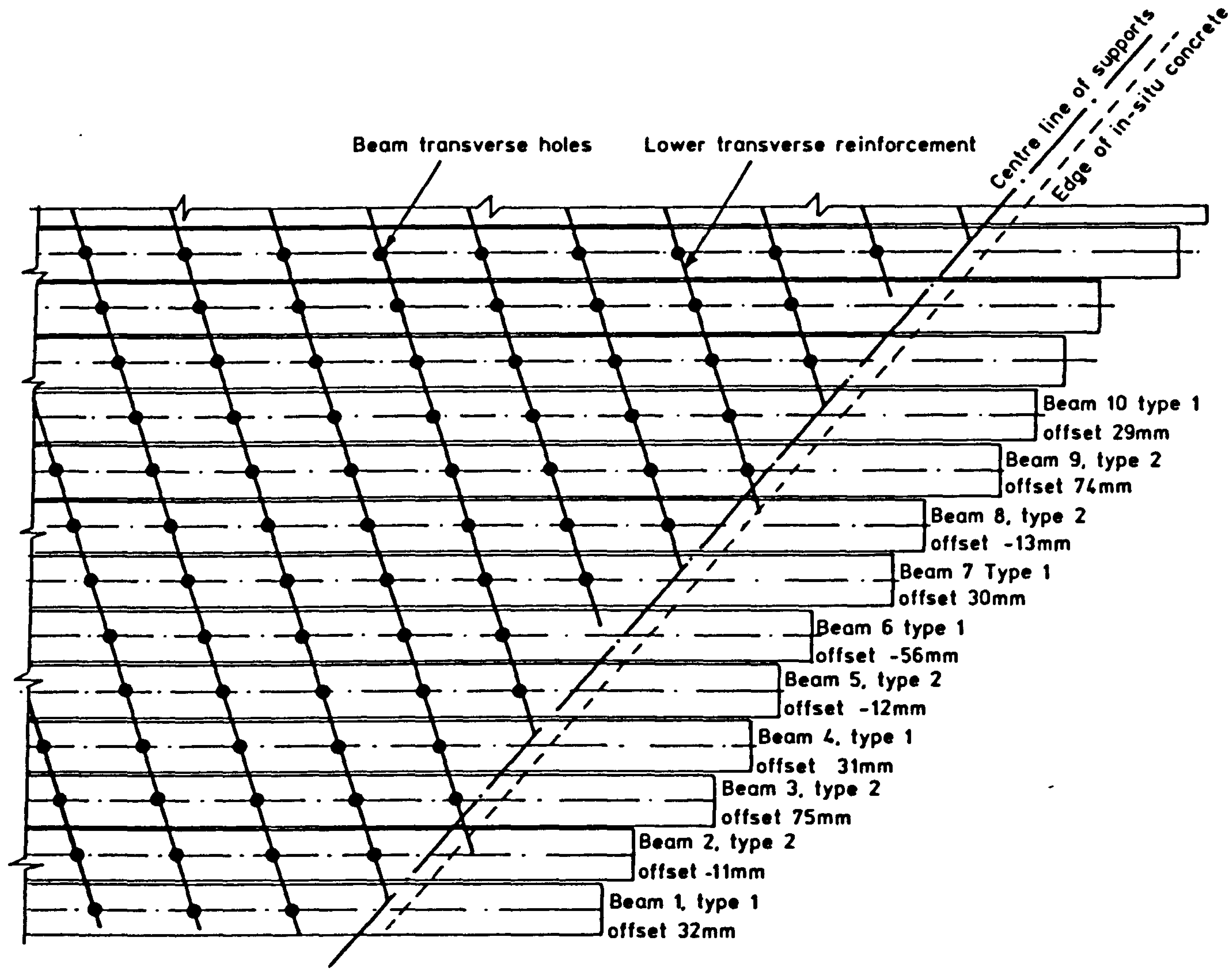

FIG. 6.11. OFFSET PRECAST BEAM DETAIL FOR MODEL DECK 2

6.6 References

1. Kong, F.K., Evans, R.H., 'Reinforced and Prestressed Concrete', Thomas Nelson and Sons Limited, 1977.

2. Clark, L.A., 'Concrete Bridge Design to BS5400', Construction Press, (1983).

3. Green, J.K., 'Detailing for standard prestressed concrete bridge beams', Cement and Concrete Association, Publication 48.018, 1973, p 21.

BAR LOCATING TABLE					
			Bending Schedule No.		
Bar	Type	Grouping	Shape	Ctrs.	No.
		Type 1			
01	R3	2*7*2	99	30	28
01	R3	2*11*2	99	24	44
01	R3	2*64*1	99	60	128
02	Y6	2*1	20		2
		Type 2			
01	R3	2*7*2	99	30	28
01	R3	2*7*2	99	18	28
01	R3	2*6*2	99	36	24
01	R3	2*60*1	99	60	120
02	Y6	2*1	20		2

NOTES

1 Concrete 52.5/6

2 Cover - General 5mm. min

PRESTRESSING

3 All Tendons to BS5896 -1980

4 Tendon forces
1 = 49.5kN
2 = 49.5 kN
3 = 49.5kN
4 = 23.5kN
5 = 23.3kN

5 Minimum cube strength of transfer 40N/mm.

6 Tendon sizes:-
1-3 7.9mm ϕ low relaxation 7 wire strand
4-5 5mm ϕ low relaxation triple indented wire

FIG. 6.12. NOTES AND BAR LOCATING TABLE FOR MODEL DECK 2 PRECAST BEAMS

BAR LOCATING TABLE					
			Bending Schedule No.		
Bar	Type	Grouping	Shape	Ctrs	No.
01	Y6	1*29*3/4		261	102
02	Y6	1*71*1		97	71
03	R3	1*17*1		150	17

NOTES

1 In-situ Concrete 45/6

2 Cover 7mm. min

3 Bar spacing measured parallel to the deck centre line and perpendicular to the deck centre line.

FIG. 6.13. NOTES AND BAR LOCATING TABLE FOR MODEL DECK 2 IN-SITU RC SLAB

PAGE

NUMBERING

AS ORIGINAL

7. TESTING OF MODEL DECK 2

7.1 Main testing programme

The testing programme for Model 2 was divided into a number of different stages, with each stage representing a different limit state and/or HB vehicle position.

The first three testing stages were designed to reproduce, as closely as possible, the effects of traffic loading on a full size bridge deck. The final two stages allowed the effects of loading the model up to and past the ultimate limit state to be examined. The model was then loaded to failure.

The HB vehicle load positions that were selected can be seen in Figure 7.1. It will be noticed that only one bogie of the HB vehicle was applied to the model deck at any one time. This was because a combination of the vehicle dimensions given in BS5400 Part 2 (1978) and the geometry of the model ensured that the addition of a second bogie would not give the worst effects. In total, there were five stages and a description of each is given below:-

Stage 1 An HB bogie was located in position 2 and no HA loading or footpath live loading was applied. This arrangement gave the worst transverse sagging moments. The HB bogie load was increased to 45 units of serviceability limit state intensity and cycled 100 times to facilitate any incipient crack growth.

Stage 2 The HB bogie was located in position 3. SLS HA UDL loading was applied to lane 1 and SLS level footpath live loading was applied to both footpaths. Again the HB bogie load was increased to 45 units of serviceability limit state intensity and cycled 100 times.

Stage 3/1 The HB bogie was located in position 1a. The same UDL loading as for stage 2 was applied, except that the HA UDL loading was switched to lane 2. The HB bogie load was increased to 45 units of serviceability limit state intensity and cycled 40 times.

Stage 3/2a The HB bogie was located in position 1a. Additional loading was applied to factor the self weight and density correction loading for the ULS. ULS HA UDL and KEL (at midspan) was applied to lane 2. ULS level footpath loading was applied to both footpaths. The HB bogie load was increased in 8 increments to 180 units of ultimate limit state intensity.

Stage 3/2b The HB bogie was located in position 1b. The same UDL and KEL loadings as for stage 3/2a were used. The HB bogie load was progressively increased in increments until failure of the deck occurred.

HB bogie position 2 was directly over the midpoint of the slab. The centre of bogie position 3 fell upon the transverse centre line, however, it was moved towards the free edge of the deck until the load pads just touched the outer edge of the footpath.

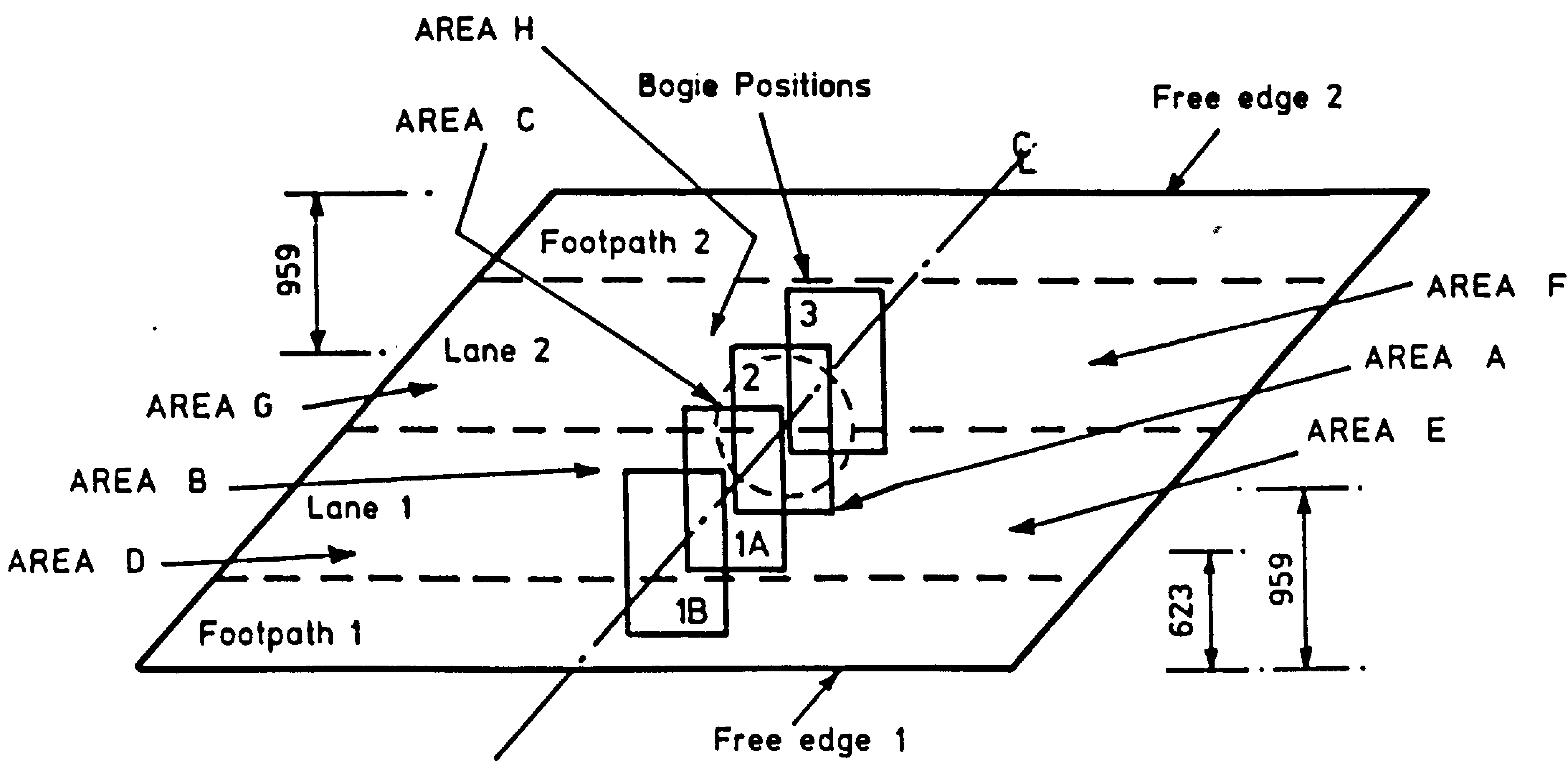

Top Surface

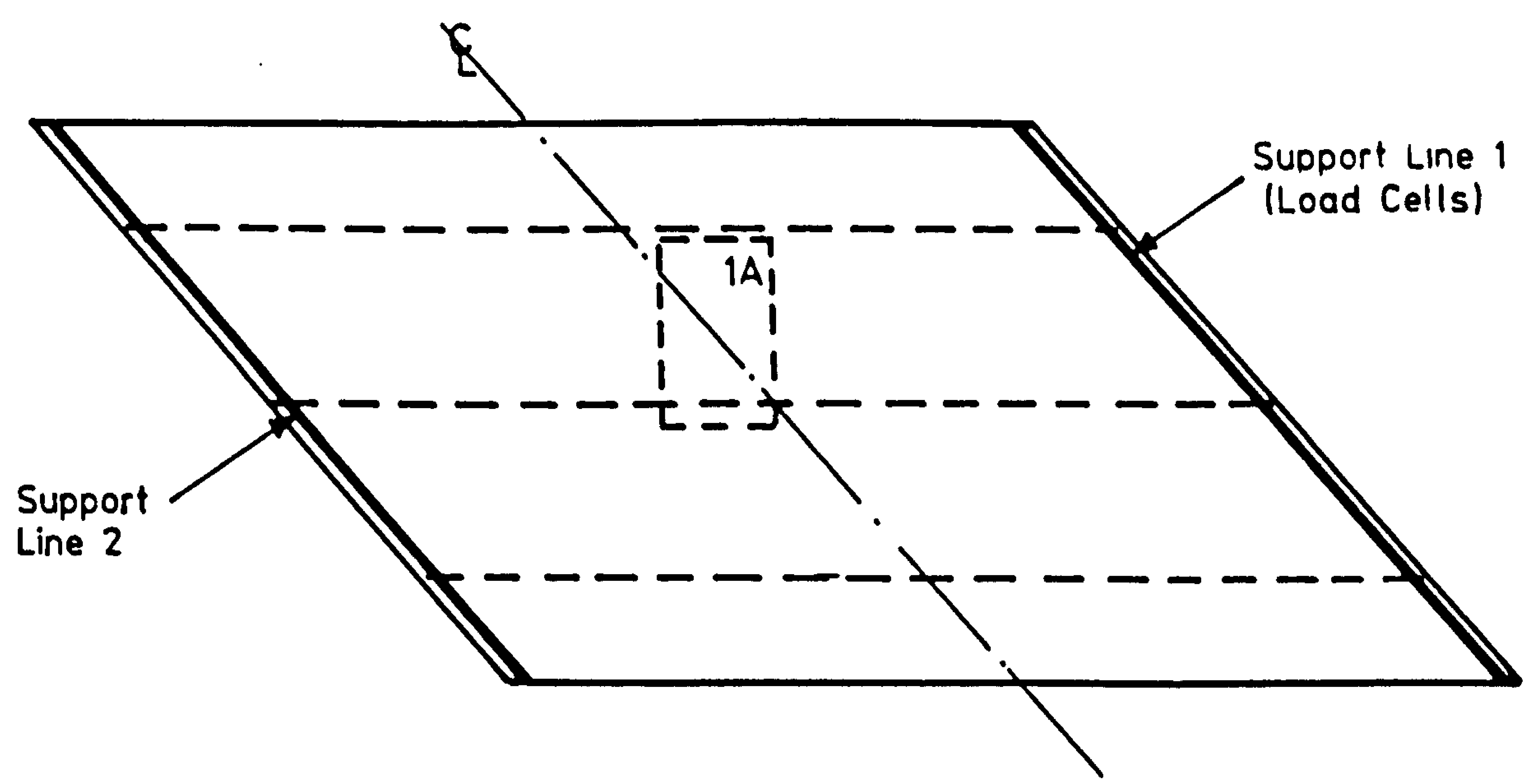

Soffit Surface

FIG. 7. 1. PLAN OF MODEL 2 SHOWING THE DETAILS REFERRED TO IN THE TEXT

The geometry of this bridge deck would permit the widening of the carriageway at a future date, thus reducing the size of, or completely removing, the footpaths from the deck. In the light of this, it was felt that an HB bogie position nearer to the free edge would provide useful and interesting results, hence position 1b was added to the HB bogie test locations.

General views of model 2 undergoing testing can be seen in Figure 7.3, while a timetable of the construction and testing events is presented in Table 7.1.

Event Dates	Description of Event
13-5-85 to 9-8-85	Precast Beams Cast
21-10-85	In-situ Concrete Cast
23-1-86 to 31-1-86	Stage 1 Serviceability Limit State Testing
7-2-86 to 11-2-86	Stage 2 Serviceability Limit State Testing
25-2-86 to 26-2-86	Stage 3/1 Serviceability Limit State Testing
28-2-86 to 4-3-86	Stage 3/2a Ultimate Limit State Testing
1-4-86 to 2-4-86	Stage 3/2b Test to Failure
3-4-86	End of Testing

TABLE 7.1 Timetable of Events for Model 2

A plot showing the load-deflection history of a point at mid-span, close to the free edge of model 2 during testing can be seen in Figure 7.4. The load on the HB bogie forms the ordinate of this figure. The apparent 'false-zero' that can be seen on this plot is caused by the small bogie load that was applied to cater for the density correction and superimposed dead loading in the vicinity of the bogie. All of

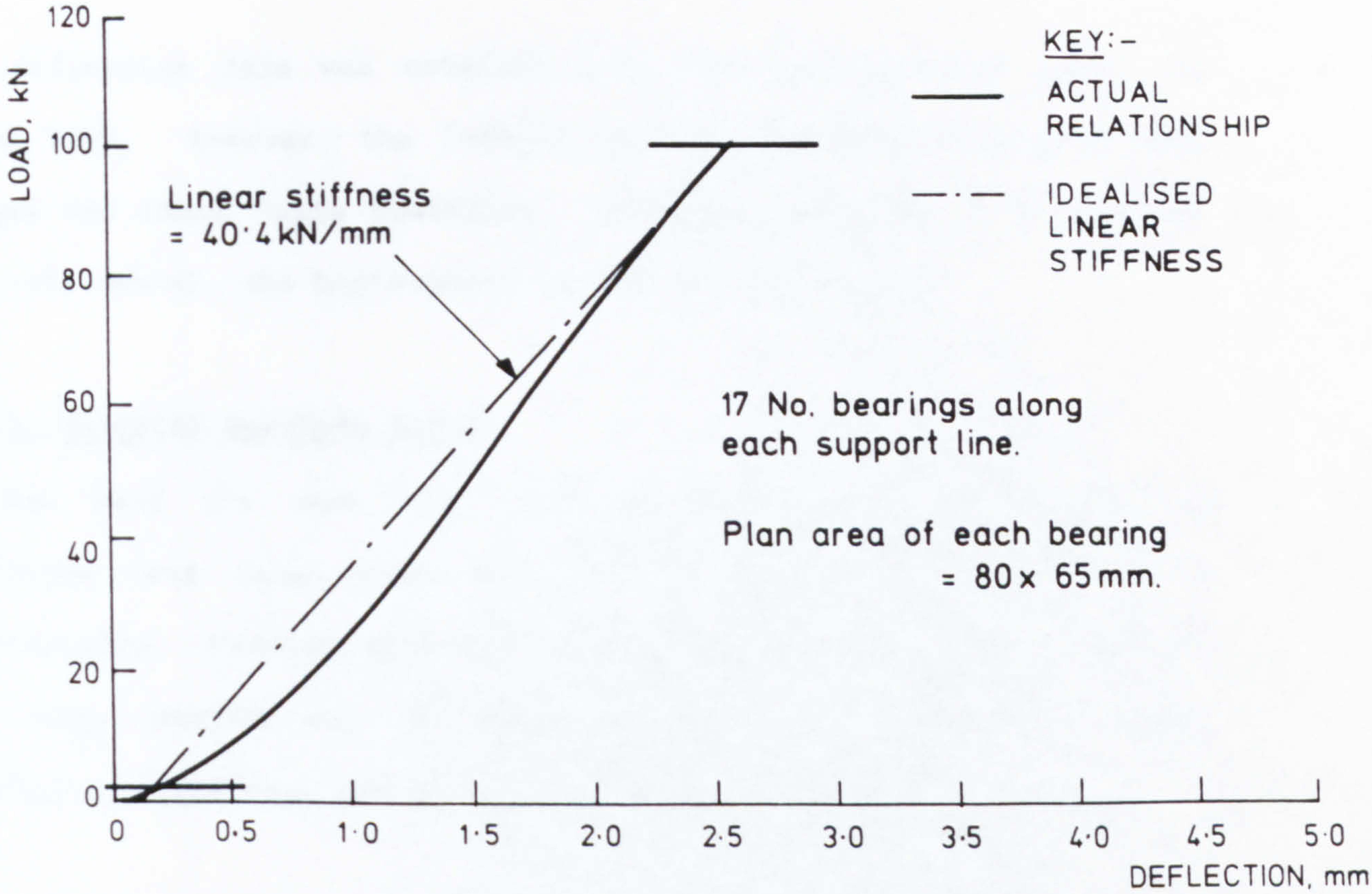

FIG. 7. 2. LOAD - DEFLECTION RELATIONSHIP FOR THE BEARINGS USED IN THE TEST ON MODEL 2

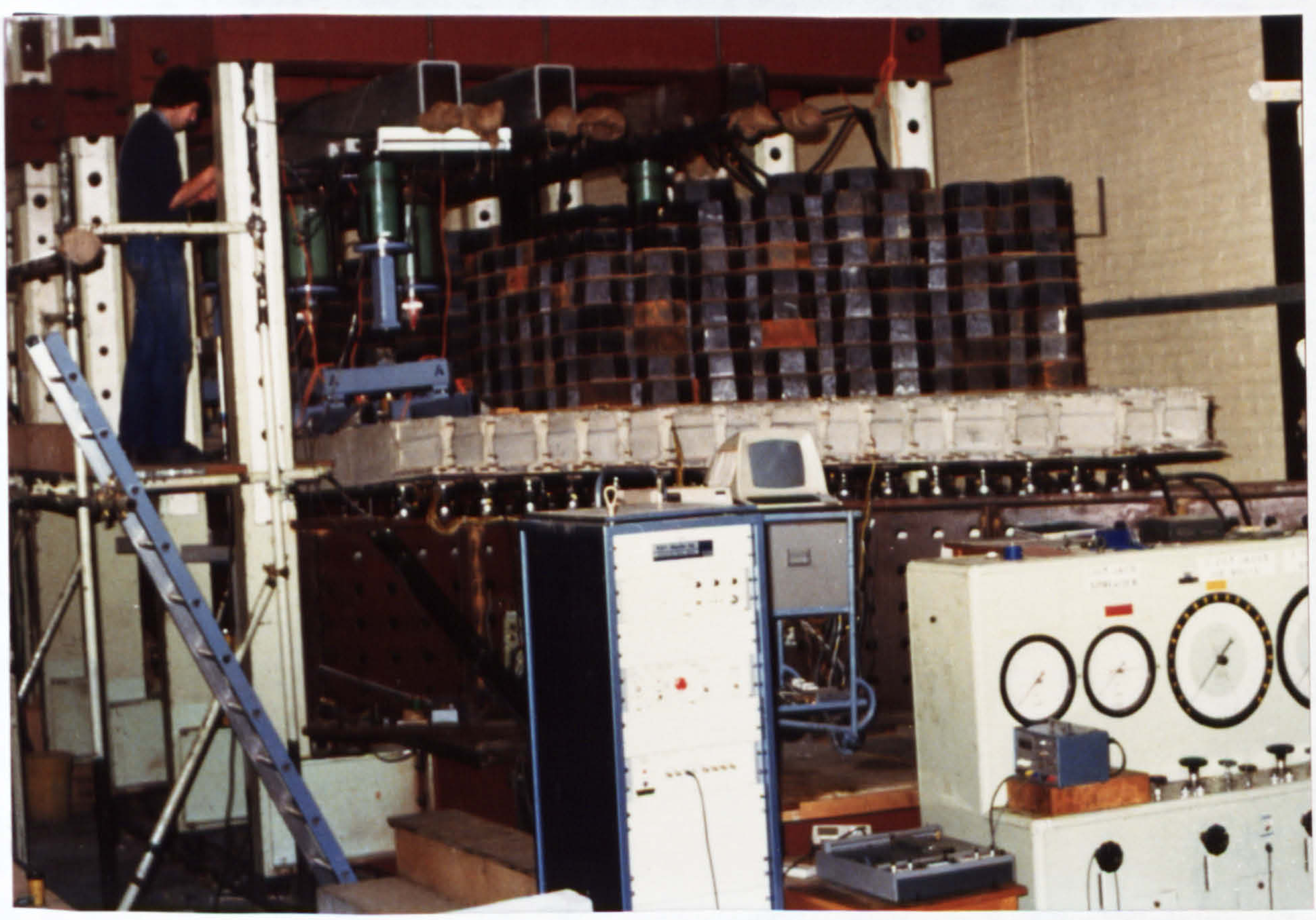

FIG. 7.3. MODEL 2 DURING THE FINAL STAGES OF TESTING

the deflection data was obtained from the same position under the model deck. However, the loading data was acquired during several stages and hence bogie positions. Reference to Table 1 of Appendix 7.2 will reveal, the bogie position for each data point.

7.1.1 Material Specimen Tests

As had been the case with model 1, numerous standard concrete specimens were taken from the concrete mixes used for the model construction. Results from the standard tests, conforming to BS 1881, that were carried out on these specimens at predetermined times yielded the data that can be seen in Tables 7.2 and 7.3.

Precast Concrete				
Mix No	Cast Date	Average strength at release (sample size) (age at release)	Average strength at 28 days (sample size)	
		100mm cubes (crushed) N/mm^2	100mm cubes (crushed) N/mm^2	150mm cylinders (split) N/mm^2
1	13-5-85	45.7 (3) (7 days)	61.2 (6)	3.6 (3)
2	29-5-85	43.3 (3) (5 days)	60.7 (6)	3.3 (3)
3	20-6-85	48.6 (3) (7 days)	58.2 (6)	3.4 (3)
4	17-7-85	42.6 (5) (6 days)	60.5 (6)	3.4 (3)
5	9-8-85	52.1 (3) (10 days)	59.8 (6)	-

TABLE 7.2 Summary of Precast Concrete Specimen Release and 28 Day Test Results

FIG. 7.4. PLOT OF LOAD-DEFLECTION HISTORY FOR MODEL 2

Mix No	Cast Date	Average strength at 7 days (sample size)	Average strength at 28 days (sample size)	
		100mm cubes (crushed) N/mm^2	100mm cubes (crushed) N/mm^2	150mm cylinders (split) N/mm^2
1	21-10-85	32.8 (4)	45.3 (4)	2.8 (2)

TABLE 7.3 Summary of In-situ Concrete Specimen 7 and 28 Day Test Results

The majority of the specimens were either 100mm cubes or 150mm x 300mm cylinders. However, a few 150mm cubes were also cast. 10 cylinders were retained for use in tests to obtain the concrete stress strain curves.

The specimens for the precast concrete were tested at either release, generally at about 5-7 days, although in one case at 10 days; 28 days; or, while the model deck was being tested. The specimens for the in-situ concrete were tested at either 7 days, 28 days, or with the model deck. A statistical analysis of the results from tests carried out while the model was being tested can be seen in Table 7.4.

Test Description	Sample Size	Mean N/mm^2	Standard Deviation N/mm^2
<u>Precast Concrete</u>			
100mm cubes (crushed)	29	74.6	4.13
150mm cylinders (split)	9	4.29	0.43
<u>In-Situ Concrete</u>			
100mm cubes (crushed)	8	58.71	2.21
150mm cubes (crushed)	3	52.3	0.72
150mm cylinders (split)	3	3.66	0.36

TABLE 7.4 Statistical Analysis of Results from Specimens Tested with the Model Deck

The 150mm x 300mm concrete cylinders that had been retained for stress-strain curve tests were capped at both ends with dental plaster, to obtain a reasonably uniform stress distribution, and loaded at a rate of 0.25 $N/mm^2/sec$. Three sets of De-mec points had been attached to each specimen periphery, in an identical way to that described for the cylinder tests for model 1. After the capping had hardened, each specimen was bedded in with a load of 0.2 of its expected cylinder strength. The load was then reduced, before being increased in increments to failure. Control of the tests was difficult at high levels with the load control machine that was employed. However it was possible to obtain failure strains approaching 3500×10^{-6} in many cases. The inclined nature of the final parts of the stress-strain curves shown in Figure 7.5 suggests that the full ductility of the concrete was not realised during these tests.

The average strength of the cylinders can be seen from Figure 7.5 to be about 7% below that predicted from the generally accepted value given by $0.8 \times f_{cu}$. However, the inclination at the end of the curves leads one to the conclusion that the tests were terminated before the full strength was realised, possibly by vibration and load fluctuations in the machine. During the testing, it was observed that the apparent strength could be enhanced if the test was accelerated. However, for all the specimens used to obtain the stress-strain curves, the tests lasted approximately 45 minutes. It is proposed to use the measured initial modulus together with a cylinder strength of $0.8 \times f_{cu}$, obtained from the cube crushing tests for calculation purposes.

Tests were also carried out upon samples of the prestressing and reinforcing steel that were used in model 2. The four types of material employed were: 7.9mm Ø, seven wire prestressing strand; 5mm Ø triple indented prestressing wire; 6mm Ø 'Torbar' high yield reinforcement wire; and 3mm Ø 'Mild' steel reinforcement. Two samples of each of the prestressing steel types were taken from the material used for each set of beams cast. In addition, a total of four samples of each of the reinforcement types were also selected for testing. Each sample, approximately 350mm long, was tested in a similar way to those tested for model 1. The results of the tests showed that all four steel types exhibited good consistency, with a variation of strength, over the test population, of approximately ± 1.5%. The stress-strain curves for each of the 4 steel types can be seen in Figures 7.6 and 7.7.

7.1.2 Bearing Stiffness Test

The bearings that were used to support model 2 were similar in most respects to those used for model 1, the major difference being the type of rubber that was selected.

The model bearings were designed to exhibit a similar response to that of elastomeric bearings which are often used in the full size structures. The plan dimensions of each bearings were 80mm x 65mm, with the longest edge aligned perpendicular to the beam axes. Through the depth, each bearing consisted of a thin steel sheet sandwiched between two sheets of rubber, each approximately 6 mm thick. The top of this unit was attached to the model with adhesive, while the bottom rested upon a steel block 20mm thick. The steel block, which ensured an even distribution of stress, was supported by the spherical load

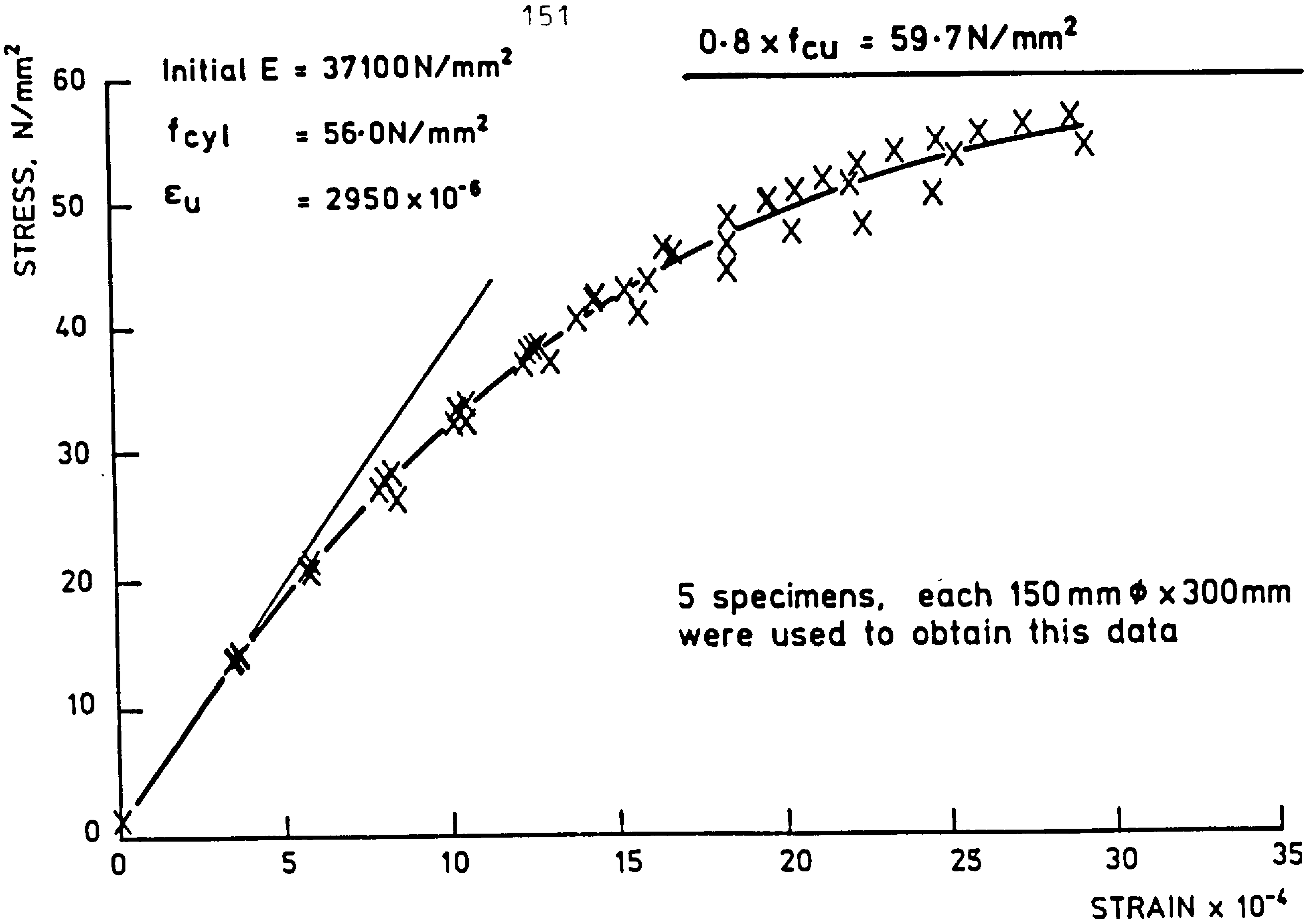

i) Precast Concrete

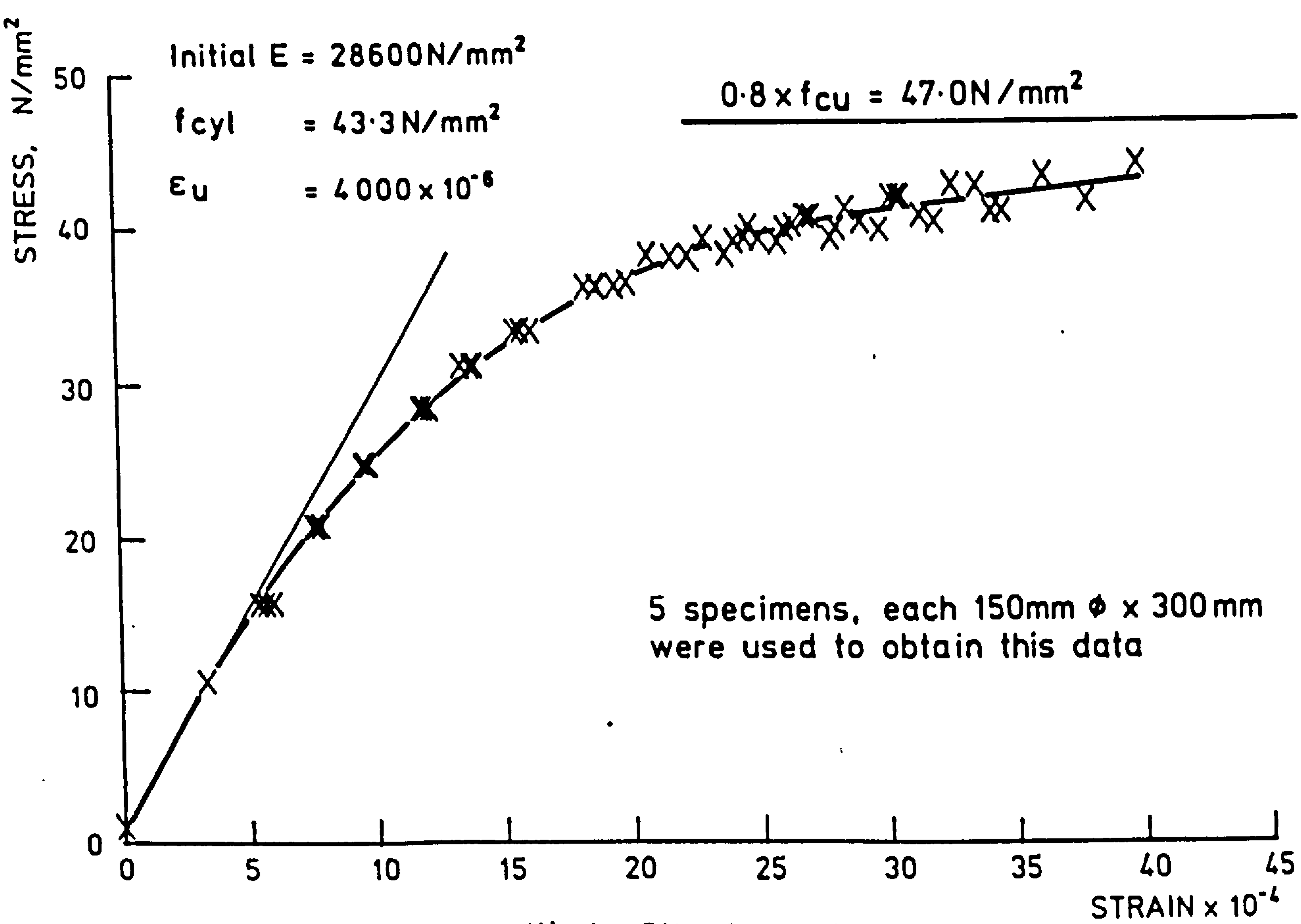

ii) In-Situ Concrete

FIG. 7.5. STRESS-STRAIN CURVES FOR THE CONCRETE THAT WAS USED IN MODEL 2

button of either the load cells or dead end supports as appropriate. The rubber sheets were attached to the other components using contact adhesive.

To ascertain the bearing load-deflection characteristics, 4 specimen units were tested in a 100 kN capacity, compressive test machine. This relationship can be seen in Figure 7.2. It will be noticed that the relationship is non-linear for approximately the first 25 kN, thereafter, it becomes relatively linear. The model self-weight amounted to about 2 kN per support and the maximum reaction forces were of the order of 100 kN. Therefore, for the analyses, it is proposed to use a bearing stiffness of 40.4 kN/mm, which is the value calculated from the gradient of a line drawn between the points where the curve crosses these two load ordinates. This can be seen in Figure 7.2. The corresponding full size bearing stiffness is 141 kN/mm. This approach will underestimate the stiffness of the bearings towards the acute corner end of the supported edge, where reactions are low, by approximately 25%. The critical bearings are located at obtuse corner end of the support line, where reaction loads will be far higher, and these supports will be modelled with the greatest accuracy.

During the testing of isolated bearings, it was noticed that the bearings underwent irreversible damage at load levels approaching 100 kN, such that unloading and subsequent retesting yielded a significantly different relationship. However, it is proposed to use the monotonic test results for analytical purposes. This is because, any load reversals that occured would be confined to the serviceability limit state testing when the absolute size of the reactions was relatively low. During the serviceability limit state

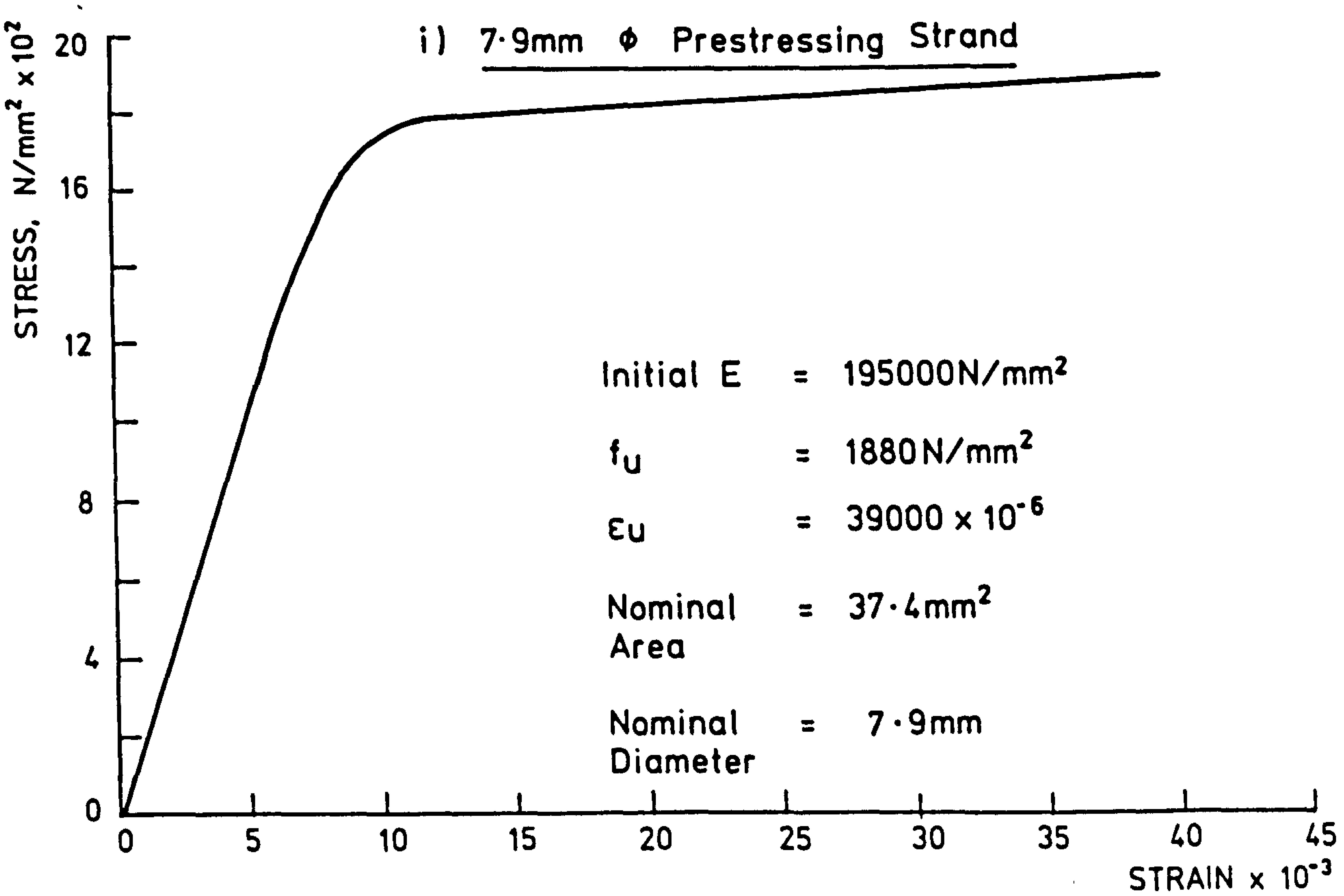

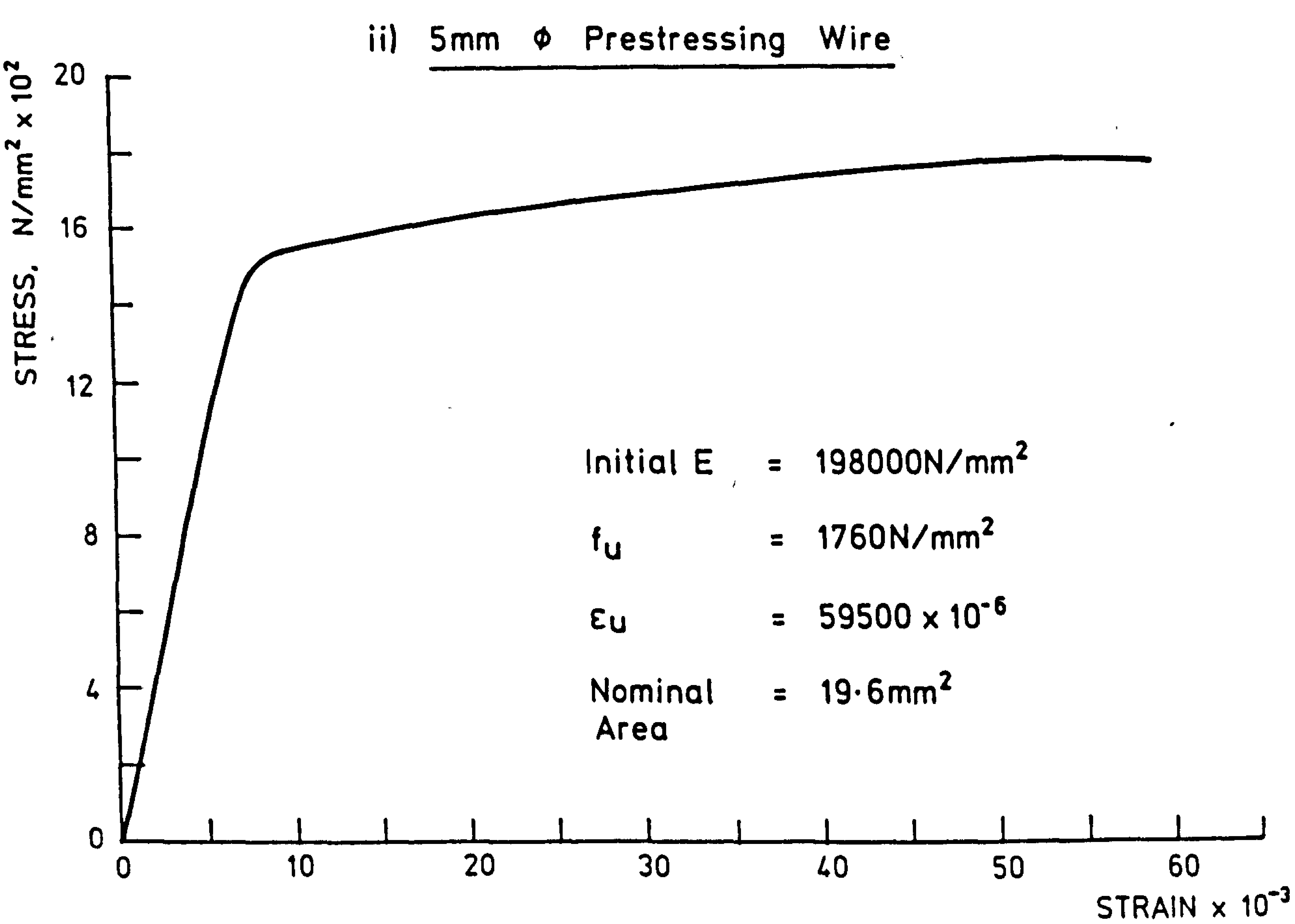

FIG. 7.6. STRESS - STRAIN CURVES FOR THE PRESTRESSING STEEL USED IN MODEL 2

testing the maximum reaction was 24.1 kN while the corresponding maximum reaction during the ultimate limit state testing at a load intensity of 4.0 x ULS was 45.7 kN. During the failure testing the maximum recorded reaction was 153.4 kN.

7.1.3 Model Deck Tests

While model 2 was being constructed, the locations of the transducers were being selected. Some, notably the weldable strain gauges, had to be cast inside the model during construction; however, the majority were attached to the surface of the model after the concrete had cured. The locations of each of the transducers attached to the model can be obtained from the figures of Appendix 7.2. It will be seen from these figures that the transducers were arranged in a consistent manner, to allow effective and meaningful data to be obtained. The arrangements were designed to pick up information along lines parallel to the supports, most notably on 1/4, 1/2 and 3/4 span lines. In addition to the 112 transducers, there were 168 De-mec points, of 100mm gauge length, attached to the model soffit. The positions of these can be seen in Figure 6 of Appendix 7.2. The electrical transducers, load cells, electrical resistance strain gauges and linear voltage displacement transducers were found to give good repeatability over a period of a few days. The De-mec point readings were not as consistent. However, they exhibited an acceptable repeatability. The datum for all the experimental readings is the model self weight, with no additional loading of any kind.

With the benefit of hind-sight, it was felt, with the first model test, that leaving only a small fraction of the top surface visible for inspection during testing was unfortunate. Inspection after the end of the testing revealed dense cracking in the covered areas, and

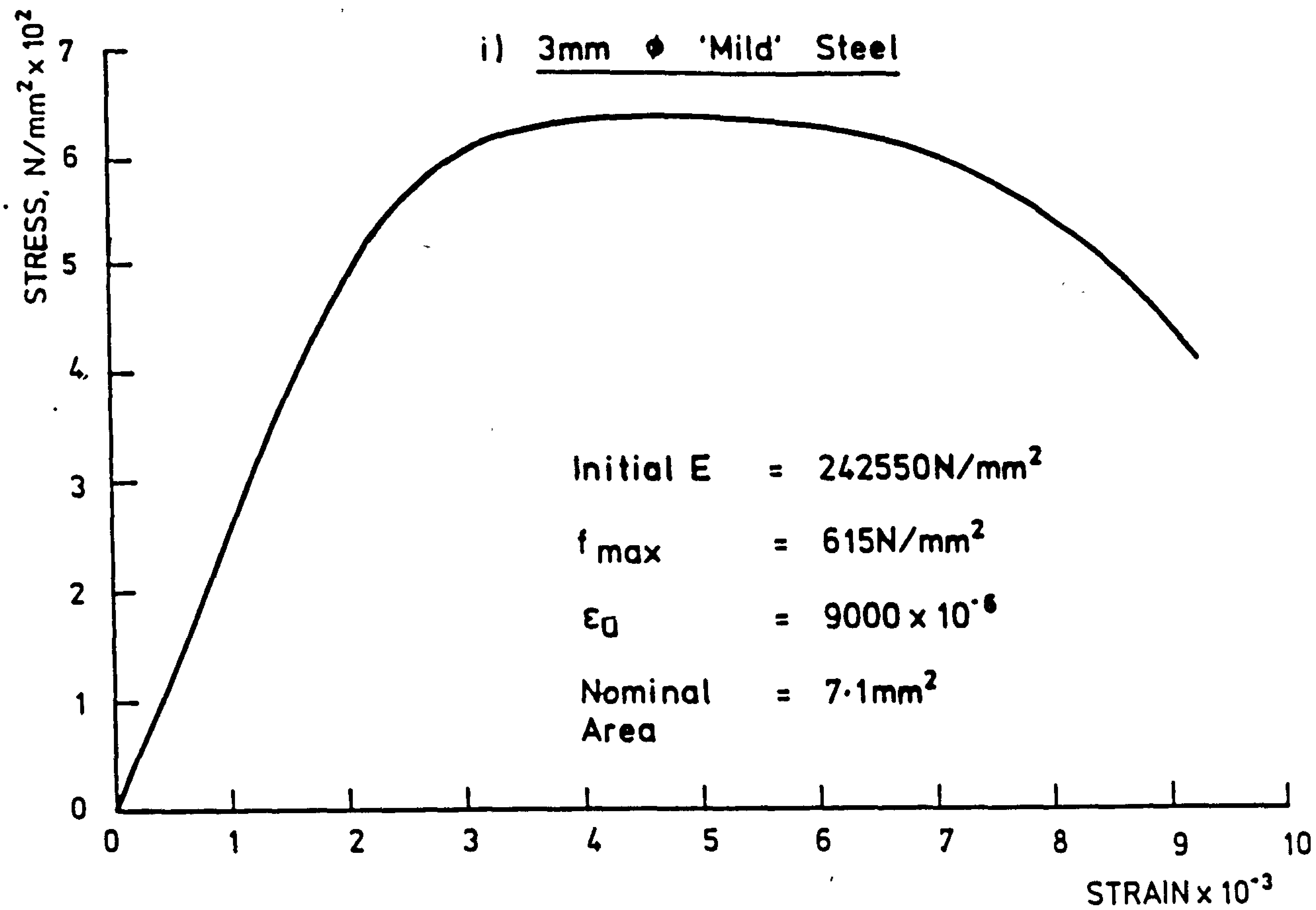

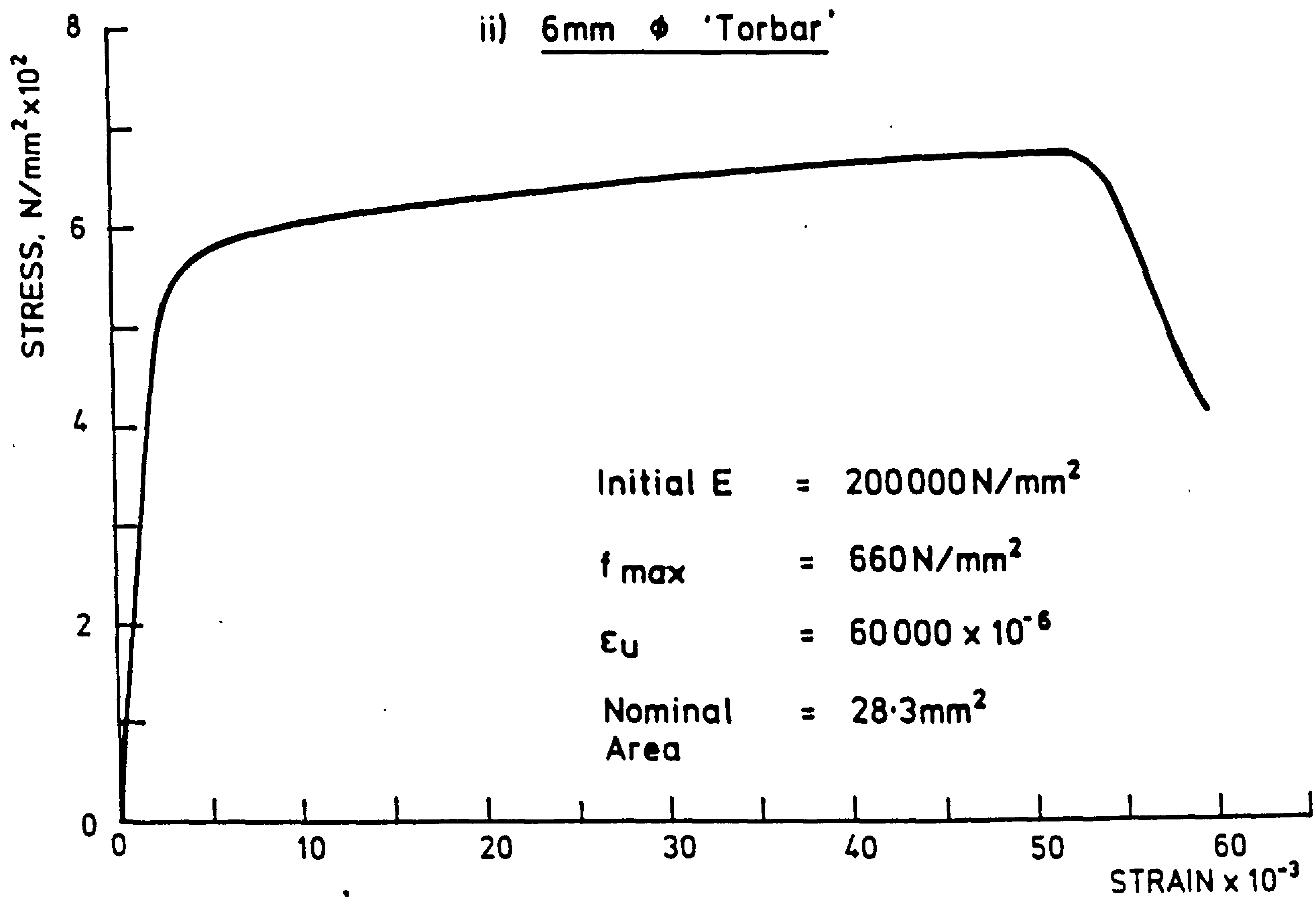

FIG. 7.7. STRESS-STRAIN CURVES FOR THE REINFORCING STEEL USED IN MODEL 2

it would have been useful to know the load stages at which it occurred. Therefore, for the second model test, extra hydraulic jacks, besides the ones of the HB bogie, were employed to simulate some of the UDL and KEL loadings. The load distribution framework that was attached to the bottom of each of the three extra jacks, see Plate 7.1, allowed a near uniform load distribution to be applied, whilst also allowing visual inspection of the top surface. However, it was not practical to use extra jacks to simulate all of the UDL loading. Therefore, black steel weights were still used for loading at each end of lane 2. A UDL simulation jack or 'load spreader' was positioned at mid-span in lane 2 to facilitate the application of the KEL loading during the final stages. The two remaining load spreaders were positioned at approximately 1/4 and 3/4 span, stradling lane 1 and footpath 1. All UDL loading was continued only as far as one slab depth from the support lines, thus allowing inspection of the top surface near the bearing.

After the testing programme had begun, it was realised that the early age cracking that had occurred on top of model 2 would make the monitoring of the early applied load cracking difficult. For, even though the visible non-structural cracks had been marked and filled with resin, some very narrow cracks, which only became visible after loading, confused the issue. However, during the later stages of testing, it was possible to monitor which cracks were structurally active and in which direction, thus identifying many of the early age cracks that had not been visible to the unaided eye.

The load intensities that were used for the testing were obtained from BS5400 Part 2 (1978). The partial safety factors (γ_{f1}) correspond to combination 1 of Table 1 of BS5400 Part 2 (1978). 45 units of HB bogie loading were considered at both the serviceability and ultimate limit states.

Initially, the deck was loaded with a total of 19.36 tonnes of uniformly distributed loading, 13.3 tonnes of black weights and 58.76 kN distributed amongst the extra load spreaders and the HB bogie. No further live loading was applied, so that the worst case for transverse sagging moments would be achieved with the HB bogie in its initial central position.

With the bogie in the central position, and with all compensation loads applied, a scan of all transducers was carried out. There was no indication of cracking and the deflection measurements showed that the model was behaving in a relatively linear manner, when account is taken of the inherent scatter in readings at low load levels.

The HB bogie load was increased to the SLS intensity of 80.8 kN and, after the model had been allowed to settle, another set of readings was obtained. An inspection of the model revealed that no cracking was apparent. As part of the procedure to simulate repeated highway loading, the HB bogie force was cycled up to the SLS intensity 20 times. The deflection readings revealed that the displacement under the mid-point of the slab was 2.54mm before the application of the bogie and 3.96mm with the bogie. After unloading, the displacement returned to 2.93mm, giving a residual displacement of 0.39mm. However, during the subsequent 20 cycles, there was only an increase of 0.08mm in the residual displacement. Thus, it would appear that the majority of the material damage, in this case, was caused by the initial load application, with the further 20 cycles causing little extra damage.

To complete the repeated highway loading simulation for stage 1, 80 more cycles were completed with visual inspections and transducer scans after each set of 20 cycles. On none of these occasions were cracks apparent on the top, soffit or sides of the model. The deflection measurements at the end of the 100 cycles revealed that the displacement under the SLS HB bogie loading had only increased to 4.05mm while, without bogie loading, it was 2.94mm. Thus, the structural response had become slightly non-linear with the first application of the HB bogie. The time taken to carry out the 100 cycles for stage 1 was approximately $4^{3/4}$ hours.

For stage 2, and subsequently for stage 3/1, one half of the SLS level HA UDL loading equal to 1.52 tonnes per lane was applied to both lanes 1 and 2. This loading was intended to produce effects similar to those of 'average' traffic loading. SLS level footpath live loading of 0.52 tonnes per footpath was also applied to both footpaths. The HB bogie was placed in position 3 and the load level increased to the UDL compensation level, after which a set of readings were taken. 45 units of scaled HB loading was then placed on the model bogie and the slab allowed to stabilise for approximately 15 minutes before a set of readings were taken. During this time, a visual inspection was carried out, and it was observed that a crack had formed in the in-situ concrete along the side of the free edge close to the bogie position. The crack extended approximately 110mm up from the top of the beam soffit flange in a vertical direction, the maximum width of the crack was approximately 0.08mm.

The HB bogie load was cycled 100 times in 20 cycle sets. After each set of 20 cycles, the model was inspected and a set of readings taken. During the 100 cycles, no more cracks were seen to appear. The deflection measurements displayed a similar trend to stage 1, with a no bogie load deflection of 3.75mm under the mid-point of the slab and a deflection of 4.77mm with the first application of the bogie load. With subsequent unloading, the deflection returned to 4.06mm, an increase in residual displacement of 0.31mm. After the 100 cycles had been completed, the no bogie load deflection was 4.11mm while, with the bogie load on, it was 4.92mm.

For stage 3/1 the UDL loading regime remained the same. However, the HB bogie was moved from position 3 to position 1a and the load spreaders moved to suit the new bogie position. The HB bogie load was applied to the compensation value, and a set of readings taken. The HB bogie load was then increased to provide the serviceability limit state bogie load level of 80.8 kN and, during the subsequent visual inspection, a new crack was noticed on the edge with the previously uncracked in-situ concrete. This crack was similar in size, shape and location to the crack in the opposite edge in-situ concrete. After details of this crack had been noted, and a set of readings taken, the load cycling was begun. However, for this stage, the number of cycles was reduced to 40, instead of the previous 100, to reduce the risk of a mechanical failure in the testing equipment. It was felt that this reduction was justified, bearing in mind the small increased effect that was observed during the first two stages with the 100 cycles.

The end of stage 3/1 completed the serviceability limit state testing of model 2. The next stages, 3/2a and 3/2b, formed the ultimate limit state and failure testing of the model. For stage 3/2a the uniformly distributed loading was rearranged and refactored for the ultimate limit state. This resulted in 1.09 tonnes of extra self-weight (to account for the 0.15 in the ULS value of γ_{f1} of 1.15), 18.67 tonnes of density correction and 4.56 tonnes of superimposed dead loading being evenly distributed over the model surface using black weights and load spreaders. In addition, a total of 1.55 tonnes was applied to the foot paths as live loading and 4.76 tonnes of HA UDL was applied to lane 2. Also, 1.30 tonnes of HA KEL loading was applied to lane 2 at mid-span.

After the black weights and load spreaders had been rearranged and refactored for the ultimate limit state testing, the load on the HB bogie, which was in position 1a, was increased to 0.5 x the ULS HB bogie load level. (In this section, ULS HB bogie load level is taken to mean 45 units of one HB bogie factored for the ULS, hence 0.5 x ULS HB bogie load level means $22^{1/2}$ units of 1 bogie with a partial safety factor, γ_{f1}, of 1.30.) The model was then allowed to stabilise at this level, while a visual check of the model surfaces was carried out. It is believed that there were no live load cracks visible on the top surface. However, as was mentioned earlier, spotting new cracks was difficult on model 2, because of the effects of the early age cracking that had occurred. After readings had been taken from all of the model transducers and de-mec points, the load on the bogie was increased to 1.0 x ULS level.

After a period of settling down, the model was checked for cracks and other interesting developments. It was apparent that there were a number of new cracks along both free edges and on the top surface along both support lines. Along the free edge nearest the bogie (free edge 1, see Figure 7.1) there were three new cracks, all vertical and starting just above the top of the precast flange. They were between 50mm and 105mm long, and their widths varied from 0.03mm to 0.05mm. There were two extra cracks upon free edge 2, their shape and dimensions were similar to those on free edge 1. The cracks above support lines 1 and 2 were relatively numerous and were in similar positions with respect to the different beams. General details of these cracks can be seen in Figure 7.8. Their lengths were in the range 15mm to 25mm, while their widths varied from 0.05mm to 0.1mm. Their orientation was generally perpendicular to the supported edges, and hence it has been deduced that they were not related to the early age cracking. However, many of these support line cracks maintained their initial size and width throughout the majority of the test, suggesting that they were not active. Therefore, their formation may have been due purely to the form of construction, with the extra long beams, that was used for the model. At this stage, no cracks were detected in any of the model's precast concrete.

Shortly after the model had been loaded to 1.5 * the ULS HB bogie load level, a power supply fault caused momentary overload of the slab with an intensity of approximately 2.4 * the ULS HB bogie load level. Following the repair and reconnection of the power supply, the model was reloaded to a bogie load intensity of 1.5 * the ULS HB bogie load level. However, from the load-deflection plot that was being produced by the equipment during the test, it was apparent that the current maximum deflection was approximately 0.8mm greater than it had been before the overload. Thus, it was decided that any crack checking at this level would not be valid. However, a set of transducer readings were obtained, before the load intensity was increased to 2.0 * the ULS HB bogie load level. After the model had been given time to settle down, it was inspected.

The previously marked cracks had extended slightly, while new cracks had appeared in the in-situ concrete, in the same areas and with approximately the same orientations as the cracks that had been spotted earlier. Moreover, a major new development in the model behaviour was apparent, with the appearance of five small cracks in the prestressed concrete forming the soffit of the model. These cracks, covering a small area around the mid-point of the slab, were contained within individual beam flanges, some covering the complete flange, while others were only across a part of a flange. Their widths varied from 0.07mm to 0.15mm while their orientations showed no apparent pattern. These cracks may have been formed during the previous overload and hence may have just reopened at this load level.

After the state of the model at 2.0 x the ULS HB bogie load level had been well documented and a set of transducer and de-mec readings taken, the load intensity was increased to 2.5 x the ULS HB bogie load level. The increased time that the model took to stabilise at the higher load levels was indicative of the increased material damage that was occurring. For instance, although the load level was increased from 2.0 to 2.5 x the ULS HB bogie load level in approximately one minute, over the subsequent 20 minute settling time, the incremental 'creep' deflections were approximately three times the 'instantaneous' incremental deflections.

The model appeared to be behaving in a similar way to a homogeneous slab, with no visible breakdown between the precast and in-situ concretes. The maximum deflection on the transverse centre line had reached 13.5mm by this time. The spread of the crack pattern had also increased quite considerably, with cracks now extending across approximately 5/6 of the model slab width, in a band approximately 400mm wide. The cracks were oriented approximately parallel to the transverse centre-line. However, there was a small bias towards an orientation that would have been perpendicular to the free edge. The cracks were well distributed, with the crack spacing generally in the range 150mm to 200mm.

This form of composite construction produces cracks that are discontinuous. This phenomenon is thought to be caused by the variations of the applied prestress in the soffit concrete of the discrete beams. A variation in the prestress is unavoidable, given the many variables encountered during the beam manufacture. However, it leads to cracks that appear to 'jump' across beams, although, during the later stages of testing, when the soffit surface strains are much higher, these cracks give the appearance of being semi-continuous. As the crack directions on neighbouring beams tended to be similar, it is reasonable to suppose that when they formed, the composite deck was behaving structurally as a continuous slab.

The measurement of crack widths on the soffit of model 1 with a good degree of accuracy and repeatability was very difficult. Therefore, a novel approach for crack width measurement was used for model 2. At discrete increments, after several new cracks had been detected, the testing programme was held for a period of time, while De-mec points were attached to the model surface across the new cracks. The crack widths were then measured, along with an initial 'crack' De-mec reading. During subsequent load increments, readings from these 'crack' De-mec points were taken and hence the crack widths calculated. The relative increases in the crack widths from when the De-mec points were attached could be measured to a precision of ± 0.001mm. Even though the absolute crack width still depends upon the initial crack width reading, a greater accuracy was expected, due to the increased time and care that could be taken with the single set of initial readings.

The first set of 'crack' De-mec points were attached at the current load level of 2.5 * the ULS HB bogie load level and the initial measurements revealed that the crack widths were in the range 0.04mm to 0.15mm. The tabulated readings from these points can be seen in Table 7.5, while the positions of the points are shown in Figure 7.9.

After the model details had been recorded and a set of transducer readings taken, the load intensity was increased to 3.0 * the ULS HB bogie load level, with a corresponding increase in the maximum deflection to 18.1mm. Further cracks were noticed above the support lines upon the top surface. These cracks were narrow and were oriented approximately perpendicular to the supports. Some of the cracks were seen to disappear under the black weights that occupied a large part of lane 2, so the full extent of the cracking could not be ascertained. The soffit crack pattern had only increased its coverage by a small amount, although the width of the measured cracks had approximately doubled.

A set of transducers readings was taken and the load intensity increased to 3.5 * the ULS HB bogie load level. There were no new developments at this load intensity so, after the model inspection had been carried out, the transducer readings were taken and the load intensity was increased to 4.0 x the ULS HB bogie load level and allowed to stabilise. From the load-deflection plot that the equipment was continuously producing, it was apparent that the structure had become highly non-linear. However, there was obviously

Level	Crack Widths (mm)														
	1	2	3	4	5	6	7	8	9	10	11	12	13	14	15
15	0.12	0.13	0.15	0.11	0.15	0.13	0.20	0.19	0.23	0.17	0.20	0.17	0.14	0.14	0.15
16	0.28	0.21	0.24	0.20	0.26	0.19	0.31	0.34	0.43	0.30	0.37	0.28	0.30	0.28	0.28
17	0.01	0.01	0.01	0.01	0.01	0.01	0.01	0.01	0.02	0.02	0.01	0.01	0.01	0.01	0.01
18	0.11	0.10	0.09	0.06	0.09	0.06	0.17	0.17	0.22	0.13	0.17	0.12	0.11	0.09	0.10
19	0.26	0.19	0.19	0.14	0.20	0.14	0.34	0.38	0.46	0.37	0.41	0.24	0.23	0.22	0.21
20	0.39	0.25	0.26	0.20	0.28	0.19	0.45	0.57	0.67	0.52	0.59	0.34	0.32	0.31	0.28
22	0.70	0.36	0.44	0.33	0.49	0.31	1.58	1.68	1.24	1.58	1.31	0.62	0.55	0.57	0.48
24	1.05	0.50	0.78	0.46	0.74	0.43	****	****	1.68	****	****	0.70	0.62	0.89	0.70

TABLE 7.5 CRACK WIDTHS THAT WERE MEASURED AT THE LOCATIONS GIVEN IN FIG. 7.9 DURING THE TEST ON MODEL 2

a large amount of resistance capacity remaining, assuming that the model would fail in a ductile manner.

The maximum deflection at this stage was 26.91mm; the maximum measured concrete compressive strain was 1077 x 10^{-6}; the maximum measured lower longitudinal tendon strain was 6467 x 10^{-6}, which is approximately 77% of the yield strain; while the four supports nearest to the obtuse corner were supporting 48% of the total support line applied load (i.e. 48% of 349 kN = 167 kN). The soffit crack pattern had spread a little further from the transverse centre-line, although the direction of cracking was still predominantly parallel to the transverse centre-line. The crack pattern suggested that the eventual failure mechanism for bogie load position 1a may have been a simple sagging yield line across the centre of the slab. The widths of the measured soffit cracks were in the range 0.19mm to 0.43mm. While narrow, well distributed cracks had appeared along free edge 1 in the in-situ concrete, many of the cracks continued down through the precast concrete and across the model soffit.

With the load on the HB bogie at 4.0 x the ULS intensity, stage 3/2a testing was concluded. During this stage, there was generally a 4-hour time interval between load increments, with all of the load increments being applied over two consecutive days.

The unexpected strength of the model necessitated the installation of extra jacking equipment before the test to failure, stage 3/2b, with the HB bogie in position 1b, could begin. A load level of 4.0 x the ULS HB bogie load level was the realistic maximum jacking capacity for the test rig, if the load was applied vertically from above. Therefore, to obtain the extra capacity for stage 3/2b, 3 high tensile steel bars were passed through 40mm diameter holes that had been drilled in the model deck. These bars, whose centroid of force coincided with that of the HB bogie, were secured to the model top surface and at the bottom to hydraulic jacks inside the lower framework of the testing rig.

Although load intensities equivalent to 0.5, 1.0 and 1.5 * the ULS HB bogie load intensities were applied at the start of the stage 3/2b programme, the subsequent description of the model behaviour begins at a load intensity equivalent to 2.0 * the ULS HB bogie load level. This is because there were no significant developments during the lower load increments.

During the latter part of stage 3/2b, the displacement of a point under the HB bogie was used as the control variable. Thus, the servo-control testing equipment varied the load being applied through the HB bogie until the desired displacement was achieved. During this stage of the test, the load applied by the extra load distributor jacks was automatically kept constant.

The tension jacking system was not activated until the load level reached 2.0 x the ULS HB bogie load level. Up to this stage, all of the load was provided by jacks from above. When the 2.0 x ULS HB load intensity was reached, the load was transferred to the tension jacking system smoothly. This was possible because the HB bogie jacks were working in the displacement control mode. Although the tension jacking system load was maintained at 2.0 x the ULS HB load level, and the actual load on the HB bogie was varied by the servo-control system as the test progressed, for ease of assimilation, load intensities quoted refer to the effective total HB bogie load. That is, the sum of the top and the lower tension jacking loads.

The model settled down in a relatively short time at 2.0 x the ULS HB bogie load level and this allowed the visual inspection and reading collection to be carried out quite quickly. There was no apparent extension to the crack pattern, while the readings from the measured crack widths were comparable with those measured at a load intensity of 3.0 x the ULS HB bogie load in the previous bogie position.

The load level was then increased to 2.5 x the ULS HB bogie load level and then to 3.0 x the ULS HB bogie load level. At both of these levels, after the model had been allowed to settle, a visual inspection was carried out, which revealed that no significant changes had occurred and sets of readings were obtained.

When the model was inspected after a load intensity of 3.5 x the ULS HB bogie load had been applied, it was discovered that the crack pattern was developing further. Although there were a few new cracks, the majority of the visible activity resulted in the extension of the existing cracks. The widths of a number of the measured cracks were now greater than the maximum widths recorded in the previous bogie position, see Table 7.5. The maximum displacement reached 30.7mm.

From this load intensity, it was not practical to increase the load in equal increments. The displacement control mode that was in operation made it difficult to maintain even an approximate load level with the extent of material damage that the slab was beginning to experience. Therefore, the next readings were obtained with the HB bogie load intensity at 4.32 x the ULS HB bogie load level.

At this stage, the maximum displacement had increased to 42.1mm; the maximum principal compressive concrete strain to 1373×10^{-6}; and the maximum tendon tensile strain which was recorded just under the bogie position, to 6980×10^{-6}. The end support in the obtuse corner was taking approximately 107 kN, i.e. 30% of the applied load attracted to the line of bearings on support line 1. A crack, inclined at 45°, with its base approximately one slab depth from the support line, was visible in the in-situ concrete of the free edge, however, it did not continue through the precast flange.

From the overall crack pattern in the vicinity of the obtuse corner, it was deduced that the end two beams were experiencing large torsional moments caused by the large obtuse corner reaction. It was thought that this could lead to the isolation of the edge beams from the rest of the model, by separation of the in-situ and precast concretes. The crack pattern on the soffit was well developed, with cracks across the full width of the model, and extending to approximately one metre each side of the transverse centre line. The crack spacing was generally in the range 60mm to 100mm and of particular interest were the fork of 'Y' shaped cracks. These were normally contained within one beam width and appeared to show a change in the direction of active cracking. The phenomenon can be clearly seen in Figure 7.9 in the position corresponding to area B of Figure 7.1. Although bogie position 1b was only a small distance from the previous bogie position 1a, it may well have been sufficient to reorientate the principal strain directions, causing the divergent cracks.

It is also interesting to note that the soffit cracks on the half of the slab nearest support line 1, area A of Figure 7.1, were typically parallel to the transverse centre line, whereas those in area B tended to fan out from under the bogie position towards free edge 2. The measured crack widths were in the range 0.19mm to 0.67mm.

Along the elevation of free edge 1, more cracks had developed, between existing cracks and also extending the crack pattern towards the supports. The existing cracks were beginning to curl over at the top, tending to the horizontal direction. This was especially true of those cracks adjacent to the HB bogie. The horizontal portion of the cracks was generally about 40mm from the top surface. However, the few cracks away from the bogie that had turned towards the horizontal were approximately 100mm from the top surface.

The top surface cracking in the obtuse corner, and above support line 1, was now quite extensive. The prevailing orientations can be seen in Figure 7.8. However, the cracking above support line 2 appeared to be stagnent with no further developments.

For the next increment, the maximum deflection was increased to 57.8mm, with a corresponding increase in the bogie load to 5.01 x the ULS HB bogie load level. There was a general increase in the crack widths, with some new cracks developing on the soffit and top surface. The width of the shear crack had increased significantly, and the load on the obtuse corner reaction was 123 kN. Three more inclined cracks had also opened up. One, about halfway between the existing inclined crack and the support line, appeared to be a progression of an earlier, nearly vertical, flexural crack, while the other two were at

0.75 and 1.5 slab depths further away from the support line than the initial crack. By this stage, the deck had lifted off the support in the acute corner.

The controlling displacement was next increased to 74.6mm. The bogie load intensity increased to be equivalent to 5.61 * the ULS HB bogie load intensity. The soffit crack pattern had now developed quite extensively in area B, reaching to within 0.5 metres of the support line in some parts. The soffit cracks in area A, which were still approximately parallel to the transverse centre-line, had only progressed as far as 1200mm from the support line 1, except under the three beams nearest the free edge, where cracking was visible almost up to the support line. The widths of the measured soffit cracks were quite large, with a maximum of 1.68mm.

Crushing of the concrete was apparent on the top surface in between the axles of the HB bogie and continuing inwards as far as the third wheel of the bogie. The direction of crushing was approximately perpendicular to the free edge.

There were interesting developments in area C, over the central zone of the model. There appeared to be bands of material aligned in the longitudinal direction, and approximately 40mm wide, which were undergoing transverse crushing and longitudinal sliding. The bands were located either above the in-situ concrete between adjacent beams, or directly above the web of a particular beam.

After a set of readings had been obtained, the maximum displacement was increased to 89.8mm, with a corresponding increase in the load intensity to 6.02 x the ULS HB bogie load level. The visible top cracking covered almost the whole of the obtuse corner region that was accessible, while the shear crack that had appeared initially along free edge 1, now had a vertical displacement of approximately 3mm near to the corner, while along the side face, there was a relative sideways displacement of about 2mm at the bottom, with none at the top. Lift-off from the bearings had also extended to the second support in from the acute corner. The obtuse corner bearing was taking 153 kN, which was about 34.5% of the total load on support line 1. The maximum measured concrete compressive strain was approximately 2100 x 10^{-6} and the corresponding maximum longitudinal tendon strain was about 11000 x 10^{-6}. Both measurements were taken close to the HB bogie. However, they were far enough away for the influence of the 3 dimensional stress system around the immediate areas of load application to be neglected.

For the next increment, the control displacement was increased to 116.2mm, while the HB bogie load showed a small reduction to 5.97 * the ULS HB bogie load level. The deflections were large enough for the deflected shape of different regions of the model to be observed. It was apparent that the acute corner quadrant, area D of Figure 7.1, was moving as a rigid body, whereas there appeared to be large twisting of the obtuse corner quadrant, area E. It was also observed that separation was occuring between the in-situ concrete and the precast concrete on the obtuse corner side of the third beam in from the obtuse corner. This can be clearly seen in Plate 7.2. The gap between the two concretes was approximately 1-2mm and could have been caused by the obtuse corner of the model attempting to twist up and away from the rest of the model. The main soffit crack widths were generally up to about 4mm. At this stage, the corner bearing was taking 149 kN, which was approximately 33.8% of the load acting upon support line 1.

As the displacement was being increased to the next incremental value, at least two tendons were heard to rupture. It is difficult to establish where these failures occurred. However, it is thought that the ruptured tendons were located under lane 1, towards the middle of the slab. After the tendon failure, the displacement level was held and, after stabilisation, the load intensity had reduced to 5.10 * the ULS HB bogie load level. The control deflection at this stage was 156mm while the maximum recorded top surface concrete compressive strain was approximately 3000 x 10^{-6}. The vertical displacement of the shear crack near the obtuse corner had increased to about 5mm while the adjacent separation of the in-situ and precast concretes was about 3mm. Separation was also apparent between the other beams and their associated in-situ concrete along support line 1, although the gaps were no more than 1.5mm.

A load of 300 kN was maintained on the tension jacking system while the other hydraulic jacks were unloaded and removed. After the visible model details had been recorded and photographed, the black steel weights were removed from lane 2. Subsequent inspection of the top surface revealed very extensive cracking in this lane, this can be seen in Figure 7.8. The cracking in area G was similar to that found in the comparable position on model 1 and resembled short stubby cracks at a small angle, say 20° to the general direction of the line of cracks. It has been suggested that these may have been caused by in-plane shear causing a 'tearing' action between adjacent beams. The cracks that could be seen at the far end of lane 2, area F, were more typical of reinforced concrete slabs, see Figure 7.8. The failure crack pattern along the free edge adjacent to the HB bogie can be seen in Plate 7.4. Before the photographs of the complete model faces were taken, a mesh of symbols was marked on the model to allow interpretation.

7.1.4 Core Samples

Six 150mm cores were cut from model 2 after the test failure had been completed. The locations from which the cores were taken where chosen carefully to allow a detailed analysis of the different structural actions that had been observed during the test. These chosen locations can be seen in Figure 7.11. Unless otherwise stated, all the cracks which are described in the subsequent section, were located in the insitu concrete.

Core 1

The first core was cut from an area adjacent to the loaded acute corner, an area which had suffered little damage during the test to failure. In the preceding text it was mentioned that during the test the loaded acute corner region appeared to move as a rigid body and, therefore, suffered little damage. This is confirmed by inspection of the crack pattern plots in Figure 7.8 and 7.9. This core was used as a datum by which the other cores were judged. It also enabled the effectiveness of the resin injection of early age cracking to be examined. From the appearance of core 1 it was apparent that the early age cracking was restricted to the region between the top of the upper transverse bars and the top surface. Through the depth, the cracks tapered until they were almost invisible to the naked eye about 3mm above the reinforcing bar. No void was visible below the top transverse reinforcing bars.

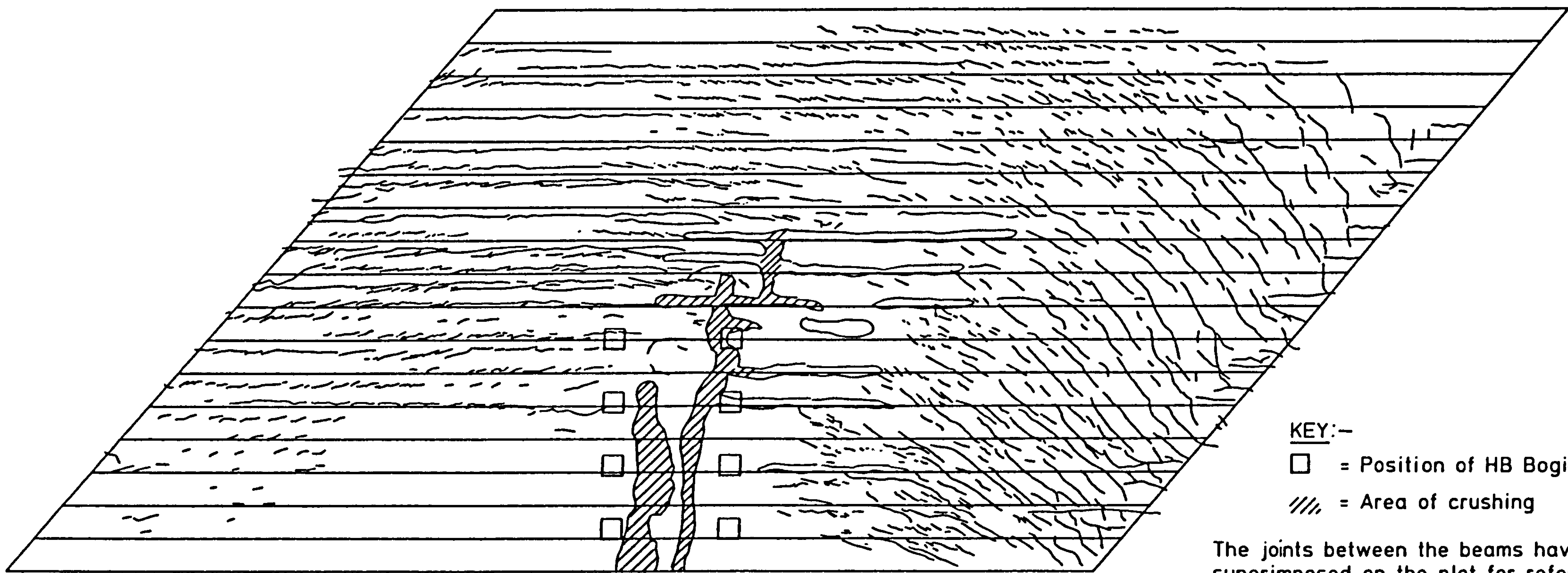

Plan view from above

KEY:-

□ = Position of HB Bogie pads

//// = Area of crushing

The joints between the beams have been superimposed on the plot for reference

FIG. 7.8. PLOT OF THE CRACK PATTERN ON THE TOP SURFACE OF MODEL 2 AT FAILURE

Throughout the rest of core 1 very few other cracks were visible. There was no separation between the component parts of the composite construction, in fact about 50% of the interfaces were either invisible to the naked eye or could only be located by the different shades of the precast and insitu concretes.

Both the precast and insitu concrete exhibited little air entrainment with good compaction throughout the whole section depth. The actual section depth as measured from the cores was within 1mm of the design value. The cores showed that prestressing and reinforcement had been accurately placed with the through depth positioning errors between 1mm and 1.5mm in most cases. The dimensional accuracy of the beams was good with the deviation from the design profile being generally less than 1.5mm.

Core 2

The location of core 2 was selected to allow the top cracking towards support line 1 to be investigated. The cracking around core 2 exhibited similar characteristics to cracking which is typical in reinforced concrete bridge decks. However it was not known how the composite construction had effected the formation and propagation of these cracks.

There was clear separation on both sides of the precast beam which can be seen in Plate 7.8 however, no cracks were visible in the precast concrete on the soffit of the core. The separation along the interface closest to the near free edge was widest at the bottom. The 'crack' width was approximately 0.35mm, tapering to almost nothing at the top. On the opposite side of the web the converse was true, with the widest separation of approximately 0.2 mm being at the top of the

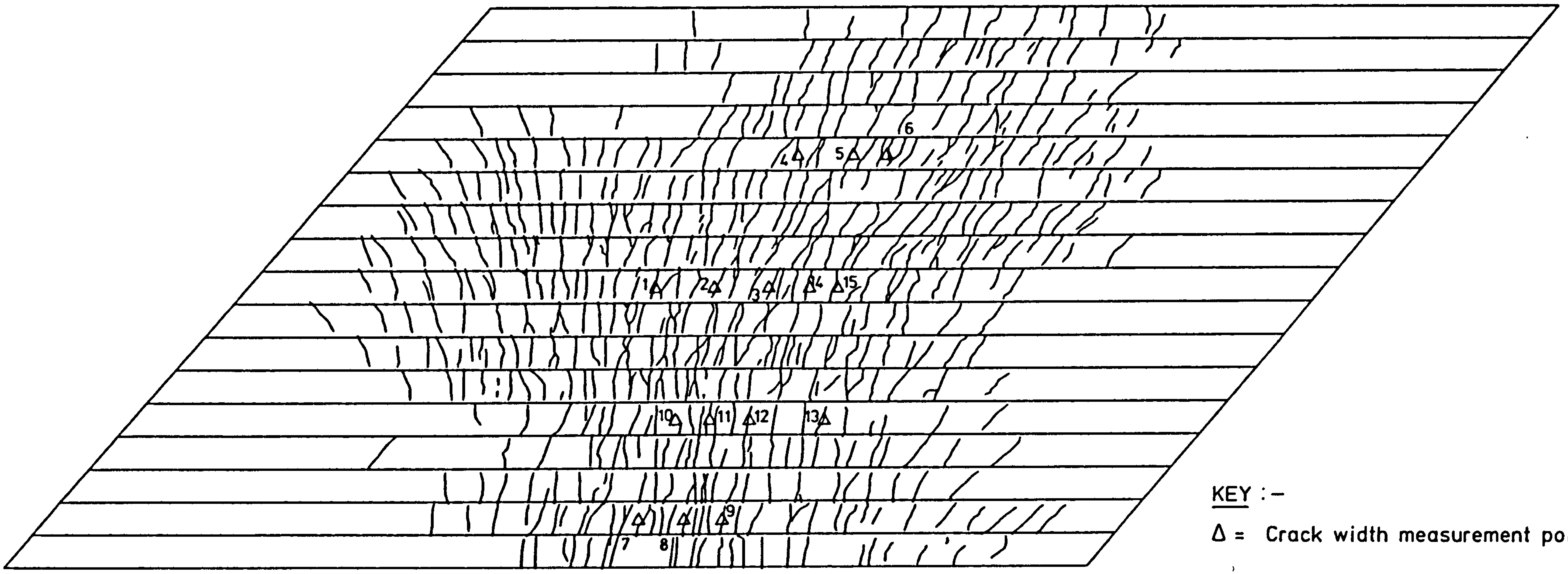

Plan view from above

KEY :-

Δ = Crack width measurement points

FIG. 7.9. PLOT OF THE CRACK PATTERN ON THE SOFFIT OF MODEL 2 AT FAILURE

section. The top cracking was aligned at approximately 45° to the line of the beams, however, it was not possible to ascertain if the cracks passed through the web of the precast beam.

Core 3

This core was located close to the midpoint of the model deck and was used to investigate the unusual damage that was present in the central region of the model. When removed, the core had suffered a great deal of damage during the test and hence was very broken up, as can be seen in Plate 7.8.

During the model test, the area around core 3 would have been subject to large bending moments both parallel and perpendicular to the beam axis with large co-existing shear forces, especially perpendicular to the beam axis.

The high transverse bending and shear forces had resulted in separation of the insitu and precast concretes along the upper portion of the interface on the free edge 1 (see Figure 7.1 for definition of free edge 1) side of the precast beam, which would be expected with transverse hogging moments. This separation which was 0.35mm wide at the top tapered to zero half way down the section with full composite action being maintained in the lower half of the section on free edge 1 side of the beam. In a shear situation the compression strut would be expected to form between this part of the lower half of the section and the corresponding upper half of the next beam towards free edge 1. This is confirmed by the presence of shear cracks, in the insitu concrete, at approximately 60° to the soffit, orientated in this direction.

Plan view from above

FIG. 7.10. PLOT SHOWING THE TOP SURFACE FAILURE CRACK PATTERN SUPERIMPOSED UPON THE SOFFIT FAILURE CRACK PATTERN FOR MODEL 2

It is interesting to note that, as the separation of the interface decreases towards section mid-depth, horizontal cracks begin to form through the web of the precast beam.

The top of core 3 exhibits an unusual phenomenon whereby the top layer of concrete, approximately 12mm thick, appears to have separated from the rest of the concrete mass in small sheets. It is possible that the shear displacement of adjacent beams acting in conjunction with the insitu/precast separation, the presence of top transverse steel and the high longitudinal bending moments has resulted in the separation of this top layer of concrete from the rest of the mass.

Core 4

The location of core 4 was chosen to allow further investigation of the 'tearing' type cracking that was observed on the top surface of the model.

Initial observation revealed little indication of damage. However, it was seen that separation of the insitu and precast concretes was present for the majority of the interface above the top of the bottom flange which would suggest a nett hogging moment perpendicular to the beams.

The longitudinal bending moment magnitude was sufficient to cause the formation of one very small and thin crack in the soffit precast concrete. In fact, after the load had been removed the only evidence of a crack that was left was the line that had been drawn with a pen to mark the crack location. Repeated attempts with a 0.01mm microscope failed to find the actual crack. Therefore, one must assume that the crack was thin enough to allow the prestressing steel to close the crack completely on unloading. It is interesting to note that no longitudinal bending cracks were visible in the insitu concrete. However, it is possible that the cracks formed and were closed by the prestress. However, for this to be realistic, either the prestressed concrete retarded the onset of insitu cracking and therefore any cracks that did form would be thin and easy to close, or, there was a pre-stress in the insitu concrete, caused by creep between the time of insitu casting and testing thus retarding the onset of cracking.

The 'tearing' type cracking was apparent on the top surface of the core however no unusual phenomenon were observed around the periphery of the core just below the top surface and as mentioned earlier the only damage that was observed was separation of the precast and insitu concretes.

Core 5

This core was removed from the central region of the model slab about 1 slab depth from the HB bogie. The model slab around core 5 was subject to large bending moments and shear forces during the model test. Consequently, this core was severely damaged hence making interpretation of its appearance difficult.

During the test the principal bending moments would have been orientated approximately parallel and perpendicular to the beam axis. The longitudinal moment would probably be sagging with the transverse moment hogging and the major moment parallel to the beams. This is confirmed by cracks parallel to the beams on the top surface and perpendicular to the beams on the soffit.

There was considerable separation visible on this core tapering from approximately 0.7mm at the bottom to 0.05mm at the top. There was one horizontal crack passing through the insitu concrete at a depth of 50mm from the top surface. The top half of the precast beam was largely intact. However, there was multiple cracking and other damage which was centred around the junction between the web and lower flange. This cracking was very variable in direction from approximately 60° to the soffit to almost parallel with the soffit.

Core 6

This core was removed from the obtuse corner region of the model slab, see Figure 7.11. During the later stages of model testing a shear crack was visible in the insitu concrete along the free edge approximately 1.5 slab depths from the obtuse corner support. Core six was positioned 1.5 slab depths in from the free edge adjacent to the visible shear crack. Also of interest in this region was the separation of insitu and precast concretes that was clearly visible at the supported edge.

This core again showed good compaction and aggregate distribution, see Plate 7.9. Several distinct cracks were visible around the periphery of the core. A few could be seen in the precast concrete. However, the majority were in the insitu concrete. Those in the precast concrete were significantly narrower.

The cracks in the insitu concrete that were visible along the free edge side of the core were generally inclined at 30°-40° to the soffit, suggesting that they were caused by high shear forces in the obtuse corner region. A diagram of those cracks is given in Figure

7.12. Interestingly, however, there was one contra-inclined crack which would be typical of a 'reverse' shear situation.

These cracks were full of debris and were rather jagged in form, hence accurate width measurement was difficult. The best estimates indicated that cracks A and B, see Figure 7.12 were approximately 0.20mm wide whereas crack C was approximately 0.05mm wide.

Face B, see Figure 7.12 revealed one major crack which was again inclined at 45° to the soffit and was probably caused by high shear forces from the obtuse corner reactions. The width of this crack was approximately 0.2mm which is comparable to those on the opposite face. There was a second crack in the top portion of face B which appeared to curl round from a horizontal to a vertical direction. This crack was again about 0.20mm wide.

Cracks were visible on the top surface of the core with an orientation approximately perpendicular to the supported edges, suggesting that the principal hogging moments were approximately parallel to the supported edges in this region. Where these top cracks intersected the periphery of the core their vertical orientation could also be seen. The largest of these cracks were visible for approximately 50mm below the top surface and were vertical.

Along the axis of the precast beams, separation was visible at most of the precast-insitu interfaces. On face C, see Figure 7.12, there was clear separation of 0.3mm along the free edge side of the precast beam with a tapering separation down the other side of 0.3mm at the top and zero at the bottom.

Some almost horizontal cracks were visible in the precast section in the direction of face C. The two major ones were located at the top flange/web interface and the bottom flange/web interface. The top one was about 0.1mm wide while the lower one was about 0.05mm wide. It was not possible at this stage to ascertain the orientation of these cracks through the length of the precast beam.

On the opposite side, face D, there was again separation although it was not as severe as that found on face C. The free edge side had an almost uniform separation of 0.25mm through the depth of the section. The opposite side showed low separation on the vertical interfaces. However, there was separation of 0.2mm on the inclined interface at the top flange-web junction. There was only one crack visible in the precast concrete on this face. It was approximately horizontal and was about 30mm above the top of the bottom flange. It was not possible to establish the crack width because of the damage that had been caused by the core cutter.

Subsequently, an attempt was made to inject the cracks in the core with Ultra-Violet sensitive epoxy resin before the core was sliced in half along the centre line of the beam using a diamond tipped disk cutter. It was hoped that the UV sensitive dye in the epoxy resin would allow the detection of narrow cracks that would normally be invisible. However, after the core had been cut in half it was realised that the resin had not seeped through the cracks in the web.

A second attempt to increase the visibility of the cracks was then made. UV sensitive epoxy resin was allowed to flow over the cut surface cracks in the hope that it would seep into the surface cracks. After the epoxy resin had hardened the cut core was placed upon a rock grinding/polishing table so that the epoxy resin left on the cut surface was ground away, the result can be seen in Plate 7.9 where the white lines show the presence of cracks.

Fortunately, the cut had intersected one of the transverse holes that passed through the beams. These holes were used for the transverse reinforcement. Inspection of this intersection revealed that there had been practically complete filling of the transverse hole by the insitu concrete, see Plate 7.9.

Inspection of the cut surface adjacent to face A revealed three inclined and one horizontal crack. One of the inclined cracks was located about two thirds of the overall depth up from the soffit, the second was at mid-depth while the third was a third up. All three were inclined at approximately 30° to the soffit. The horizontal crack was located close to the junction between the top of the precast beams and the insitu concrete, in fact for some of its length it appears to run along the junction. Where it deviates from the junction, the crack appears to be adopting a smoother profile than that of the interface itself. Therefore, it would appear that due to incompatible stress fields caused by the different load histories, and material moduli of the precast and insitu concretes, the two concretes lost their initial composite nature. For the majority of the insitu/precast interface this could be achieved by the breakdown of interface bond. However, the rough nature of the top interface has caused the separation to adopt a path which allows a smoother progression than the actual interface junction itself.

The top inclined crack was 0.2mm wide at its intersection with face C narrowing to 0.05mm mid-way through the core and it was not visible 40mm away from its extrapolated intersection with face D.

The lower crack only became visible 70mm from face D as it passed through the insitu concrete that filled the transverse hole. By the time the crack intersected face D it had a width of 0.3mm. It was difficult to locate the crack at mid-depth even by the use of a micro-scope, hence a crack width measurement of 0.03mm is only very approximate.

Discussion of Core Cracking

The inclinations of cracks seen in the cores are dependent upon stress conditions prevailing at the time of their formation. Of particular interest is the cracking of core 6. In the presence of vertical shear only, one would expect a shear crack to form at 45° to the soffit. However, the sections in question were also subjected to varying amounts of axial stress. With reference to the Mohr's circle diagram of Figure 7.13, points a and b refer to orthogonal sections subjected solely to shear, and point c refers to a section which is also subjected to an axial compression. Such points occur in the upper region of the insitu material and through a large proportion of the prestressed precast material. The angle between the section with stresses represented by c and the principle tensile direction has increased and therefore the angle between direction c and the crack direction has decreased. For an axial compressive stress equal in magnitude to the applied shear stress, one would expect the crack to form at 30° to the soffit.

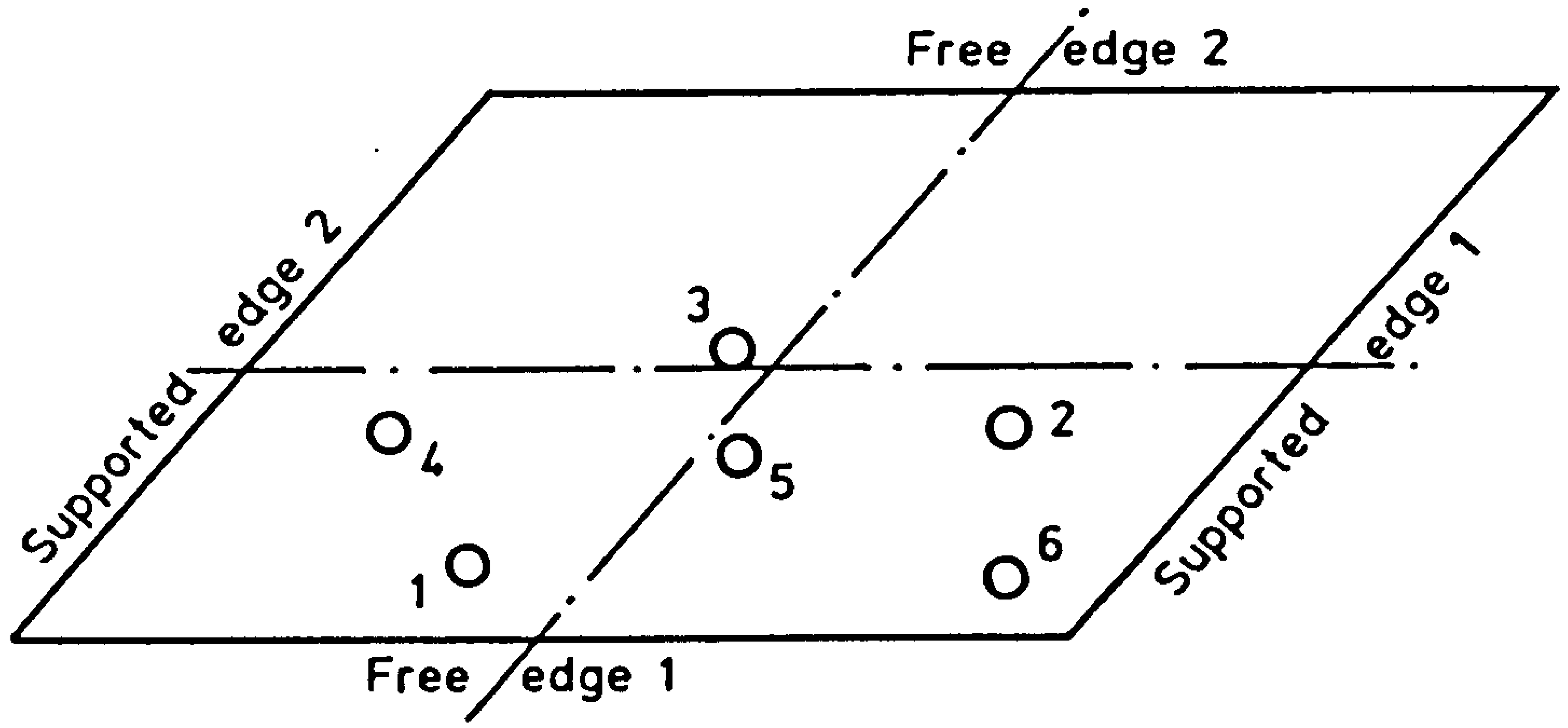

FIG. 7.11. MODEL 2 CORE LOCATIONS

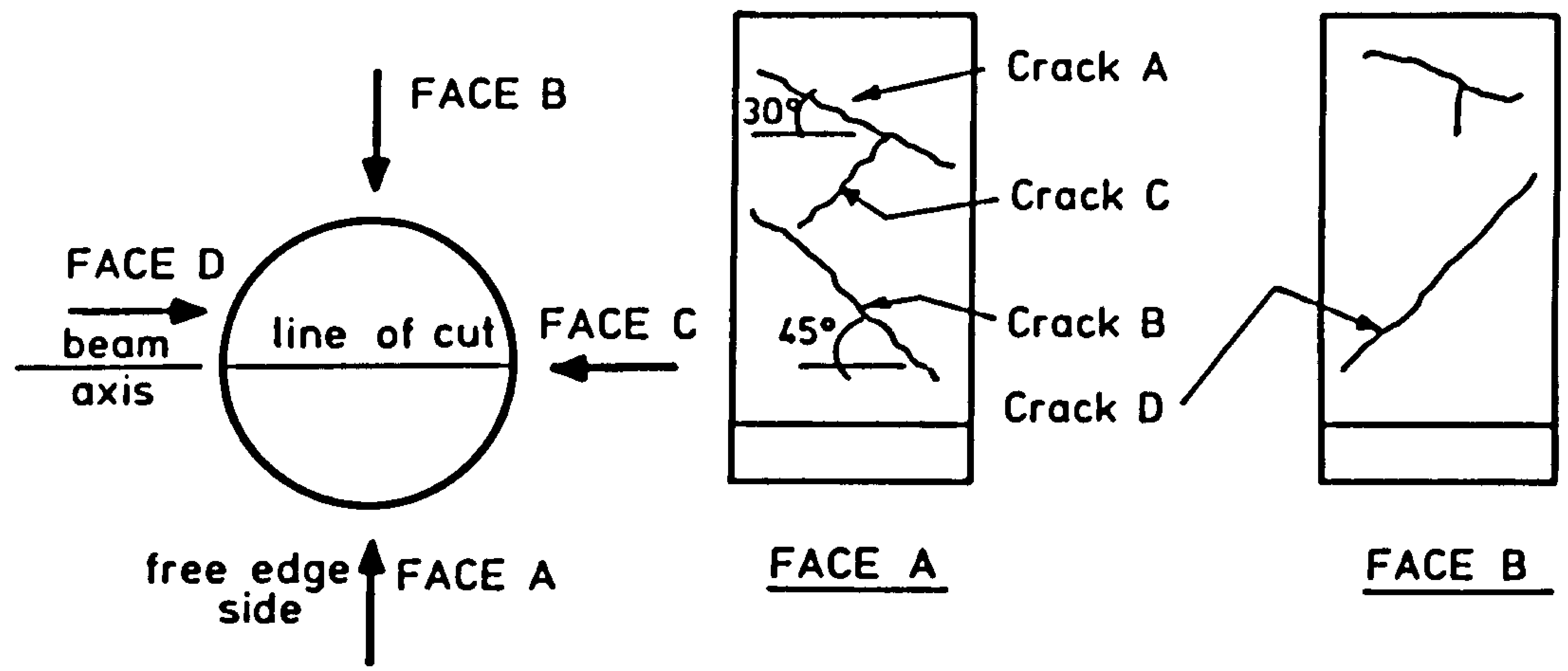

FIG. 7.12. CORE 6 IN-SITU CONCRETE CRACK PATTERN

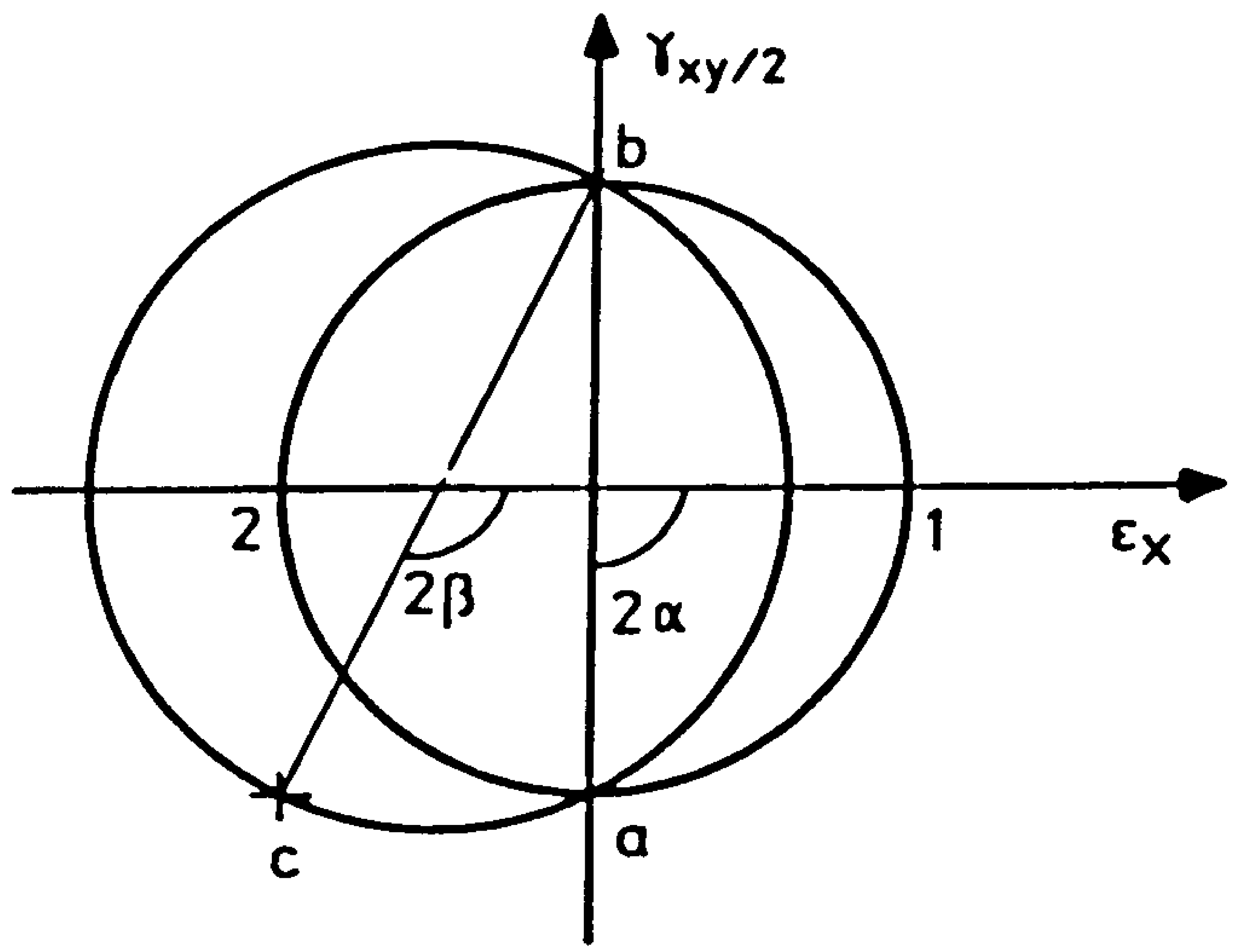

FIG. 7.13. MOHR'S CIRCLE SHOWING INTERACTION OF AXIAL AND SHEAR STRAIN FOR CORE 6

From Figure 7.12 it can be seen that the lower shear crack in the in-situ concrete of core 6 formed at approximately 45°. This suggests that only negligible in-plane direct stresses were acting at the time of its formation. Plate 7.9 shows the cracking on a parallel vertical slice through the same core and illustrates the cracking in the prestressed concrete. All of the cracks shown in this plate are at about 30° to the soffit. Thus at the time of the formation of the crack at mid-depth, continuity between the beams and the adjacent in-situ concrete can no longer be assumed to exist. Locally, at least, there must have been separation and slip at the interface, resulting in a complicated three dimensional state of stress.

7.2 Results Processing

After the test upon model 2 had been completed, the readings that had been recorded by the computer were retrieved and checked for consistency. Then, the readings that would allow the most efficient assessment of the structural response to be carried out were selected. These readings were formed into tables and have been presented in Appendix 7.2. Also contained within that appendix are diagrams showing the exact location of every transducer and de-mec point that was attached to model 2. The test results are assessed and compared with analytical predictions in Chapter 11.

7.3 Investigation of 'Tearing' Crack Phenomenon

The three types of cracking that were evident on the top surface of the model can be seen in Figure 7.8 and Plate 7.5. In area E (see Figure 7.1), the cracking is similar to that observed in monolithic reinforced concrete slabs. In the opposite obtuse corner zone there are continuous tensile cracks parallel to the beams. However in areas D and H, there are 'tearing' type cracks. These are aligned in the general direction of the precast beams, although the short individual stubby cracks which make up these lines are orientated at between 15° and 30° to the beam direction.

If an element of concrete in a top region of the model slab, which includes the in-situ/precast interface is considered, and is subject to a biaxial stress field, then the principal directions are usually inclined to the beam axes, see Figure 7.14. If the principal stresses are transformed to directions parallel and perpendicular to the interface, two direct stresses σ_n and σ_t and a shearing stress τ_{nt} are obtained, see Figure 7.15.

Thus $$\sigma_n = \sigma_1 \cos^2 \theta + \sigma_2 \sin^2 \theta \qquad (7.1)$$

$$\sigma_t = \sigma_1 \sin^2 \theta + \sigma_2 \cos^2 \theta \qquad (7.2)$$

$$\tau_{nt} = (\sigma_2 - \sigma_1) \sin \theta \cos \theta \qquad (7.3)$$

Generally, σ_n compresses or extends the concretes either side of the interface. If the two concretes have different 'E' values, then σ_n could theoretically have a significant effect upon the interface behaviour. There will be a discontinuity in σ_n across the interface. However, in reality, although the concretes will have very different strengths, their elastic moduli are likely to be similar and, therefore, it will be assumed that σ_n has a negligible effect upon the interface behaviour.

The resistance to sliding between the two concretes is provided by a combination of many factors. Probably the most significant being chemical bond, physical roughness, reinforcement dowel action and friction. Dowel action is ignored, on the basis that it will not have a significant effect until after initial slippage. A resistance to slippage at the interface, τ_{tot}, can be defined to be:

$$\tau_{tot} = \tau_i + \tau_f = \tau_i + \sigma_{norm} \tan \phi \qquad (7.4)$$

Where τ_i is the interface shear stress that is required to break the initial chemical bond and cohesion. τ_f is the shear stress required to overcome the frictional restraint. σ_{norm} is the direct stress normal to the interface, while ϕ is the materials' angle of friction.

If the stress system σ_n, σ_t and τ_{nt} acts upon the interface, which is just on the point of slipping then, equation 7.4 can be re-written as

$$\tau_{nt} = \tau_i + \sigma_t \tan \phi \quad \text{Rearranging gives} \quad \tan \phi = \frac{\tau_{nt} - \tau_i}{\sigma_t} \qquad (7.5)$$

Substituting equations 7.2 and 7.3 into 7.5 gives

$$\tan \phi = \frac{(\sigma_2 - \sigma_1) \sin \theta \cos \theta - \tau_i}{\sigma_1 \sin^2 \theta + \sigma_2 \cos^2 \theta} \qquad (7.6)$$

Introducing a stress ratio $R = \sigma_2/\sigma_1$,

$$\tan \phi = \frac{\sigma_1 (R - 1) \sin \theta \cos \theta - \tau_i}{\sigma_1 (\sin^2 \theta + R \cos^2 \theta)} \qquad (7.7)$$

If, initially, it is assumed that the only resistance to sliding is frictional, then τ_i can be set equal to zero and introducing an apparent angle of friction, ϕ'

$$\tan \phi' = \frac{(R - 1) \sin \theta \cos \theta}{\sin^2 \theta + R \cos^2 \theta} \qquad (7.8)$$

Thus, there are three unknowns, the two variables R and θ and the apparent angle of friction ϕ'. From the plots of principal top surface strains recorded during the tests, it can be deduced that the in-plane principal strains in most of the regions subject to "tearing"

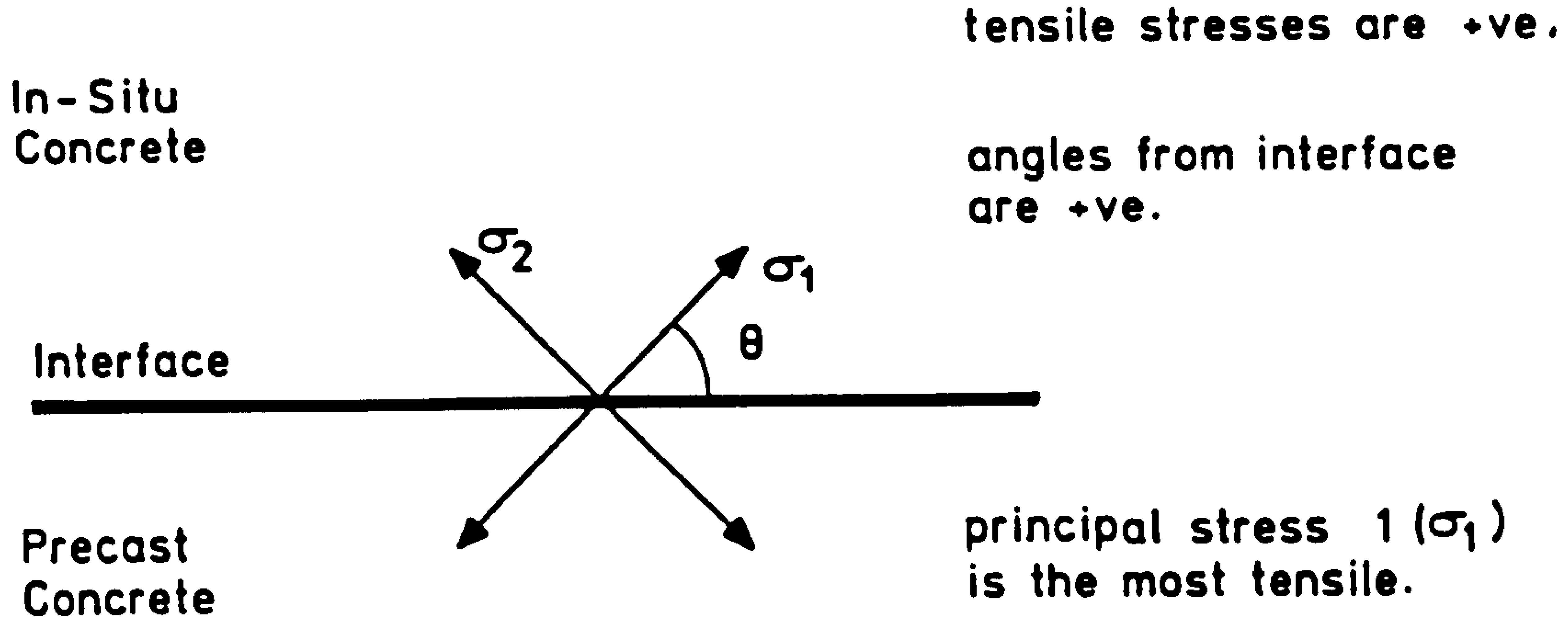

FIG. 7.14. NOTATION ADOPTED FOR STRESS REGIME AT PRECAST/IN-SITU INTERFACE

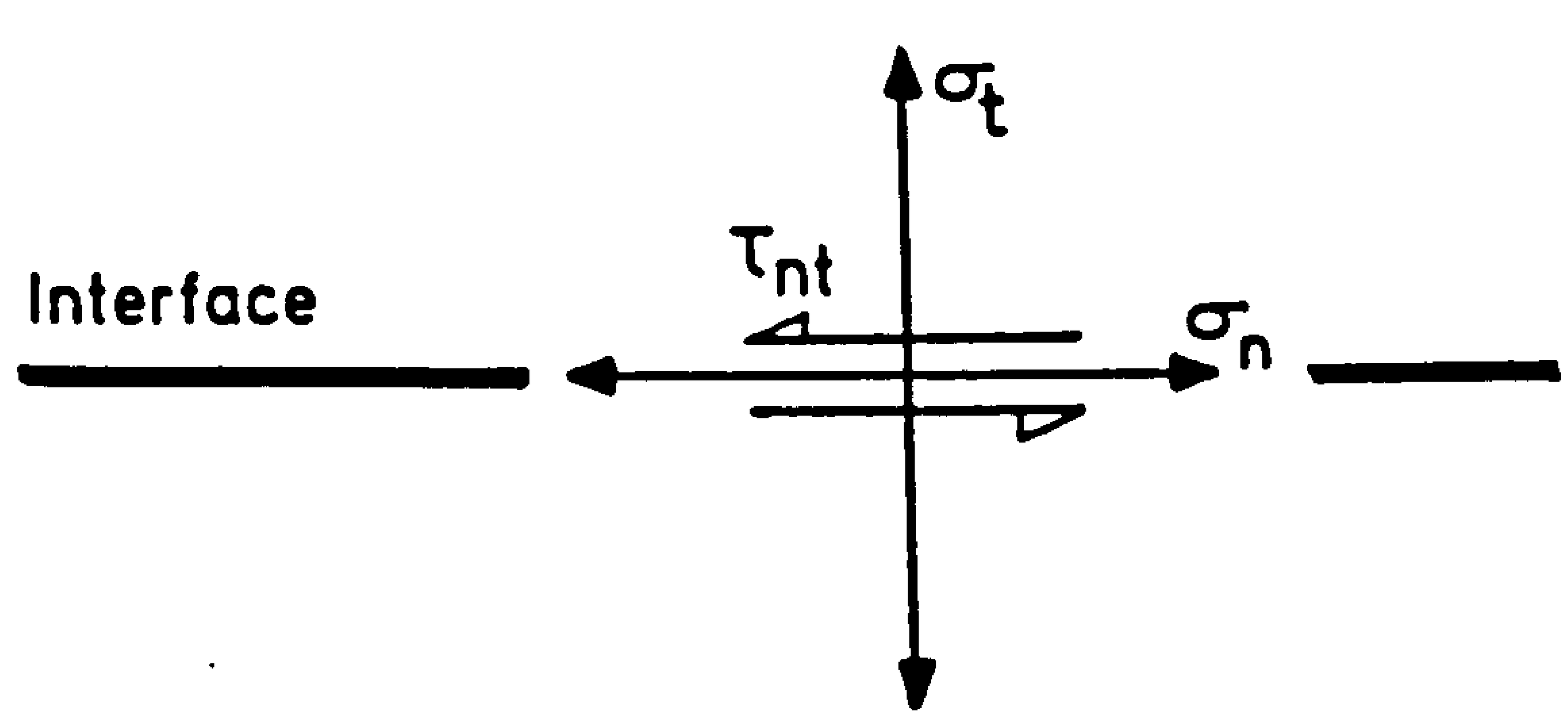

FIG. 7.15. STRESS SYSTEM AFTER TRANSFORMATION TO THE INTERFACE DIRECTION

cracking were of opposite sign. From finite element analyses, the elastic stress ratio R in these regions was in the range -8 to -1, with -5 being the predominant value ($\sigma_2 = -\sigma_1$ to $\sigma_2 = -8\ \sigma_1$).

In Figure 7.16, the lower limits to the apparent angles of friction, that will prevent interface slippage are shown for ranges of R and θ. Predicted negative values of ϕ' shown are meaningless, and are obtained when the normal stress on the interface, σ_t, is tensile. Plots showing the interface normal stress and the interface shear-stress, for various stress ratios (R) and principal angles (θ) have also included in Figure 7.16. To allow easier interpretation, the absolute value of the interface shear stress has been plotted.

Consider the case when R = -5, ($\sigma_2 = -5$, $\sigma_1 = 1$). For $0 < \theta < 66°$ the normal stress on the interface is compressive and reduces with an increase in θ. The magnitude of the shear stress along the interface increases with an increase in θ. Therefore, the required apparent angle of friction to prevent slipping increases with θ.

From examination of the cracking and the finite element stress predictions, it can be seen that when the principal tensile stress is at between 95° and 85° to the interface (opposite obtuse corner to area E), the top cracks are continuous. In area E (see Figures 7.1 and 7.9) where the principal tensile stresses have rotated to approximately 50° to the interface, the top surface cracking is again continuous. However, in the regions where rotation of the principal angles is in the range 50° to 85° (areas D and H), the top surface cracks are discontinuous and take on the 'tearing' appearance. These three regions can clearly be seen in Figure 7.8.

NON-DIMENSIONALISED INTERFACE NORMAL STRESS FOR DIFFERENT STRESS RATIOS.

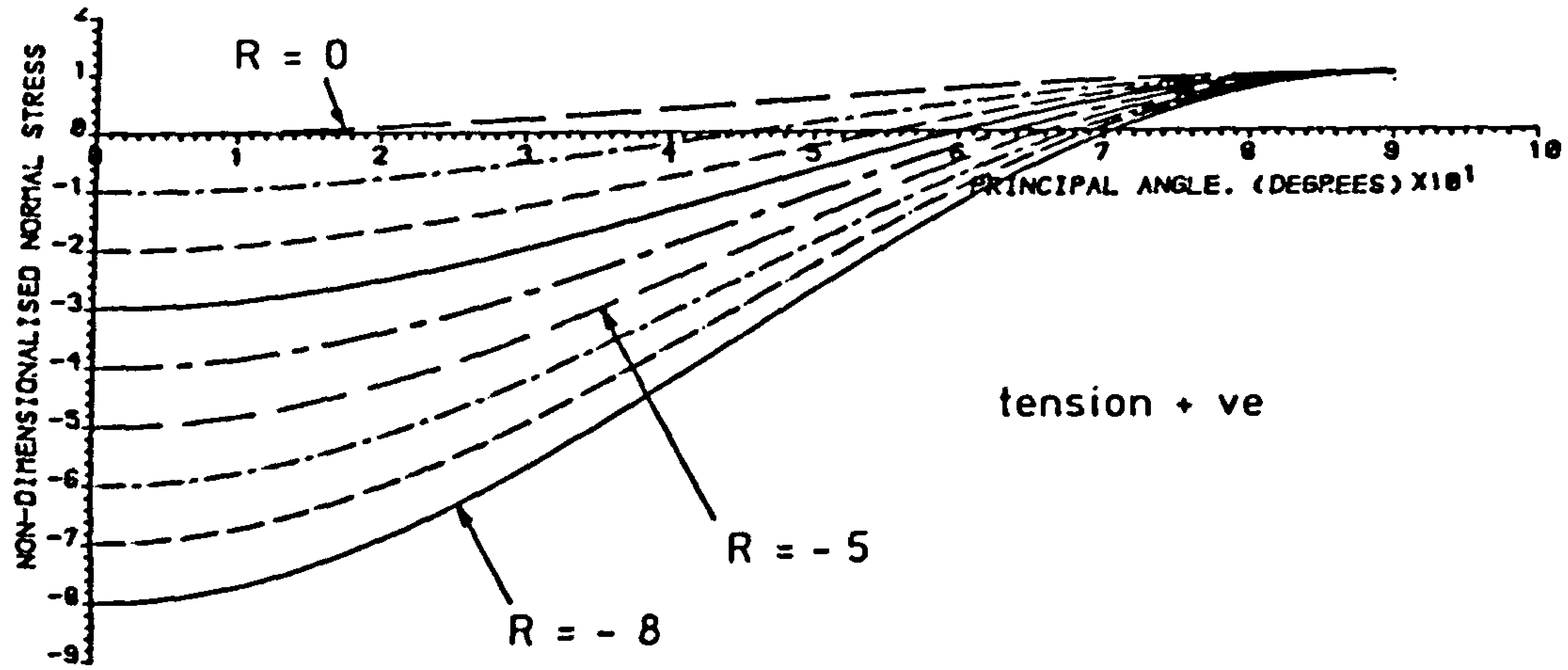

NON-DIMENSIONALISED INTERFACE SHEAR STRESS FOR DIFFERENT STRESS RATIOS.

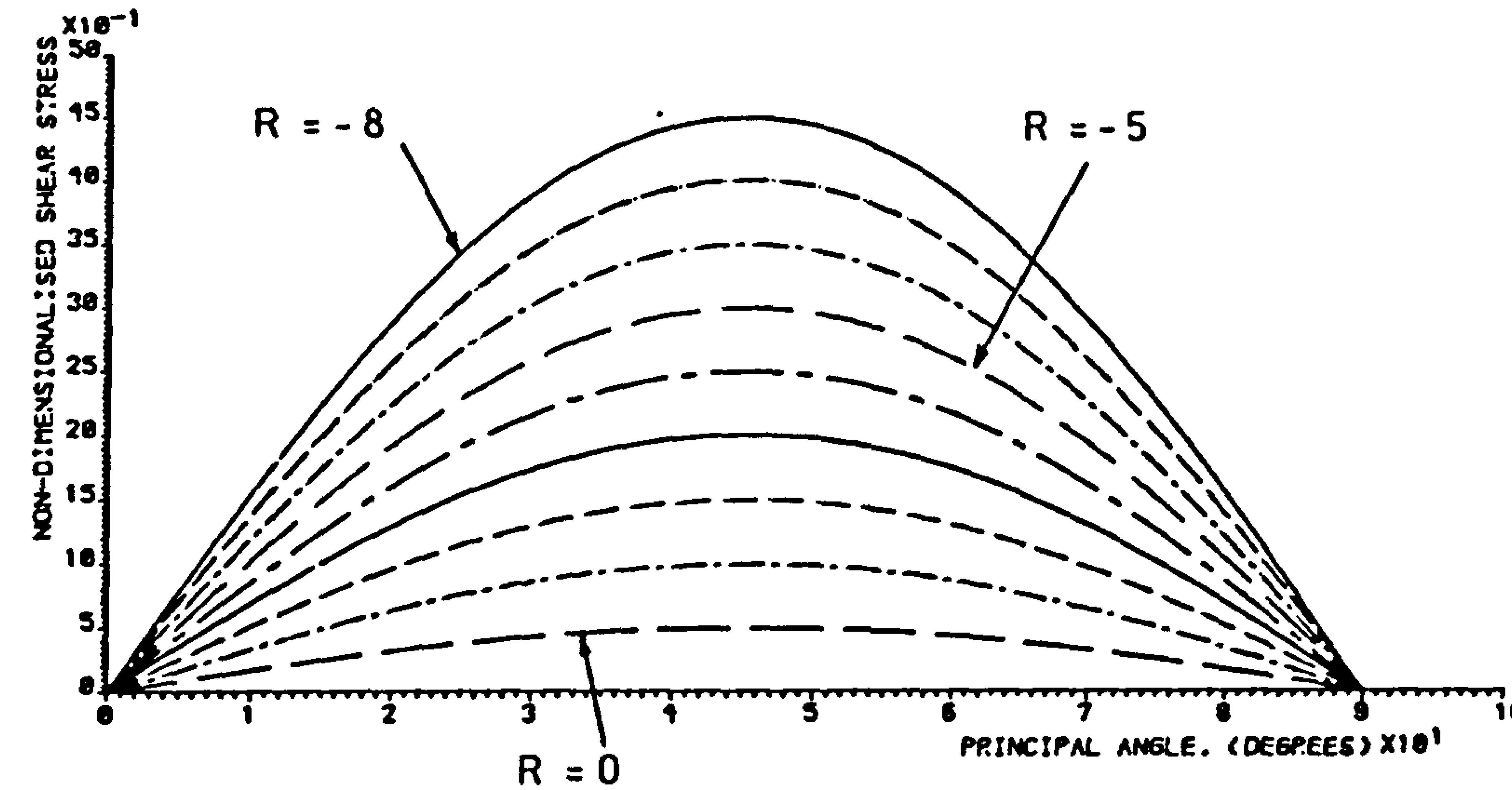

REQUIRED ANGLE OF FRICTION FOR 'NO SLIP' FOR DIFFERENT STRESS RATIOS.
ASSUMING A PURELY FRICTIONAL RESTRAINT

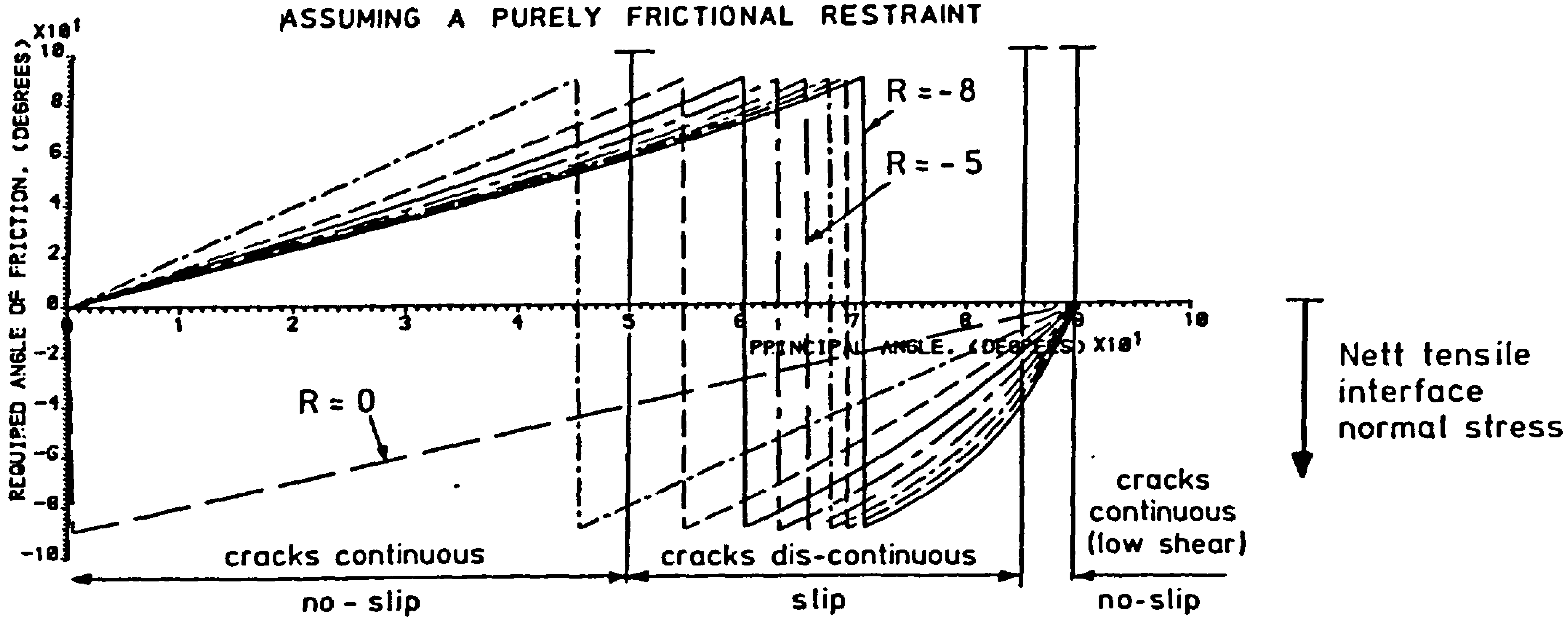

KEY: -

R = Stress ratio.

Each line represents a situation with constant stress ratio (R) and rotating principal angle.
The principal angle is the angle +ve anti-clockwise from the interface to the most tensile stress

FIG. 7.16. REQUIRED ANGLE OF FRICTION AT THE PRECAST / IN-SITU INTERFACE FOR 'NO-SLIP' ASSUMING A PURELY FRICTIONAL RESTRAINT

If one considers the typical stress ratio of -5, then the required apparent angle of friction to prevent slipping at the interface of the in-situ and precast concretes would appear to be 63°, for an angle of rotation of the principal stresses of 50°. At principal angles below this, the interface normal stress is more compressive while the shear stress magnitude is reduced, hence one would expect less likelihood of slipping. At principal angles between 85° and 95°, the interface shear stress is low and unable to overcome the shear capacity, hence slippage is unlikely.

Between these two no-slip regions, there are areas where slip is seen to occur (areas D and H), with principal angles between 50° and 85°. At the higher end of this range, there is a tensile stress across the interface and, therefore, one would expect that as soon as the shear stress was large enough to overcome the restraint factors mentioned above a tearing type cracking appearance would result. Towards the lower end of this range, the interface normal stress is compressive. However, the small magnitude of compression is not capable of mobilising the required frictional force to overcome the relatively large interface shear stress. At smaller principal angles, the interface normal compressive stress is larger, while the shear stress is reduced. A sufficiently large frictional force is mobilised, and the tearing appearance of the crack pattern ceases.

One would expect the angle of friction of concrete on concrete to be largely dependent upon the roughness of the two surfaces and hence a large variation in possible values for the angle of friction would be expected. However, a general value of 37° has been suggested, see section 2.1.3. It will be recollected that the precast beams were cast against steel side moulds with a smooth surface. However, small air bubbles did adhere to the moulds during casting and hence the resulting precast beam surfaces did have irregularities. These small bubble holes will have increased the effective roughness when the insitu concrete was cast, thus increasing the physical restraint to slipping.

If one includes the cohesion term τ_i in the calculations, then a knowledge of the absolute magnitude of the stresses, rather than a simple ratio would be required. From section 2.1.3, and equation 2.2, the interface shear capacity is given by

$$\tau_{tot} = 0.07\ f_{cu} + \tan \phi\ \sigma_{norm} \tag{7.9}$$

The cohesive term in this equation, $0.07\ f_{cu}$, is equal to τ_i used in previous equations. After initial breakdown of bond, the value of the cohesive term will probably be severely reduced. With a precast concrete cube strength of $-74.6\ N/mm^2$ and an in-situ concrete strength of $-58.7\ N/mm^2$ for model 2, then a typical composite value of $-66.2\ N/mm^2$ can be calculated from $\sqrt{(74.6 \times 58.7)}$. Using this value and the equation above, the cohesion term is equal to $-4.63\ N/mm^2$.

From equation 7.8, defining the interface shear capacity in terms of the apparent angle of friction, ϕ'

$\tau_{nt} = \tan \phi'\ \sigma_t$. With $\phi' = 63.4°$ $\quad \tau_{nt} = 1.99\ \sigma_t$

At breakdown $\tau_{tot} = \tau_{nt}$ and $\sigma_{norm} = \sigma_t$, hence

$$1.99\ \sigma_t = -4.63 + 0.75\ \sigma_t$$

$$\therefore \sigma_t = \frac{-4.63}{1.99 - 0.75} = -3.72\ N/mm^2 \quad \text{hence } \tau_{nt} = 1.99\ \sigma_t = -7.41\ N/mm^2$$

Using equations 7.2 and 7.3, the magnitude of the principal stresses at breakdown, for a stress ratio R of -5 and a principal angle of 50° can be obtained. Using,

$$\sigma_t = \sigma_1 \sin^2\theta + \sigma_2 \cos^2\theta \text{ and } \tau_{nt} = (\sigma_2 - \sigma_1) \sin\theta \cos\theta$$

then for R = -5,

$$\sigma_t = \sigma_1 (\sin^2\theta - 5 \cos^2\theta) \text{ and } \tau_{nt} = - 6\, \sigma_1 \sin\theta \cos\theta$$

With the principal angle $\theta = 50°$,

$$\sigma_t = -1.48\, \sigma_1,\ \tau_{nt} = -2.95\, \sigma_1 \quad \text{and} \quad \sigma_2 = -5\, \sigma_1$$

$$\therefore \quad \sigma_1 = \frac{\sigma_t}{-1.48} = \frac{-3.72}{-1.48} = 2.51 \text{ N/mm}^2 \quad \text{and} \quad \sigma_2 = -12.57 \text{ N/mm}^2$$

From the Finite Element predictions, it is probable that this situation would be encountered in areas D and H during the middle stage of testing, at load levels beyond those considered for ultimate limit state design.

7.4 Tests on Longitudinal Strips

In addition to the test upon model 2, subsidiary tests were also carried out upon 1:3.5 models of longitudinal strips of the prototype deck. The tests on the longitudinal strips are fully described in Appendix 7.1.

These separate tests provided useful information on the flexural stiffness and failure history for a longitudinal strip of the composite construction. The specimens used for these tests were nominally identical, to allow an appraisal of result scatter due to material property variations and experimental errors.

The excellent correlation between the results of the two tests can be seen in Figure 4 of Appendix 7.1. The results suggested that the restraint of the precast concrete severely retarded the onset of cracking in the insitu concrete while the initial flexural stiffness agreed closely with the theoretical stiffness calculated with an 'E' value obtained from specimen tests.

Cracking in both tests was well distributed at an interval of approximately 100mm. During the latter stages of the test there was limited evidence of cracks closing while others became dominant. However, this effect may have been restrained by the excellent bond properties of the prestressing strand and the minimal moment redistribution given the determinate nature of the structure.

BLANK IN ORIGINAL

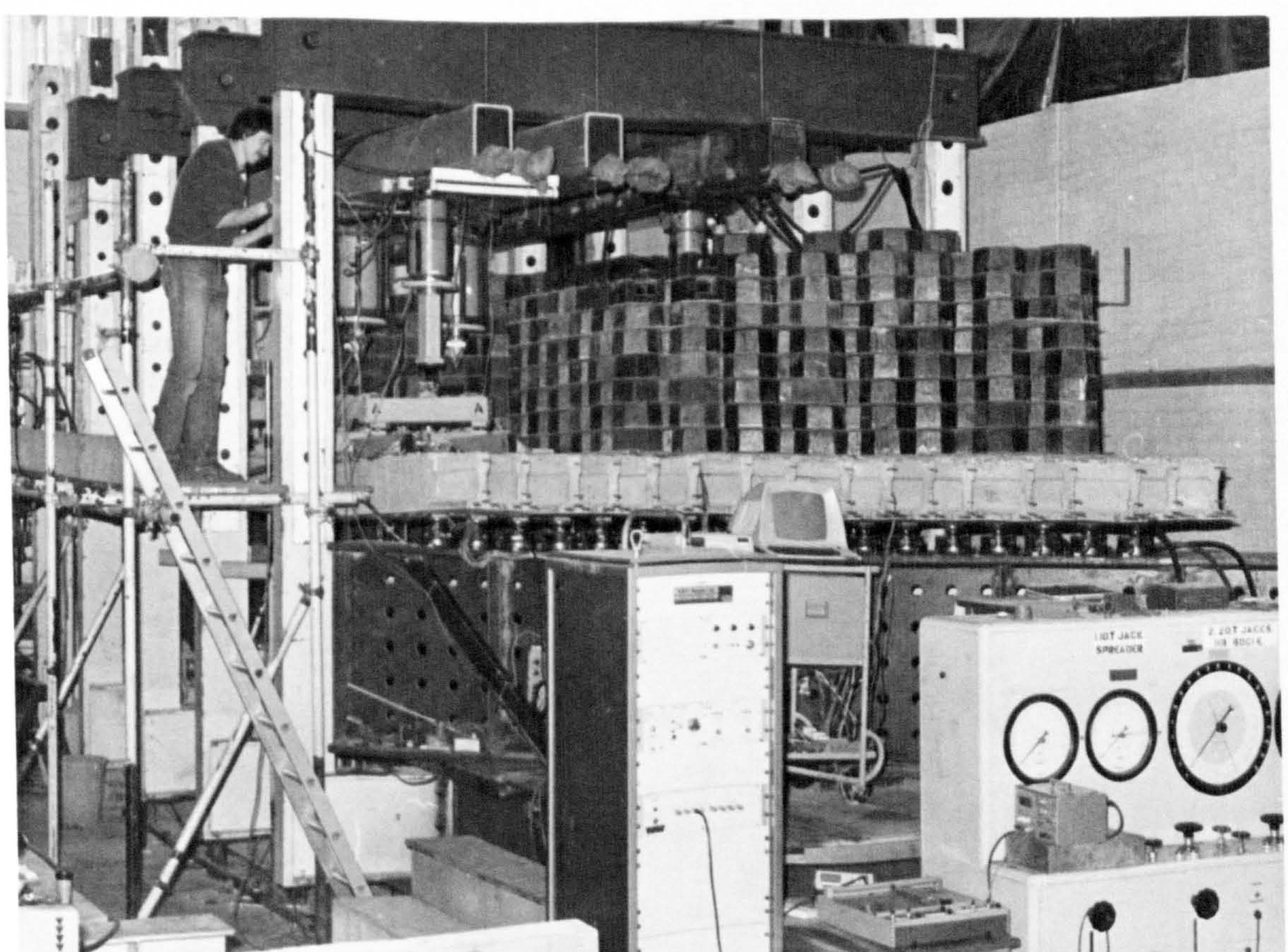

PLATE 7.1 GENERAL VIEWS OF MODEL 2 DURING TESTING

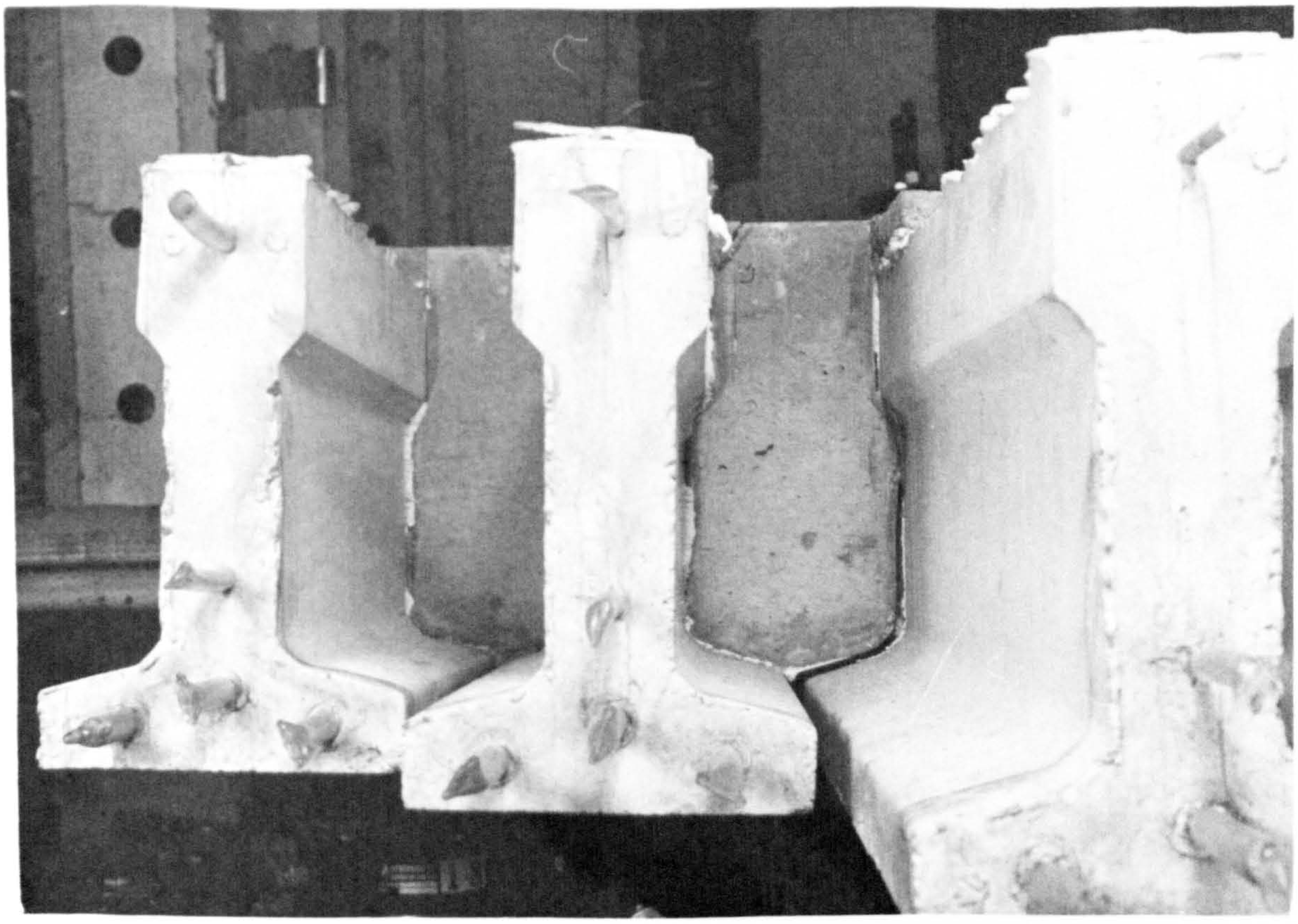

PLATE 7.2 BREAKDOWN OF COMPOSITE ACTION IN MODEL 2

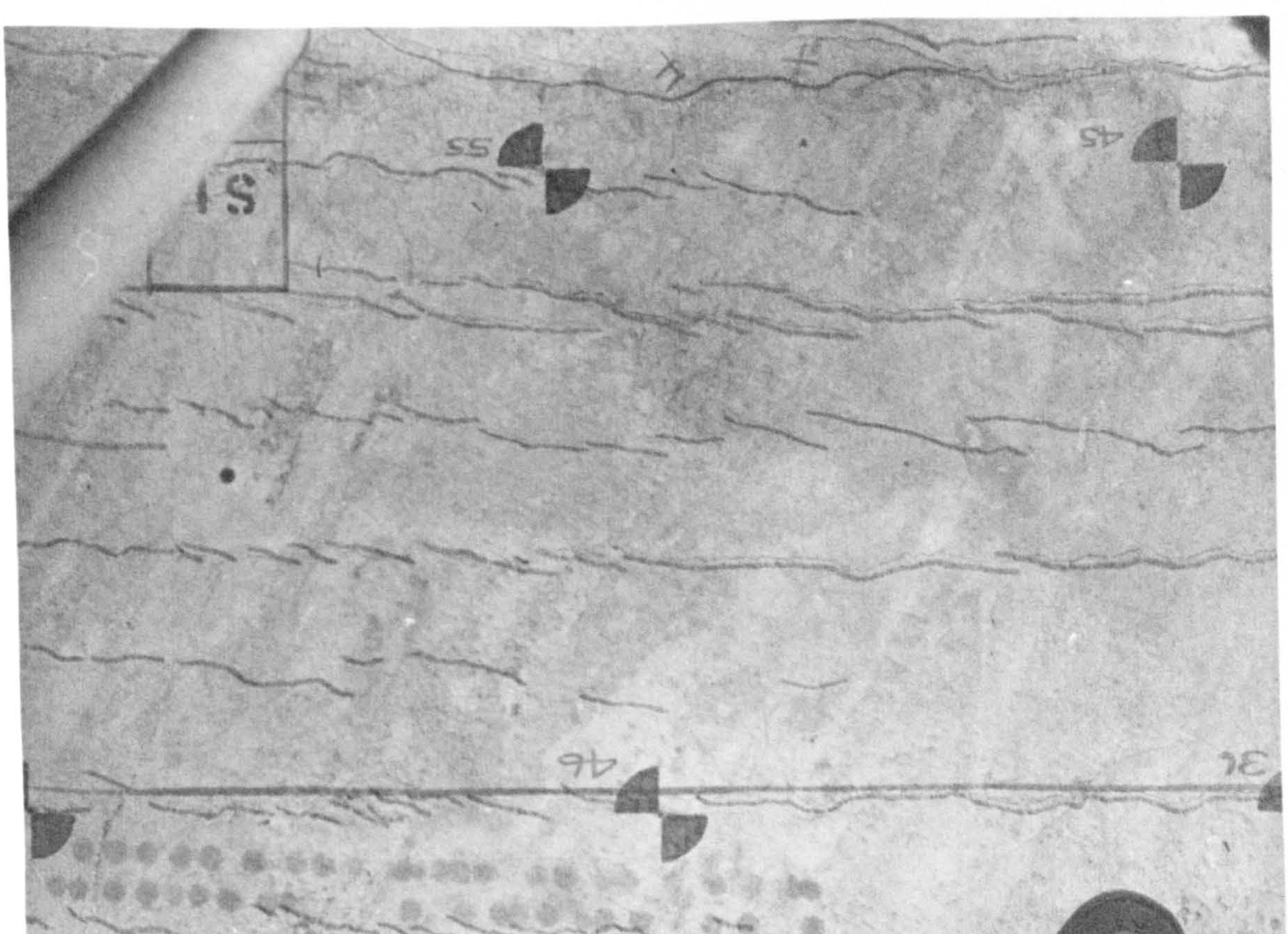

PLATE 7.3 THE 'TEARING' TYPE CRACKING THAT WAS VISIBLE ON THE TOP SURFACE OF MODEL 2

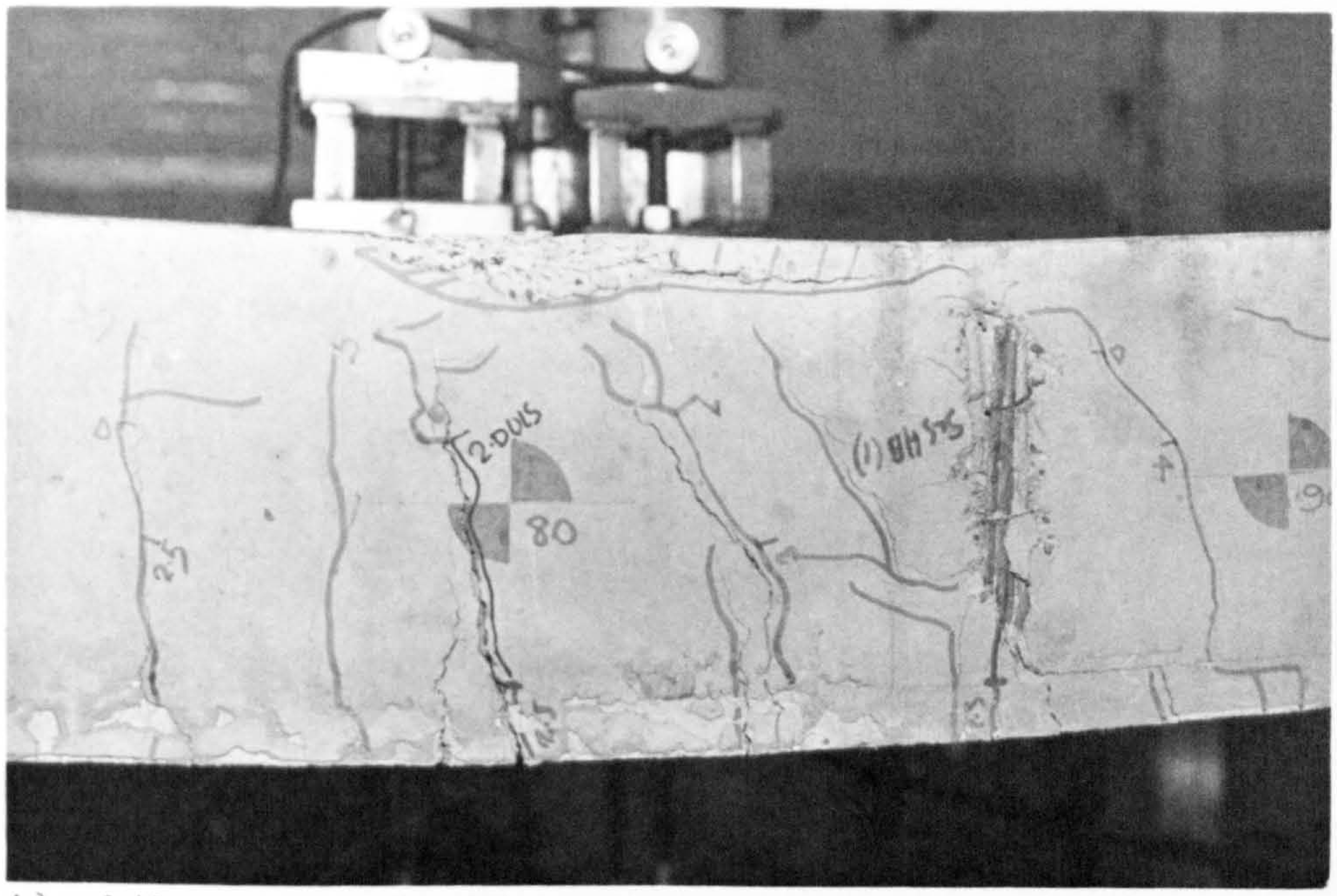

i) Adjacent to the HB bogie

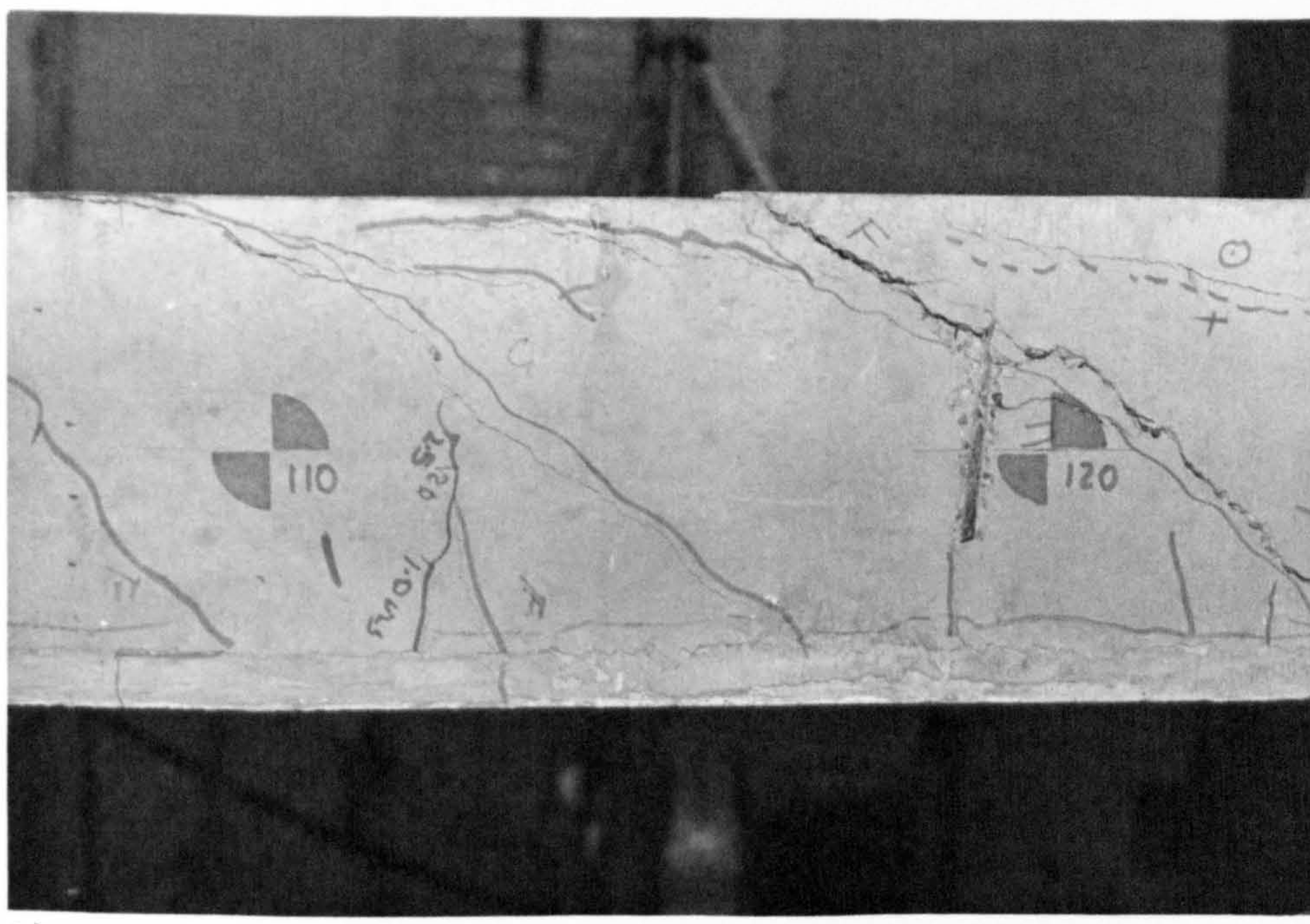

ii) Approximately 2½ slab depths from the obtuse corner

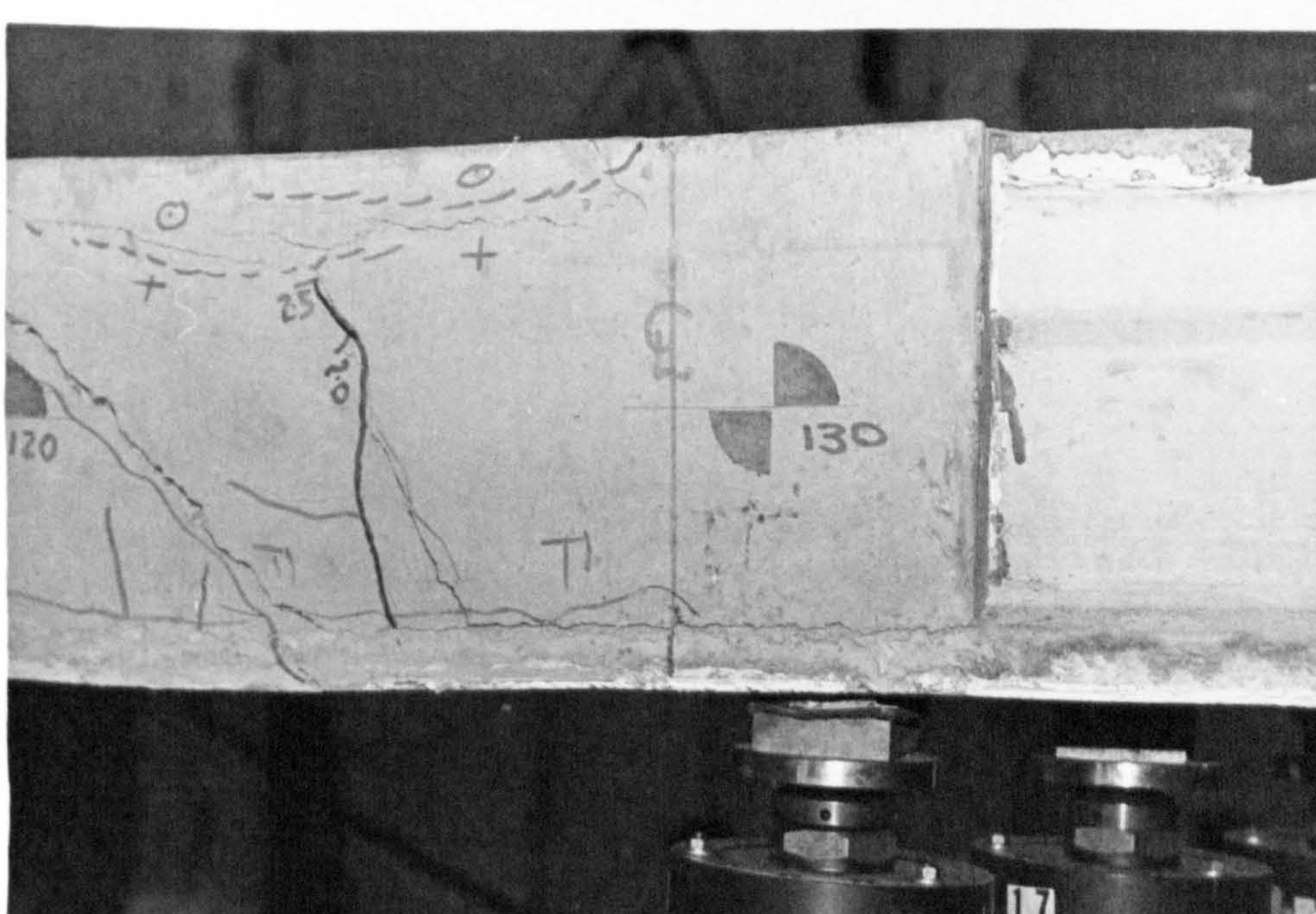

iii) Adjacent to the obtuse corner

PLATE 7.4 CRACK PATTERN ALONG THE LOADED FREE EDGE OF MODEL 2

PLATE 7.5. MODEL 2 TOP SURFACE CRACK PATTERN

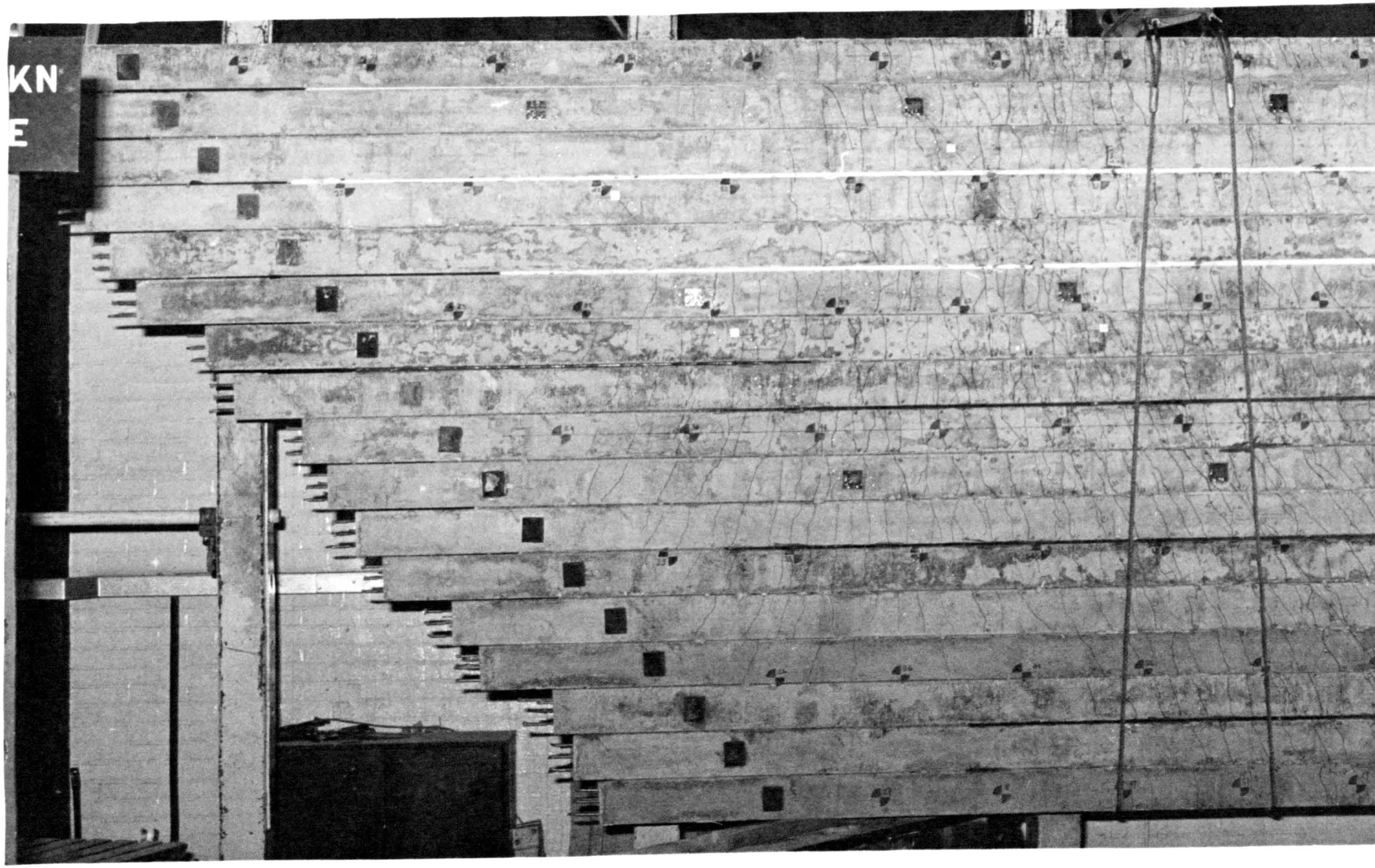

PLATE 7.6 MODEL 2 SOFFIT CRACK PATTERN FOR THE HALF REMOTE FROM THE OBTUSE CORNER

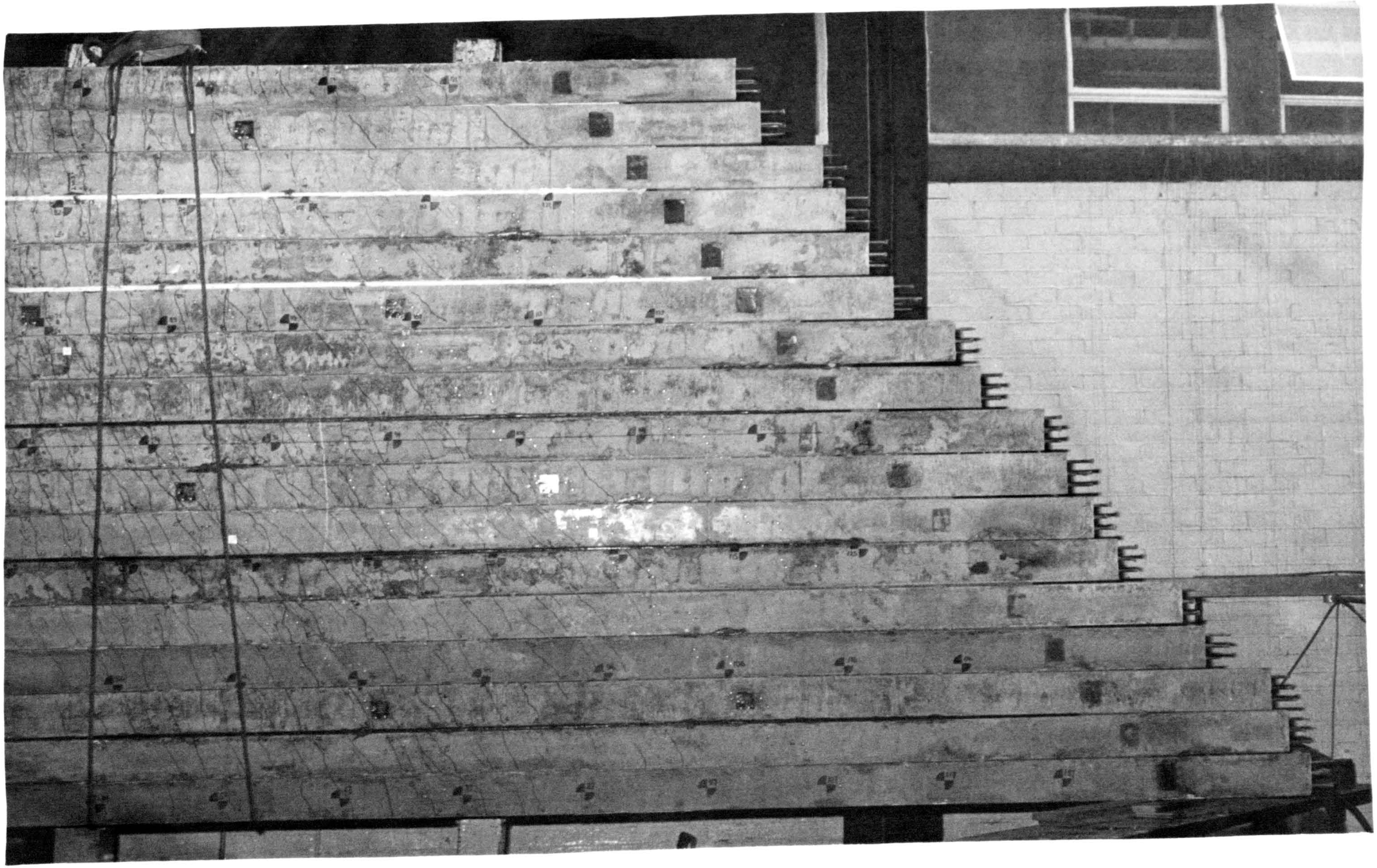

PLATE 7.7 MODEL 2 SOFFIT CRACK PATTERN FOR THE OBTUSE CORNER HALF

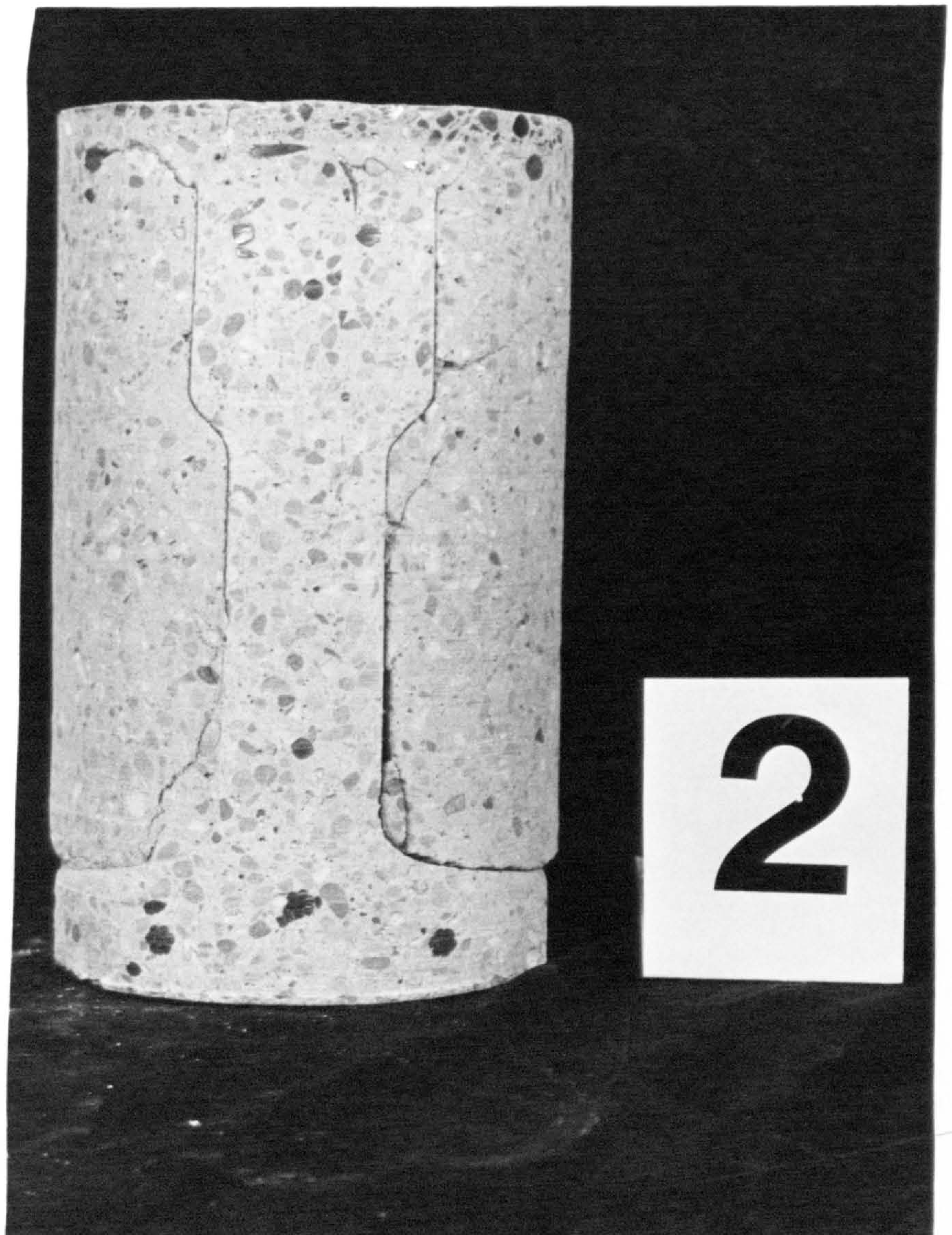

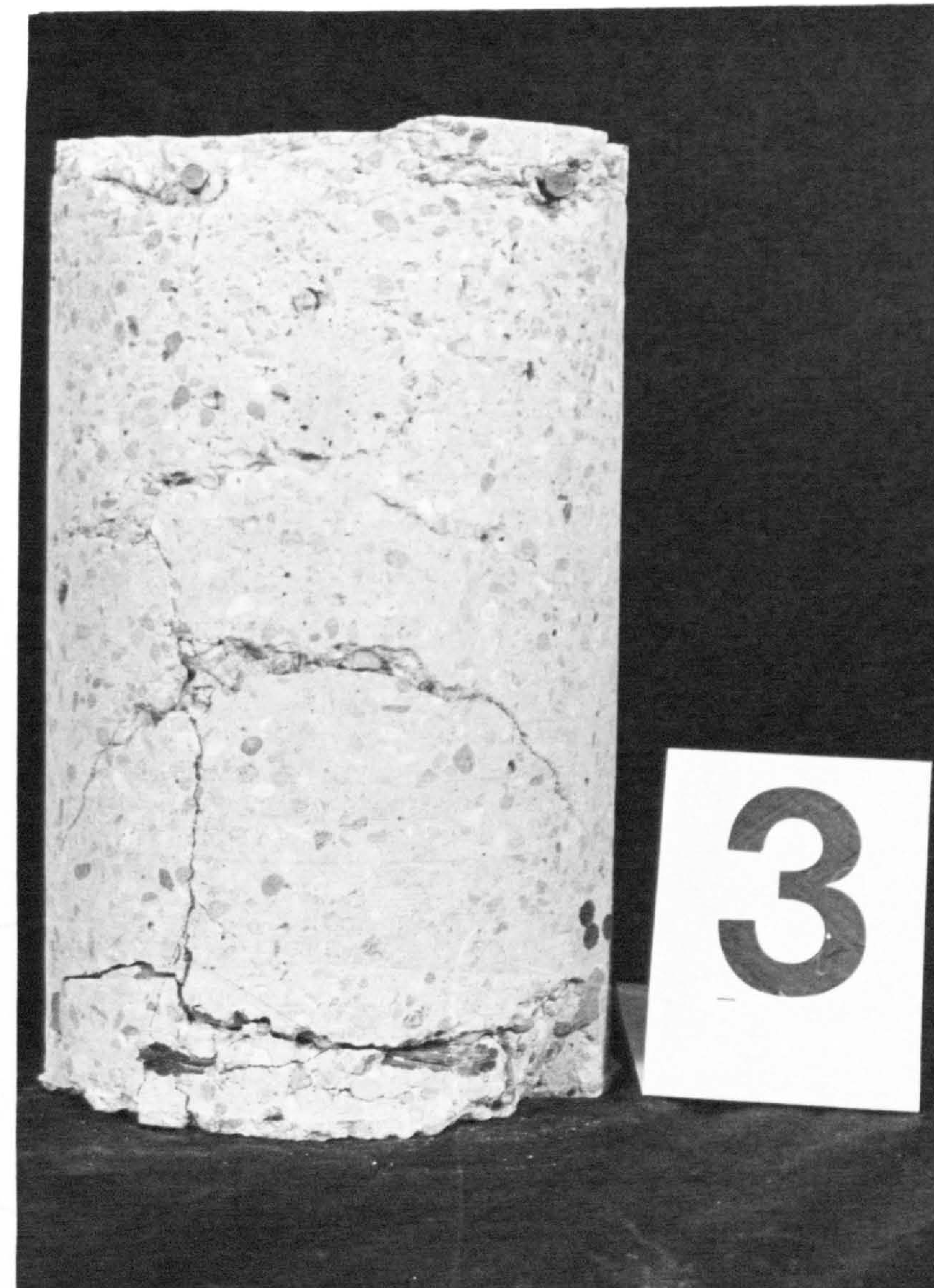

PLATE 7.8 CONCRETE CORES THAT WERE REMOVED FROM MODEL 2

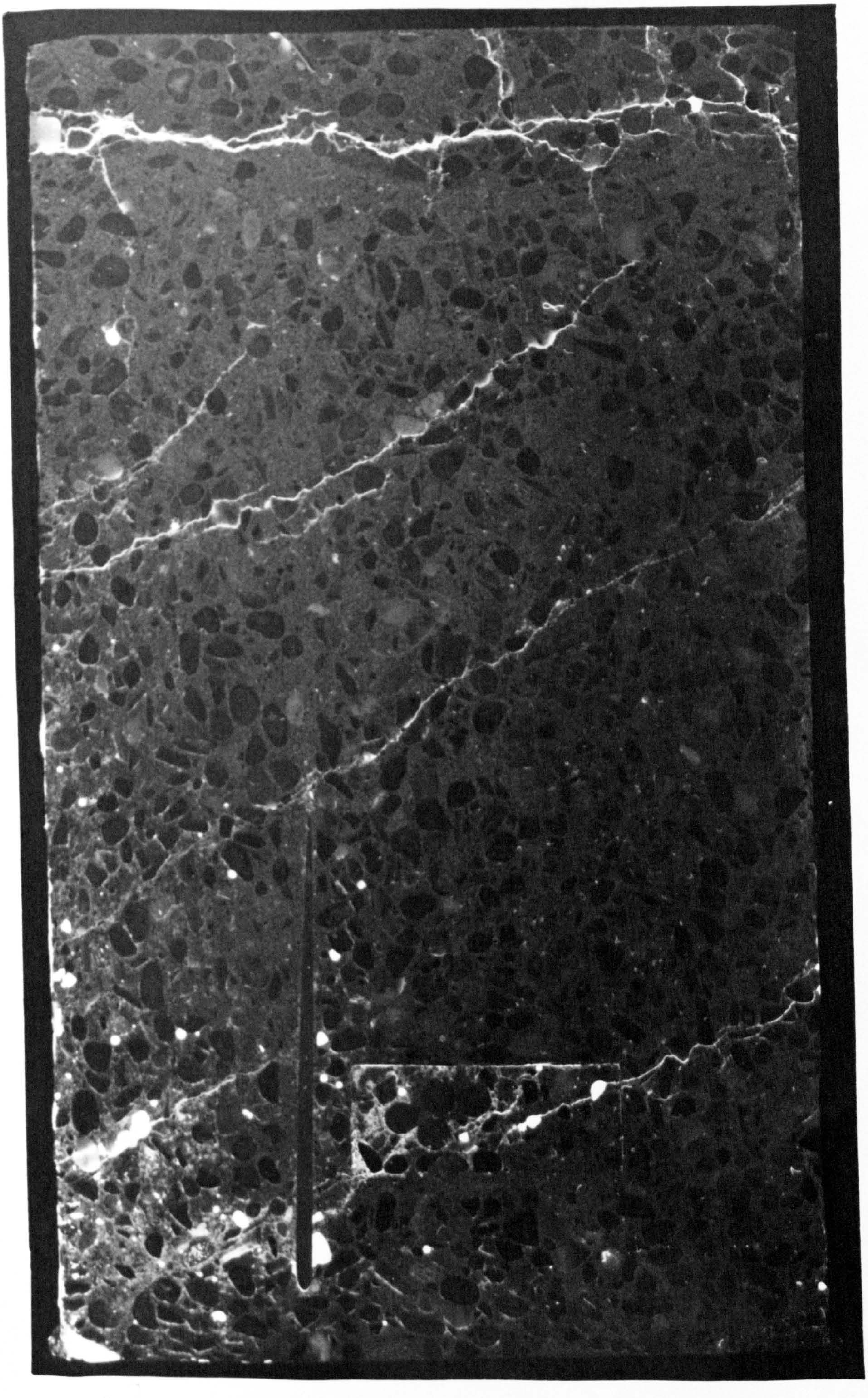

PLATE 7.9 PRECAST CONCRETE CRACK PATTERN ON THE CUT FACE OF CORE 6

APPENDIX 5.1 Moment-Curvature Relationship for the Composite Beams of Model 1

Introduction

Composite beams were formed incorporating 1, 2 and 3 prestressed beams, respectively, as described in Appendix 2.5 of Research Report No TRR 842/368, produced for the Transport and Road Research Laboratory (hereafter referred to as the Report). The information provided on the moment-curvature relationship was, however, less than anticipated, due to the premature bond failures. A further two composite beams incorporating 1 pretensioned beam were, therefore, constructed and tested. The first beam was called the Control Beam and the second beam, which had welded end plates, was called the New Beam.

The gradients of the moment-curvature graphs, before cracking of the pretensioned beams, are given in Table 1. For reference, the cube strengths of the precast beams ($f_{cu,p}$) and the insitu concretes ($f_{cu,i}$) are also tabulated.

Table 1 Uncracked Flexural Stiffnesses

Beam	EI = M/X (kNm^2/m)	$f_{cu,p}$	$f_{cu,i}$
1	11650	56.4	42.1
New Beam	12150	57.0	38.2
2	15080	61.7	37.7
3	14680	56.4, 61.7	45.0

It is apparent that the composite beams with insitu concrete sandwiched between pretensioned beams are stiffer than those with only one pretensioned member. The EI value from a transformed section calculation, using E values determined from strain gauged cylinders, is 14,400 kNm^2/m.

This suggests that pre-structural cracking (due to restraint of early thermal contraction) reduced the effective stiffness of the composite members. However, the tensile stiffness of the sandwiched insitu concrete is largely retained until cracking of the pretensioned members.

The moments (per composite beam) at which cracking was detected in the prestressed beams were 11.6, 10.5, 12.4 and 10.8 kN.m, respectively. Detection of first cracking is notoriously difficult, and the values listed must be regarded as very approximate. No trend is evident from the values.

<u>Test of Control Beam</u>

The beam was set up with the testing arrangements shown in Figure 1. At the time of testing, the cube strengths of the precast and insitu concretes were 57.1 N/mm^2 and 40.6 N/mm^2, respectively.

The steel strains have been plotted against the moments at the strain gauged sections in Figure 10 of Appendix 2.5 of the Report and typical

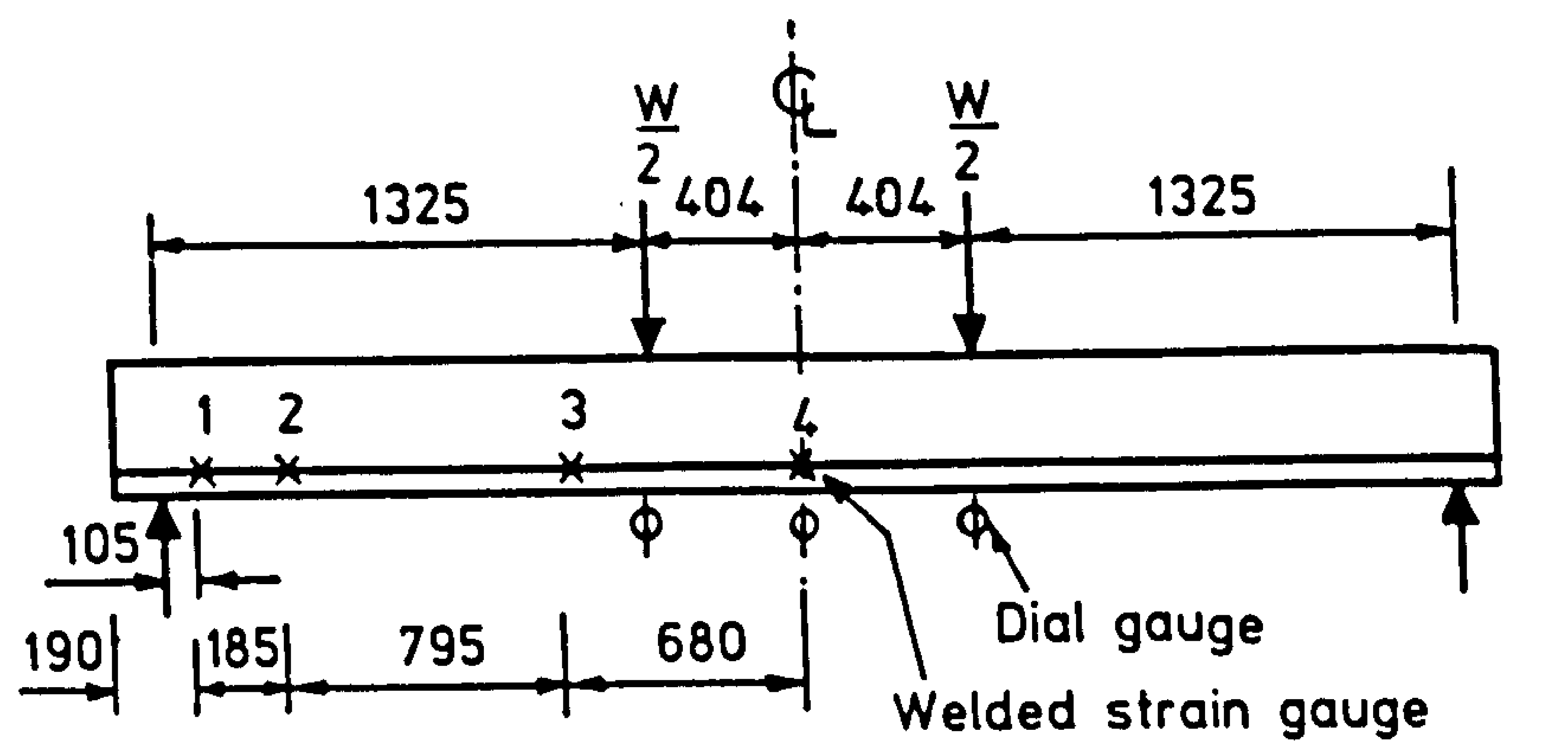

FIG. 1. TEST ARRANGEMENT FOR CONTROL AND NEW BEAM

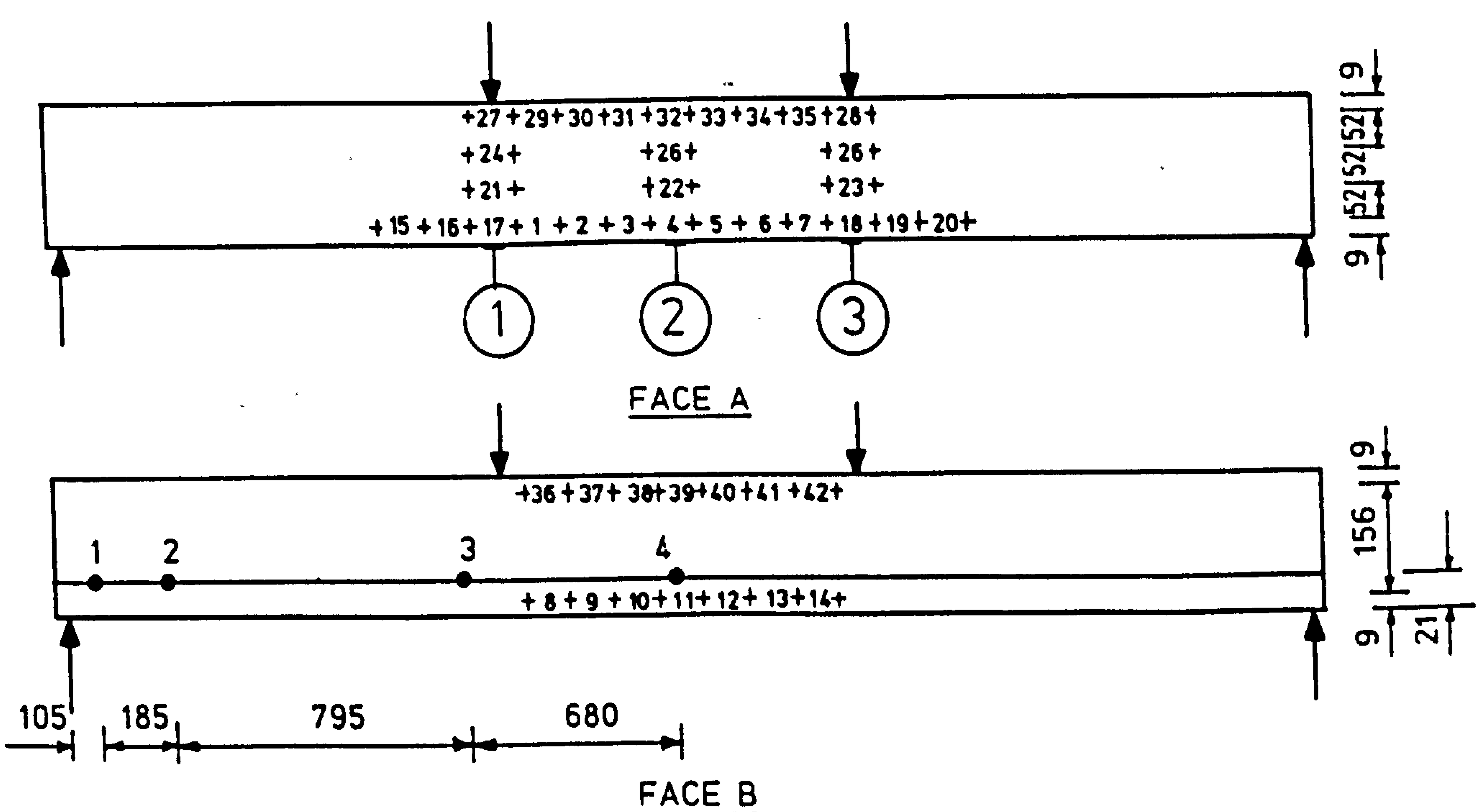

FIG. 2. TRANSDUCER AND DE-MEC POINT LOCATIONS FOR NEW BEAM

stress-strain curves for the tendons are shown in Figure 4. The measured strain in the tendons, before failure, suggests that yielding was taking place.

The moment-curvature relationship has been plotted in Figure 5, the continuously curved nature of the initial part of the graph for the Control Beam is due to an experimental error. Because of an unnoticed change in the load cell scale setting, the beam was loaded to beyond initial cracking before any deformation readings were taken. The graph shown is for a second test on the beam, with the locked-in curvature ignored. Test results are given in Tables 2 to 4, for reference. No separation of insitu and precast concretes was observed. The crack pattern at failure is shown in Plate 1 and, as can be seen, the visible cracks were continuous across the precast and insitu concrete interfaces.

<u>Test of New Beam</u>

The "New Beam" was tested 11 weeks after release of the tendons, using the arrangement shown in Figure 1. The test was delayed to enable much of the creep in the concrete gripping the tendons to take place, so that bond conditions were similar to those in the beams of the model bridge. The 28 day cube strength of the precast beam was 57 N/mm^2 and the strength of the insitu concrete at the time of testing was 38.2 N/mm^2. The corresponding split cylinder strengths were 3.8 N/mm^2 and 3.4 N/mm^2, respectively.

The steel strains have been plotted against the moments at the strain gauged sections in Figure 12 of Appendix 2.5 of the Report. Measured

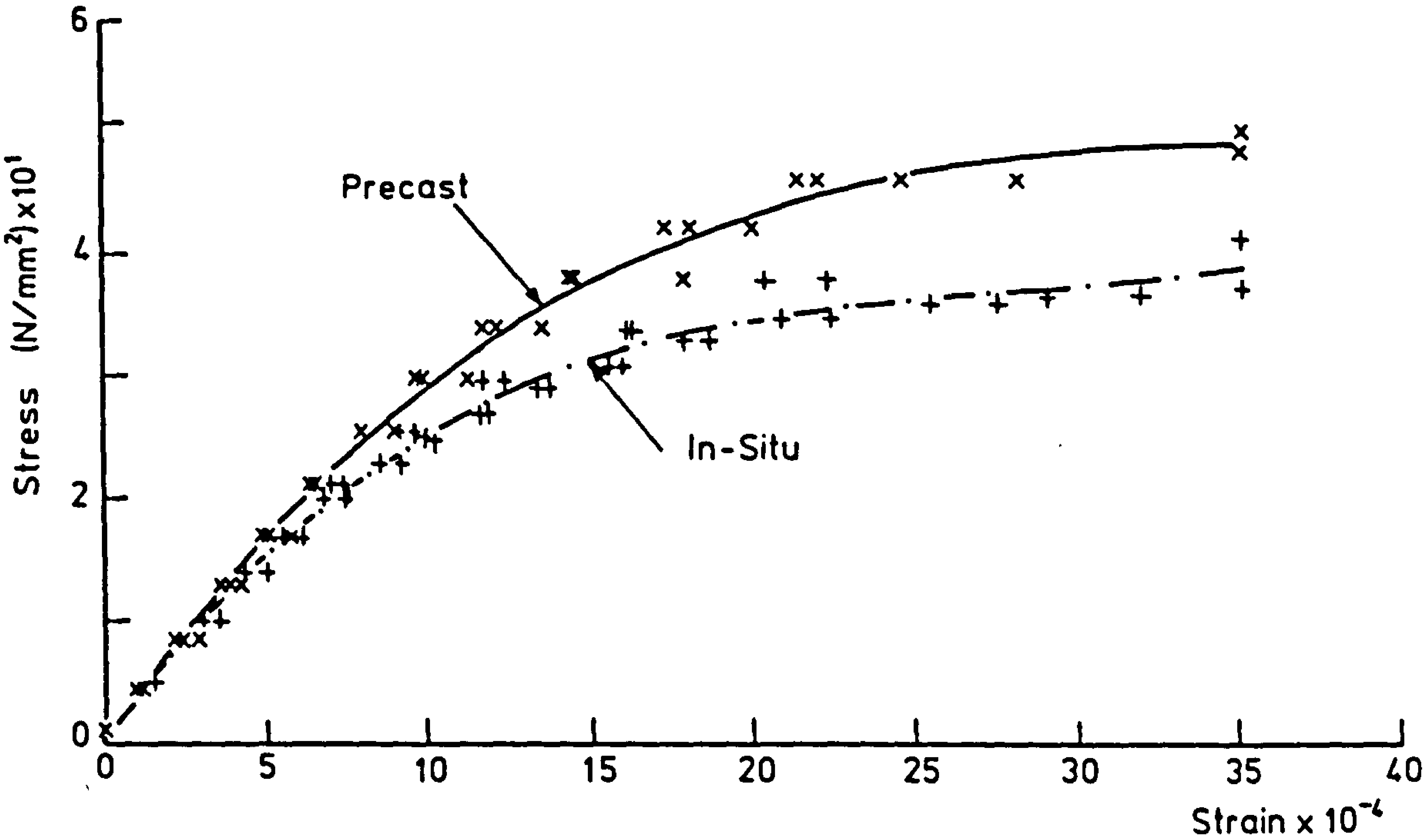

FIG. 3. CONCRETE STRESS-STRAIN DIAGRAM

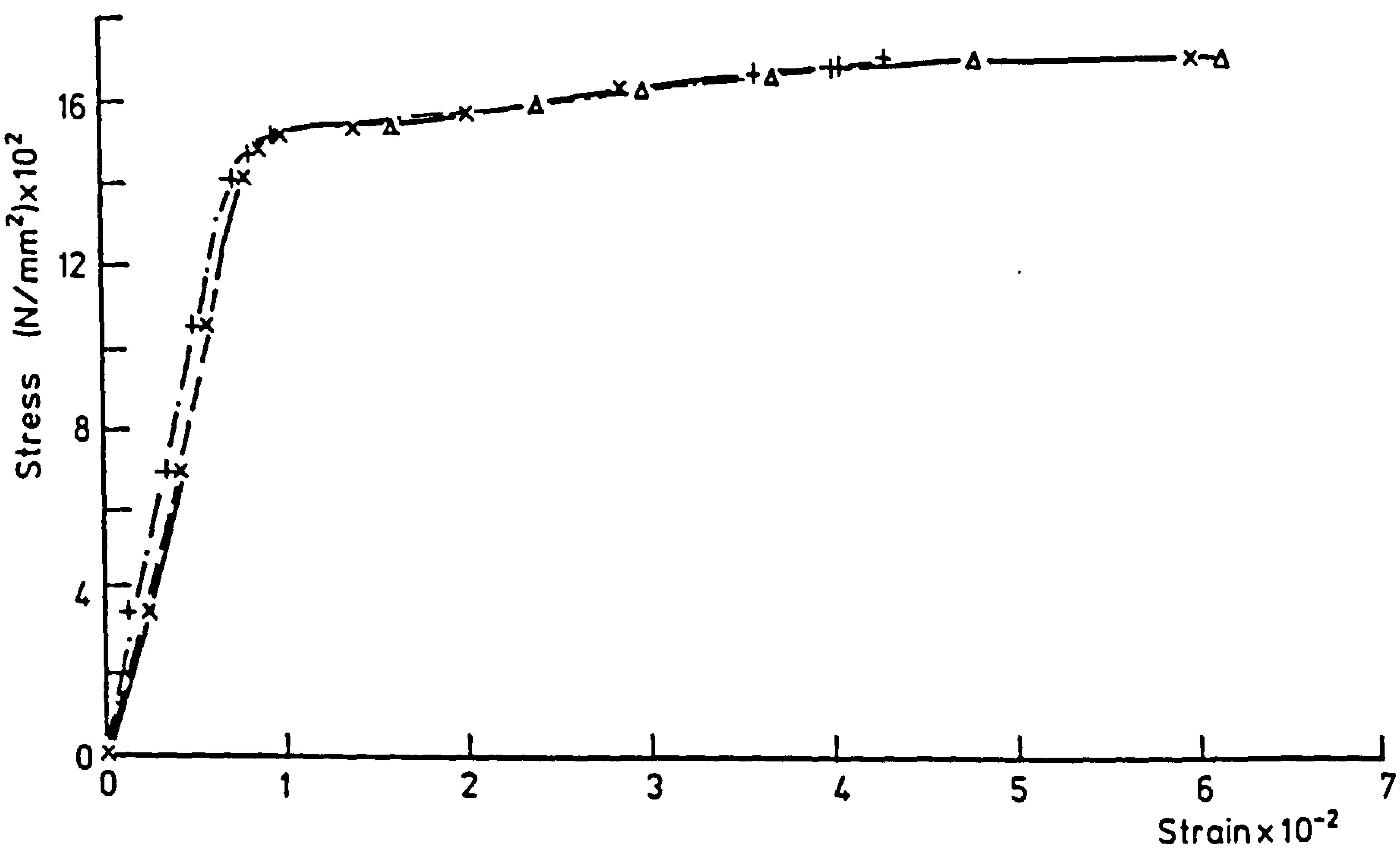

FIG. 4. TENDON STRESS-STRAIN DIAGRAM.

Table 2 Control Beam Deflections

Load, W (x 10^3N)	Moment (x 10^6Nmm)	Moment/mm (x 10^6Nmm/mm)	Deflections (mm)		
			d_1	d_2	d_3
0	0.88	0.06	0	0	0
5	4.13	0.029	1.85	1.91	1.87
7	5.43	0.038	2.56	2.70	2.61
10	7.38	0.051	3.69	3.95	3.76
13	9.33	0.065	4.94	5.34	5.03
15	10.63	0.074	6.03	6.54	6.13
17	11.93	0.083	7.29	7.94	7.38
18	12.58	0.087	7.98	8.69	8.06
19	13.23	0.092	8.62	9.42	8.72
21	14.53	0.101	10.46	11.45	10.57
23	15.83	0.110	14.50	16.00	14.67
24	16.48	0.114	17.68	19.50	17.90
25	17.13	0.119	20.40	22.48	20.65
26	17.78	0.124	23.83	27.24	24.05
0	0.88	0.06	1.36	2.56	2.08
26	17.78	0.124	25.90	29.81	26.36
27	18.43	0.128	31.18	35.77	31.58
28	19.08	0.133	41.07	47.23	41.44

Table 3 Control Beam Curvatures

(based on deflection measurements)

Moment (x 10^6Nmm)	Moment/mm (x 10^6Nmm/mm)	Curvature, K (x 10^{-6}mm^{-1})
0.88	0.06	0
4.13	0.029	0.62
5.43	0.038	1.44
7.38	0.051	2.81
9.33	0.065	4.44
10.63	0.074	5.75
11.93	0.083	7.56
12.58	0.087	8.38
13.23	0.092	9.38
14.53	0.101	11.69
15.83	0.110	17.69
16.48	0.114	21.38
17.13	0.119	24.44
17.78	0.124	41.25
0.88	0.06	10.50
17.78	0.124	46.00
18.43	0.128	54.88
19.08	0.133	74.69

deflections, steel strains and concrete strains are given in Tables 5 to 7, while a typical stress-strain relationship for the concrete is given in Figure 3. The locations of the gauge lengths for the concrete strain readings are shown in Figure 2. Calculated curvatures are presented in Tables 8 a-b. Plots of the moment-curvature relationships, based on average strains over the constant moment zone, and on deflection measurements, are compared in Figure 6. As can be seen, the overall degree of agreement is good.

It can be seen from Figure 5 that the moment-curvature relationships for the New Beam and Beam 1 are similar, to the start of bond failure in Beam 1. The ultimate moments of the Control Beam and the New Beam are similar. These observations suggest that the welded end plates had little effect on the behaviour of the composite beam, before cracking of the prestressed beam, and on its ultimate load.

Strain readings from the first two load increments indicate that the neutral axis depth was approximately 68% of the section depth from the top surface. This suggests that there was a greater difference between the moduli for the insitu and precast concretes than was found from specimen testing. A possible reason for this is thought to be micro-cracking of the insitu concrete due to restraint of early thermal cracking.

The results indicate that cracking did not take place until the fifth load increment was applied. Cracks propagated fairly rapidly, at spacings of 100-150 mm, and with some crack tips about 80 mm above the soffit. There were some 200 mm gaps between cracks and these areas

Table 4 Control Beam Steel Strains

Load, W ($x10^3$N)	Gauge 1		Gauge 2		Gauge 3		Gauge 4	
	Moment ($x10^6$Nmm)	Micro-strain	Moment ($x10^6$Nmm)	Micro-strain	Moment ($x10^6$Nmm)	Micro-strain	Moment ($x10^6$Nmm)	Micro-strain
0	0.11	-120	0.29	1710	0.81	4560	0.88	4770
5	0.36	-10	0.99	1670	3.51	4630	4.13	4850
7	0.46	30	1.27	1690	4.59	4670	5.43	4910
10	0.61	10	1.69	1690	6.21	4710	7.38	4960
13	0.76	50	2.11	1750	7.83	4790	9.33	5100
15	0.86	40	2.39	1750	8.91	4860	10.63	5270
17	0.96	60	2.67	1770	9.99	4890	11.93	5420
18	1.01	10	2.81	1710	10.53	4830	12.58	5520
19	1.06	80	2.95	1780	11.07	4920	13.23	5660
21	1.16	80	3.23	1780	12.15	4960	14.53	5900
23	1.26	90	3.51	1780	13.23	5020	15.83	6190
24	1.31	100	3.65	1790	13.77	5190	16.48	6470
25	1.36	100	3.79	1790	14.31	5440	17.13	6730
26	1.41	110	3.93	1790	14.85	5730	17.78	7050
0	0.11	70	0.29	1700	0.81	4720	0.88	4900
26	1.41	110	3.93	1790	14.85	5740	17.78	7290
27	1.46	140	4.07	1800	15.39	5680	18.43	7860
28	1.51	150	4.21	1820	15.93	5510	19.08	8630

	Gauge 1	Gauge 2	Gauge 3	Gauge 4
Before release	5828	5910	5860	6050
After release	959	2910	5310	5470
3 hrs after release	734	2520	5240	5400
24 hrs after release	578	2240	5130	5290
14 days after release	113	1670	4820	4985
Before testing (50 days)	-120	1710	4560	4770

remained uncracked with further loading. The test was stopped when unacceptably large deflections had been sustained. The maximum recorded steel strain was approximately 95% of the initial yield strain. However, at this stage there was a gradual breakdown in bond on the side of the beam with the ungauged tendons. When this reached the end plate, part of the tensile force was applied at the beam end and the action was between that of a bonded and an unbonded pre-tensioned member.

Table 5 New Beam, Concrete Strains

Gauge	Moment (Nmm x 10^6)											
	0.88	4.13	7.38	10.63	12.58	14.53	15.83	17.13	18.43	19.08	17.78	15.83
1	0	-74	-194	-338	-427	-629	-700	-647	-563	-	-	-
2	0	-79	-216	-405	-663	-2303	-3566	-5290	-8545	-	-	-
3	0	-49	-168	-371	-448	-1065	-1516	-1972	-2291	-	-	-
4	0	-68	-165	77	-585	-1395	-2036	-2698	-3611	-	-	-
5	0	14	-161	-315	-432	-1243	-1945	-2722	-3673	-	-	-
6	0	?	-	-	-	-	-	-	-	-	-	-
7	0	-54	-199	-364	-470	-1079	-2170	-3145	-4431	-	-	-
8	0	-50	-187	-334	-443	-349	-279	-248	-212	-228	-192	-273
9	0	-38	-170	-338	-432	-1721	-2667	-3787	-5448	-9532	-9120	-6472
10	0	-75	-183	-364	-414	-963	-1598	-2284	-3185	-4891	-4691	-3326
11	0	-51	-188	-373	-493	-1681	-2606	-3436	-4414	-5528	-5101	-3808
12	0	-60	-208	-422	-778	-1586	-1948	-2369	-2624	-2598	-2379	-2001
13	0	-54	-229	-373	-329	-1898	-3116	-4815	-8074	-18024	-36040	-
14	0	-94	-228	?	-489	-478	-469	-458	-421	-447	-439	-419
15	0	-52	-157	-273	-312	-435	-525	-808	-800	-	-	-
16	0	-67	-166	-304	-352	-332	-315	-276	-255	-	-	-
17	0	-80	-210	-382	-448	-1528	-2617	-4080	-5784	-	-	-
18	0	-74	-164	-304	-400	-244	-236	-185	-171	-	-	-
19	0	-66	-171	-315	-399	-1732	-2551	-3673	-4976	-	-	-
20	0	-45	-159	-259	-324	-451	-522	-927	-1661	-	-	-
21	0	-4	-40	-101	-139	-908	-1517	-2394	-3338	-	-	-
22	C	85	80	32	-31	-439	-822	-1166	-1669	-	-	-
23	0	53	-24	-69	-119	-788	-1273	-1915	-2649	-	-	-
24	0	69	126	168	203	99	17	-208	-459	-	-	-
25	0	101	161	206	226	150	56	-43	-136	-	-	-
26	0	61	103	185	216	119	-7	-149	-316	-	-	-
27	0	177	267	423	533	748	920	1129	1344	-	-	-
28	0	128	257	435	549	855	1081	1333	1578	-	-	-
29	0	199	343	533	625	858	1007	1251	1540	-	-	-
30	0	184	321	501	634	959	1200	1474	1894	-	-	-
31	0	172	328	447	623	865	1106	1356	1573	-	-	-
32	0	178	326	462	579	848	1033	1212	1409	-	-	-
33	0	185	272	452	549	780	933	1134	1319	-	-	-
34	0	218	364	544	641	956	1156	1400	1662	-	-	-
35	0	170	294	458	537	831	1088	1354	1657	-	-	-
36	0	250	414	541	646	964	1170	1413	1751	2165	2130	1818
37	0	155	281	449	564	831	989	1220	1497	1940	1950	1606
38	0	209	346	521	640	860	1008	1188	1394	1631	1633	1388
39	0	211	383	567	680	969	1161	1363	1592	1825	1821	1464
40	0	132	262	406	531	797	1008	1210	1437	1721	1799	1459
41	0	114	205	380	480	812	1352	1320	1678	2528	4152	-
42	0	229	386	582	710	1005	1162	1380	1687	2303	3971	-

NOTE: All strains shown as microstrains. Compression strains positive.

Table 6 New Beam, Deflections

Load, W (x 10^3N)	Moment (x 10^{+6}Nmm)	Deflections (mm)		
		1	2	3
0	0.88	0	0	0
5	4.13	1.69	1.88	1.72
10	7.38	3.49	3.85	3.53
15	10.63	5.68	6.21	5.69
18	12.58	7.34	8.04	7.33
21	14.53	12.54	13.84	12.56
23	15.83	16.78	18.53	16.84
24	16.48	19.24	21.27	19.37
25	17.13	22.21	24.45	21.22
26	17.78	25.93	28.42	25.80
27	18.43	29.39	32.16	29.16
28	19.08	40.64	44.57	40.15
26	17.78	51.52	55.06	48.24
23	15.83	67.44	70.13	58.87

Table 7 New Beam Steel Strains

Load, W ($x10^3$N)	Gauge 1		Gauge 2		Gauge 3		Gauge 4	
	Moment ($x10^6$Nmm)	Micro-strain	Moment ($x10^6$Nmm)	Micro-strain	Moment ($x10^6$Nmm)	Micro-strain	Moment ($x10^6$Nmm)	Micro-strain
0	0.11	-2200	0.29	760	0.81	4280	0.88	4360
5	0.36	-2190	0.99	780	3.51	4345	4.13	4450
10	0.61	-2180	1.69	790	6.21	4410	7.38	4535
15	0.86	-2180	2.39	805	8.91	4485	10.63	4660
18	1.01	-2175	2.81	815	10.53	4535	12.58	4785
21	1.16	-2170	3.23	830	12.15	4600	14.53	5440
23	1.26	-2170	3.51	835	13.23	4650	15.83	5700
24	1.31	-2170	3.65	840	13.77	4700	16.48	5870
25	1.36	-2165	3.79	840	14.31	4775	17.13	6055
26	1.41	-2165	3.93	850	14.85	4915	17.78	6270
27	1.46	-2165	4.07	850	15.39	5050	18.43	6440
28	1.51	-2160	4.21	850	15.93	5060	19.08	6810
26	1.41	-2170	3.93	850	14.85	5020	17.78	5890
23	1.26	-2170	3.51	840	13.23	4960	15.83	4960

	Gauge 1	Gauge 2	Gauge 3	Gauge 4
Before release	5890	5800	5780	5900
After release	144	2670	5240	5330
3 hrs after release	-248	2070	5190	5260
24 hrs after release	-340	1910	5070	5150
14 days after release	-1878	650	4680	4725
Before testing (100 days)	-2200	760	4280	4360

Table 8a Curvatures Calculated From Deflections

Moment ($\times 10^6$Nmm)	Moment/mm ($\times 10^6$Nmm/mm)	Curvature ($\times 10^{-6}$mm^{-1})
0.88	0.006	0
4.13	0.028	2.19
7.38	0.051	4.25
10.63	0.074	6.56
12.58	0.087	8.81
14.53	0.101	16.12
15.83	0.110	21.50
16.48	0.114	24.56
17.13	0.119	34.19
17.78	0.123	31.94
18.43	0.128	36.06
19.08	0.133	52.19
17.78	0.123	64.75
15.83	0.110	87.19

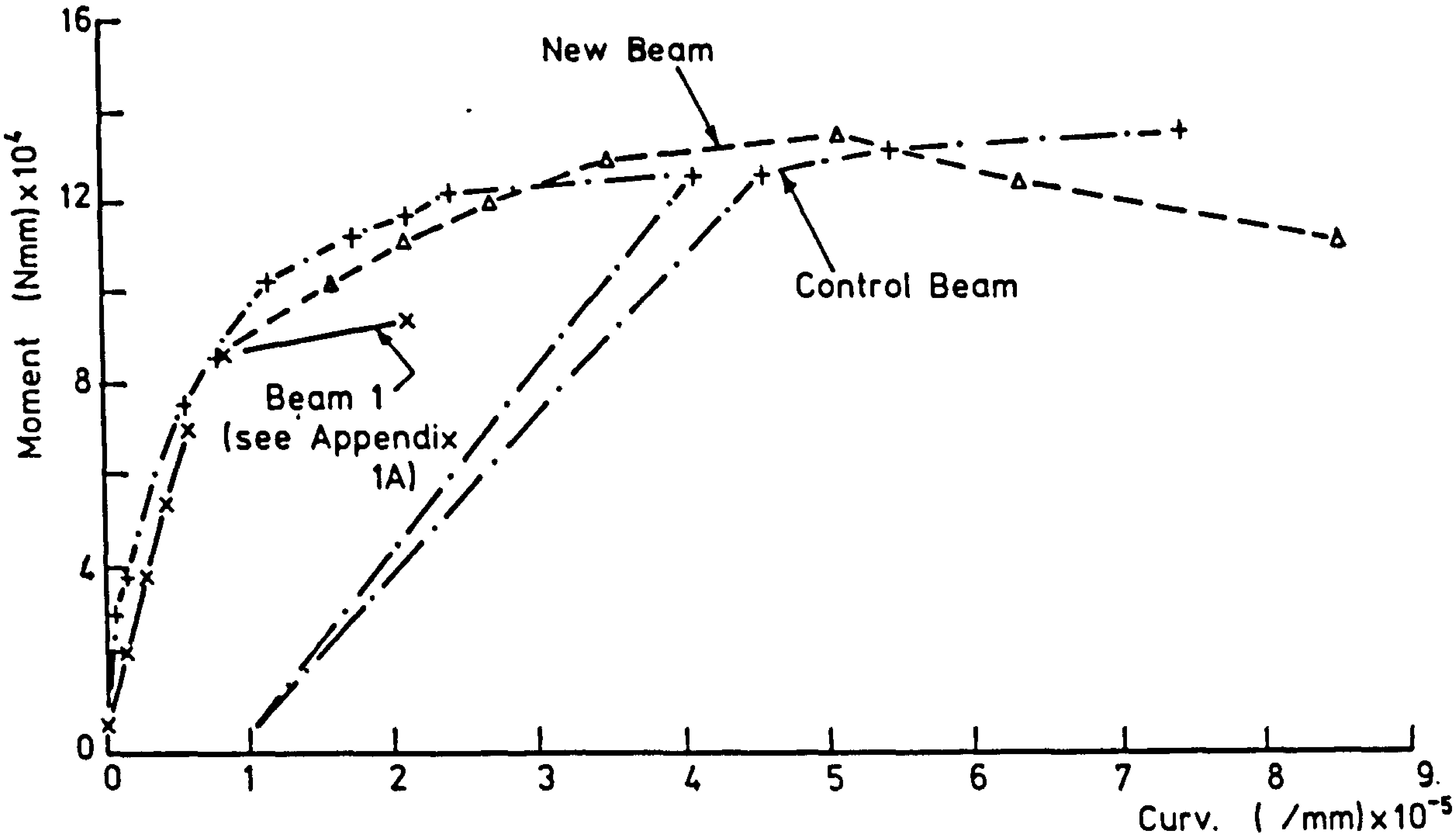

FIG. 5. MOMENT-CURVATURE

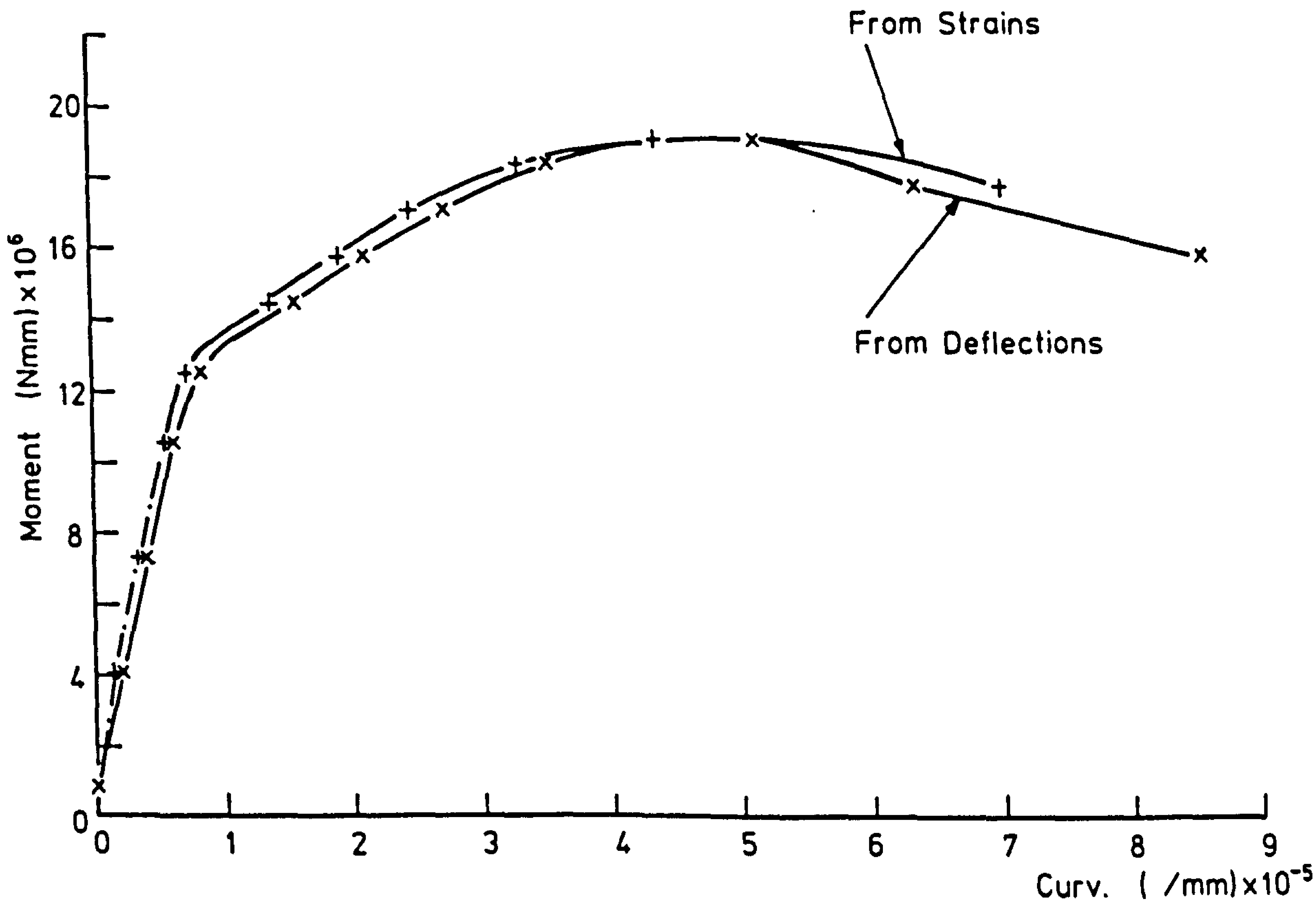

FIG. 6. MOMENT-CURVATURE RELATIONSHIP FOR NEW BEAM

Table 8b Curvatures Calculated From Strains

Moment ($x10^{6}$Nmm)	Moment/mm ($x10^{6}$Nmm/mm)	Average Microstrains		Curvature ($x10^{-6}mm^{-1}$)
		Top	Bottom	
0.88	0.006	0	0	0
4.13	0.028	186	-62	1.61
7.38	0.051	323	-195	3.36
10.63	0.074	489	-363	5.53
12.58	0.087	603	-492	7.11
14.53	0.101	881	-1261	13.91
15.83	0.110	1098	-1894	19.43
17.13	0.119	1305	-2605	25.39
18.43	0.128	1578	-3653	33.97
19.08	0.133	2016	-5891	51.34
17.78	0.123	4494	-8280	82.95
15.83	0.110	n.a.	n.a.	n.a.

BLANK IN ORIGINAL

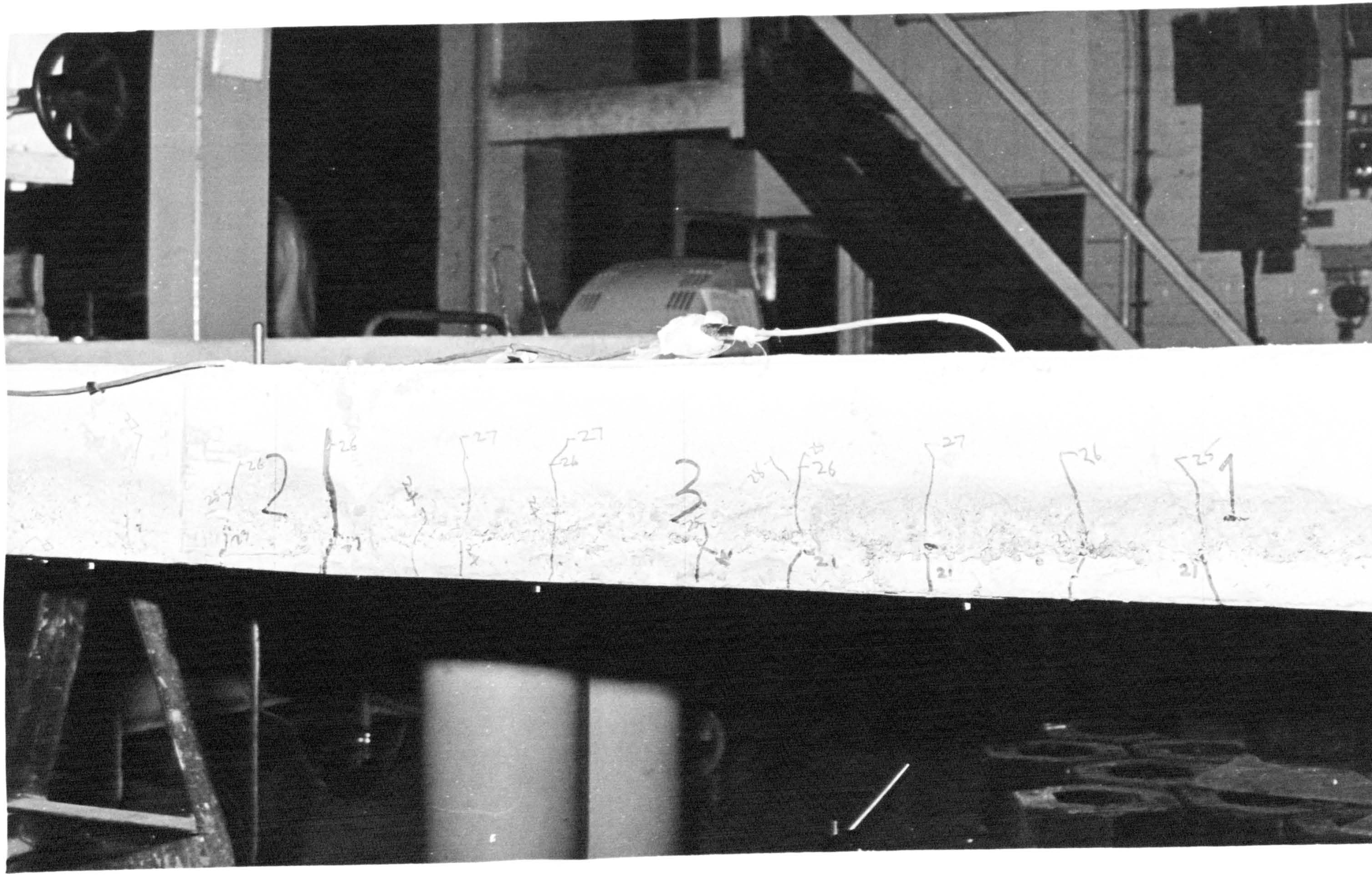

Plate 1 Failure Crack Pattern of Control Beam

APPENDIX 5.2 - Study of Transverse Section of Model 1

Introduction

Some of the rejected prestressed beams for the first model were sawn into 440 mm lengths and used to form two composite beams representing a transverse slice of the model, see Fig. 1 and Plates 1, 2. These beams were then tested to study stiffness changes with the development of cracking.

Tests on Beams Representing Transverse Section

Cracking in the transverse beams initiated at the junctions of the precast beam segments. Some of their surfaces profiles tended to follow the beam segment outlines, whereas others were nearly vertical, see Plate 3. Strains were recorded on continuous lines of Demec points, with 100 mm gauge lengths. The Demec points were located on the beam sides, 10 mm from the top and soffit surfaces. Most of the gauge lengths spanned precast beam flange junctions, but a few were confined to the flanges of the precast beam segments.

For reference, measured strains on side A of the second beam tested are given in Tables 1 and 2. As can be seen from these results, there were considerable variations in strain readings in the compression zone, but there was no obvious distinction between readings from gauge lengths above the beam segment junctions and from those above the beam segment flanges. On the soffit, the variation in strains is much greater, and the strains on gauge lengths confined to the flanges are both small and difficult to interpret. However, for the purposes of analysis, the readings suggest that it is reasonable to assume there is negligible stress in the concrete between the cracks.

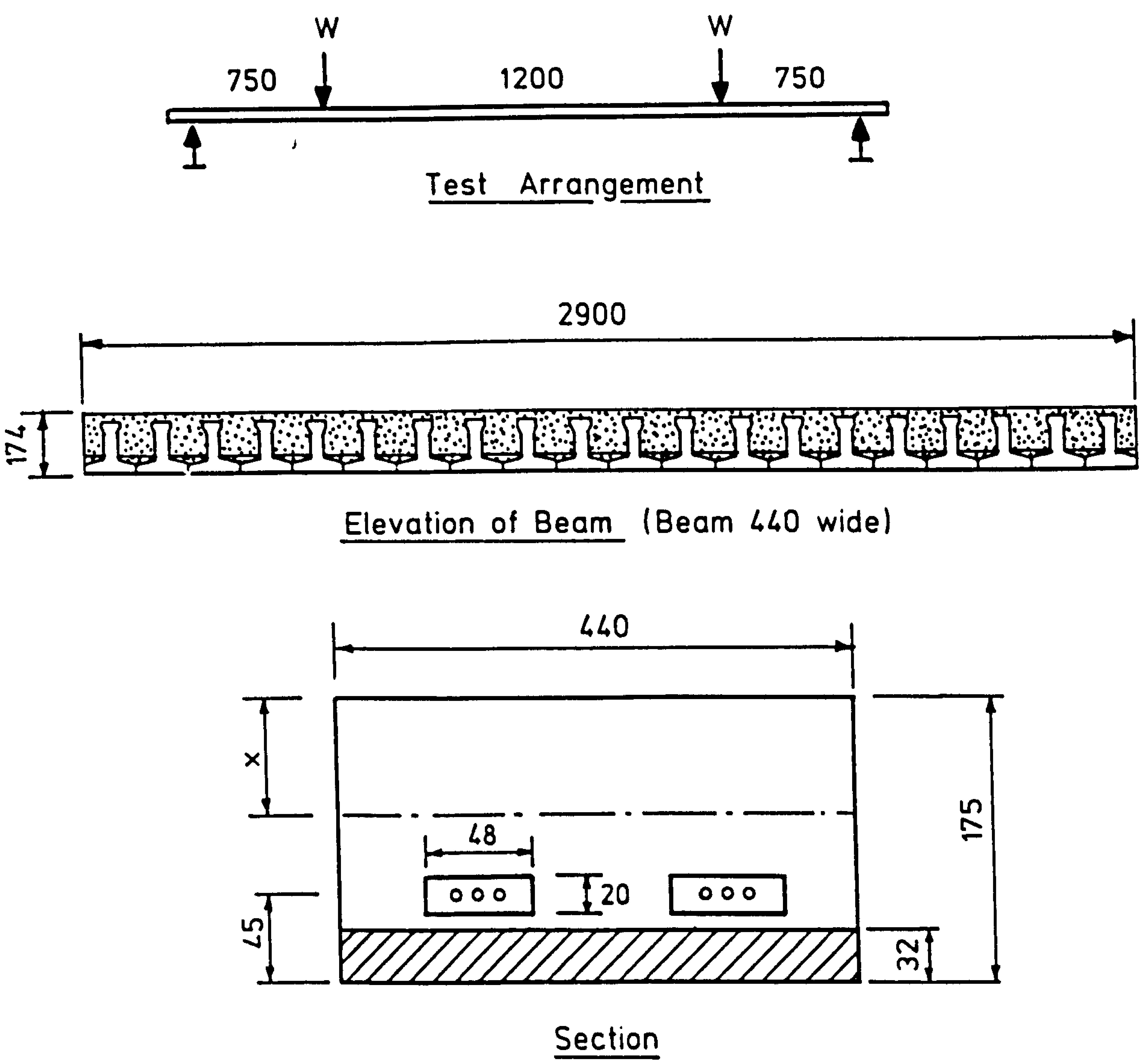

FIG. 1. BEAM TEST ON TRANSVERSE SECTION

Gauge	Moment (kNm)						
	0	1.875	3.75	7.5	9.375	11.25	12.0
1	0	0	80	150	260	300	350
2*	0	40	140	400	520	620	680
3	0	30	180	300	450	520	590
4	0	30	170	300	400	500	550
5*	0	70	200	360	430	490	500
6	0	70	190	440	480	580	650
7	0	60	150	370	360	400	397
8	0	40	130	310	380	410	450
9*	0	90	200	360	430	510	550
10	0	50	200	260	370	390?	450
11	0	70	150	330	390	460	510
12*	0	90	180	330	400	470	530
13	0	100	200	380	430	510	560

Table 1: Micro-strains on top gauge line

(*Gauge length above beam segment flange)

Gauge	Moment (kNm)						
	0	1.875	3.75	7.5	9.375	11.25	12.0
1	0	50	990	4730	5830	7900	10360
2*	0	30	70	110	80	110	110
3	0	20	-20	0	1710	2690	3430
4	0	-30	2320	4520	5660	7400	9640
5*	0	-30	-80	-140	-260	-260	-340
6	0	90	240	2470	3470	4940	6510
7	0	-20	250	1060	5190	7330	9410
8	0	-40	-60	1400	2070	3110	4110
9*	0	-40	-90	-70	-80	-50	-10
10	0	500	1310	2990	4830	7070	10270
11	0	50	200	2670	3280	4230	4920
12*	0	-50	-50	-130	-140	-130	-70
13	0	-10	840	4140	5440	7990	10970

Table 2: Micro-strains on bottom gauge line

(*Gauge length over beam segment flange)

Stiffness Properties

In Fig. 2, the deduced moment-curvature relationships for the constant moment zone are shown. The curvatures were calculated using the strain readings and the assumption of linear strain distribution over the beam depth, and from deflection readings at centre span and at the load points using the assumption of circular bending over the constant moment zone. It can be seen that the two methods gave a very satisfactory degree of agreement. The load-central deflection graphs for two beams are shown in Fig. 3.

Up to a moment of about 7.5 kNm, the stress-strain distribution in the compression block is approximately linear. This deduction is based on the assumption of a linear strain distribution over the depth of the beam and the test results shown in Fig. 4. For the purposes of calculation, a constant value of Young's Modulus for the insitu concrete of 26 kN/mm^2 has been taken.

Using $A_s = 170\ mm^2$, $E_s = 200\ kN/mm^2$, $E_c = 26\ kN/mm^2$, and the assumptions of zero tensile stress capacity and a linear stress-strain relationship in compression, the calculated depth of the neutral axis is 25 mm.

Using the averages of recorded strains over the constant moment zones and the assumption of linear strain variation with depth, the deduced neutral axis depths are as given in Table 3. These results show that as

Moment (kNm)	1.875	3.75	7.5	9.375	11.25	12.0
Depth (mm)	102	62	34	30	27	24

Table 3: Neutral Axis Depths

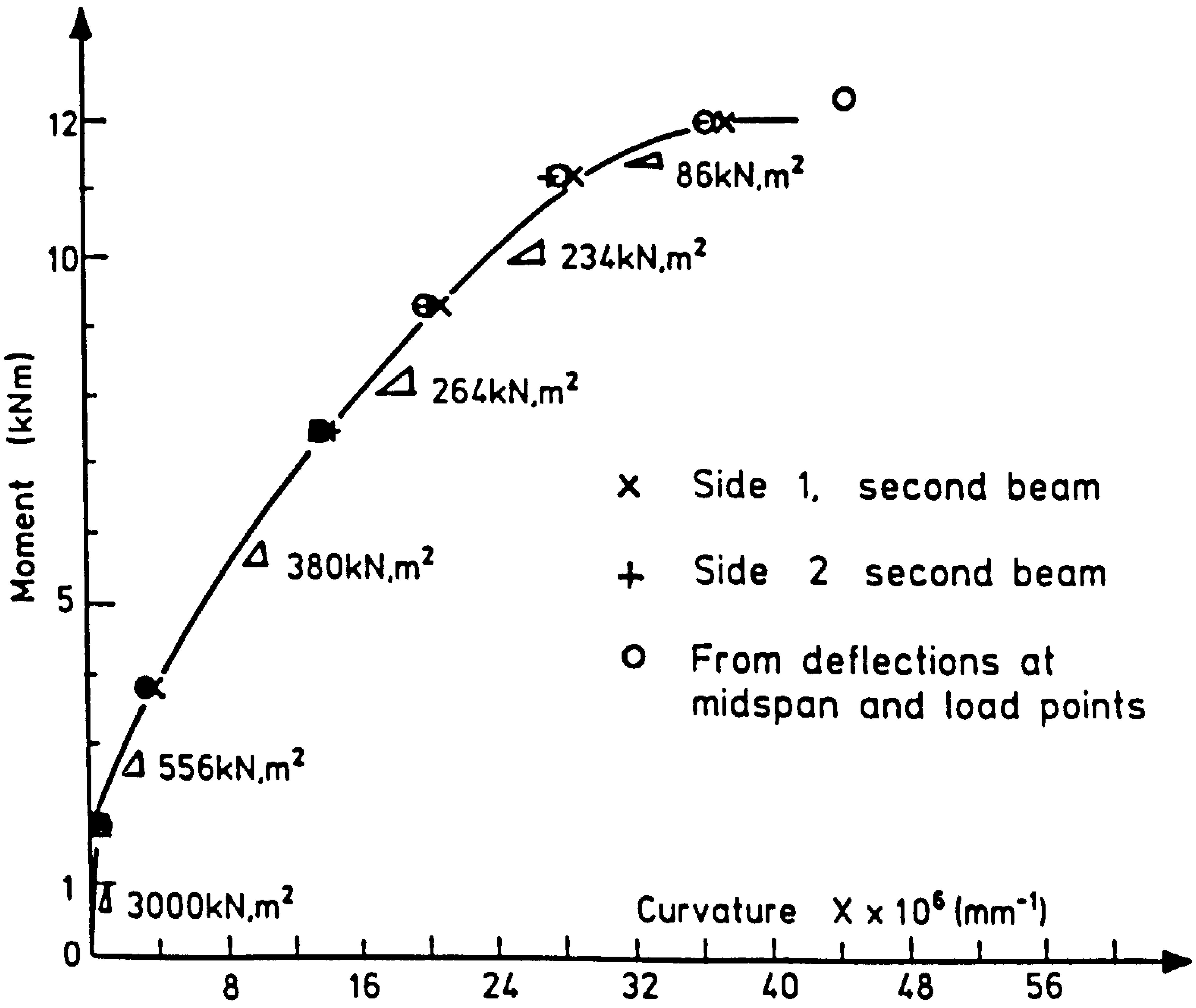

FIG. 2. MOMENT CURVATURE OF TRANSVERSE SECTION BASED ON STRAINS AVERAGED OVER 1200 mm AND DEFLECTIONS.

cracking develops over the constant moment zone, the neutral axis depth approaches the theoretical value calculated using the assumptions described above.

From the readings in Table 2, it can be seen that a single crack had developed with the applied moment at 1.875 kNm; 4 cracks had developed at 3.75 kNm; and 8 cracks had developed at 7.5 kNm. The corresponding average neutral axis depths based on the strains at the cracked sections only are 24 mm, 29 mm and 28 mm, respectively.

For design purposes, as cracking develops with sustained loading and with repetition of live load applications, use of the calculated neutral axis depth for predicting the effects of both short and long term loading seems reasonable. However, the appropriate value of Young's Modulus should, of course, be used for the two cases.

For the purposes of non-linear analysis of short term load effects, it seems reasonable to ignore tension stiffening effects at cracked sampling stations.

Before the onset of cracking, the calculated EI value for the beam is 2730 kNm^2. This value is based on a concrete section of depth 142 mm, and a Young's Modulus of 26 kN/mm^2. The value based on the Moment-Curvature graph of Fig. 2 is 3000 kNm^2. The agreement between the values is reasonable, as the strain readings are subject to maximum error under low moments.

Incremental average values of flexural stiffness are shown on Fig. 2. The calculated value for an elastic, cracked section is 435 kNm^2. It can be seen that the calculated value gives a reasonable prediction of

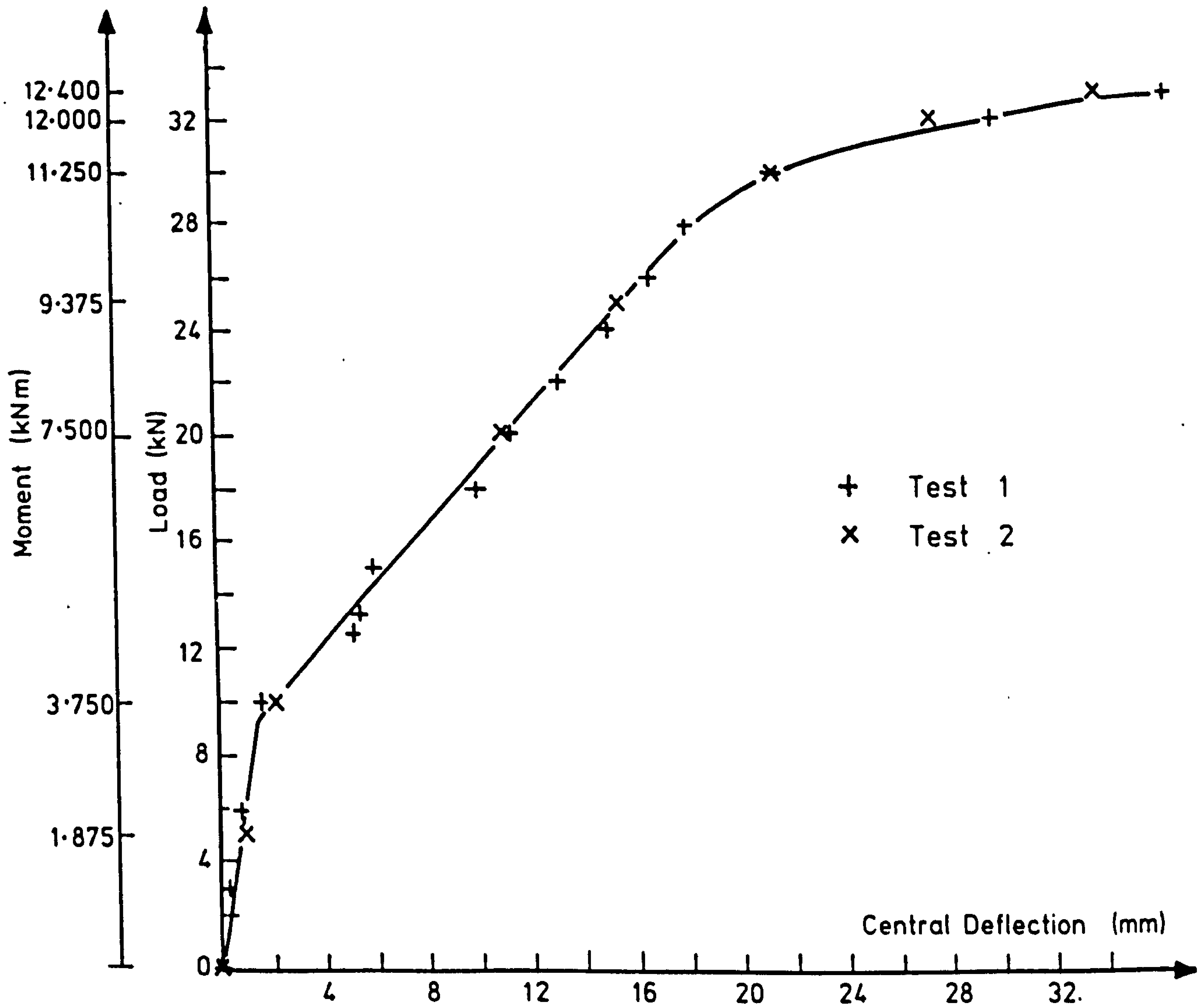

FIG. 3. LOAD CENTRAL DEFLECTION OF TRANSVERSE SECTION.

the average flexural stiffness over the range M = 1.875 kNm to M = 7.5 kNm of 468 kNm^2. This result confirms that it is reasonable to neglect the concrete in the tension zone when determining the average stiffness. At higher moments, there is softening of the concrete due to the high level of strain in the compression block, and a non-linear analysis is required to determine the flexural stiffness.

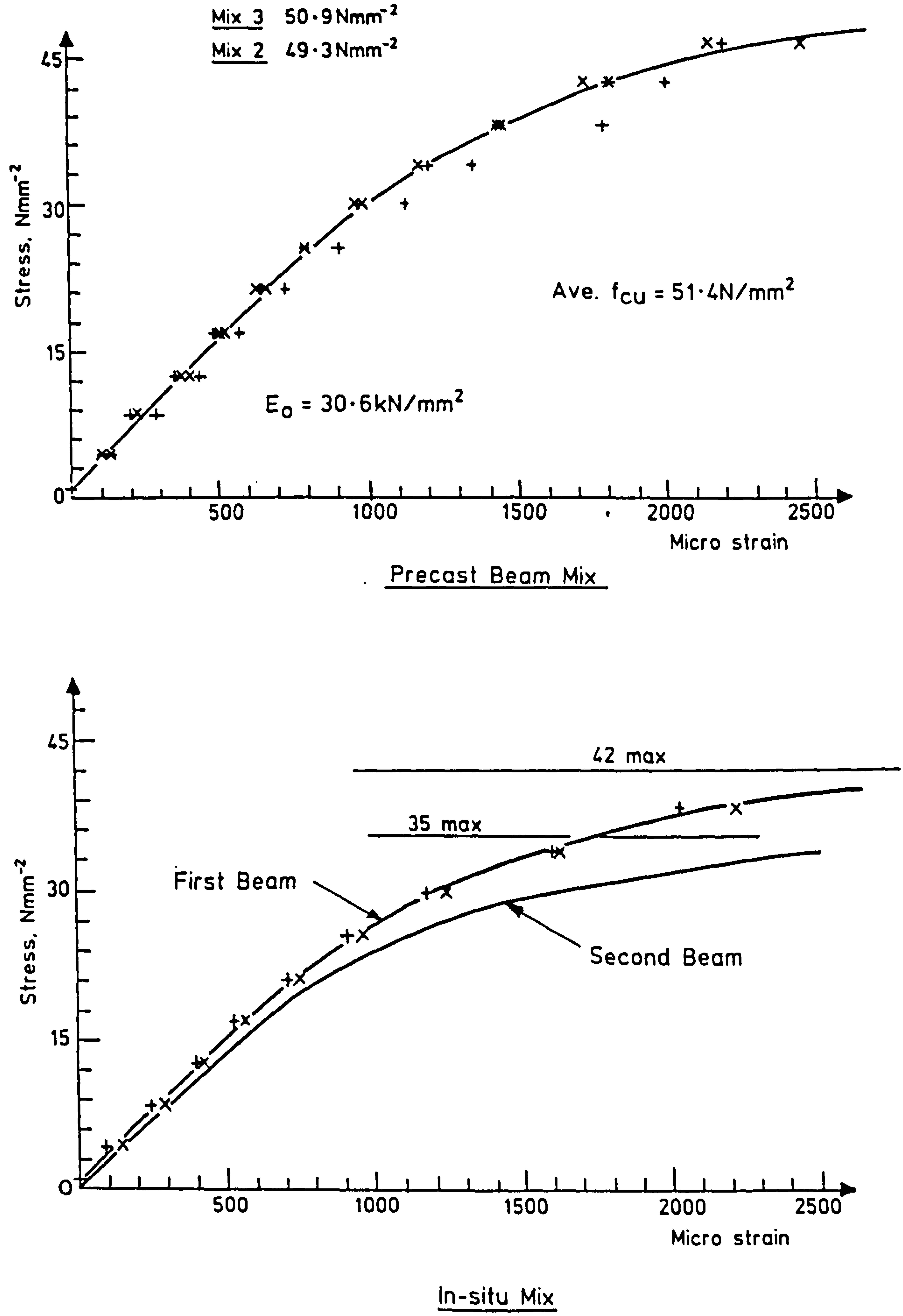

FIG.4. CONCRETE STRAIN-STRESS CURVES.

BLANK IN ORIGINAL

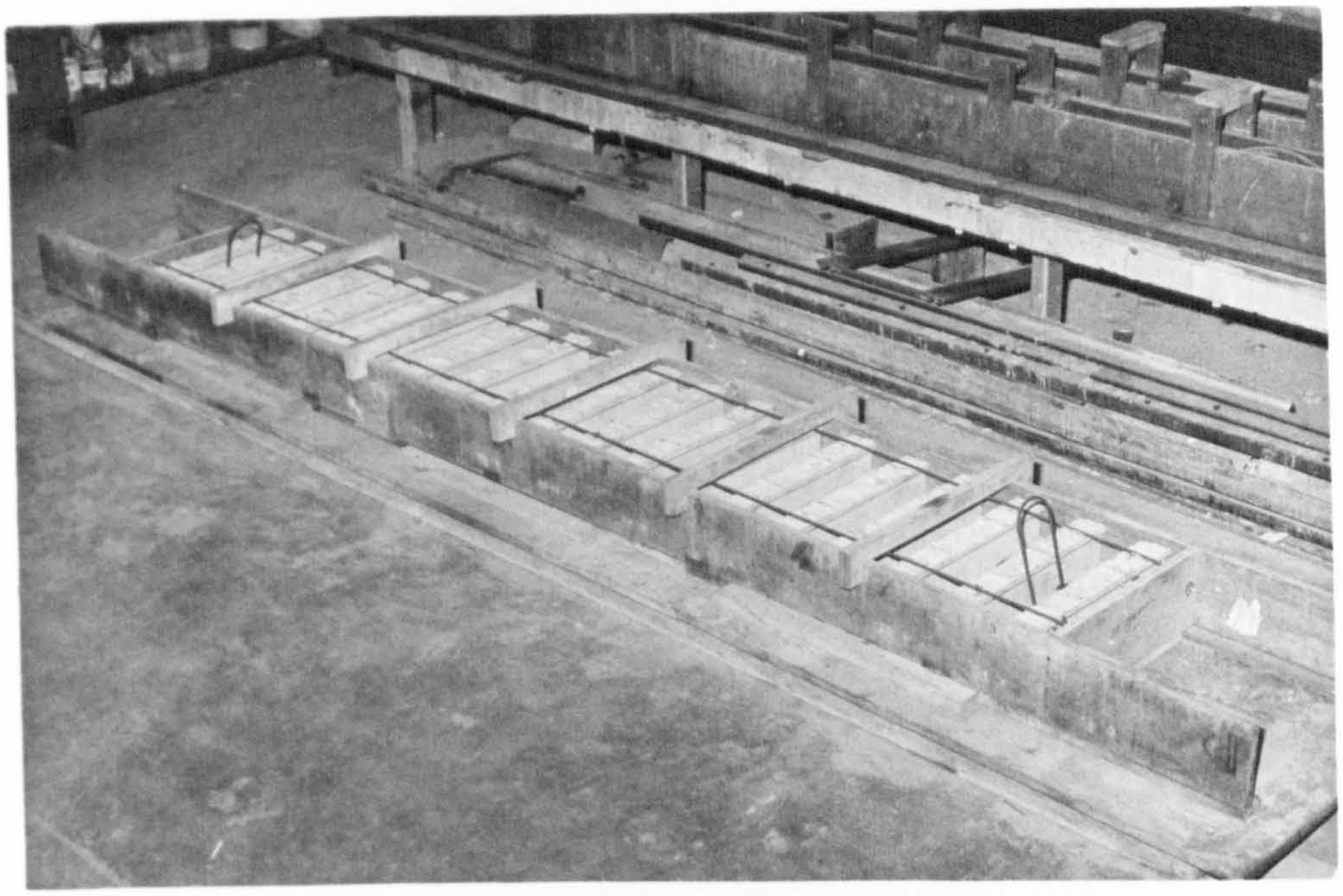

PLATE 1 Beam Segments in Mould

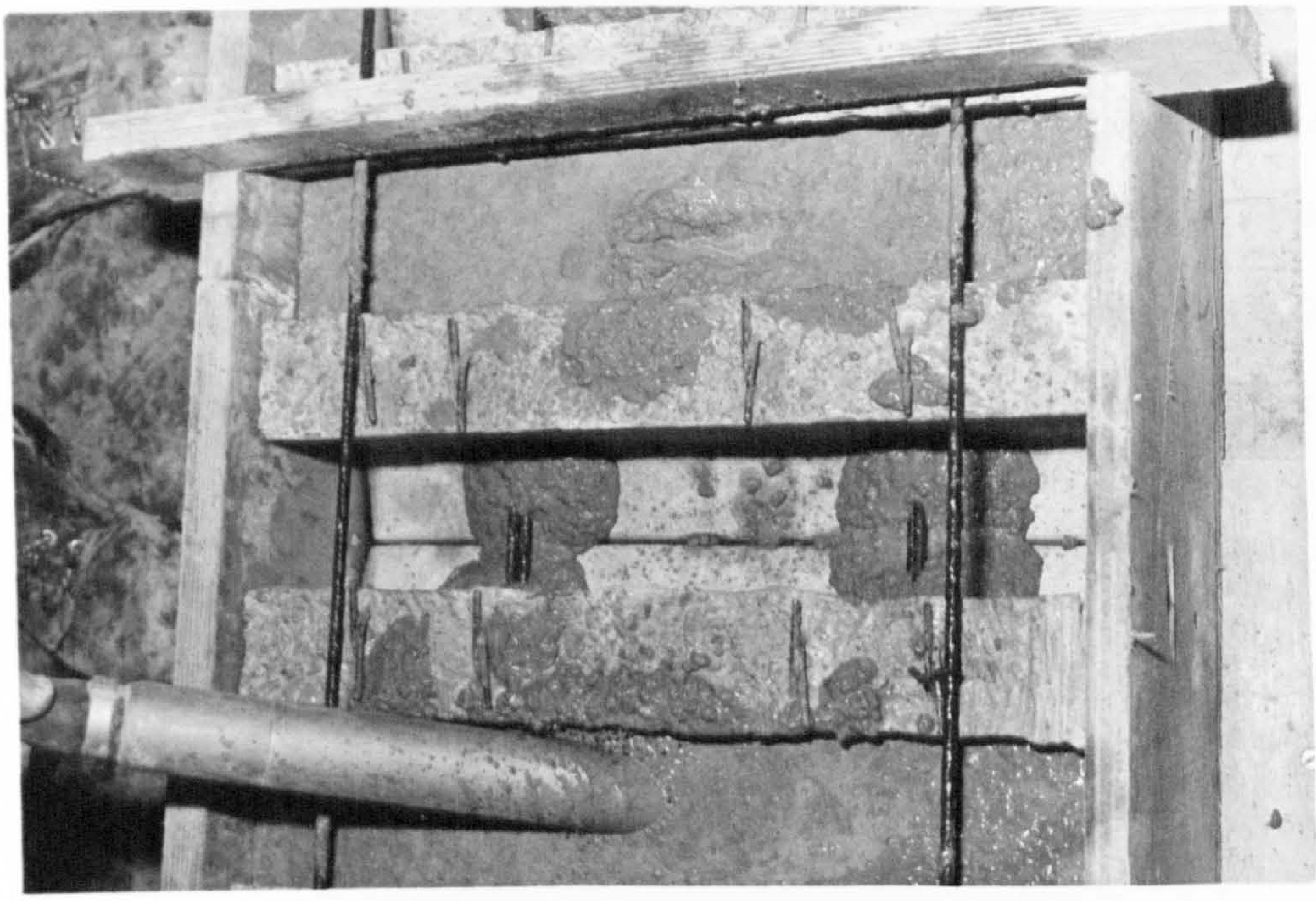

PLATE 2 Vibration of in-situ Concrete

PLATE 3 Crack Pattern on Elevation

PAGE

NUMBERING

AS ORIGINAL

APPENDIX 5.3 Numerical Results from Model 1 Tests

This appendix contains the main test data obtained for Model 1. Tables of values are presented for each transducer. The transducers are identified by reference numbers at the top of each Table and their locations are given on Figures 1 to 6. The particular load regimes corresponding to readings are defined by the numbers given in the first column of each Table. The meaning of these numbers is explained in Table 1.

There are two Tables which relate to the strain gauge rosettes on the slab top surfaces, Tables 3 & 4. The first table gives the raw readings from each arm of the rosette. The second Table presents the derived principal strains and angle for each complete rosette reading.

Level	Scan No	Bogie load (kN)	Disp level (mm)	Comment
1	1 & 2	0	0.0	Deck Self Weight only (Datum)
2	6 & 7	0	-1.12	'1' + Density correction and Super Dead Load, both factored for SLS
3	11 & 12	0	-2.30	'2' + 1/3 HA UDL over complete slab area
4	13 & 14	81.4	-3.51	'3' + 45 units of one HB Bogie factored for SLS in position 2
5	16 & 17	0	-2.60	As for '3', HB Bogie load removed
6	20 & 21	82.2	-3.05	'3' + 45 units of one HB Bogie factored for SLS in position 3
7	23	0	-2.17	As for '3', HB Bogie load removed
8	24	81.6	-5.01	'3' + 45 units of one HB Bogie factored for SLS in position 1
9	25	0	-3.62	As for '3', HB Bogie load removed
10	26	0	-3.61	'1' + Density Correction and Super Dead Load, both factored for ULS
11	27	0	-3.10	'10' + Full HA UDL in Lane 2 and 1/3 HA UDL in Lane 3, both factored for ULS
12	28	95	-5.61	'11' + 45 units of one HB Bogie factored for ULS in position 1
13	29	144.	-7.38	'11' + 1.5 * (45 units of one HB Bogie factored for ULS) in position 1
14	30	190.	-11.83	'11' + 2.0 * (45 units of one HB Bogie factored for ULS) in position 1
15	35	229.	-17.74	'11' + 2.4 * (45 units of one HB Bogie factored for ULS) in position 1
16	36 & 37	256.	-24.12	'11' + 2.7 * (45 units of one HB Bogie factored for ULS) in position 1
17	38	273.	-32.51	'11' + 2.9 * (45 units of one HB Bogie factored for ULS) in position 1
18	39	290.	-40.38	'11' + 3.0 * (45 units of one HB Bogie factored for ULS) in position 1
19	40	307.	-55.92	'11' + 3.2 * (45 units of one HB Bogie factored for ULS) in position 1

20	41	312.	-65.76	'11' + 3.27 * (45 units of one HB Bogie factored for ULS) in position 1
21	42	312.	-78.95	'11' + 3.27 * (45 units of one HB Bogie factored for ULS) in position 1
22	43	306.	-92.30	'11' + 3.2 * (45 units of one HB Bogie factored for ULS) in position 1
23	44	307.	-102.58	'11' + 3.2 * (45 units of one HB Bogie factored for ULS) in position 1
24	45	304.	-117.49	'11' + 3.2 * (45 units of one HB Bogie factored for ULS) in position 1
25	46	290.	-137.10	'11' + 3.0 * (45 units of one HB Bogie factored for ULS) in position 1

TABLE 1 Key For The Load Levels Used in The Presentation of Model 1 Testing Results

NOTE: Bogie positions refer to those given in Figure 5.6

	Level												
	1	2	3	4	5	6	7	8	9	10	11	12	13
Sum of Reactions (kN)	0	113.4	142.2	216.8	134.8	203.2	134.4	220.0	129.0	126.4	172.2	272.4	323.2
Expected Reaction (kN)	0	130.3	162.9	244.3	162.9	245.1	159.6	241.2	159.6	158.6	204.9	299.9	349.0
Error (%)	0	12.9	12.7	11.2	17.2	17.0	15.7	8.7	19.1	20.3	15.9	9.1	7.3

	Level											
	14	15	16	17	18	19	20	21	22	23	24	25
Sum of Reactions (kN)	367.2	395.6	416.2	430.2	446.4	461.0	461.2	462.6	457.6	458.6	456.6	436.6
Expected Reaction (kN)	395.6	433.8	461.6	478.1	494.7	511.7	516.9	516.9	510.9	511.9	508.9	494.9
Error (%)	7.1	8.8	9.8	11.1	9.7	9.9	10.7	10.5	10.4	10.3	10.3	11.7

TABLE 2 THE CORRELATION BETWEEN THE ACTUAL REACTION READINGS AND THOSE EXPECTED FROM THE APPLIED LOADING FOR MODEL 1

NOTE: Load cell output errors could give a variation of ± 16.2 kN on the total reaction reading

LEVEL	Support Load Cell Reading (kN)																					
	1	2	3	4	5	6	7	8	9	10	11	12	13	14	15	16	17	18	19	20	21	22
1	0	0	0	0	0	0	0	0	0	0	0	0	0	0	0	0	0	0	0	0	0	0
2	2.27	1.74	1.17	1.46	1.15	0.3	1.35	1.25	1.63	2.25	2.34	0.63	2.23	2.11	2.85	3.05	3.90	2.89	4.14	5.42	6.18	6.28
3	2.99	2.08	1.47	1.67	1.54	0.35	1.69	1.56	1.99	2.71	3.00	3.04	2.70	2.57	3.44	3.74	4.57	3.42	4.87	6.39	7.27	7.91
4	2.35	1.82	1.72	1.93	2.17	0.58	2.34	2.44	3.14	4.37	5.65	5.29	4.93	5.01	6.19	6.91	7.67	5.86	7.46	9.33	10.0	11.3
5	3.14	1.95	1.69	1.47	1.76	0.27	1.73	1.55	1.97	2.67	2.86	3.13	2.64	2.40	3.34	3.57	4.13	3.09	4.39	6.01	6.59	6.98
6	7.21	5.95	3.57	4.01	3.77	0.91	3.05	3.28	3.86	4.97	6.02	5.08	4.21	3.95	4.80	4.82	5.32	3.79	4.88	6.06	5.88	6.20
7	3.27	1.75	1.57	1.05	1.49	0.25	1.56	1.47	2.04	2.76	3.15	3.37	2.73	2.49	3.32	3.45	3.84	2.91	4.19	5.96	6.68	7.59
8	2.27	1.01	1.38	0.60	1.48	0.10	1.67	1.56	2.13	3.05	3.62	3.82	3.10	3.22	4.36	4.99	6.44	5.88	8.46	12.9	16.6	21.3
9	3.26	1.72	1.61	0.81	1.6	0.14	1.61	1.47	2.00	2.76	3.22	3.38	2.71	2.58	3.40	3.65	4.12	3.12	4.40	5.79	6.03	5.11
10	3.23	1.64	1.64	0.74	1.57	0.10	1.56	1.39	1.90	2.68	3.04	3.26	2.61	2.46	3.30	3.52	4.05	3.14	4.32	5.83	6.15	5.33
11	3.94	2.08	2.02	1.21	2.33	0.50	2.29	2.27	2.93	3.92	5.20	4.72	4.01	3.94	4.89	5.33	5.73	4.31	5.50	6.71	6.64	5.92
12	2.58	1.11	1.60	0.83	2.06	0.43	2.25	2.31	2.99	4.20	5.57	5.18	4.41	4.63	5.87	6.73	8.25	7.34	10.1	14.9	18.7	24.2
13	1.96	0.69	1.38	0.66	1.94	0.45	2.29	2.43	3.17	4.46	5.96	5.5	4.81	5.21	6.58	7.69	9.47	8.57	12.1	18.2	24.7	33.2
14	0.48	0	0.94	0.29	1.83	0.54	2.49	2.85	3.86	5.79	8.47	8.50	8.55	10.1	7.78	7.87	9.12	8.33	11.9	19.4	27.9	36.7
15	0	0	0	0	1.63	0.73	3.45	4.79	6.75	5.56	8.07	9.28	9.89	13.4	9.76	14.3	10.3	6.67	9.58	15.9	26.6	42.5
16	0	0	0	0	0.69	0.58	3.71	5.99	9.09	5.99	7.86	10.0	10.8	16.3	10.5	14.4	8.54	4.16	7.89	15.2	28.0	51.6
17	0	0	0	0	0	0.41	3.90	7.08	11.1	6.68	7.31	10.3	11.8	16.3	9.61	14.4	12.1	6.07	13.7	11.5	22.7	52.5
18	0	0	0	0	0	0.33	4.90	10.4	9.45	5.55	6.92	11.9	15.1	13.6	9.13	15.9	14.6	8.26	12.2	9.15	20.6	57.7
19	0	0	0	0	0	0	4.21	13.9	8.43	4.96	6.57	13.7	17.8	12.2	11.0	13.1	15.5	11.3	14.2	13.2	15.9	57.9

20	0	0	0	0	0	2.55	6.35	9.56	5.93	4.24	9.17	18.0	13.2	11.7	11.8	13.0	15.7	11.8	14.2	14.0	13.5	59.1
21	0	0	0	0	0	1.91	5.33	10.5	6.18	4.33	9.22	19.0	13.0	12.1	13.0	12.9	15.0	12.1	14.0	14.6	11.9	59.2
22	0	0	0	0	0	2.17	5.38	10.6	5.97	3.80	9.14	20.0	12.4	12.3	13.8	11.7	14.1	12.2	15.1	18.0	20.1	44.9
23	0	0	0	0	0	1.83	4.74	11.3	5.96	3.90	9.21	22.1	12.5	12.1	14.8	11.4	16.1	11.6	17.5	19.8	12.1	45.4
24	0	0	0	0	0	1.76	4.59	11.4	6.89	3.26	9.67	23.4	12.3	12.6	16.2	11.8	18.5	7.53	16.9	18.2	7.75	48.1
25	0	0	0	0	0	2.56	3.92	10.5	8.64	7.68	18.1	11.2	11.1	12.0	14.0	9.77	20.0	5.53	15.7	17.3	6.92	46.3

Table 3 Support Reaction Readings Taken During the Test on Model 1

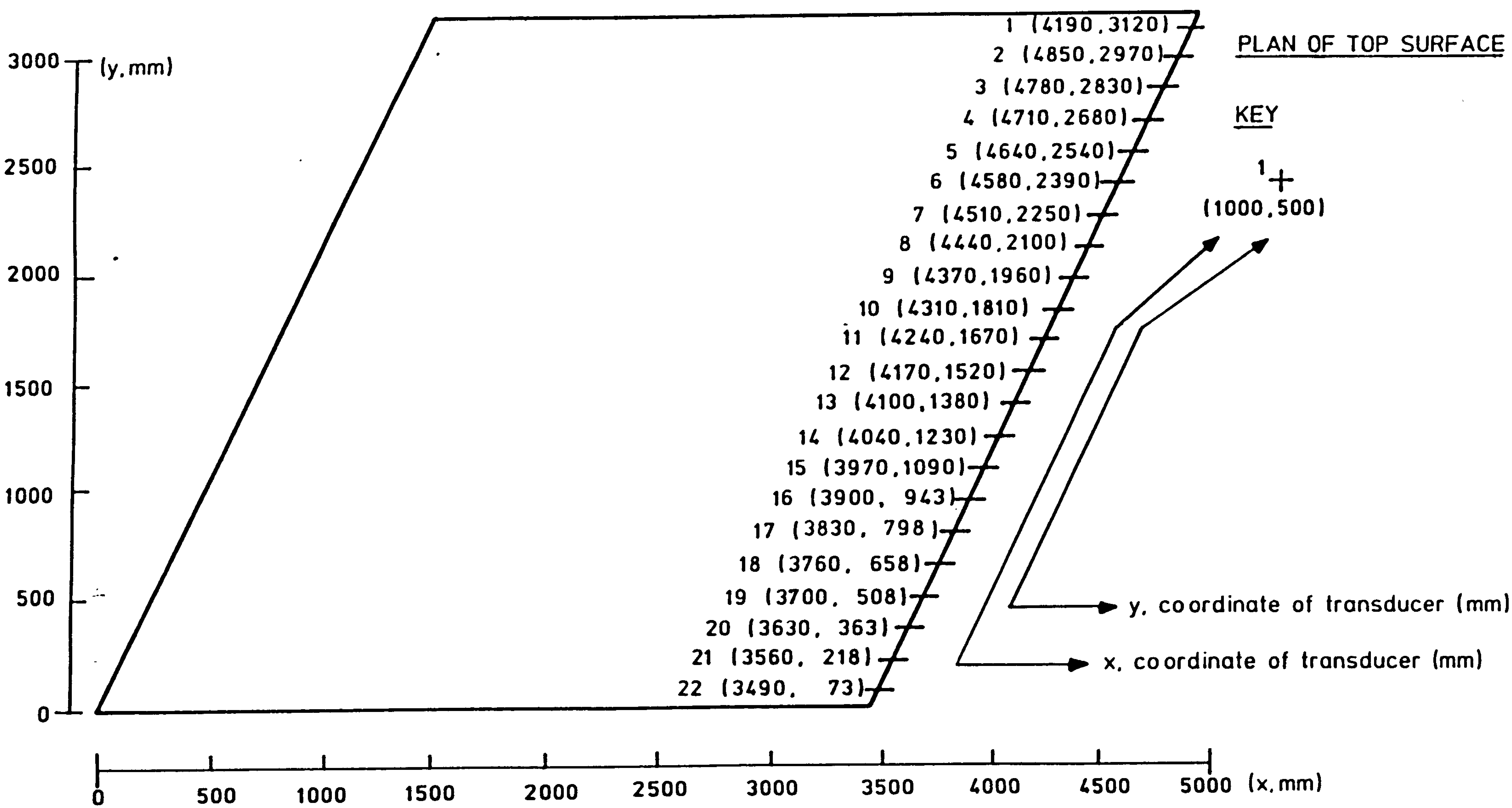

FIG. 1. POSITIONAL INFORMATION FOR MODEL 1 SUPPORTS

Level	Arm	Top Surface Strain Gauge Rosette Readings (Raw) ($\mu\epsilon$)										
		1	2	3	4	5	6	7	8	9	10	11
1	1	0.	0.	0.	0.	0.	0.	0.	0.	0.	0.	0.
	2	0.	0.	0.	0.	0.	0.	0.	0.	0.	0.	0.
	3	0.	0.	0.	0.	0.	0.	0.	0.	0.	0.	0.
2	1	-118.	-114.	-133.	-113.	-132.	-123.	-103.	-142.	-84.	-99.	-76.
	2	-95.	-135.	-126.	-102.	-84.	-111.	-81.	-129.	-73.	-111.	-74.
	3	-12.	-11.	-24.	-15.	2.	-8.	-8.	-20.	-11.	-45.	-7.
3	1	-154.	-148.	-176.	-151.	-174.	-162.	-134.	-185.	-107.	-129.	-98.
	2	-123.	-177.	-167.	-136.	-109.	-147.	-105.	-169.	-95.	-142.	-96.
	3	-12.	-12.	-33.	-22.	4.	-11.	-9.	-26.	-17.	-52.	-11.
4	1	-226.	-229.	-300.	-258.	-254.	-247.	-214.	-306.	-167.	-180.	-152.
	2	-185.	-266.	-285.	-241.	-162.	-217.	-159.	-273.	-131.	-236.	-135.
	3	-1.	-10.	-73.	-69.	14.	-4.	-11.	-75.	-24.	-161.	-11.
5	1	-162.	-165.	-211.	-179.	-188.	-178.	-150.	-225.	-112.	-146.	-104.
	2	-129.	-197.	-197.	-163.	-113.	-169.	-112.	-201.	-97.	-160.	-103.
	3	5.	-4.	-36.	-30.	10.	-14.	-3.	-31.	-19.	-57.	-12.
6	1	-196.	-201.	-271.	-285.	-352.	-219.	-195.	-310.	-157.	-232.	-139.
	2	-163.	-237.	-255.	-255.	-193.	-201.	-135.	-260.	-104.	-166.	-113.
	3	12.	9.	-25.	-23.	19.	-3.	20.	8.	3.	13.	-1.
7	1	-247.	-242.	-295.	-257.	-278.	-247.	-207.	-296.	-174.	-221.	-169.
	2	-201.	-277.	-267.	-230.	-184.	-232.	-162.	-259.	-152.	-223.	-160.
	3	-72.	-71.	-83.	-76.	-54.	-69.	-49.	-75.	-69.	-103.	-66.

8	1	-472.	-409.	-472.	-352.	-353.	-467.	-353.	-403.	-243.	-289.	-239.
	2	-363.	-488.	-426.	-318.	-247.	-415.	-311.	-389.	-277.	-354.	-279.
	3	-106.	-120.	-108.	-80.	-76.	-101.	-91.	-103.	-113.	-147.	-88.
9	1	-317.	-310.	-366.	-304.	-322.	-327.	-270.	-346.	-213.	-269.	-211.
	2	-262.	-356.	-330.	-273.	-223.	-308.	-221.	-310.	-201.	-286.	-207.
	3	-111.	-106.	-98.	-96.	-82.	-109.	-76.	-95.	-99.	-131.	-91.
10	1	-307.	-300.	-361.	-303.	-320.	-318.	-266.	-344.	-213.	-267.	-209.
	2	-255.	-346.	-325.	-272.	-222.	-301.	-217.	-306.	-199.	-283.	-206.
	3	-108.	-104.	-101.	-101.	-85.	-114.	-78.	-98.	-104.	-140.	-96.
11	1	-318.	-308.	-400.	-340.	-362.	-340.	-290.	-385.	-231.	-293.	-224.
	2	-258.	-357.	-362.	-314.	-247.	-322.	-231.	-340.	-206.	-314.	-210.
	3	-83.	-83.	-114.	-115.	-76.	-113.	-69.	-103.	-99.	-172.	-90.
12	1	-500.	-421.	-520.	-390.	-393.	-499.	-384.	-447.	-262.	-313.	-254.
	2	-373.	-510.	-470.	-362.	-272.	-444.	-333.	-429.	-292.	-391.	-290.
	3	-75.	-94.	-118.	-91.	-66.	-99.	-84.	-107.	-110.	-183.	-82.
13	1	-618.	-500.	-603.	-421.	-415.	-606.	-443.	-490.	-274.	-331.	-274.
	2	-453.	-613.	-539.	-393.	-289.	-529.	-401.	-492.	-346.	-452.	-337.
	3	-76.	-102.	-116.	-77.	-59.	-93.	-91.	-113.	-120.	-197.	-86.
14	1	-1039.	-799.	-858.	-497.	-460.	-882.	-548.	-637.	-268.	-401.	-279.
	2	-790.	-974.	-659.	-439.	-318.	-757.	-520.	-630.	-414.	-602.	-387.
	3	-94.	-155.	-72.	-58.	-43.	-114.	-72.	-88.	-135.	-103.	-111.
15	1	-1378.	-939.	-1143.	-605.	-519.	-1131.	-760.	-747.	-258.	-488.	-299.
	2	-1042.	-1251.	-834.	-493.	-348.	-902.	-688.	-732.	-452.	-753.	-429.
	3	-120.	-171.	-58.	-101.	-45.	-52.	-107.	-102.	-130.	-204.	-132.
16	1	-1713.	-1095.	-1315.	-666.	-533.	-1309.	-924.	-863.	-252.	-505.	- 305.
	2	-1266.	-1441.	-945.	-572.	-348.	-1001.	-897.	-884.	-503.	-777.	-464.
	3	-114.	-223.	-53.	-178.	-37.	-18.	-221.	-153.	-167.	-256.	-136.

17	1	-2127.	-1271.	-1548.	-796.	-542.	-1558.	-1057.	-926.	-290.	-481.	- 324.
	2	-1525.	-1688.	-1099.	-637.	-347.	-1123.	-1106.	-1024.	-547.	-916.	-488.
	3	-164.	-249.	-46.	-193.	-31.	-16.	-335.	-258.	-114.	-494.	-131.
18	1	-2562.	-1471.	-1743.	-877.	-556.	-1771.	-1226.	-1007.	-330.	-506.	-349.
	2	-1818.	-1929.	-1288.	-653.	-342.	-1288.	-1358.	-1155.	-587.	-1125.	-538.
	3	-226.	-317.	-88.	-208.	-25.	-16.	-465.	-313.	-131.	-696.	-111.
19	1	-3111.	-1783.	-2010.	-972.	-556.	-2122.	-1497.	-1156.	-393.	-535.	-182.
	2	-2222.	-2344.	-1544.	-697.	-334.	-1598.	-1741.	-1375.	-667.	-1280.	-666.
	3	-305.	-427.	-159.	-88.	-24.	-18.	-573.	-370.	-92.	-811.	823.
20	1	-3467.	-1966.	-2212.	-1026.	-553.	-2416.	-1681.	-1319.	-447.	-611.	-145.
	2	-2493.	-2633.	-1722.	-728.	-324.	-1859.	-1917.	-1560.	-762.	-1340.	-739.
	3	-355.	-469.	-202.	-40.	-23.	-41.	-515.	-370.	-91.	-833.	1019.
21	1	-4060.	-2270.	-2685.	-1202.	-578.	-3050.	-2134.	-1575.	-527.	-711.	-118.
	2	-2803.	-3200.	-2094.	-845	-342.	-2326.	-2334.	-1878.	-920.	-1539.	-908.
	3	-424.	-536.	-239.	-28.	-26.	-72.	-533.	-426.	-104.	-958.	1246.
22	1	-4141.	-2338.	-2767.	-1226.	-574.	-3295.	-2499.	-1746.	-621.	-745.	-292.
	2	-2812.	-3408.	-2293.	-874.	-338.	-2617.	-2575.	-2125.	-1072.	-1609.	-839.
	3	-449.	-525.	-362.	-4.	-26.	-188.	-420.	-442.	135.	-1011.	1894.
23	1	-4141.	-2353.	-2843.	-1255.	-576.	-3428.	-2793.	-1888.	-663.	-797.	-398.
	2	-2775.	-3527.	-2391.	-898.	-338.	-2869.	-2744.	-2303.	-1174.	-1678.	-863.
	3	-491.	-539.	-404.	1.	-25.	-419.	-314.	-438.	210.	-1027.	1785.
24	1	-4122.	-2372.	-2932.	-1303.	-572.	-3459.	-3294.	-2083.	-778.	-857.	-393.
	2	-2754.	-3643.	-2497.	-930.	-331.	-2884.	-3005.	-2531.	-1429.	-1749.	-968.
	3	-523.	-549.	-446.	-11.	-24.	-408.	-135.	-434.	272.	-1039.	1650.

25	1	-4027.	-2281.	-3003.	-1360.	-555.	-2436.	-3863.	-2344.	-887.	-1114.	-338.
	2	-2677.	-3662.	-2519.	-965.	-316.	-2018.	-3394.	-2718.	-1794.	-1849.	-1030.
	3	-551.	-549.	-446.	-59.	-26.	-131.	-53.	-384.	530.	-945.	1829.

TABLE 4 TOP SURFACE STRAIN GAUGE ROSETTE READINGS TAKEN DURING THE TEST ON MODEL 1

NOTE: Arm 1 is inclined at 180° to the x-axis, arm 2 at 135° and arm 3 at 90°. Where + ve angles are measured anti-clockwise

Level	Quantity	Top Surface Strain Gauge Rosette Readings (Principal) ($\mu\epsilon$)										
		1	2	3	4	5	6	7	8	9	10	11
1	ϵ_1	0.	0.	0.	0.	0.	0.	0.	0.	0.	0.	0.
	ϵ_2	0.	0.	0.	0.	0.	0.	0.	0.	0.	0.	0.
	θ	0.	0.	0.	0.	0.	0.	0.	0.	0.	0.	0.
2	ϵ_1	-5.	26.	-6.	-2.	5.	8.	-1.	-3.	-4.	-24.	6.
	ϵ_2	-126.	-152.	-150.	-126.	-134.	-139.	-110.	-158.	-92.	-120.	-89.
	θ	75.	63.	69.	71.	82.	71.	76.	71.	73.	62.	68.
3	ϵ_1	-1.	38.	-10.	-5.	7.	10.	0.	-4.	-6.	-26.	6.
	ϵ_2	-165.	-198.	-199.	-168.	-177.	-183.	-142.	-207.	-118.	-155.	-115.
	θ	75.	63.	70.	71.	82.	71.	76.	71.	72.	63.	68.
4	ϵ_1	20.	64.	-37.	-41.	20.	26.	-1.	-48.	-16.	-105.	7.
	ϵ_2	-247.	-302.	-337.	-286.	-260.	-277.	-224.	-332.	-175.	-237.	-170.
	θ	74.	63.	70.	70.	81.	71.	78.	72.	77.	49.	71.
5	ϵ_1	19.	53.	-10.	-10.	13.	13.	5.	-7.	-9.	-29.	6.
	ϵ_2	-176.	-223.	-237.	-199.	-191.	-206.	-158.	-249.	-122.	-175.	-123.
	θ	74.	63.	70.	71.	83.	69.	77.	71.	73.	64.	68.
6	ϵ_1	33.	80.	15.	11.	21.	29.	30.	42.	7.	25.	11.
	ϵ_2	-218.	-272.	-311.	-319.	-354.	-251.	-205.	-344.	-162.	-245.	-151.
	θ	73.	63.	70.	71.	86.	70.	78.	73.	81.	78.	74.
7	ϵ_1	-62.	-9.	-57.	-56.	-52.	-42.	-42.	-53.	-61.	-77.	-51.
	ϵ_2	-256.	-304.	-321.	-277.	-280.	-274.	-214.	-318.	-182.	-246.	-184.
	θ	77.	63.	72.	72.	85.	70.	78.	73.	75.	67.	70.
8	ϵ_1	-91.	2.	-63.	-45.	-72.	-59.	-64.	-51.	-59.	-64.	-26.
	ϵ_2	-487.	-531.	-517.	-386.	-357.	-509.	-380.	-456.	-297.	-372.	-302.
	θ	79.	61.	72.	71.	83.	72.	73.	69.	62.	59.	62.

9	ϵ_1	-100.	-28.	-66.	-73.	-80.	-77.	-64.	-66.	-84.	-89.	-69.
	ϵ_2	-328.	-388.	-398.	-327.	-324.	-359.	-282.	-374.	-228.	-310.	-233.
	θ	77.	62.	72.	72.	85.	70.	77.	72.	71.	64.	68.
10	ϵ_1	-97.	-28.	-71.	-79.	-84.	-82.	-68.	-72.	-90.	-102.	-75.
	ϵ_2	-318.	-377.	-391.	-325.	-322.	-349.	-276.	-371.	-266.	-305.	-231.
	θ	77.	62.	72.	73.	85.	70.	77.	73.	72.	64.	68.
11	ϵ_1	-70.	2.	-79.	-85.	-73.	-77.	-58.	-74.	-88.	-132.	-72.
	ϵ_2	-331.	-392.	-434.	-369.	-365.	-375.	-301.	-414.	-243.	-333.	-242.
	θ	77.	62.	72.	71.	84.	70.	78.	73.	74.	63.	71.
12	ϵ_1	-58.	43.	-68.	-48.	-60.	-52.	-54.	-49.	-55.	-91.	-18.
	ϵ_2	-517.	-558.	-571.	-433.	-399.	-546.	-414.	-505.	-317.	-405.	-317.
	θ	79.	61.	72.	70.	83.	72.	73.	69.	63.	57.	63.
13	ϵ_1	-56.	69.	-57.	-25.	-52.	-36.	-46.	-33.	-29.	-64.	2.
	ϵ_2	-638.	-671.	-662.	-473.	-422.	-663.	-488.	-570.	-365.	-464.	-362.
	θ	79.	61.	72.	70.	82.	73.	71.	67.	59.	55.	60.
14	ϵ_1	-44.	116.	-27.	-5.	-32.	-36.	7.	20.	21.	129.	16.
	ϵ_2	-1089.	-1069.	-903.	-550.	-471.	-961.	-628.	-746.	-424.	-632.	-405.
	θ	77.	61.	77.	72.	81.	73.	69.	68.	54.	57.	57.
15	ϵ_1	-55.	240.	-10.	-65.	-36.	31.	-19.	21.	72.	84.	14.
	ϵ_2	-1443.	-1350.	-1191.	-641.	-528.	-1214.	-847.	-870.	-459.	-777.	-445.
	θ	78.	59.	78.	75.	82.	75.	71.	68.	52.	55.	56.
16	ϵ_1	-40.	237.	-1.	-135.	-29.	65.	-94.	9.	88.	36.	38.
	ϵ_2	-1787.	-1555.	-1367.	-708.	-541.	-1392.	-1051.	-1025.	-506.	-797.	-479.
	θ	78.	60.	79.	74.	83.	76.	69.	67.	49.	54.	55.
17	ϵ_1	-93.	299.	12.	-161.	-24.	54.	-150.	-47.	121.	-917.	50.
	ϵ_2	-2198.	-1819.	-1606.	-828.	-549.	-1628.	-1243.	-1138.	-555.	-59.	-506.
	θ	79.	59.	79.	77.	83.	78.	66.	64.	51.	135.	55.

18	ϵ_1	-152.	290.	-8.	-191.	-20.	69.	-207.	-55.	139.	-1133.	99.
	ϵ_2	-2637.	-2079.	-1823.	-894.	-561.	-1856.	-1483.	-1265.	-600.	-69.	-560.
	θ	80.	60.	78.	81.	85.	78.	63.	63.	53.	130.	56.
19	ϵ_1	-213.	307.	-51.	-57.	-20.	107.	-192.	-35.	208.	-1295.	1428.
	ϵ_2	-3202.	-2517.	-2118.	-1002.	-559.	-2247.	-1879.	-1491.	-693.	-50.	-786.
	θ	80.	59.	77.	80.	85.	77.	62.	61.	55.	129.	58.
20	ϵ_1	-249.	383.	-77.	-3.	-21.	116.	-93.	14.	255.	-1349.	1749.
	ϵ_2	-3572.	-2819.	-2336.	-1063.	-555.	-2573.	-2103.	-1703.	-793.	-95.	-875.
	θ	80.	59.	76.	79.	86.	76.	63.	62.	55.	130.	58.
21	ϵ_1	-340.	592.	-86.	15.	-23.	113.	-52.	48.	325.	-1550.	2186.
	ϵ_2	-4145.	-3398.	-2839.	-1245.	-581.	-3235.	-2615.	-2049.	-956.	-119.	-1058.
	θ	81.	58.	76.	79.	86.	76.	64.	62.	55.	130.	57.
22	ϵ_1	-378.	742.	-159.	48.	-23.	42.	66.	126.	668.	-1621.	2772.
	ϵ_2	-4212.	-3606.	-2971.	-1279.	-577.	-3525.	-2985.	-2314.	-1154.	-135.	-1170.
	θ	82.	57.	74.	79.	86.	75.	66.	61.	57.	130.	62.
23	ϵ_1	-434.	824.	-183.	57.	-23.	-146.	166.	187.	817.	-1686.	2594.
	ϵ_2	-4198.	-3717.	-3065.	-1311.	-578.	-3701.	-3272.	-2514.	-1270.	-137.	-1208.
	θ	83.	57.	74.	78.	86.	74.	68.	61.	57.	131.	63.
24	ϵ_1	-472.	904.	-206.	44.	-22.	-137.	326.	258.	1035.	-1755.	2523.
	ϵ_2	-4173.	-3826.	-3172.	-1358.	-574.	-3731.	-3775.	-2775.	-1541.	-142.	-1266.
	θ	83.	56.	73.	79.	87.	74.	70.	61.	57.	132.	61.
25	ϵ_1	-509.	993.	-219.	-11.	-24.	83.	427.	307.	1585.	-205.	2825.
	ϵ_2	-4070.	-3823.	-3230.	-1408.	-556.	-2651.	-4343.	-3035.	-1943.	-1854.	-1334.
	θ	84.	56.	74.	79.	87.	74.	71.	63.	57.	48.	61.

TABLE 5 PRINCIPAL TOP SURFACE STRAINS DURING THE TEST ON MODEL 1

NOTE: θ refers to the direction of the strain ϵ_1, angles are measured +ve anti-clockwise from the x-axis.

FIG. 2. POSITIONAL INFORMATION FOR MODEL 1 TOP SURFACE STRAIN GAUGES (ROSETTES)

Level	Weldable Strain Gauge Readings ($\mu\epsilon$)											
	1	2	3	4	5	6	7	8	9	10	11	12
1	5180.	5320.	5060.	5200.	5200.	4990.	5110.	16180.	0.	0.	0.	0.
2	5238.	5376.	5116.	5257.	5258.	5048.	5168.	16241.	-7.	-5.	15.	14.
3	5251.	5391.	5129.	5270.	5274.	5065.	5182.	16256.	-14.	-11.	15.	13.
4	5311.	5456.	5206.	5343.	5325.	5128.	5265.	16321.	-12.	-9.	32.	16.
5	5258.	5404.	5136.	5283.	5280.	5077.	5193.	16272.	-21.	-16.	12.	7.
6	5281.	5429.	5172.	5325.	5291.	5090.	5266.	16380.	-31.	-22.	15.	-2.
7	5252.	5398.	5132.	5278.	5271.	5070.	5190.	16276.	-22.	-19.	15.	9.
8	5359.	5487.	5208.	5329.	5402.	5201.	5233.	16308.	-20.	-21.	73.	85.
9	5271.	5420.	5144.	5291.	5296.	5098.	5197.	16286.	-21.	-17.	43.	41.
10	5269.	5421.	5142.	5294.	5295.	5098.	5197.	16289.	-18.	-13.	44.	43.
11	5277.	5422.	5158.	5297.	5296.	5096.	5220.	16308.	-31.	-31.	30.	21.
12	5379.	5496.	5230.	5340.	5421.	5216.	5254.	16327.	-31.	-34.	62.	67.
13	5476.	5559.	5291.	5370.	5544.	5423.	5283.	16340.	-34.	-39.	118.	106.
14	6168.	5828.	5454.	5435.	6142.	6451.	5357.	16377.	-45.	552.	250.	203.
15	6682.	6478.	6193.	5482.	6501.	7282.	5431.	16408.	-29.	656.	321.	491.
16	7277.	6846.	6512.	5492.	7066.	7958.	5479.	16428.	48.	903.	353.	778.

17	7890.	7169.	6874.	6050.	7678.	8602.	6270.	16452.	246.	1083.	363.	1348.
18	8942.	7284.	7212.	6259.	8190.	9200.	6492.	16484.	398.	1250.	404.	1384.
19	13024.	*****	7802.	6586.	8660.	9034.	6665.	16522.	667.	1455.	633.	1532.
20	13619.	*****	8273.	6826.	8982.	8742.	6755.	16527.	859.	1546.	744.	1679.
21	14309.	*****	8851.	7085.	*****	*****	6848.	16557.	1081.	1537.	954.	1996.
22	14804.	*****	9443.	7415.	*****	*****	6880.	16557.	1308.	1431.	1293.	2450.
23	15070.	*****	9521.	7821.	*****	*****	6949.	16555.	1479.	1355.	1428.	3055.
24	*****	*****	9611.	8407.	*****	*****	7011.	16562.	1637.	1264.	1667.	4052.
25	*****	*****	9525.	6648.	*****	*****	7031.	16559.	1827.	1240.	2075.	5208.

TABLE 6 WELDABLE STRAIN GAUGE READINGS TAKEN DURING THE TEST ON MODEL 1

Level	Soffit Strain Gauge Readings ($\mu\epsilon$)											
	1	2	3	4	5	6	7	8	9	10	11	12
1	0.	0.	0.	0.	0.	0.	0.	0.	0.	0.	0.	0.
2	26.	29.	34.	68.	73.	69.	72.	70.	45.	44.	45.	46.
3	40.	45.	50.	97.	102.	96.	97.	95.	64.	62.	61.	64.
4	59.	68.	81.	160.	179.	190.	199.	166.	119.	116.	106.	98.
5	59.	70.	69.	126.	134.	124.	130.	121.	84.	83.	85.	89.
6	64.	75.	78.	146.	170.	177.	234.	267.	110.	121.	144.	172.
7	-11.	-11.	-6.	50.	65.	61.	64.	64.	10.	15.	19.	30.
8	25.	45.	55.	204.	201.	151.	104.	78.	58.	43.	20.	29.
9	-19.	-11.	-8.	65.	82.	66.	57.	50.	3.	7.	5.	18.
10	-13.	-6.	-3.	67.	84.	68.	60.	53.	11.	11.	8.	20.
11	0.	12.	22.	92.	113.	105.	109.	106.	37.	45.	38.	49.
12	55.	81.	99.	261.	258.	209.	167.	140.	103.	89.	57.	65.
13	88.	122.	146.	401.	378.	287.	205.	164.	142.	116.	72.	76.
14	139.	198.	241.	496.	*****	454.	309.	224.	195.	139.	118.	117.
15	151.	239.	330.	*****	*****	1478.	376.	240.	176.	130.	139.	106.
16	184.	315.	295.	*****	*****	*****	446.	265.	185.	147.	153.	134.

FIG. 3. POSITIONAL INFORMATION FOR MODEL 1 WELDABLE STRAIN GAUGES ON PRESTRESSING WIRE AND REINFORCEMENT (LINEAR)

17	222.	384.	254.	*****	*****	*****	1352.	287.	208.	375.	223.	133.
18	246.	462.	276.	*****	*****	*****	*****	321.	171.	367.	208.	151.
19	302.	508.	303.	*****	*****	*****	*****	373.	163.	*****	347.	356.
20	302.	527.	304.	*****	*****	*****	*****	379.	172.	*****	843.	1822.
21	330.	558.	322.	*****	*****	*****	*****	381.	175.	*****	1107.	2483.
22	352.	573.	348.	*****	*****	*****	*****	382.	202.	*****	*****	2799.
23	373.	575.	351.	*****	*****	*****	*****	389.	219.	*****	*****	3050.
24	574.	572.	341.	*****	*****	*****	*****	393.	220.	*****	*****	3499.
25	*****	560.	307.	*****	*****	*****	*****	385.	205.	*****	*****	*****

TABLE 7 SOFFIT STRAIN GAUGE READINGS TAKEN DURING THE TEST ON MODEL 1

FIG. 4. POSITIONAL INFORMATION FOR MODEL 1 SOFFIT STRAIN GAUGES (LINEAR)

Level	Displacement Transducer Reading (mm)											
	1	2	3	4	5	6	7	8	9	10	11	12
1	0.00	0.00	0.00	0.00	0.00	0.00	0.00	0.00	0.00	0.00	0.00	0.00
2	-1.12	-1.83	-1.67	-1.72	-1.62	-1.44	-1.86	-1.03	-1.34	-1.51	-1.24	-1.60
3	-2.30	-2.67	-2.45	-2.47	-2.74	-1.76	-2.59	-1.68	-2.97	-1.57	-2.97	-2.95
4	-3.51	-3.97	-3.87	-4.06	-3.87	-2.85	-4.11	-2.79	-4.17	-2.94	-3.88	-4.17
5	-2.60	-2.98	-2.72	-2.82	-2.86	-2.04	-3.18	-1.98	-3.15	-2.01	-3.08	-3.11
6	-3.05	-3.55	-3.59	-4.09	-3.38	-2.50	-5.11	-4.73	-4.34	-2.96	-4.14	-3.86
7	-2.17	-3.18	-2.90	-2.57	-3.11	-2.18	-3.37	-2.37	-3.29	-2.24	-3.60	-3.54
8	-5.01	-5.51	-4.51	-3.66	-5.04	-4.10	-3.88	-2.96	-4.19	-3.23	-3.86	-4.83
9	-3.62	-3.55	-3.07	-2.69	-3.35	-2.62	-3.35	-2.62	-3.38	-2.38	-3.44	-3.36
10	-3.61	-3.37	-2.87	-2.56	-3.18	-2.46	-3.28	-2.53	-3.25	-2.28	-3.27	-3.43
11	-3.10	-4.13	-4.00	-3.71	-3.77	-3.26	-4.32	-3.78	-4.16	-3.41	-3.72	-4.07
12	-5.61	-6.29	-5.62	-4.76	-5.68	-4.91	-4.91	-4.15	-5.02	-4.32	-4.14	-5.39
13	-7.38	-7.80	-6.76	-5.51	-6.96	-6.03	-5.32	-4.46	-5.60	-4.88	-4.46	-6.29
14	-11.83	-11.94	-9.86	-7.30	-10.06	-8.90	-6.28	-5.07	-7.20	-6.15	-5.22	-8.73
15	-17.74	-17.37	-13.68	-9.40	-14.40	-12.51	-7.21	-5.24	-8.89	-7.77	-6.35	-12.13
16	-24.12	-23.22	-17.85	-11.53	-18.95	-16.56	-7.63	-5.32	-10.85	-9.25	-7.22	-15.67

17	-32.51	-30.63	-22.69	-13.75	-25.12	-21.69	-8.03	-5.30	-13.02	-10.83	-8.14	-19.91
18	-40.38	-37.56	-27.50	-16.30	-30.83	-26.50	-8.62	-5.13	-15.39	-12.71	-9.34	-24.03
19	-55.92	-50.71	-35.19	-20.43	-41.48	-35.42	-9.37	-4.29	-19.35	-15.98	-11.19	-31.37
20	-65.76	-59.16	-41.20	-23.82	-48.48	-41.11	-10.25	-3.31	-22.58	-18.58	-12.94	-36.46
21	-78.95	-69.63	-48.35	-27.70	-57.49	-48.13	-11.35	-2.18	-26.06	-21.81	-14.88	-42.62
22	-92.30	-80.68	-55.56	-31.22	-67.25	******	-11.91	-0.76	-29.51	-24.64	-16.56	-48.79
23	-102.58	-89.22	-61.35	-34.18	-75.06	******	-12.48	0.31	-32.41	-27.06	-18.02	******
24	-117.49	-101.63	-69.71	-38.40	-86.81	******	-13.17	2.03	******	-30.36	-20.22	******
25	-137.10	-118.06	-80.72	-43.82	-103.59	******	-12.71	5.48	******	-34.13	-22.95	******

TABLE 8 DISPLACEMENT TRANSDUCER READINGS TAKEN DURING THE TEST ON MODEL 1

Level	De-mec Point Numbers and Readings ($\mu\epsilon$)											
	1	2	3	4	9	15	22	28	32	35	42	47
1	0.	0.	0.	0.	0.	0.	0.	0.	0.	0.	0.	0.
2	28.	7.	20.	76.	****	102.	79.	110.	59.	56.	57.	63.
3	66.	10.	20.	92.	164.	110.	106.	117.	73.	94.	82.	77.
4	79.	26.	59.	175.	211.	252.	236.	237.	151.	169.	139.	142.
5	12.	-42.	-15.	82.	106.	93.	70.	89.	35.	52.	27.	34.
6	55.	7.	37.	127.	199.	200.	221.	283.	67.	118.	90.	153.
7	59.	19.	31.	95.	184.	139.	119.	146.	69.	88.	64.	79.
8	92.	9.	36.	218.	264.	183.	125.	136.	94.	90.	32.	27.
9	34.	-34.	-9.	74.	171.	106.	83.	101.	18.	44.	3.	32.
10	13.	-67.	-29.	30.	134.	74.	72.	75.	-4.	15.	-8.	8.
11	73.	3.	23.	105.	197.	154.	142.	154.	48.	77.	64.	69.
12	170.	84.	67.	292.	400.	205.	202.	191.	115.	91.	95.	95.
13	195.	94.	90.	446.	474.	318.	222.	222.	161.	149.	94.	103.
14	302.	175.	160.	2158.	1559.	490.	322.	279.	201.	179.	164.	159.
18	2723.	471.	281.	12417.	7750.	2905.	1281.	394.	204.	388.	239.	189.

TABLE 9a SOFFIT DE-MEC POINT STRAIN READINGS TAKEN DURING THE TEST ON MODEL 1, LONGITUDINAL DIRECTION

FIG. 5. POSITIONAL INFORMATION FOR MODEL 1 DISPLACEMENT TRANSDUCERS

Level	De-Mec Point Numbers and Readings ($\mu\epsilon$)											
	5 19	6 20	7 21	8 23	10 24	11 25	12 26	13 27	14 29	16 30	17 31	18
1	0. 0.	0. 0.	0. 0.	0. 0.	0. 0.	0. 0.	0. 0.	0. 0.	0. 0.	0. 0.	0. 0.	0. 0.
2	-24. 31.	-26. 35.	-11. 68.	-6. 2.	2. 18.	43. 17.	11. 11.	67. 14.	18. 36.	31. -10.	5. 1.	22.
3	-24. 25.	-42. 34.	-24. 43.	-9. 12.	-29. 20.	23. 10.	-9. -2.	38. 4.	26. 17.	14. -30.	-12. -19.	13.
4	-35. 119.	-21. 119.	-2. 146.	57. 78.	8. 83.	86. 43.	**** 20.	98. 38.	85. 46.	96. -6.	77. 27.	85.
5	-95. -47.	-80. -20.	-45. 6.	-35. -53.	-85. -38.	-11. -73.	-80. -79.	-30. -51.	-24. -44.	-26. -29.	-69. -56.	-66.
6	-56. -13.	-60. -5.	-39. 1.	-26. 4.	-70. 20.	-25. 2.	-59. -21.	-13. -6.	-31. 0.	-39. -37.	-40. -46.	-36.
7	-70. -7.	-38. 4.	-9. 48.	-9. 13.	-53. 17.	16. 5.	-29. -21.	23. -25.	-9. 3.	-1. -40.	-15. -58.	-13.
8	-119. -48.	-82. -32.	-47. -18.	-50. -52.	-87. -43.	-55. -55.	-71. -80.	-22. -88.	-39. -65.	-47. -79.	-80. -84.	-63.
9	-103. -36.	-102. -26.	-77. 5.	-58. -49.	-80. -42.	-22. -57.	-71. -70.	-32. -78.	-39. -61.	-59. -97.	-68. -96.	-39.
10	-133. -44.	-128. -29.	-104. -28.	-71. -65.	-128. -46.	-50. -69.	-113. -94.	-54. -95.	-72. -75.	-64. -110.	-76. -127.	-41.

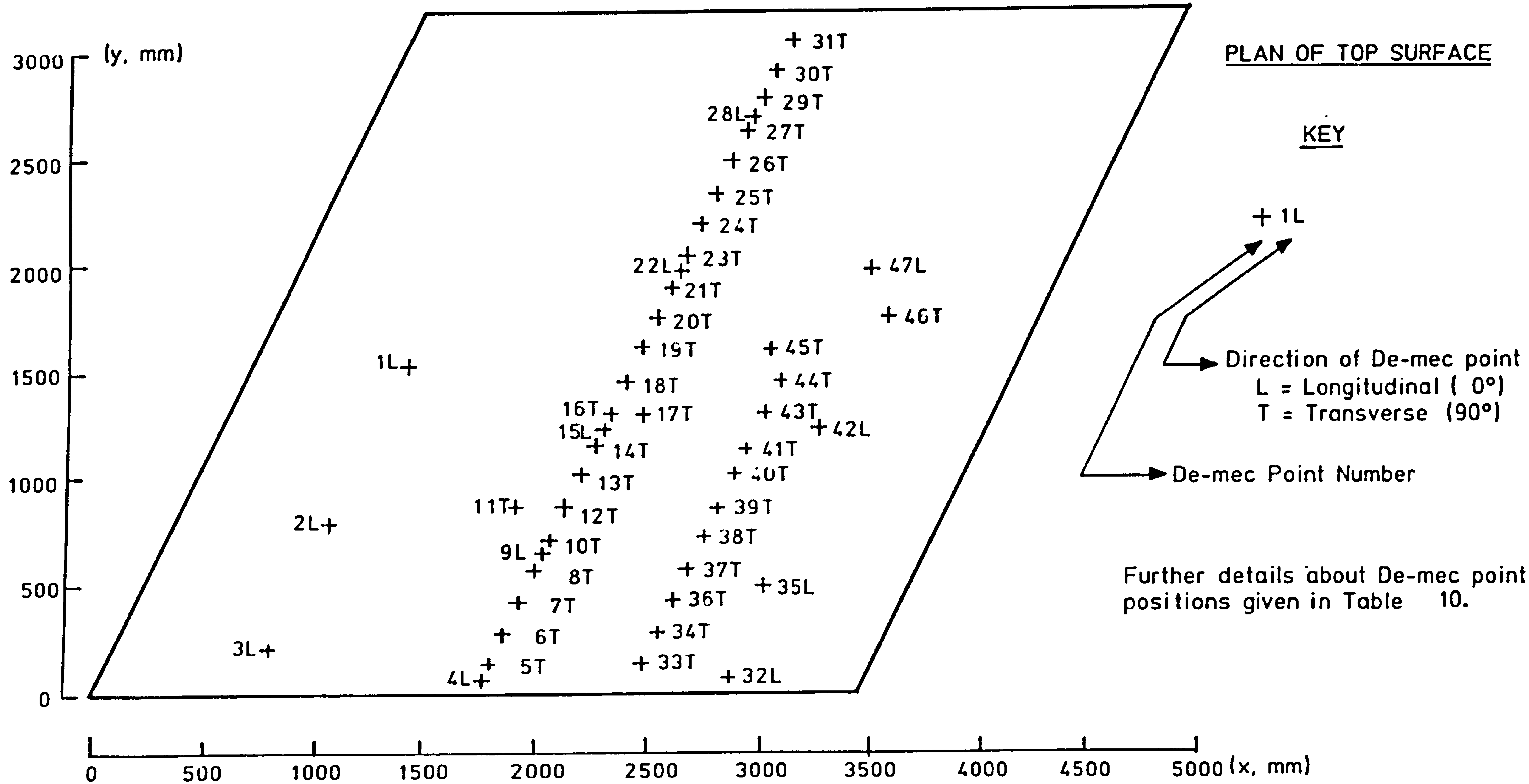

FIG. 6. POSITIONAL INFORMATION FOR MODEL 1 DE-MEC POINTS

11	-80.	-78.	-50.	-26.	-71.	-5.	-45.	6.	-12.	-10.	-48.	19.
	-11.	0.	41.	-28.	-21.	-31.	-60.	-58.	-48.	-76.	-110.	
12	-87.	-77.	-52.	-1.	-33.	25.	-47.	16.	-9.	-31.	-29.	-1.
	5.	7.	7.	-45.	-30.	-56.	-87.	-72.	-65.	-75.	-99.	
13	-100.	-60.	-62.	27.	-21.	-1.	-43.	33.	11.	-31.	-40.	-16.
	-7.	-19.	11.	-52.	-57.	-69.	-92.	-82.	-56.	-63.	-78.	
14	-77.	1089.	-50.	2406.	3.	25.	713.	58.	-27.	-69.	248.	-38.
	-56.	-56.	-44.	-80.	-51.	-88.	-86.	-94.	-70.	-66.	-88.	
18	-65.	7156.	-149.	10925.	2351.	330.	3126.	302.	-27.	-149.	1643.	1014.
	-241.	-80.	30.	-83.	-400.	-320.	-268.	-249.	-181.	-103.	-109.	

TABLE 9b SOFFIT DE-MEC POINT STRAIN READINGS TAKEN DURING THE TEST ON MODEL 1, TRANSVERSE DIRECTION AT MID-SPAN

Level	De-mec Point Numbers and Readings ($\mu\epsilon$)											
	33	34	36	37	38	39	40	41	43	44	45	46
1	0.	0.	0.	0.	0.	0.	0.	0.	0.	0.	0.	0.
2	40.	8.	-4.	3.	-12.	10.	23.	12.	-19.	-19.	23.	2.
3	8.	-34.	-23.	-6.	-20.	-18.	0.	1.	14.	11.	25.	-5.
4	35.	-20.	10.	20.	6.	26.	34.	61.	69.	59.	54.	58.
5	-43.	-121.	-61.	-74.	-68.	-79.	-88.	-65.	-29.	-46.	-36.	-57.
6	4.	-66.	-52.	-20.	-65.	-65.	-71.	-29.	-30.	-73.	-37.	-26.
7	-1.	-48.	-44.	-45.	-14.	-39.	-31.	-4.	22.	29.	16.	-19.
8	-51.	-94.	-96.	-91.	-66.	-83.	-54.	-30.	-38.	-41.	-36.	-65.
9	-58.	-104.	-96.	-84.	-78.	-96.	-63.	-54.	-60.	-47.	-43.	-41.
10	-65.	-145.	-121.	-115.	-82.	-83.	-91.	-59.	-59.	-64.	-53.	-79.
11	-38.	-90.	-71.	-92.	-33.	-57.	-53.	-27.	-16.	-16.	-8.	-30.
12	-47.	-72.	-64.	-64.	-48.	-45.	-43.	9.	-11.	-2.	-11.	-17.
13	-42.	-69.	-64.	-58.	-15.	-29.	-7.	95.	-8.	17.	-19.	-11.
14	-20.	-25.	-46.	-41.	492.	24.	150.	2838.	-20.	107.	3.	47.
18	-87.	9993.	4863.	837.	7477.	-183.	2844.	7529.	2511.	2851.	-244.	194.

TABLE 9c SOFFIT DE-MEC POINT STRAIN READINGS TAKEN DURING THE TEST ON MODEL 1, TRANSVERSE DIRECTION AT QUARTER SPAN

Point No	X coordinate (mm)	Y coordinate (mm)	Z coordinate (mm)	Angle to x-axis (degrees)	Comment
1	1400.	1520.	-87.	0.	Along beam 11
2	1060.	798.	-87.	0.	Along beam 6
3	794.	218.	-87.	0.	Along beam 2
4	1760.	73.	-87.	0.	Along beam 1
5	1800.	145.	-87.	90.	Between beams 1&2
6	1870.	290.	-87.	90.	Between beams 2&3
7	1930.	435.	-87.	90.	Between beams 3&4
8	2000.	580.	-87.	90.	Between beams 4&5
9	2040.	653.	-87.	0.	Along beam 5
10	2070.	725.	-87.	90.	Between beams 5&6
11	1910.	870.	-87.	90.	Between beams 6&7
12	2140.	870.	-87.	90.	Between beams 6&7
13	2200.	1020.	-87.	90.	Between beams 7&8
14	2270.	1160.	-87.	90.	Between beams 8&9
15	2310.	1230.	-87.	0.	Along beam 9
16	2340.	1310.	-87.	90.	Between beams 9&10
17	2490.	1310.	-87.	90.	Between beams 9&10
18	2410.	1450.	-87.	90.	Between beams 10&11
19	2470.	1600.	-87.	90.	Between beams 11&12
20	2540.	1740.	-87.	90.	Between beams 12&13
21	2610.	1890.	-87.	90.	Between beams 13&14
22	2640.	1960.	-87.	0.	Along beam 14
23	2680.	2030.	-87.	90.	Between beams 14&15
24	2740.	2180.	-87.	90.	Between beams 15&16
25	2810.	2320.	-87.	90.	Between beams 16&17

26	2880.	2470.	-87.	90.	Between beams 17&18
27	2950.	2610.	-87.	90.	Between beams 18&19
28	2980.	2680.	-87.	0.	Along beam 19
29	3020.	2760.	-87.	90.	Between beams 19&20
30	3080.	2900.	-87.	90.	Between beams 20&21
31	3150.	3050.	-87.	90.	Between beams 21&22
32	2870.	73.	-87.	0.	Along beam 1
33	2490.	145.	-87.	90.	Between beams 1&2
34	2560.	290.	-87.	90.	Between beams 2&3
35	3020.	508.	-87.	0.	Along beam 4
36	2620.	435.	-87.	90.	Between beams 3&4
37	2690.	580.	-87.	90.	Between beams 4&5
38	2760.	725.	-87.	90.	Between beams 5&6
39	2830.	870.	-87.	90.	Between beams 6&7
40	2890.	1020.	-87.	90.	Between beams 7&8
41	2960.	1160.	-87.	90.	Between beams 8&9
42	3270.	1230.	-87.	0.	Along beam 9
43	3030.	1310.	-87.	90.	Between beams 9&10
44	3100.	1450.	-87.	90.	Between beams 10&11
45	3050.	1600.	-87.	90.	Between beams 11&12
46	3580.	1740.	-87.	90.	Between beams 12&13
47	3520.	1960.	-87.	0.	Along beam 14

TABLE 10 POSITIONAL INFORMATION FOR THE DE-MEC POINTS THAT WERE ATTACHED TO MODEL 1

NOTE: All de-mec points had a 100 mm gauge length

When tested in a calibration bar with a precision of better than 100 $\mu\epsilon$ in 40000 $\mu\epsilon$ the de-mec unit gave results with a standard deviation of 25 $\mu\epsilon$

PAGE

NUMBERING

AS ORIGINAL

APPENDIX 7.1 Moment-Curvature Relationship for the Composite Beams of Model 2

Introduction

In order to obtain moment-curvature information about model 2 two composite beams were constructed, hence forth the beams will be called longitudinal sections, and tested, see Plate 1. Each longitudinal section incorporated one prestressed beam and each was similar to those described in Appendix 5.1 for model 1.

The two longitudinal sections were nominally identical so that a direct comparison between the two sets of test results would allow a critical appraisal of accidental and random errors to be carried out.

The arrangement that was used for the longitudinal section tests can be seen in Figure 1 while the locations of the de-mec points and displacement transducers are given in Figure 2. Geometrical accuracy checks on each of the sections revealed good quality construction with errors generally less than 1mm. 100mm cubes and 150mm x 300mm cylinders were cast from the mixes used to construct the sections. The material properties were obtained from tests carried out on these specimens at the same time as the main section tests. The cube strength from 100mm cube tests for the insitu concrete was 62 N/mm^2 with a standard deviation of 1.6 N/mm^2 from a sample of 4 and for the precast concrete it was 66 N/mm^2 with a standard deviation of 1.2 N/mm^2 from a sample of 3. The split cylinder strength obtained from Brazilian tests on 150mm Ø x 300mm cylinders was 3.68 N/mm^2 with a standard deviation of 0.21 N/mm^2 from a sample of 3 for the insitu concrete while tests on the precast concrete yielded values of 4.12 N/mm^2 with a standard deviation of 0.44 from a sample of 2. The material stress-strain relationships were obtained from strain gauged compression and tension tests, for the concrete and steel respectively. These tests were carried out at the same time as the longitudinal section tests and the results can be seen in Figure 3.

Test of longitudinal section 1

Before any load was applied to the beam the initial pre-camber was measured at 14mm at mid-span relative to the supports.

Poor surface finish on the sides of the insitu concrete hindered the spotting of the first cracks. However, the test observation that there was not significant cracking in the section for the first three load increments up to a load of 27 kN is supported by the load-deflection plot of Figure 4. The small change in the beam stiffness upon application of the third load increment, see Figure 4, suggests that limited cracking was present.

The first crack was spotted during the test at a load of 30.34 kN and this is supported by both the load-deflection response and the de-mec strain readings.

During subsequent load increments the cracking intensity increased to cover the whole constant moment zone, and beyond, at an average

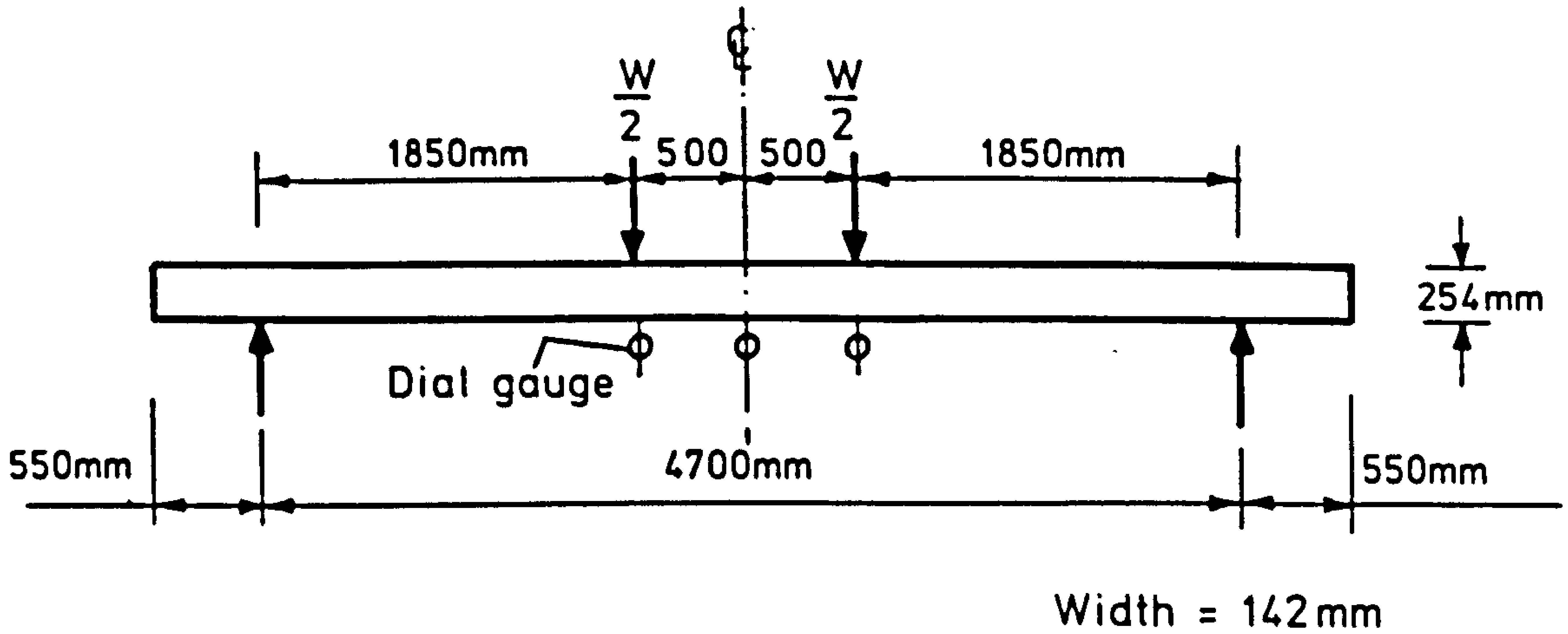

FIG. 1 TEST ARRANGEMENT FOR MODEL 2 LONGITUDINAL SECTIONS

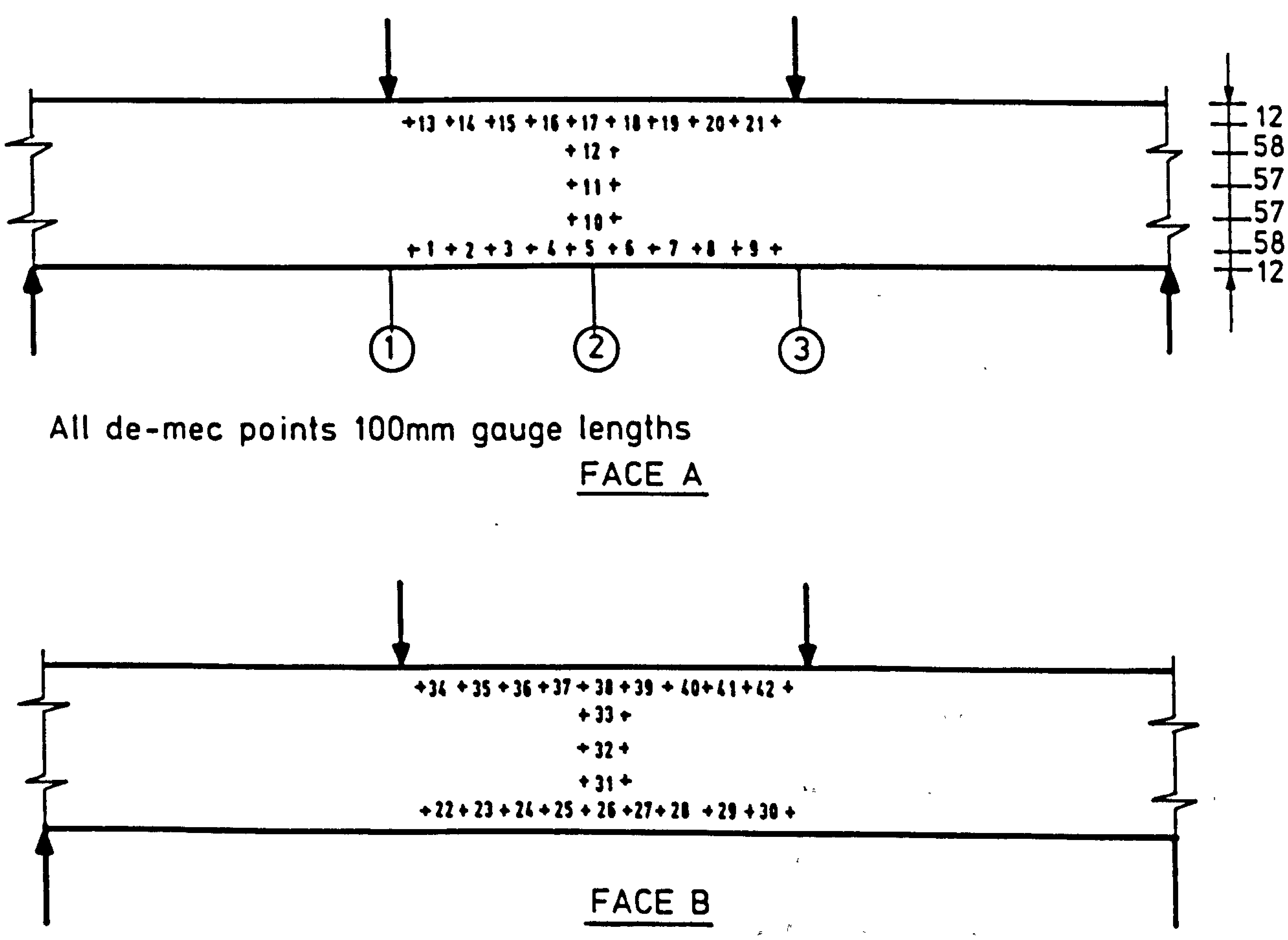

FIG 2 TRANSDUCER AND DE-MEC POINT LOCATIONS FOR MODEL 2 LONGITUDINAL SECTIONS

spacing of 100mm. Generally, the cracks propagated to within 50mm of the top surface, although several progressed as far as 25mm from the top.

At a load of 52.33 kN several of the de-mec points could not be used because either the concrete had crushed resulting in de-mec points falling off or the tensile strain had exceeded the 30,000 micro strain limit of the de-mec gauge. Such points are denoted by '-' in Tables 5 to 10.

There was a great deal of crushing and spalling around the top surface of the beam as well as large cracks approximately 4-5mm wide along the soffit when the mid-span displacement had reached 141.2mm with an applied load of 50.06 kN.

Failure occurred by rupture of one or more of the lower prestressing tendons. After failure there was still an upward prestress camber of approximately 5mm in the end few metres of the beam. A side view of the longitudinal section after failure can be seen in Plate 2.

Test of Longitudinal Section 2

As with section 1 no cracks were noticed in the concrete for the first two load increments up to 18 kN. However, at 27 kN two cracks were noticed in the insitu concrete along the side of section 2. Each crack progressed approximately 40mm vertically upwards from its intersection with the top of the precast flange. At a load level of 31 kN the cracking was well distributed with a spacing of

Stress-strain relationship for the precast concrete.

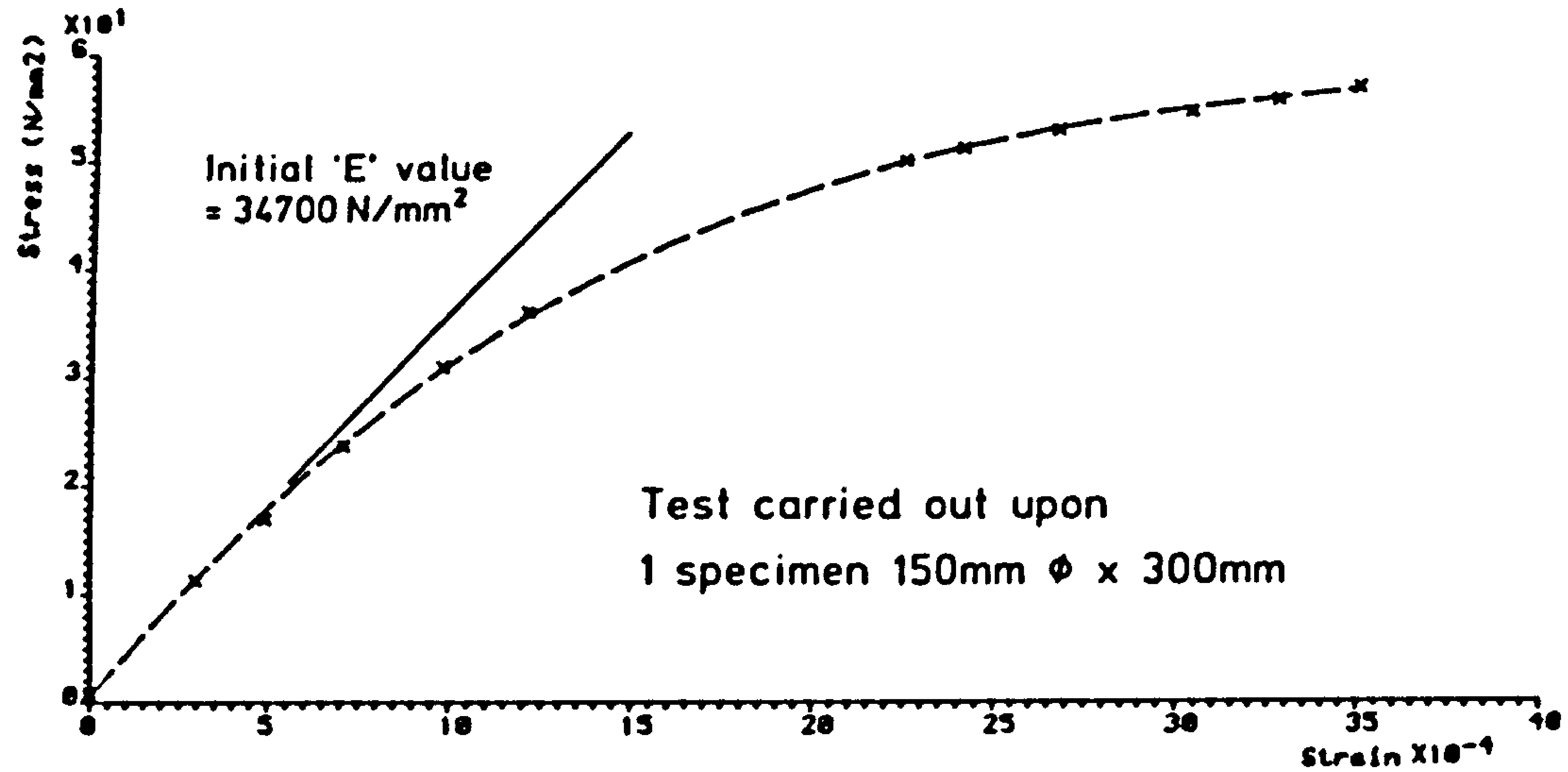

Stress-strain relationship for the in-situ concrete.

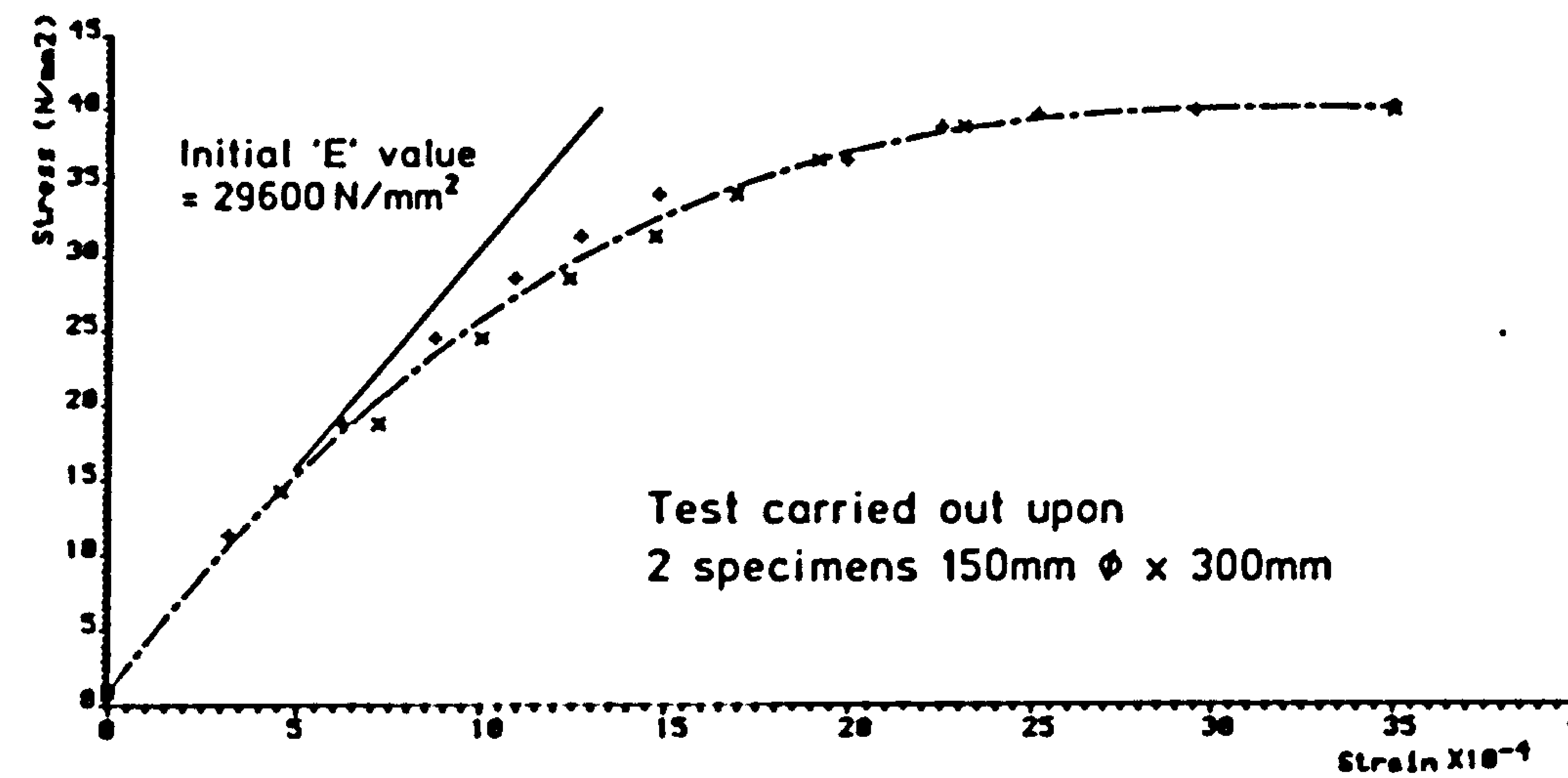

Stress-strain curve for the 7.9mm dia. prestressing strand.

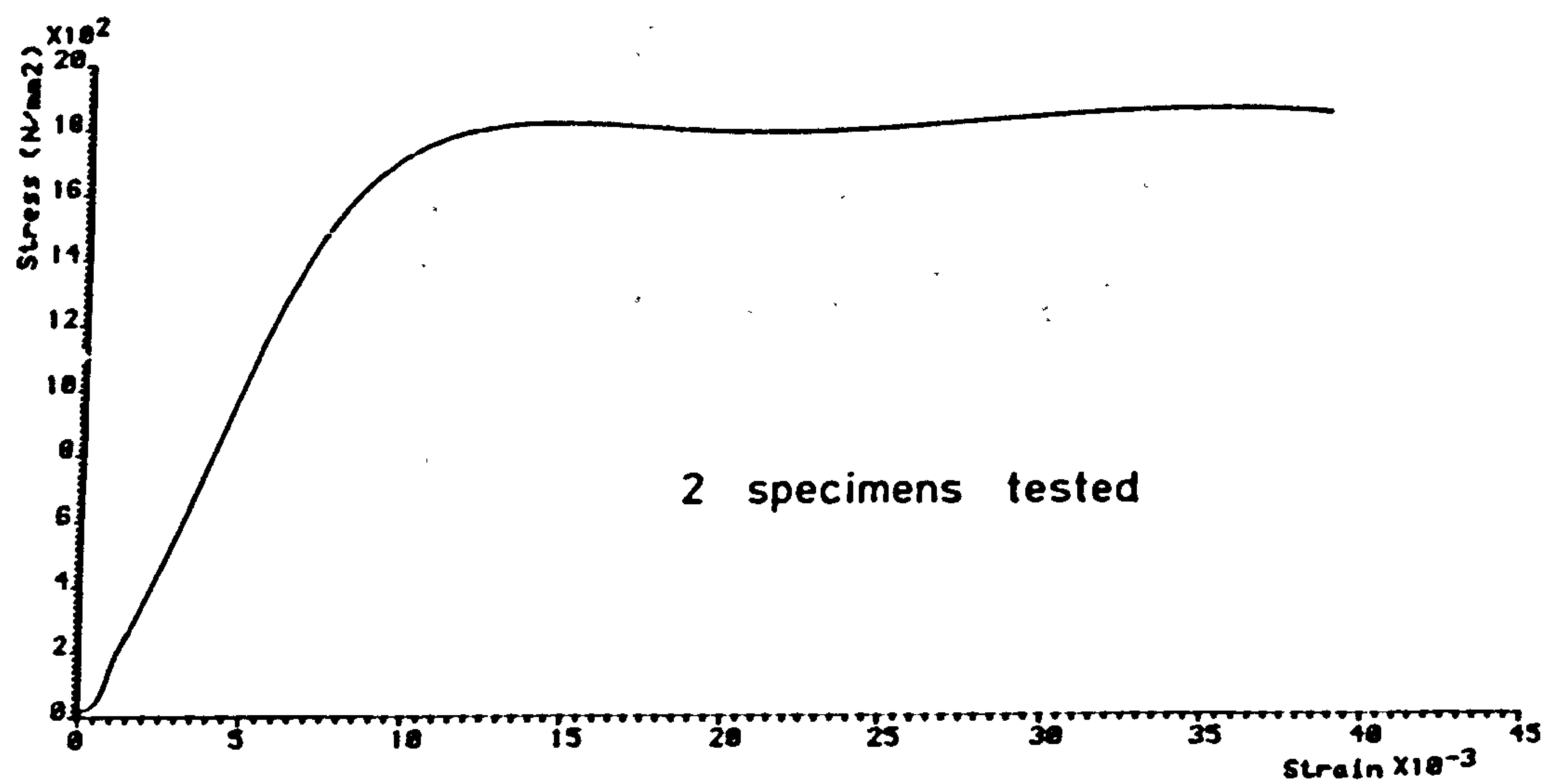

FIG. 3. STRESS-STRAIN RELATIONSHIP FOR THE MODEL 2 LONGITUDINAL SECTION MATERIALS

approximately 110 to 140mm and an average height above the beam soffit of 80 to 100mm.

During the middle and later stages of the test, it was thought necessary to allow conditions to stabilise for between 20 and 60 minutes after each load increment before transducer readings were taken.

Crushing and spalling of the top of the surface concrete adjacent to mid-span was evident when the mid-span displacement reached 125mm at a load level of 52.6 kN.

A catastrophic failure was caused by rupture of all three lower prestressing tendons. After failure the beam retained no load carrying capacity and therefore unlike beam 1 no readings were taken after failure.

Discussion

A plot showing the change in NA depth with increasing depth can be seen in Figure 4, the NA depth was calculated from average strains. It will be noted that the NA is initially significantly below the mid-section depth at the beginning of the test which is unusual considering the similar strengths and 'E' values for the two concretes. It is surprising that for section 1 the depth of the NA changes during the second load increment while the load-deflection and moment curvature plots indicate a linear response. Inspection of Table 3 reveals very similar average strains for each side at both the

Plot of load against deflection for model 2 longitudinal sections.

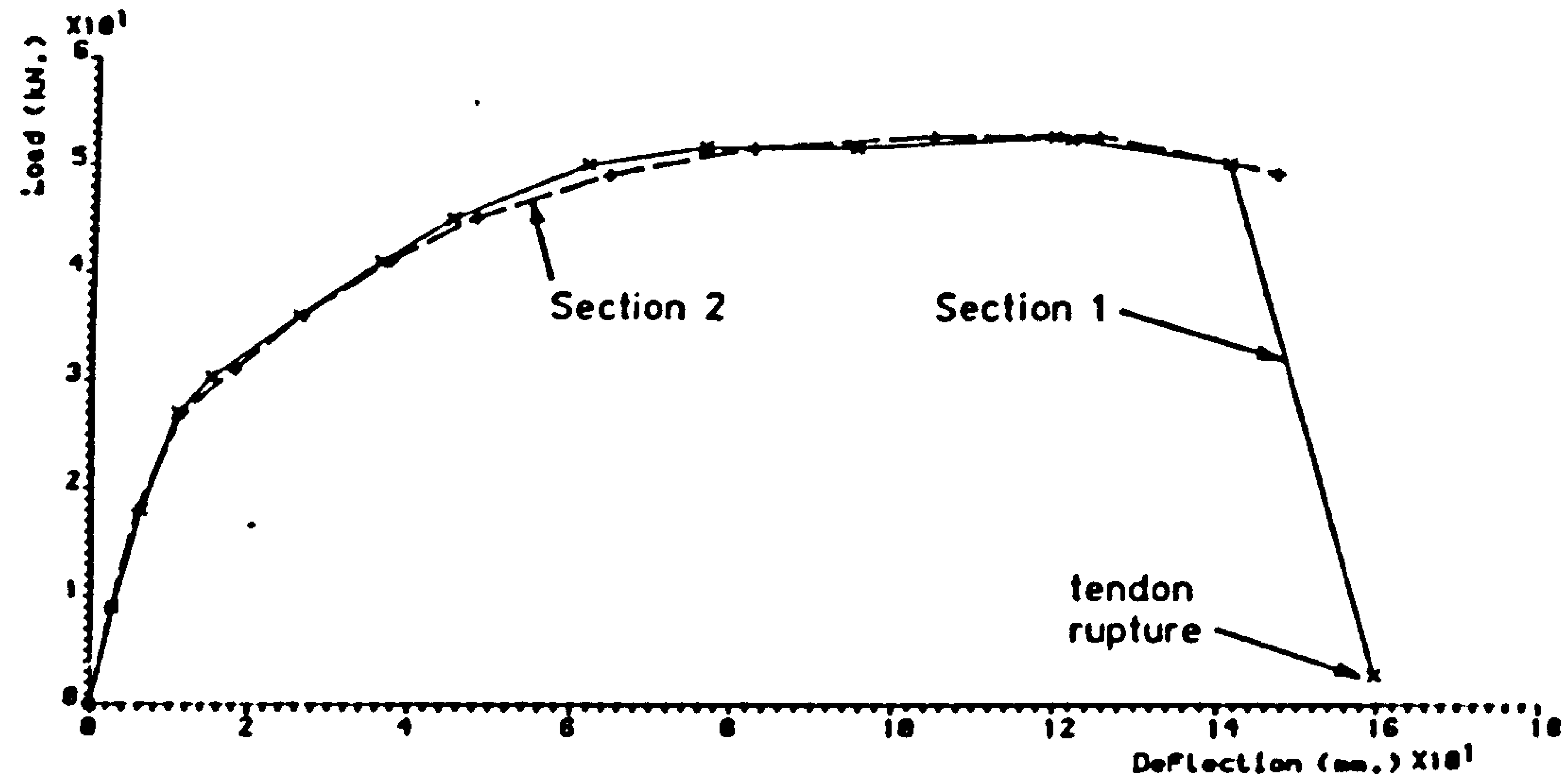

Plot of moment against curvature for model 2 longitudinal sections.

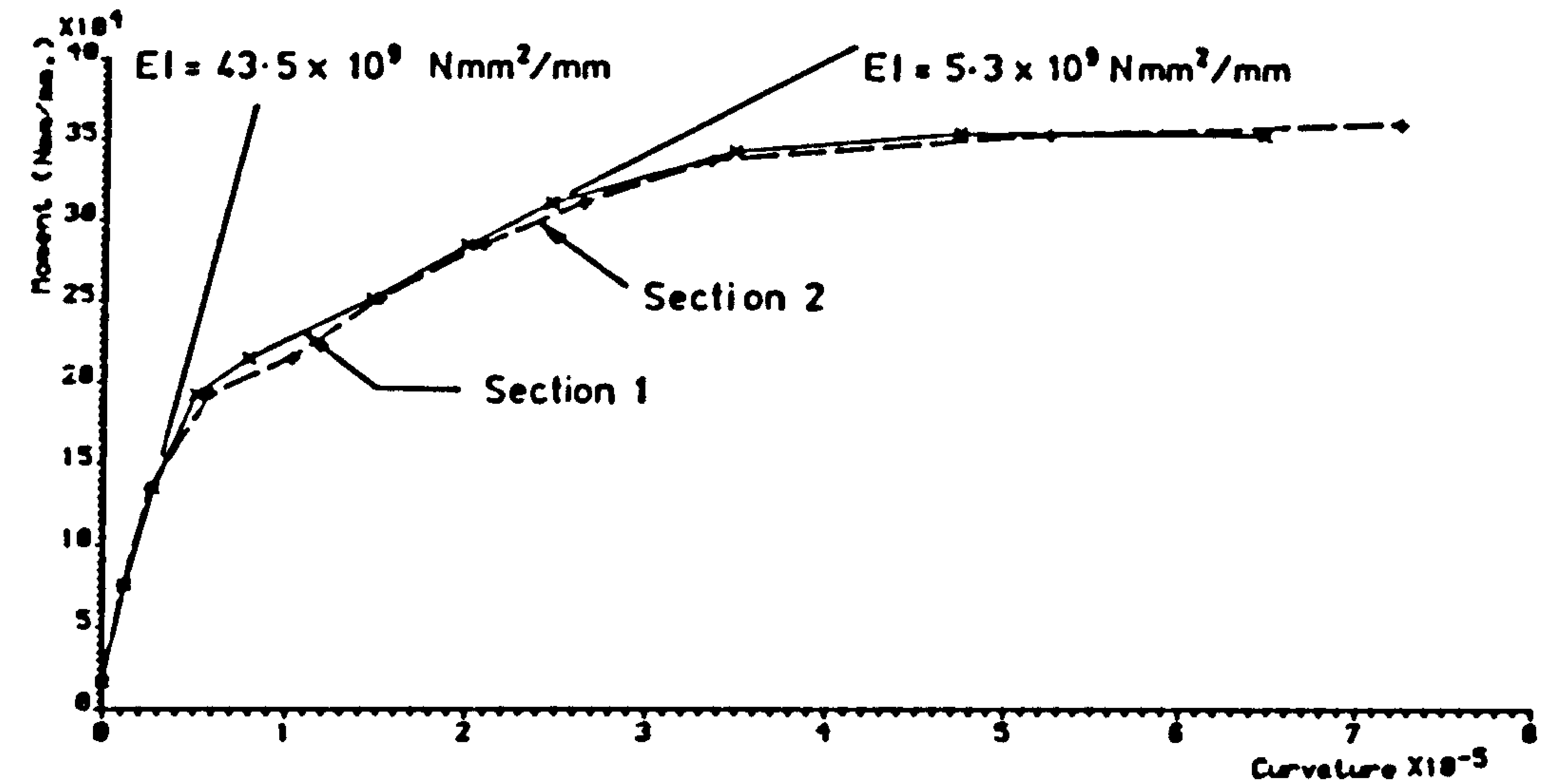

Plot of moment against NA depth for model 2 longitudinal sections.

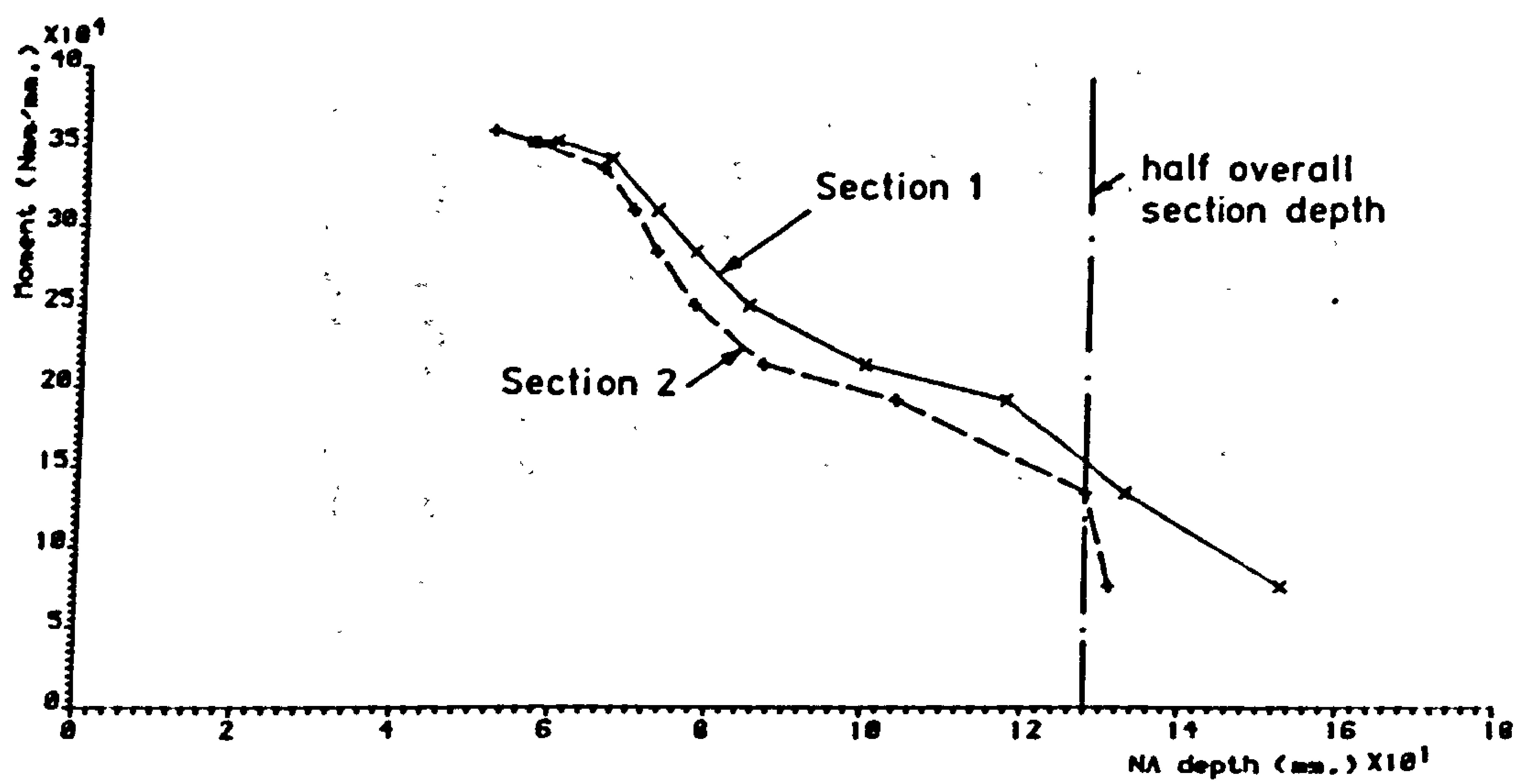

FIG. 4. PLOTS OF MODEL 2 LONGITUDINAL SECTION TEST RESULTS

top and bottom of the section thus reducing the possibility of transducer drift and other errors.

It can be seen from Plate 2 that generally the cracks progressed as far as 50mm from the top surface which is in agreement with the predicted NA depth of approximately 50mm from Figure 4.

From the moment-curvature comparison in Figure 4 it can be seen that the initial flexural stiffness is 43.5×10^9 Nmm^2/mm which compares very favourably with the flexural stiffness of 46.7×10^9 Nmm^2/mm that was calculated in Chapter 8 for the linear finite element analysis.

Both the load-deflection plots and moment-curvature plots of Figure 4 indicate that very little cracking occurred at a load of 18 kN or a moment of 135×10^3 Nmm/mm with limited cracking between this load and 27 kN. From Table 3 and 4 we can see that the average lower strain at a load of 18 kN is 297 $\mu\epsilon$ for section 1 and 300$\mu\epsilon$ for section 2. From the stress-strain curves in Figure 3 and the previously mentioned split cylinder strengths we can deduce that the cracking strain for the insitu concrete is approximately 124 $\mu\epsilon$. This would therefore suggest that the pre-strained precast concrete severely retarded the onset of cracking in the insitu concrete. It may be argued that the insitu concrete was not effectively strain free at the start of the tests, caused maybe by creep as a result of the prestress loading. It is interesting to examine the relevant dates which are; release of the prestress beams, 13-5-85; casting of insitu concrete 18-6-85; and testing on 4-9-85 and 8-10-85. The 11 and 16 week gaps between the insitu casting and the testing may have allowed compressive

Plot of moment against curvature for model 2 longitudinal section 1.

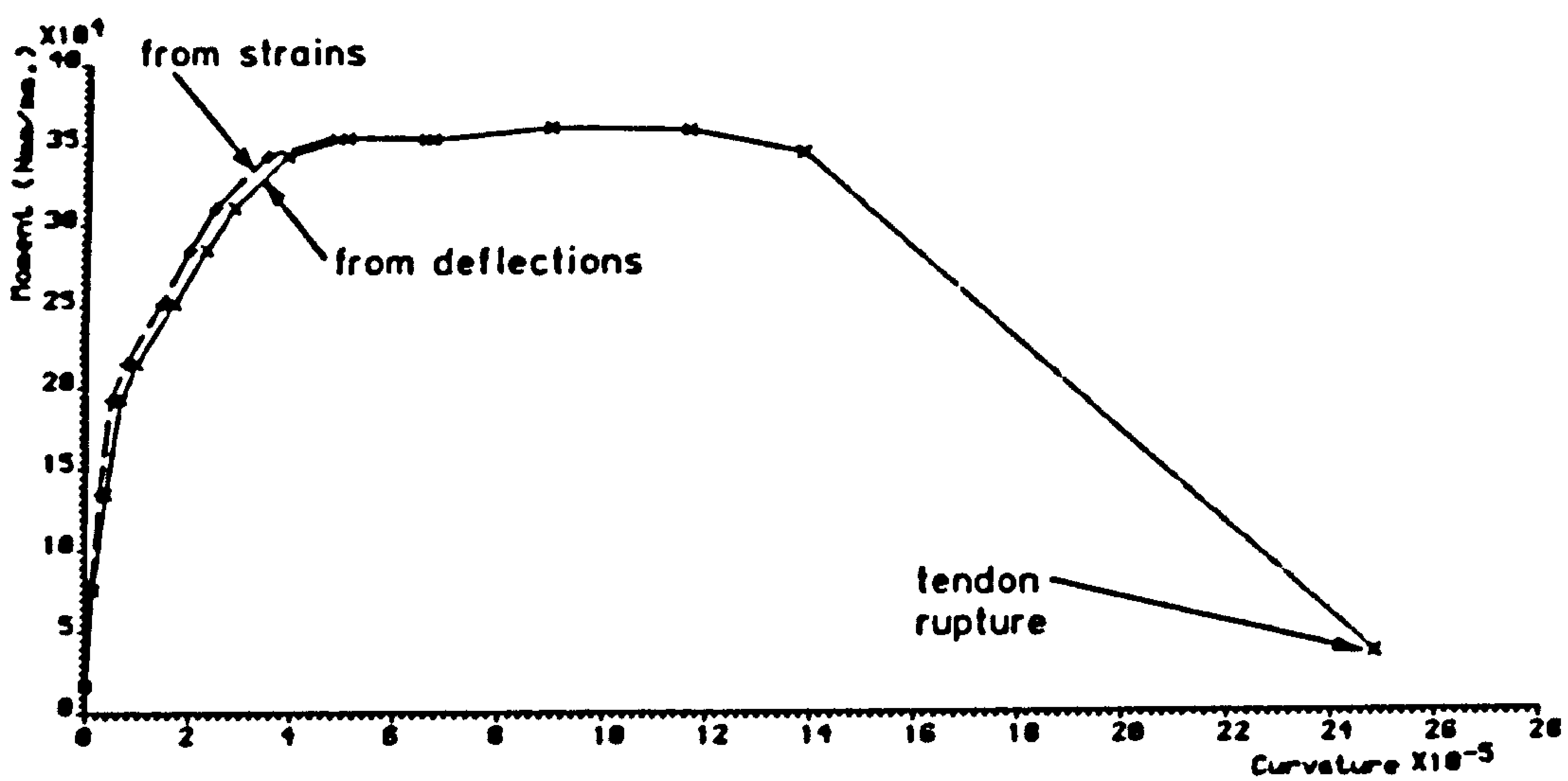

Plot of moment against curvature for model 2 longitudinal section 2.

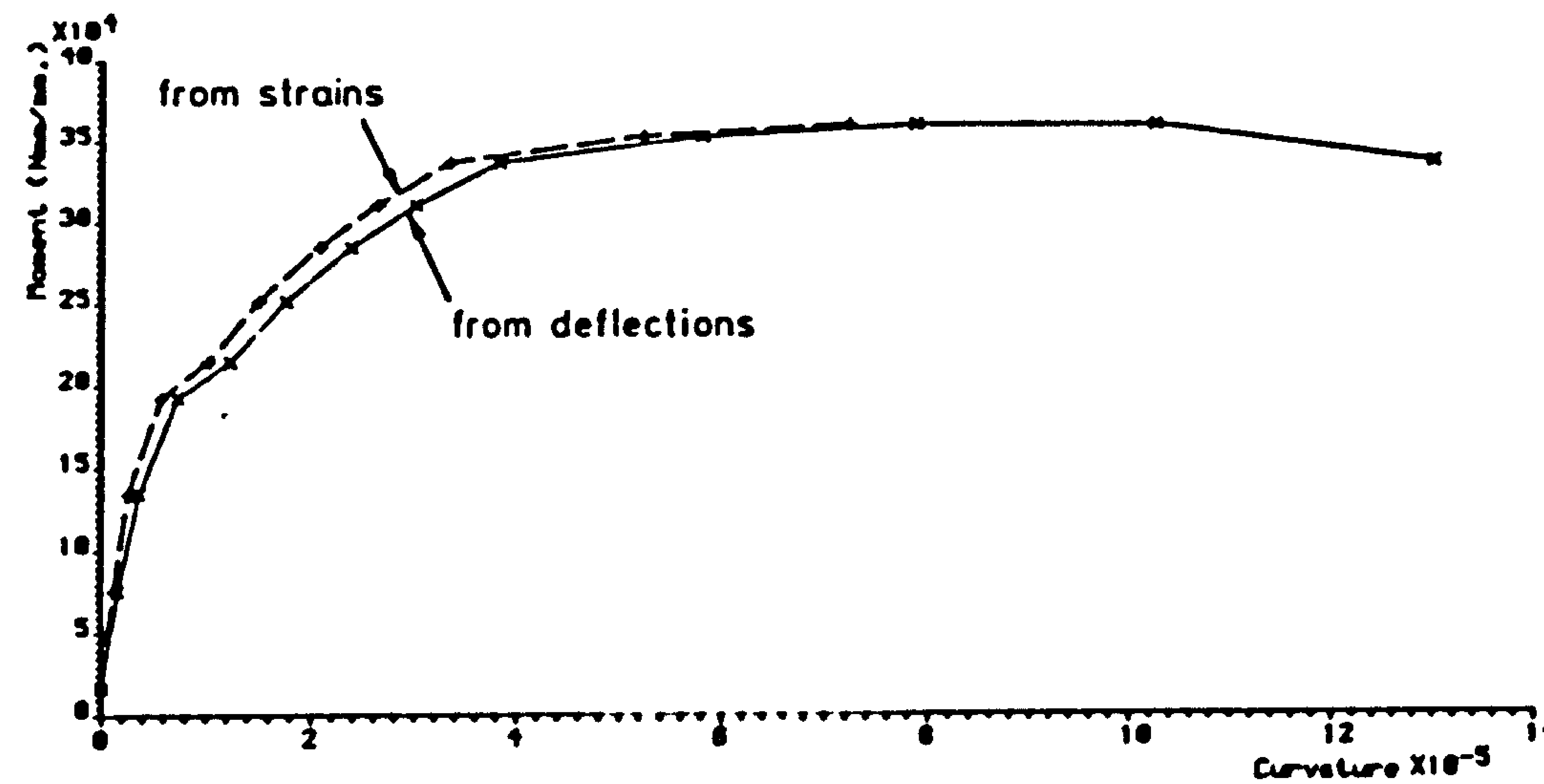

FIG. 5. COMPARISONS BETWEEN CURVATURES DERIVED FROM DEFLECTIONS AND THOSE DERIVED FROM STRAINS FOR MODEL 2 LONGITUDINAL SECTIONS

pre-strains to develop in the lower regions of the insitu concrete. The central deflection required to give the increase in strain at 18 kN above the deduced cracking strain is approximately 3.5mm which is not unreasonable when one recalls that the initial pre-camber at the beginning of the tests was 14mm.

Load (kN)	Moment x 10^6(Nmm/mm)	Deflections (mm)			Curvature x 10^{-6}
		Gauge 1	Gauge 2	Gauge 3	
0	0.017	0	0	0	0
9	0.076	2.48	2.67	2.49	1.48
18	0.135	5.76	6.23	5.70	4.00
27	0.193	9.87	10.76	9.92	6.92
30.34	0.215	13.66	14.92	13.71	9.88
36	0.252	23.83	26.02	23.95	17.04
41	0.285	33.11	36.11	33.36	23.00
45	0.311	41.42	45.12	41.74	28.32
50	0.343	56.40	61.50	56.93	38.68
51.60	0.354	69.45	76.18	70.29	50.48
51.58	0.353	85.96	94.99	87.24	67.12
52.59	0.360	107.42	119.53	109.23	89.64
52.33	0.358	106.3	121.60	107.81	116.36
50.06	0.344	124.36	141.18	123.39	138.44
2.78	0.036	143.81	159.79	113.59	248.72

TABLE 1 DEFLECTIONS AND DERIVED CURVATURES FOR MODEL 2 LONGITUDINAL SECTION 1

Load (kN)	Moment x 10^6 (Nmm/mm)	Deflections (mm)			Curvature x 10^{-6}
		Gauge 1	Gauge 2	Gauge 3	
0	0.017	0	0	0	0
9	0.076	2.41	2.60	2.39	1.60
18	0.135	5.40	5.84	5.37	3.64
27	0.193	10.4	11.33	10.42	7.36
31	0.215	16.44	17.99	16.45	12.36
36	0.252	24.26	26.46	24.22	17.76
41	0.285	34.36	37.33	34.32	23.92
45	0.311	44.26	47.98	44.17	30.12
49	0.337	59.67	64.11	58.95	38.36
51.50	0.353	75.33	82.19	74.52	58.12
52.59	0.360	95.15	104.43	94.00	78.84
52.59	0.360	112.80	124.98	111.48	102.72
49.05	0.337	131.81	147.03	129.73	130.08

TABLE 2 DEFLECTIONS AND DERIVED CURVATURES FOR MODEL 2 LONGITUDINAL SECTION 2

Load (kN)	Moment $\times 10^6$ (Nmm/mm)	Average Strains ($\mu\epsilon$)						Curvature $\times 10^{-6}$ (/mm)	Average NA depth (mm)
		Top points 13-21	Top points 34-42	Average	Bot points 1-9	Bot points 22-30	Average		
0	0.017	0	0	0	0	0	0	0	-
9	0.076	-167	-169	-168	105	105	105	1.19	153
18	0.135	-322	-338	-330	308	286	297	2.73	133
27	0.193	-519	-557	-538	643	611	627	5.07	118
30.34	0.215	-677	-726	-702	1127	1147	1137	7.99	100
36	0.252	-1036	-1108	-1072	2278	2338	2308	14.70	85
41	0.285	-1266	-1353	-1310	3200	3380	3290	20.00	78
45	0.311	-1441	-1566	-1504	4048	4300	4174	24.69	73
50	0.343	-1837	-2014	-1926	5911	6256	6084	34.83	67
51.60	0.354	-2134	-2395	-2265	8307	8927	8617	47.31	60
51.58	0.353	-2628	-2930	-2779	11622	12618	12120	64.78	57

TABLE 3 AVERAGE STRAINS AND DERIVED CURVATURES FOR MODEL 2 LONGITUDINAL SECTION 1

Load (kN)	Moment $\times 10^6$ (Nmm/mm)	Average Strains $\times 10^{-6}$						Curvature $\times 10^{-6}$ (/mm)	Average NA depth (mm)
		Top points 13-21	Top points 34-42	Average	Bot points 1-9	Bot points 22-30	Average		
0	0.017	0	0	0	0	0	0	0	-
9	0.076	-142	-131	-137	120	135	128	1.15	131
18	0.135	-314	-292	-303	278	321	300	2.62	128
27	0.193	-549	-532	-541	793	819	806	5.86	104
31	0.215	-779	-779	-779	1607	1591	1599	10.34	87
36	0.252	-1006	-1002	-1004	2495	2479	2487	15.18	78
41	0.285	-1281	-1278	-1280	3544	3523	3534	20.93	73
45	0.311	-1527	-1532	-1530	4573	4536	4555	26.46	70
49	0.337	-1805	-1822	-1814	5913	5875	5894	33.51	66
51.50	0.353	-2360	-2386	-2372	9707	9653	9680	52.40	57
52.59	0.360	-2890	-2923	-2906	13794	13726	13760	72.46	52

TABLE 4 AVERAGE STRAINS AND DERIVED CURVATURES FOR MODEL 2 LONGITUDINAL SECTION 2

Load (kN)	De-mec Point Strain Readings ($\mu\epsilon$)																	
	1	2	3	4	5	6	7	8	9	22	23	24	25	26	27	28	29	30
0	0	0	0	0	0	0	0	0	0	0	0	0	0	0	0	0	0	0
9	119	120	108	110	120	70	92	74	128	91	115	150	103	92	98	86	114	95
18	306	308	291	306	333	297	275	323	330	256	304	323	259	274	298	279	295	284
27	514	613	638	524	711	768	370	1110	528	590	559	632	500	524	565	557	1045	522
30.34	1021	1094	1166	1192	1251	1381	395	1804	833	944	1234	1134	1112	887	891	1112	1848	1156
36	1990	2218	2742	2373	2316	2198	1568	3484	1613	1922	2346	2584	2217	1962	1713	2102	3958	2236
41	2850	2982	4114	3261	3261	2881	2406	5237	1806	2786	3195	3971	3110	2958	2462	2903	5691	3340
45	3679	3812	5326	4066	4111	3564	3155	6757	1960	3547	3969	5172	3916	3838	3159	3588	7230	4276
50	5698	5455	7644	6095	5557	5022	4722	10903	2099	5220	5516	7450	5776	5411	4586	5009	10752	6579
51.60	8913	7550	9816	10392	6202	6794	6320	16752	2022	8162	7525	9630	10051	6202	6363	6685	16120	9606
51.58	12758	10308	14433	14237	7118	10006	9284	24491	1963	11844	10216	14154	13878	7242	9582	9558	23709	13381
52.59	16226	13702	21200	18395	10463	14186	13357	-	1920	15185	13294	20774	17950	10415	13569	13511	-	19224
52.33	18358	19415	-	22382	15948	17285	16436	-	2030	17364	19126	-	21671	-	16482	16617	-	23130
50.06	18125	28587	-	23875	16457	17460	16591	-	1666	17051	28363	-	23627	-	16606	16727	-	23389
2.78	19129	-	-	24461	17398	19479	18993	-	1525	18462	-	-	24539	-	18355	18332	-	25317

TABLE 5 READINGS FROM LOWER LINES OF DE-MEC POINTS ON MODEL 2 LONGITUDINAL SECTION 1

Load (kN)	De-Mec Point Strain Readings ($\mu\epsilon$)									
	5	10	11	12	17	26	31	32	33	38
0	0	0	0	0	0	0	0	0	0	0
9	-125	-111	-21	29	120	-156	-83	-25	59	92
18	-298	-196	-21	128	333	-312	-148	-23	126	274
27	-466	-211	86	371	711	-507	-168	-24	194	524
30.34	-611	-166	293	763	1251	-683	-220	87	389	887
36	-964	-173	649	1471	2316	-1053	-276	398	1113	1926
41	-1194	-60	1011	2113	3261	-1281	-35	734	1770	2958
45	-1392	-55	1299	2708	4111	-1480	-31	1046	2374	3838
50	-1742	107	1859	3713	5557	-1896	45	1604	3461	5411
51.60	-1981	269	2169	4148	6202	-2222	163	2014	4089	6202
51.58	-2346	384	2540	4829	7118	-2583	636	2383	4710	7242
52.59	-2839	859	3916	7173	10463	-3196	977	3726	7073	10415
52.33	-3369	1646	6239	11142	15948	-4033	1483	5907	10911	-
50.06	-3362	1402	6192	11344	16457	-4092	1330	5567	10809	-
2.78	-2492	2223	7072	12239	17398	-3260	2049	6710	12072	-

TABLE 6 READINGS FROM THROUGH DEPTH DE-MEC POINTS ON MODEL 2 LONGITUDINAL SECTION 1

Load (kN)	De-mec Point Strain Readings ($\mu\epsilon$)																	
	13	14	15	16	17	18	19	20	21	34	35	36	37	38	39	40	41	42
0	0	0	0	0	0	0	0	0	0	0	0	0	0	0	0	0	0	0
9	-158	-168	-189	-212	-125	-145	-235	-111	-159	-169	-138	-146	-153	-156	-188	-187	-179	-201
18	-310	-295	-362	-386	-298	-320	-441	153	-325	-344	-301	-311	-327	-312	-358	-356	-335	-392
27	-458	-464	-550	-538	-466	-505	-623	-482	-582	-554	-505	-505	-513	-507	-588	-601	-608	-625
30.34	-612	-607	-702	-698	-611	-652	-776	-650	-782	-742	-674	-678	-664	-683	-785	-750	-764	-791
36	-956	-977	-1075	-1057	-964	-992	-1153	-1011	-1134	-1093	-1050	-1058	-1047	-1053	-1176	-1158	-1152	-1184
41	-1171	-1199	-1301	-1268	-1194	-1241	-1448	-1215	-1357	-1331	-1282	-1299	-1279	-1281	-1407	-1416	-1422	-1456
45	-1378	-1390	-1527	-1475	-1392	-1426	-1658	-1152	-1568	-1538	-1498	-1521	-1483	-1480	-1622	-1635	-1633	-1681
50	-1718	-1736	-1890	-1815	-1742	-1807	-2055	-1816	-1944	-1973	-1912	-1934	-1881	-1896	-2084	-2081	-2159	-2198
51.60	-2009	-2037	-2164	-2156	-1981	-2022	-2321	-2166	-2346	-2324	-2256	-2257	-2305	-2222	-2437	-2456	-2625	-2667
51.58	-2374	-2453	-2700	-2653	-2346	-2517	-2976	-2752	-2881	-2785	-2766	-2810	-2819	-2583	-3020	-3120	-3299	-3165
52.59	-2768	-2977	-3345	-3258	-2839	-3127	-3618	-3464	-3437	-3254	-3475	-3605	-3518	-3196	-3957	-3799	-4081	-3777
52.33	-3028	-4206	-5170	-4002	-3369	-3761	-4307	-4346	-3896	-3437	-5094	-5945	-4068	-4033	-4700	-4260	-5152	-4133
50.06	-2953	-	-	-	-3362	-4052	-4536	-4343	-4086	-3356	-	-	-	-4092	-4948	-4445	-5984	-4351
2.78	-2140	-	-	-	-2492	-3004	-3504	-3908	-3235	-2627	-	-	-	-3260	-4174	-3646	-5088	-3479

TABLE 7 READINGS FROM UPPER LINES OF DE-MEC POINTS ON MODEL 2 LONGITUDINAL SECTION 1

Load (kN)	De-mec Point Strain Readings ($\mu\epsilon$)																	
	1	2	3	4	5	6	7	8	9	22	23	24	25	26	27	28	29	30
0	0	0	0	0	0	0	0	0	0	0	0	0	0	0	0	0	0	0
9	122	124	112	127	124	103	121	126	122	164	139	124	129	126	128	140	118	139
18	262	317	241	297	262	264	252	307	296	361	307	325	298	332	320	303	300	333
27	960	685	402	1109	642	995	574	515	1255	1186	644	1244	305	871	832	469	576	1235
31	1910	1710	352	2075	1894	1877	1695	580	2366	1910	1528	2286	422	2038	1835	390	1772	2131
36	2918	3168	300	3333	2919	2910	2772	715	3416	2742	3135	2665	1238	3044	2971	408	2875	3228
41	4053	4853	279	4749	4129	4154	4294	721	4666	3856	4830	2931	2378	4176	4267	866	3907	4486
45	5164	6499	263	6118	5346	5382	5873	695	5809	4932	6451	3420	3246	5352	5483	1446	4858	5635
49	6591	8707	218	8043	6996	7063	7870	636	7088	6306	8616	4153	4458	7012	7063	2419	5874	6963
51.50	10008	16110	166	14179	12670	12219	12515	584	8907	9613	16126	4878	9752	12674	12109	6139	6747	8841
52.59	14836	21328	103	20206	19528	17290	17617	547	12691	14466	21365	6967	13552	19388	17226	9262	8566	12743
52.59	17655	24508	-49	25433	-	21286	20511	463	15841	17293	24570	8990	16978	-	20967	10951	9791	15815
49.05	19211	27269	-75	-	-	24045	22005	400	17466	19058	27496	16936	21552	-	23471	11778	10441	17330

TABLE 8 READINGS FROM LOWER LINES OF DE-MEC POINTS ON MODEL 2 LONGITUDINAL SECTION 2

Load (kN)	De-mec Point Strain Readings ($\mu\epsilon$)									
	5	10	11	12	17	26	31	32	33	38
0	0	0	0	0	0	0	0	0	0	0
9	-145	-86	-7	55	124	-148	-81	-3	70	126
18	-332	-185	-28	110	262	-296	-140	39	234	332
27	-600	-243	62	363	642	-562	-203	214	605	871
31	-865	-193	503	1235	1894	-849	-166	619	1386	2038
36	-1099	-128	899	1949	2919	-1095	-81	984	2034	3044
41	-1391	-64	1359	2797	4129	-1418	-25	1415	2839	4176
45	-1665	45	1844	3645	5346	-1716	55	1859	3644	5352
49	-1991	215	2521	4822	6996	-2101	227	2527	4791	7012
51.50	-2765	1119	5039	8934	12670	-2953	1107	4990	8819	12674
52.59	-3643	2250	8044	13888	19528	-3961	2129	7853	13557	19388
52.59	-7400	4053	13305	22618	-	-6964	3479	12637	21738	-
49.05	-	3555	16426	-	-	-	2480	15210	27972	-

TABLE 9 READINGS FROM THROUGH DEPTH DE-MEC POINTS ON MODEL 2 LONGITUDINAL SECTION 2

Load (kN)	De-mec Point Strain Readings ($\mu\epsilon$)																	
	13	14	15	16	17	18	19	20	21	34	35	36	37	38	39	40	41	42
0	0	0	0	0	0	0	0	0	0	0	0	0	0	0	0	0	0	0
9	-108	-155	-128	-149	-145	-151	-140	-142	-158	-139	-129	-142	-104	-148	-132	-124	-152	-106
18	-269	-336	-290	-339	-332	-336	-305	-293	-321	-303	-255	-311	-279	-296	-282	-276	-334	-287
27	-481	-571	-518	-584	-600	-583	-526	-507	-564	-528	-454	-536	-537	-562	-544	-523	-566	-530
31	-724	-785	-727	-800	-865	-852	-758	-717	-777	-750	-694	-768	-797	-849	-793	-764	-798	-791
36	-928	-1021	-963	-1041	-1099	-1085	-980	-915	-1012	-959	-968	-995	-999	-1095	-1047	-976	-954	-1022
41	-1215	-1280	-1224	-1345	-1391	-1363	-1261	-1166	-1277	-1213	-1168	-1237	-1281	-1418	-1332	-1264	-1294	-1294
45	-1440	-1550	-1460	-1633	-1665	-1619	-1493	-1369	-1511	-1463	-1398	-1470	-1570	-1716	-1590	-1540	-1522	-1515
49	-1718	-1822	-1724	-1918	-1991	-1910	-1789	-1602	-1767	-1733	-1742	-1752	-1864	-2101	-1934	-1790	-1656	-1819
51.50	-2154	-2454	-2328	-2663	-2765	-2490	-2347	-1978	-2053	-2165	-2284	-2313	-2570	-2953	-2655	-2297	-2094	-2133
52.59	-2635	-2943	-2794	-3282	-3643	-3025	-2848	-2352	-2479	-2651	-2652	-2727	-3219	-3961	-3151	-2812	-2607	-2520
52.59	-3075	-3311	-3080	-2648	-7400	-3468	-3274	-2663	-2753	-2971	-2970	-2993	-3739	-6964	-3490	-3159	-2828	-2886
49.05	-3348	-3185	-1174	-949	-	-3699	-3567	-2880	-3013	-3162	-3154	-2915	-	-	-3679	-3379	-2935	-3117

TABLE 10 READINGS FROM UPPER LINES OF DE-MEC POINTS ON MODEL 2 LONGITUDINAL SECTION 2

BLANK IN ORIGINAL

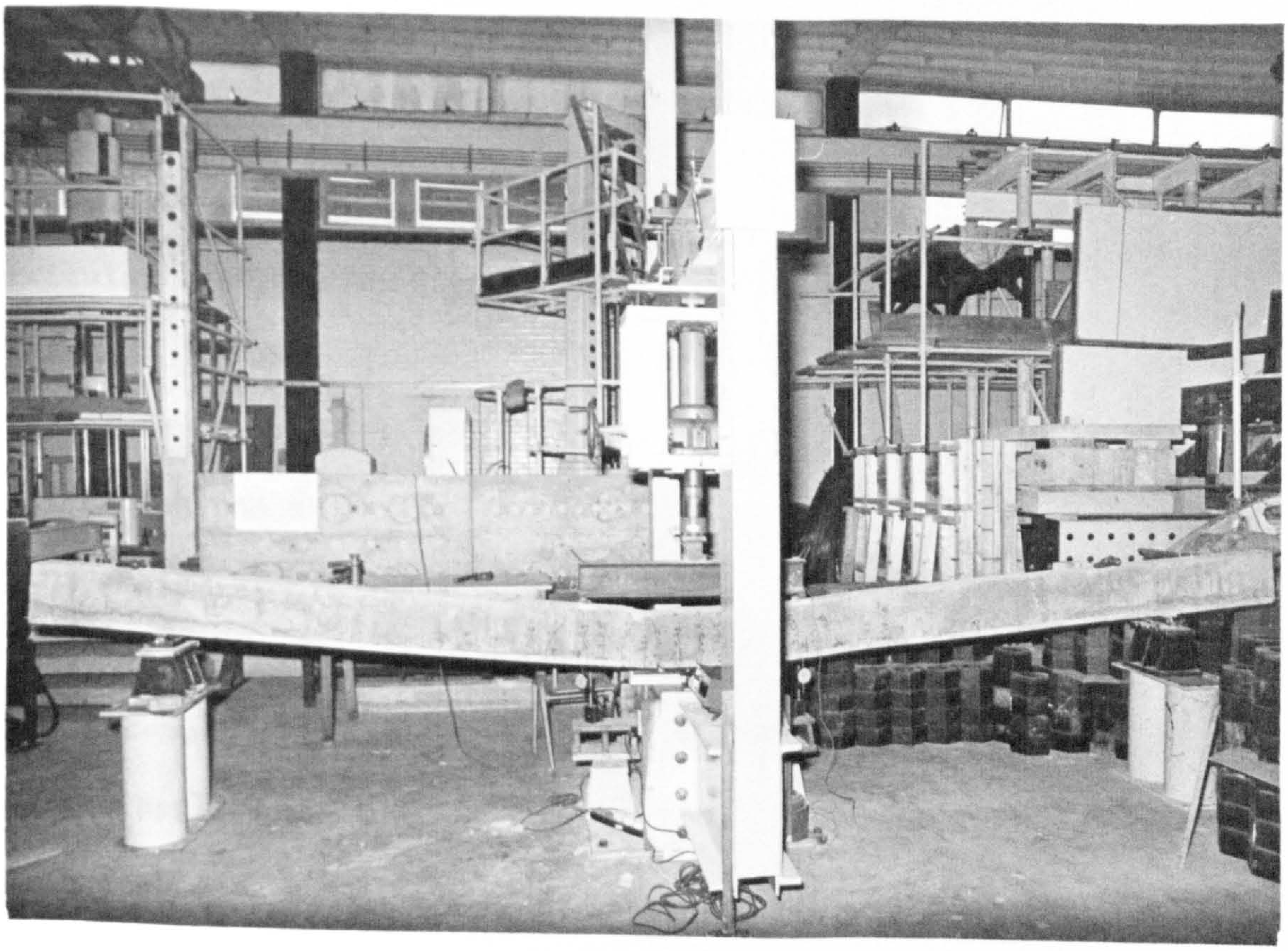

PLATE 1 MODEL 2 LONGITUDINAL SECTION 1 UNDER TEST

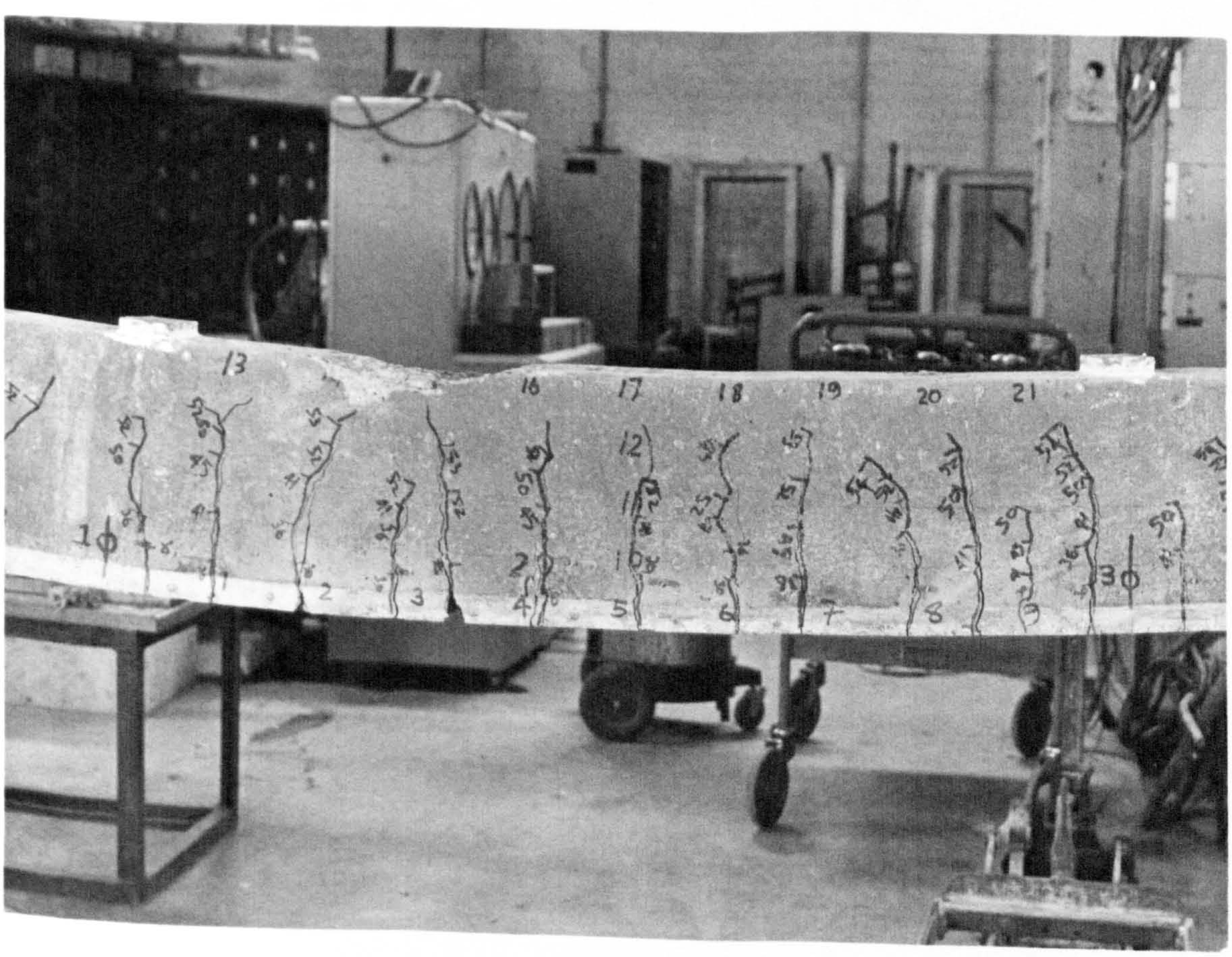

PLATE 2 FAILURE CRACK PATTERN ON MODEL 2 LONGITUDINAL SECTION 1

APPENDIX 7.2 Numerical Results from Model 2 Tests

This appendix contains the main test data obtained during the test on model 2. A separate table is presented for each type of transducer. Particular readings in each table are referred to by load level and transducer identification number. The meaning of each of the load levels is explained in Table 1. By using the identification number, the location and orientation of each of the transducers can be deduced by inspection of Figures 1 to 6.

Table 2 compares the measured total reaction load with that expected from the applied loading. While Tables 5 and 8 present the principal top surface and soffit surface strains that have been calculated using the strain gauge arm readings that are shown in Tables 4 and 7 respectively. The support reaction and displacement transducer readings are given in Tables 3 and 9. While the readings from the weldable strain gauges that were attached to the prestressing strands and the transverse reinforcement can be seen in Table 6. There is not a high level of confidence in the pre-strain readings, therefore, although the pre-strain reading for each gauge is given, the subsequent readings are quoted relative to the readings obtained with no applied loading upon the slab. Thus the datum for all the tables is the same. This method of presentation also allows easier comparisons to be made with the observed structural behaviour and the rest of the numerical results.

Level	Scan No.	Bogie Load (kN)	Disp level (mm)	Comment
1	4	0.	0.0	Deck self-weight (Datum)
2	5	0.	-2.83	'1' + Density Correction and Super Dead Load, both factored for SLS (immediately before testing in position 2)
3	19	80.8	-4.34	'2' + 45 units of one HB Bogie factored for SLS in position 2 (after cycling 100 times)
4	17	0.	-3.32	'1' + Density Correction and Super Dead Load, both factored for SLS
5	21	0.	-4.14	'1' + Density Correction, Super Dead Load, Footpath Live Loading and 1/2 HA UDL over whole slab area, all factored for SLS (immediately before testing in position 3)
6	34	80.8	-5.15	'5' + 45 units of one HB Bogie factored for SLS in position 3 (after cycling 100 times)
7	32	0.	-4.39	'1' + Density correction, Super Dead Load, Footpath Live Loading and 1/2 HA UDL over slab area, all factored for SLS
8	36	0.	-4.14	'1' + Density Correction, Super Dead Load, Footpath Live Loading and 1/2 HA UDL over slab area, all factored for SLS (immediately before testing in position 1a)
9	44	80.8	-5.90	'8' + 45 units of one HB Bogie factored for SLS in position 1a (after cycling 40 times)
10	42	0.	-4.56	'1' + Density Correction, Super Dead Load, Footpath Live Loading and 1/2 HA UDL over whole slab area, all factored for SLS
11	46	0.	-4.82	'1' + Density Correction, Super Dead Load, Footpath live loading, full HA UDL in lane 2 and full HA KEL in lane 2 at mid-span, all factored for ULS (immediately before testing in position 1a)

12	48	49	-5.85	'11' + 0.51* (45 units of one HB bogie factored for ULS) in position 1a
13	50	97.3	-7.14	'11' + 1.02* (45 units of one HB bogie factored for ULS) in position 1a
14	55	192	-11.33	'11' + 2.01* (45 units of one HB bogie factored for ULS) in position 1a
15	60	289	-18.07	'11' + 3.03* (45 units of one HB bogie factored for ULS) in position 1a
16	62	384	-26.91	'11' + 4.02* (45 units of one HB bogie factored for ULS) in position 1a
17	68	0	-9.19	'1' + Density correction, super dead load, footpath live loading, full HA UDL in lane 2 and full HA KEL in lane 2 at mid-span, all factored for ULS (immediately before testing in position 1b)
18	76	191	-18.82	'17' + 2.0* (45 units of one HB bogie factored for ULS) in position 1b
19	82	191 + 139 = 330	-30.66	'17' + 3.46* (45 units of one HB bogie factored for ULS in position 1b)
20	84	191 + 222 = 413	-42.07	'17' + 4.32* (45 units of one HB bogie factored for ULS) in position 1b
21	85	191 + 296 = 487	-57.78	'17' + 5.10* (45 units of one HB bogie factored for ULS) in position 1b
22	87	287 + 249 = 536	-74.61	'17' + 5.61* (45 units of one HB bogie factored for ULS) in position 1b
23	89	287 + 288 = 575	-89.83	'17' + 6.02* (45 units of one HB bogie factored for ULS) in position 1b
24	90	287 + 283 = 570	-116.25	'17' + 5.97* (45 units of one HB bogie factored for ULS) in position 1b

25	92	287 + 200 = 487	-156.03	'17' + 5.10* (45 units of one HB bogie factored for ULS) in position 1b

Table 1 Key for the load levels used in the presentation of Model 2 Testing Results

NOTE: Partial safety factors for SLS and ULS were obtained from BS5400 Part 2 (1978) Table 1 for combination 3

If applicable, the density correction loading also included a component for the deck self weight if its partial safety factor was greater than 1.0

During testing, while the load was being increased from level 13 to level 14, a power supply problem caused a momentary overload to a load intensity between levels 14 and 15 (an HB loading of approximately 230 kN)

When two numbers are given for the bogie load it indicates that the tension jacking system was in operation, the first number is the tension jack load and the second is the HB Bogie Load.

Bogie positions refer to those given in Figure 7.1

	Level												
	1	2	3	4	5	6	7	8	9	10	11	12	13
Sum of Reactions (kN)	0	191.2	268	191	240.6	313.6	241.4	232.4	309.8	235.2	293	342.4	387.4
Expected Reaction (kN)	0	194.7	275.3	195.3	239.3	319.9	239.7	238.7	320.4	239.7	308.8	362.4	410.7
Error (%)	0	-1.8	-2.6	-2.2	0.5	-1.9	0.7	-2.6	-3.3	-1.8	-5.1	-5.5	-5.6

	Level											
	14	15	16	17	18	19	20	21	22	23	24	25
Sum of Reactions (kN)	470	619.6	708.2	325.2	506.8	649.2	734.4	814.4	874.2	911.4	912.8	851.2
Expected Reactions (kN)	504.4	602.6	697.7	313.4	504.4	643.4	726.4	800.4	849.4	888.4	883.4	800.4
Error (%)	-6.8	2.8	1.5	3.6	0.5	0.9	1.1	1.7	2.8	2.5	3.2	6.0

TABLE 2 THE CORRELATION BETWEEN THE ACTUAL REACTION READINGS AND THOSE EXPECTED FROM THE APPLIED LOADING FOR MODEL 2

NOTE: It can be observed from Table 3, that reaction load cell number 10 did not give reasonable readings, even though there was load applied to it, until level 15 was reached

Level	Support Reaction Readings (kN)																
	1	2	3	4	5	6	7	8	9	10	11	12	13	14	15	16	17
1	0.0	0.0	0.0	0.0	0.0	0.0	0.0	0.0	0.0	0.0	0.0	0.0	0.0	0.0	0.0	0.0	0.0
2	1.8	1.1	1.6	5.1	5.4	4.8	6.2	4.2	6.6	0.1	6.2	6.2	7.7	9.2	8.3	13.3	7.8
3	1.3	1.0	1.6	6.0	6.7	6.0	8.2	6.2	9.7	0.1	8.5	10.0	10.6	13.7	9.1	20.7	14.6
4	1.7	1.1	1.8	5.9	6.1	5.1	6.7	4.8	7.1	0.1	5.9	7.0	6.9	8.8	5.5	12.8	8.2
5	1.3	0.8	1.4	5.6	5.9	5.4	7.6	5.9	8.9	0.1	7.3	9.3	9.6	12.2	8.1	17.9	13.0
6	1.5	1.0	2.1	7.9	8.4	7.4	11.0	9.0	13.4	0.1	6.7	14.1	13.8	10.3	10.9	19.9	19.3
7	1.2	0.8	1.5	6.5	6.6	5.6	8.4	6.8	10.0	0.1	4.9	10.7	10.2	7.3	8.2	16.4	15.5
8	1.5	1.0	2.0	7.3	7.4	6.1	9.2	7.2	10.6	0.1	3.3	10.9	9.3	8.0	7.6	11.0	13.7
9	0.8	0.7	1.4	6.9	7.1	5.9	10.1	8.8	12.7	0.1	4.2	14.2	13.9	12.7	12.4	18.9	24.1
10	1.5	1.0	2.0	7.7	7.4	6.1	9.5	7.7	11.0	0.1	3.1	11.1	9.8	8.5	7.9	10.8	12.4
11	2.8	1.9	4.3	11.4	10.6	7.3	11.5	9.8	14.4	0.1	9.1	8.7	8.3	9.0	10.1	13.9	13.3
12	2.1	1.4	3.6	10.6	10.3	7.4	12.2	10.7	16.0	0.1	10.8	10.6	10.1	12.6	13.3	19.6	19.8
13	1.6	1.1	3.1	10.0	10.4	7.5	12.9	11.7	17.5	0.1	12.3	13.3	11.3	16.2	16.1	24.1	24.5
14	0.6	0.6	2.2	9.2	10.7	8.3	14.8	14.6	22.1	0.1	16.1	17.9	13.0	22.2	21.2	30.9	30.5
15	0.0	0.0	1.1	8.6	11.0	8.9	17.3	19.7	24.9	28.6	21.9	16.5	16.7	32.5	29.3	42.6	30.2
16	-0.1	-0.2	1.1	7.1	10.3	9.0	18.1	20.9	27.0	31.4	23.4	19.1	20.1	42.6	37.6	45.7	41.1

17	5.2	4.4	9.2	15.8	12.8	3.3	8.9	7.7	6.6	5.5	9.0	5.7	10.0	18.2	11.8	11.7	16.8
18	2.2	2.3	6.8	14.1	13.5	4.7	12.2	10.5	8.8	6.6	12.1	6.7	13.7	26.8	23.3	32.9	56.2
19	0.2	0.6	3.4	10.8	12.7	6.1	15.3	14.1	13.4	10.3	21.1	8.7	17.4	28.9	29.2	44.8	87.6
20	-0.2	-0.2	1.6	9.1	14.4	8.5	15.9	15.7	16.9	13.1	28.3	7.9	18.4	26.4	32.5	51.2	107.7
21	-0.2	-0.6	1.0	8.0	15.3	10.6	15.3	16.0	19.9	15.4	33.4	7.1	20.0	28.4	44.0	50.4	123.2
22	0.0	-0.7	0.2	7.8	18.8	9.5	13.9	16.1	23.6	18.2	38.6	6.2	20.3	26.8	55.0	44.4	138.4
23	-0.2	-0.9	-0.7	5.5	18.9	9.8	14.8	15.4	26.3	22.0	42.0	4.9	19.7	22.6	65.9	36.3	153.4
24	-0.2	-0.9	-1.3	5.8	20.4	10.5	16.9	14.6	29.1	25.9	42.0	3.2	18.6	15.7	73.5	33.3	149.3
25	-0.2	-0.9	-1.5	1.2	28.0	9.8	18.7	13.6	29.6	31.3	39.0	0.1	16.3	4.8	76.3	32.1	127.4

TABLE 3 SUPPORT REACTION READINGS TAKEN DURING THE TEST ON MODEL 2

Level	Arm	Top Surface Strain Gauge Rosette Readings (Raw) ($\mu\epsilon$)										
		10	1	3	5	7	2	4	6	8	9	11
1	1	0	0	0	0	0	0	0	0	0	0	0
	2	0	0	0	0	0	0	0	0	0	0	0
	3	0	0	0	0	0	0	0	0	0	0	0
2	1	-24	-40	-40	-62	-83	-212	-88	-19	-75	-40	-41
	2	-30	-41	-48	-49	-75	-122	-51	-46	-53	-21	-62
	3	10	28	26	25	37	35	34	21	23	39	-4
3	1	-28	-64	-77	-116	-133	-369	-148	-25	-103	-65	-61
	2	-45	-70	-95	-94	-129	-204	-87	-75	-83	-28	-88
	3	11	34	-5	21	44	39	26	14	28	48	-9
4	1	-20	-38	-43	-62	-91	-261	-103	-17	-88	-39	-47
	2	-26	-39	-45	-47	-84	-144	-49	-48	-61	-11	-61
	3	14	28	27	26	38	31	41	24	29	38	-3
5	1	-5	-35	-42	-67	-83	-308	-96	4	-64	-35	-39
	2	-20	-36	-56	-56	-86	-163	-52	-43	-50	-1	-66
	3	29	53	22	42	65	57	45	44	56	55	-1
6	1	-3	-52	-69	-131	-149	-409	-165	-11	-104	-54	-70
	2	-38	-61	-92	-108	-148	-215	-78	-61	-78	-9	-78
	3	28	59	24	45	68	65	51	43	66	62	0
7	1	5	-27	-35	-64	-84	-321	-94	12	-68	-20	-36
	2	-11	-27	-44	-48	-87	-159	-40	-33	-47	10	-54
	3	37	58	36	54	66	59	55	55	70	54	3
8	1	44	15	-1	-20	-43	-243	-38	43	-19	16	-7
	2	16	16	2	-10	-39	-95	16	12	5	47	-14
	3	67	95	83	86	102	102	101	97	119	75	32

9	1	28	-30	-57	-77	-84	-390	-86	40	-35	-12	-15
	2	0	-26	-58	-68	-91	-181	-31	-24	-25	23	-49
	3	66	101	50	85	102	102	87	88	113	81	25
10	1	41	11	-9	-28	-51	-286	-56	42	-28	8	-16
	2	14	12	-3	-15	-50	-115	10	6	-4	46	-22
	3	67	95	81	86	99	99	103	98	116	74	29
11	1	42	6	-18	-53	-90	-334	-80	27	-73	-6	-42
	2	0	0	-17	-44	-86	-147	-1	-7	-28	44	-31
	3	67	102	87	88	104	114	109	100	125	81	25
12	1	31	-27	-56	-93	-117	-412	-108	24	-82	-33	-50
	2	-12	-29	-59	-86	-119	-198	-33	-30	-49	22	-52
	3	64	103	65	85	103	113	98	92	119	85	20
13	1	29	-58	-95	-131	-137	-497	-126	29	-87	-46	-60
	2	-17	-57	-96	-127	-152	-249	-56	-47	-65	14	-77
	3	68	112	52	87	104	118	96	93	124	87	8
14	1	-1	-192	-271	-310	-222	-653	-211	19	-169	-85	-60
	2	-43	-177	-259	-301	-281	-361	-161	-117	-168	-16	-180
	3	57	108	-62	72	70	104	-6	67	90	75	-143
15	1	-54	-425	-562	-573	-388	-839	-318	4	-236	-142	-89
	2	-89	-368	-542	-542	-476	-493	-280	-214	-280	-54	-299
	3	34	102	-231	51	51	87	-71	1	26	70	-268
16	1	-79	-690	-846	-876	-580	-1051	-379	14	-278	-168	-113
	2	-117	-595	-861	-838	-694	-655	-392	-290	-394	-89	-442
	3	32	115	-439	22	54	92	-120	-44	-51	72	-388
17	1	30	-162	37	-185	-138	-547	-204	17	-202	-33	-76
	2	1	-123	-7	-202	-160	-306	-117	-24	-105	26	-175
	3	92	92	153	10	65	69	0	51	83	40	-211

18	1	-37	-543	-330	-434	-293	-814	-274	29	-265	-65	-67
	2	-10	-377	-297	-461	-368	-589	-291	-151	-246	-56	-374
	3	109	115	105	12	52	44	-83	-11	24	80	-387
19	1	-119	-976	-789	-733	-487	-1046	-261	35	-308	-111	-85
	2	-22	-703	-739	-682	-611	-801	-468	-290	-373	-241	-721
	3	112	132	45	64	41	62	-206	-80	-30	84	-680
20	1	-191	-1291	-1109	-912	-617	-1254	-323	29	-332	-159	-170
	2	-22	-858	-1003	-859	-772	-1015	-624	-422	-443	-434	-1018
	3	128	173	10	12	22	48	-321	-147	-62	18	-860
21	1	-306	-1646	-1582	-1155	-769	-1525	-414	-39	-324	-344	-303
	2	-50	-1028	-1400	-1134	-972	-1274	-897	-620	-476	-893	-1438
	3	144	228	-46	-42	-7	36	-512	-287	-76	-144	-1061
22	1	-392	-1867	-2329	-1417	-935	-1692	-510	-114	-324	-472	-356
	2	-65	-1134	-2222	-1487	-1184	-1521	-1158	-826	-543	-1338	-1658
	3	134	256	-314	-115	-39	-43	-684	-415	-141	-436	-1180
23	1	-432	-2001	-3322	-1662	-1064	-1784	-619	-147	-332	-585	-353
	2	-44	-1195	-3207	-1849	-1384	-1695	-1453	-970	-623	-1753	-1760
	3	147	275	-483	-205	-63	-89	-843	-442	-185	-567	-1306
24	1	-504	-1938	-4069	-2144	-1209	-1786	-922	-204	-315	-568	-453
	2	-13	-1119	-4112	-2572	-1657	-1877	-2028	-1168	-734	-2532	-1894
	3	100	243	-178	-393	-119	-203	-1098	-389	-240	-352	-1402
25	1	-618	-1658	726	-2966	-1410	-1386	-1134	-297	-307	-984	-551
	2	110	-842	-654	-3517	-2014	-2449	-2968	-1550	-848	-2517	-2161
	3	37	171	-630	1634	-193	-293	-1313	-424	-286	904	-1572

TABLE 4 TOP SURFACE STRAIN GAUGE ROSETTE READINGS TAKEN DURING THE TEST ON MODEL 2

NOTE: Arm 1 is inclined at 180° to the x-axis, arm 2 at 135° and arm 3 at 90°. Where +ve angles are measured anti-clockwise.

FIG. 1. POSITIONAL INFORMATION FOR MODEL 2 SUPPORTS

Level	Quantity	Top Surface Strain Gauge Rosette Readings (Principal) ($\mu\epsilon$)										
		10	1	3	5	7	2	4	6	8	9	11
1	ϵ_1	0	0	0	0	0	0	0	0	0	0	0
	ϵ_2	0	0	0	0	0	0	0	0	0	0	0
	θ	0	0	0	0	0	0	0	0	0	0	0
2	ϵ_1	22	43	45	34	57	39	39	52	30	44	20
	ϵ_2	-35	-55	-60	-72	-102	-217	-92	-50	-82	-45	-66
	θ	63	67	65	72	70	82	79	56	76	76	58
3	ϵ_1	34	59	24	35	78	43	30	67	42	52	24
	ϵ_2	-50	-89	-106	-130	-167	-373	-152	-78	-117	-69	-94
	θ	59	66	62	73	68	85	82	53	73	80	58
4	ϵ_1	26	42	43	35	60	34	43	59	36	39	18
	ϵ_2	-31	-52	-59	-71	-113	-264	-105	-52	-96	-40	-67
	θ	63	67	67	73	69	84	83	56	76	82	60
5	ϵ_1	48	71	46	57	97	61	50	93	71	56	29
	ϵ_2	-24	-54	-66	-82	-115	-312	-101	-46	-80	-36	-70
	θ	59	67	63	71	67	84	80	53	71	83	56
6	ϵ_1	65	89	60	67	113	69	53	98	84	63	20
	ϵ_2	-41	-82	-106	-152	-194	-413	-167	-66	-122	-55	-91
	θ	54	65	62	72	68	85	85	55	73	84	65
7	ϵ_1	57	76	57	68	100	61	58	104	85	55	26
	ϵ_2	-15	-44	-56	-78	-117	-323	-97	-36	-83	-21	-59
	θ	58	67	65	72	67	86	82	54	73	85	59
8	ϵ_1	97	111	98	102	129	103	102	134	132	75	46
	ϵ_2	14	-1	-16	-35	-70	-244	-39	6	-32	16	-20
	θ	53	68	69	70	68	86	84	57	73	91	63

9	ϵ_1	97	125	73	112	145	105	93	155	137	82	62
	ϵ_2	-3	-54	-80	-104	-127	-393	-91	-27	-59	-14	-53
	θ	56	68	67	69	66	86	80	53	70	83	55
10	ϵ_1	96	112	95	101	130	101	104	139	131	75	43
	ϵ_2	12	-6	-23	-43	-82	-287	-57	0	-43	7	-30
	θ	54	68	70	71	68	87	85	57	73	94	64
11	ϵ_1	110	126	109	111	140	117	110	143	139	81	32
	ϵ_2	-1	-19	-39	-76	-127	-337	-81	-16	-86	-6	-49
	θ	51	66	68	69	68	85	85	59	76	95	73
12	ϵ_1	109	132	93	117	150	117	102	153	140	85	36
	ϵ_2	-14	-56	-83	-126	-165	-417	-112	-37	-102	-34	-66
	θ	53	67	67	69	67	85	82	56	73	88	67
13	ϵ_1	116	146	83	130	165	124	103	174	153	87	35
	ϵ_2	-20	-93	-126	-173	-198	-503	-133	-51	-117	-46	-87
	θ	53	68	67	68	66	85	80	53	71	87	62
14	ϵ_1	104	160	-26	144	176	113	6	204	143	76	-190
	ϵ_2	-49	-244	-306	-383	-327	-663	-224	-119	-222	-86	-13
	θ	56	69	69	68	63	84	76	49	68	86	121
15	ϵ_1	81	173	-176	158	208	102	-44	-214	113	71	-328
	ϵ_2	-101	-496	-616	-681	-546	-854	-345	220	-323	-144	-29
	θ	59	71	69	69	63	83	73	135	63	85	117
16	ϵ_1	86	220	-344	182	271	119	-57	-291	92	79	-486
	ϵ_2	-132	-794	-941	-1036	-798	-1077	-442	261	-421	-175	-14
	θ	60	71	66	69	63	81	66	132	58	80	117
17	ϵ_1	128	120	212	63	123	76	1	93	90	46	-218
	ϵ_2	-6	-190	-23	-238	-196	-554	-205	-26	-209	-40	-68
	θ	59	73	60	65	65	84	86	53	81	105	103

18	ϵ_1	122	154	173	124	180	90	-30	-153	71	103	-445
	ϵ_2	-51	-581	-397	-546	-422	-860	-326	171	-312	-89	-9
	θ	74	77	70	66	62	77	65	131	69	69	111
19	ϵ_1	113	199	183	194	247	142	2	-296	77	234	-834
	ϵ_2	-120	-1043	-927	-863	-693	-1126	-469	251	-415	-261	69
	θ	85	77	69	69	62	75	48	129	62	57	114
20	ϵ_1	128	232	171	167	274	168	-20	-433	83	303	-1125
	ϵ_2	-191	-1350	-1270	-1066	-869	-1373	-624	314	-477	-445	94
	θ	92	79	70	69	62	74	45	128	59	52	118
21	ϵ_1	147	281	152	174	308	198	-900	-637	102	413	-1528
	ϵ_2	-308	-1699	-1780	-1371	-1085	-1688	-27	310	-502	-901	164
	θ	94	81	71	68	62	73	132	127	57	49	122
22	ϵ_1	142	306	30	205	342	185	-1165	-846	91	430	-1748
	ϵ_2	-400	-1917	-2673	-1737	-1316	-1920	-28	318	-556	-1338	213
	θ	97	81	69	66	61	71	131	127	53	46	123
23	ϵ_1	163	322	25	236	397	201	-1461	-986	113	602	-1875
	ϵ_2	-449	-2048	-3830	-2104	-1524	-2074	-1	396	-630	-1753	215
	θ	99	82	69	64	61	69	131	129	51	45	121
24	ϵ_1	154	277	658	302	468	190	-2031	-1173	181	1615	-2004
	ϵ_2	-558	-1972	-4905	-2838	-1796	-2180	11	579	-735	-2535	150
	θ	106	83	67	62	59	66	133	132	47	46	122
25	ϵ_1	227	176	-928	2996	555	859	-2970	-1552	256	2611	-2274
	ϵ_2	-808	-1663	1023	-4329	-2158	-2539	523	831	-848	-2691	151
	θ	115	87	113	64	58	54	134	133	46	55	123

TABLE 5 PRINCIPAL TOP SURFACE STRAINS DURING THE TEST ON MODEL 2

NOTE: θ refers to the direction of the strain ϵ_1, angles are measured +ve anti-clockwise from the x-axis

FIG. 2. POSITIONAL INFORMATION FOR MODEL 2 TOP SURFACE STRAIN GAUGES (ROSETTES)

Level	Weldable Strain Gauge Readings ($\mu\epsilon$)													
	1	9	11	13	8	10	12	14	3	6	7	5	4	2
Prestrain	4200	4200	4200	4200	4200	4200	4200	4200	0	0	0	0	0	0
1	-1	0	1	0	0	0	0	0	1	1	0	-1	0	0
2	35	65	52	58	46	38	36	56	-29	-9	-6	-20	-5	56
3	87	218	204	195	179	156	137	164	-46	30	31	-75	-21	114
4	57	89	72	77	62	50	46	72	-29	10	6	-18	2	101
5	59	191	175	174	159	143	131	205	-73	14	4	-78	-50	100
6	81	233	240	235	184	168	147	246	-97	22	48	-158	-77	97
7	61	200	189	188	157	141	133	238	-84	8	19	-106	-69	91
8	32	170	168	178	127	127	118	385	-82	-8	2	-116	-70	63
9	98	118	92	79	49	20	-5	268	-117	22	43	-159	-89	93
10	42	94	87	93	47	41	30	297	-95	-7	5	-123	-71	72
11	61	159	162	178	108	111	98	409	-81	5	22	-123	-25	155
12	91	204	194	196	138	123	101	408	-112	17	38	-154	-45	173
13	149	258	246	230	178	136	100	451	-132	50	94	-173	-40	198
14	326	693	671	399	280	204	132	466	-211	261	411	-213	-1	251

15	746	1362	1285	726	439	281	159	513	-274	592	840	-247	41	366
16	1438	2267	2137	1256	881	390	186	563	-358	1108	1424	-280	108	493
17	176	171	113	159	9	12	-50	1109	-44	267	275	-96	216	307
18	943	843	515	320	134	-43	-171	995	-107	621	723	-93	135	478
19	1906	1985	1291	720	572	8	-154	1036	-373	1453	1249	148	188	893
20	2728	2780	1869	1020	1159	91	-104	1054	-369	1826	1619	415	397	1384
21	3918	4007	2682	1519	1936	393	9	1151	-333	2166	1994	672	640	1819
22	4805	5689	3498	1947	2354	646	55	1164	-418	2564	2315	888	764	2043
23	5212	6738	4315	2379	2637	775	151	1193	-448	2884	2679	945	903	2235
24	5195	7733	5343	2932	2857	887	404	1230	-236	3488	3200	774	1143	2243
25	5644	****	5861	3501	2873	967	682	1265	232	3220	3736	1013	1478	2424

TABLE 6 WELDABLE STRAIN GAUGE READINGS TAKEN DURING THE TEST ON MODEL 2

NOTE: The first row of this table gives the assumed prestrain in the tendons relative to the unstressed condition. The second and subsequent rows give the strains measured at the load levels indicated relative to load level 1 and do not include the prestrain component. The two readings were not combined in the table due to doubt about the accuracy of the prestrain reading.

Level	Arm	Soffit Strain Gauge Rosette Readings (Raw) ($\mu\epsilon$)										
		9	10	11	1	3	5	7	2	4	6	8
1	1	0	0	0	0	0	0	0	0	0	0	0
	2	0	0	0	0	0	0	0	0	0	0	0
	3	0	0	0	0	0	0	0	0	0	0	0
2	1	66	72	79	108	112	112	114	110	88	80	69
	2	48	58	64	77	85	93	82	84	76	69	46
	3	5	9	-1	0	-9	0	-5	-10	3	6	-4
3	1	88	99	115	174	211	199	176	181	130	109	89
	2	66	74	88	121	142	146	121	126	105	99	64
	3	1	-3	-8	-15	-28	-8	-19	-27	1	6	-12
4	1	77	84	90	129	143	133	130	127	99	89	78
	2	53	57	67	86	92	99	85	88	77	75	50
	3	3	-3	-5	-8	-22	-5	-11	-17	-1	4	-9
5	1	86	98	109	156	177	168	153	155	118	103	81
	2	60	67	79	104	114	125	105	106	92	92	55
	3	-2	-4	-12	-16	-31	-12	-17	-32	-1	3	-14
6	1	99	113	131	203	244	277	253	213	170	141	109
	2	76	73	101	136	146	184	154	140	118	115	71
	3	-8	-25	-22	-29	-51	-32	-41	-50	-4	-2	-23
7	1	94	107	118	170	194	206	187	168	130	113	90
	2	65	59	78	107	109	138	112	108	93	94	57
	3	-5	-21	-18	-23	-40	-23	-29	-40	-1	0	-18
8	1	81	90	104	136	176	196	182	144	123	115	91
	2	58	52	76	91	94	130	105	90	81	86	53
	3	-6	-19	-23	-22	-42	-26	-29	-43	-8	-4	-21

9	1	108	127	152	224	286	276	230	225	159	133	100
	2	76	74	99	145	150	186	143	142	119	118	67
	3	-8	-24	-27	-34	-53	-33	-38	-57	-7	0	-25
10	1	86	98	112	153	197	213	193	162	133	121	94
	2	60	55	79	98	101	138	111	99	86	90	53
	3	-9	-23	-25	-26	-46	-29	-32	-49	-11	-6	-25
11	1	94	105	126	174	228	255	244	190	165	156	127
	2	72	69	103	118	123	171	143	121	106	111	71
	3	-4	-20	-22	-25	-47	-29	-37	-50	-16	-7	-28
12	1	107	124	152	223	289	301	272	235	183	165	129
	2	81	78	114	149	157	203	165	151	128	130	79
	3	-8	-26	-28	-34	-57	-38	-44	-60	-17	-5	-30
13	1	128	148	187	292	373	373	320	292	209	182	139
	2	97	91	130	188	195	243	197	186	155	152	88
	3	-10	-33	-31	-49	-64	-49	-54	-68	-24	-9	-37
14	1	176	197	254	471	548	407	455	412	275	243	160
	2	129	114	155	323	260	206	295	270	164	182	105
	3	-25	-48	-41	-34	-83	-79	-93	-87	-86	-69	-57
15	1	226	267	328	535	514	368	487	521	346	259	190
	2	158	115	182	330	203	172	282	320	224	200	133
	3	-48	-76	-54	-56	-110	-81	-123	-115	-109	-108	-93
16	1	278	332	398	480	514	333	518	407	471	289	249
	2	194	151	214	236	182	161	224	155	335	254	196
	3	-55	-79	-55	-87	-134	-64	-151	-146	-108	-115	-117
17	1	88	99	104	251	310	220	247	168	157	141	143
	2	41	27	76	98	158	116	107	84	73	38	52
	3	-73	-77	-70	-98	-88	-81	-107	-112	-107	-101	-95

18	1	187	243	273	388	507	280	392	232	263	178	181
	2	85	79	137	153	222	153	180	109	195	114	107
	3	-83	-90	-85	-112	-122	-101	-150	-151	-128	-113	-109
19	1	267	369	423	392	481	255	421	224	326	200	202
	2	117	103	164	0	209	157	178	48	283	174	149
	3	-96	-103	-112	-126	-181	-145	-174	-222	-159	-141	-135
20	1	321	465	455	0	501	219	431	0	388	247	226
	2	128	119	229	0	194	160	172	0	352	211	179
	3	-104	-110	-86	-115	-206	-163	-189	0	-123	-196	-154
21	1	381	537	722	0	0	178	407	0	456	304	267
	2	141	141	552	0	0	154	175	0	419	226	224
	3	-113	-132	-71	-120	-223	-161	-173	0	-150	-263	-177
22	1	417	525	1154	0	0	148	381	0	468	329	296
	2	144	127	709	0	0	124	174	0	439	269	252
	3	-129	-143	-74	-137	-333	-170	-175	0	-164	-246	-207
23	1	454	523	1111	0	0	143	376	0	479	341	332
	2	155	120	632	0	0	115	191	0	604	279	297
	3	-127	-135	-50	-131	-424	-161	-163	0	-120	-199	-209
24	1	451	493	728	0	0	117	373	0	430	274	345
	2	139	65	352	0	0	87	195	0	995	105	317
	3	-125	-178	56	-124	-613	-156	-170	0	2	-183	-198
25	1	329	400	523	0	0	30	372	0	334	327	371
	2	42	-98	140	0	0	34	195	0	1308	51	311
	3	-120	-225	134	-125	-708	-171	-186	0	91	-192	-212

TABLE 7 SOFFIT STRAIN GAUGE ROSETTE READINGS TAKEN DURING THE TEST ON MODEL 2

NOTE: Arm 1 is inclined at 180° to the x-axis, arm 2 at 135° and arm 3 at 90°. Where +ve angles are measured anti-clockwise

FIG. 3. POSITIONAL INFORMATION FOR MODEL 2 STRAIN GAUGES ON PRESTRESSING WIRE AND REINFORCEMENT (LINEAR)

Level	Quantity	Soffit Strain Gauge Rosette Readings (Principal) ($\mu\epsilon$)										
		9	10	11	1	3	5	7	2	4	6	8
1	ϵ_1	0	0	0	0	0	0	0	0	0	0	0
	ϵ_2	0	0	0	0	0	0	0	0	0	0	0
	θ	0	0	0	0	0	0	0	0	0	0	0
2	ϵ_1	2	4	-9	-4	-17	-10	-11	-19	-7	-2	-6
	ϵ_2	68	77	86	113	120	123	120	119	98	88	72
	θ	79	76	74	78	76	73	78	75	72	72	80
3	ϵ_1	-4	-10	-17	-24	-38	-20	-27	-38	-10	-9	-18
	ϵ_2	93	105	124	183	221	210	185	192	141	123	96
	θ	77	76	75	78	79	77	78	77	74	71	77
4	ϵ_1	1	-6	-11	-12	-27	-14	-15	-25	-8	-4	-12
	ϵ_2	79	87	96	134	149	141	135	135	106	98	80
	θ	80	80	76	80	80	76	80	78	75	73	80
5	ϵ_1	-6	-8	-20	-23	-39	-23	-24	-42	-10	-11	-19
	ϵ_2	90	102	116	162	185	179	161	165	127	116	86
	θ	79	79	77	79	79	76	78	77	75	71	78
6	ϵ_1	-16	-31	-35	-39	-59	-44	-49	-63	-11	-15	-29
	ϵ_2	107	119	144	213	252	289	260	226	177	155	115
	θ	75	79	74	79	81	79	81	78	79	74	79
7	ϵ_1	-9	-23	-23	-28	-45	-32	-33	-49	-7	-12	-22
	ϵ_2	98	109	123	176	198	215	192	176	136	124	94
	θ	79	83	79	81	82	79	81	79	78	73	79
8	ϵ_1	-11	-22	-32	-29	-45	-34	-32	-51	-13	-11	-23
	ϵ_2	85	93	113	143	180	204	186	152	127	122	94
	θ	77	82	75	78	83	79	82	79	80	77	81

9	ϵ_1	-14	-27	-33	-43	-56	-46	-46	-68	-18	-18	-32
	ϵ_2	113	130	159	233	289	289	238	237	170	151	107
	θ	78	82	79	79	84	79	80	79	76	71	77
10	ϵ_1	-14	-25	-34	-33	-48	-38	-36	-57	-16	-14	-27
	ϵ_2	91	101	121	160	199	221	197	170	137	129	97
	θ	78	82	76	79	84	80	82	79	80	76	81
11	ϵ_1	-12	-25	-38	-34	-51	-41	-42	-60	-21	-15	-31
	ϵ_2	101	110	142	183	232	266	250	200	170	164	130
	θ	75	79	73	78	83	79	82	78	80	78	82
12	ϵ_1	-16	-31	-41	-46	-61	-52	-52	-73	-26	-19	-36
	ϵ_2	115	129	166	234	294	316	280	248	193	179	134
	θ	76	79	75	78	83	79	81	78	78	75	80
13	ϵ_1	-20	-39	-43	-61	-68	-64	-65	-83	-39	-30	-44
	ϵ_2	138	154	198	304	377	388	331	306	225	202	146
	θ	75	80	77	79	85	80	81	79	76	73	79
14	ϵ_1	-38	-54	-49	-55	-84	-83	-116	-109	-100	-95	-69
	ϵ_2	190	203	261	492	550	411	478	434	288	270	172
	θ	76	81	81	79	88	85	79	78	79	74	77
15	ϵ_1	-64	-77	-59	-69	-110	-83	-139	-136	-132	-146	-117
	ϵ_2	242	268	333	548	514	370	503	542	370	297	213
	θ	77	87	83	82	90	86	81	80	78	73	75
16	ϵ_1	-74	-80	-59	-90	-134	-66	-153	-147	-146	-174	-158
	ϵ_2	297	334	402	482	514	335	520	408	509	349	290
	θ	77	87	85	86	91	86	87	88	76	70	72
17	ϵ_1	-80	-78	-88	-100	-94	-88	-110	-123	-115	-103	-98
	ϵ_2	95	100	122	252	316	227	251	178	166	142	147
	θ	79	85	73	86	83	81	84	79	80	86	84

18	ϵ_1	-87	-90	-90	-113	-124	-112	-156	-163	-166	-134	-125
	ϵ_2	191	243	278	388	509	290	398	244	301	199	198
	θ	83	90	83	88	87	81	84	80	73	75	77
19	ϵ_1	-99	-105	-112	0	-186	-170	-179	-227	-230	-194	-171
	ϵ_2	270	370	423	0	486	279	426	228	397	253	238
	θ	85	94	89	0	85	76	85	84	70	70	73
20	ϵ_1	-105	-116	-90	0	-209	-204	-193	0	-204	-264	-202
	ϵ_2	322	471	458	0	504	260	435	0	470	314	274
	θ	87	96	85	0	86	73	85	0	70	70	71
21	ϵ_1	-113	-138	-131	0	0	-215	-179	0	-250	-330	-241
	ϵ_2	381	542	782	0	0	232	413	0	556	371	331
	θ	89	95	75	0	0	70	84	0	69	72	71
22	ϵ_1	-129	-149	-97	0	0	-219	-184	0	-275	-325	-282
	ϵ_2	417	531	1177	0	0	197	390	0	579	408	371
	θ	90	95	82	0	0	70	83	0	69	71	70
23	ϵ_1	-127	-143	-58	0	0	-205	-175	0	-340	-270	-297
	ϵ_2	454	531	1120	0	0	187	389	0	699	412	420
	θ	91	96	85	0	0	71	81	0	63	71	69
24	ϵ_1	-126	-190	54	0	0	-192	-185	0	-592	-190	-291
	ϵ_2	452	505	731	0	0	154	389	0	1023	282	438
	θ	92	98	93	0	0	71	81	0	53	83	69
25	ϵ_1	-128	-276	57	0	0	-216	-204	0	-889	-193	-293
	ϵ_2	337	451	600	0	0	75	390	0	1314	328	452
	θ	98	105	112	0	0	67	80	0	48	92	71

TABLE 8 PRINCIPAL BEAM SOFFIT STRAINS DURING THE TEST ON MODEL 2

NOTE: θ refers to the direction of the strain ϵ_1, angles are measured +ve anti-clockwise from the x-axis

FIG. 4. POSITIONAL INFORMATION FOR MODEL 2 SOFFIT STRAIN GAUGES (ROSETTES)

Level	Displacement Transducer Readings (mm)											
	1	2	3	4	5	6	7	8	9	10	11	12
1	0.02	0.00	0.00	0.02	-0.02	0.00	-0.01	-0.01	-0.02	-0.02	0.00	-0.01
2	-2.17	-1.65	-1.91	-2.83	-2.73	-2.56	-2.34	-2.62	-2.74	-2.30	-2.05	-1.70
3	-2.99	-2.60	-2.88	-4.34	-4.20	-4.05	-3.77	-3.84	-4.07	-3.59	-3.18	-2.71
4	-2.41	-1.99	-2.19	-3.32	-3.17	-2.94	-2.72	-2.87	-3.13	-2.71	-2.39	-2.03
5	-2.96	-2.54	-2.73	-4.14	-3.96	-3.75	-3.31	-3.44	-3.89	-3.36	-2.94	-2.48
6	-3.61	-3.30	-3.53	-5.15	-5.16	-5.12	-4.86	-5.17	-4.85	-4.41	-4.08	-3.71
7	-3.21	-2.83	-2.96	-4.39	-4.30	-4.11	-3.68	-3.86	-4.12	-3.64	-3.26	-2.87
8	-3.04	-2.47	-2.89	-4.14	-4.11	-4.11	-3.84	-4.12	-3.85	-3.56	-3.27	-2.92
9	-4.03	-3.66	-3.84	-5.90	-5.77	-5.55	-4.93	-4.86	-5.37	-4.84	-4.26	-3.72
10	-3.34	-2.85	-3.05	-4.56	-4.52	-4.42	-4.08	-4.24	-4.24	-3.86	-3.55	-3.19
11	-3.43	-2.99	-3.41	-4.82	-4.81	-4.87	-4.78	-5.48	-4.36	-4.16	-3.94	-3.75
12	-4.03	-3.63	-4.05	-5.85	-5.81	-5.79	-5.50	-5.94	-5.32	-4.93	-4.59	-4.15
13	-4.70	-4.27	-4.83	-7.14	-7.01	-6.94	-6.53	-6.63	-6.39	-5.86	-5.38	-4.74
14	-7.31	-6.76	-7.62	-11.33	-11.19	-10.85	-9.69	-8.82	-9.87	-8.82	-7.95	-6.65
15	-11.12	-10.11	-11.30	-18.07	-17.76	-17.07	-14.83	-12.52	-15.81	-13.83	-12.05	-9.27
16	-15.80	-14.96	-16.18	-26.91	-26.21	-25.12	-21.76	-17.92	-23.08	-19.80	-17.08	-13.14

17	-6.00	-5.09	-6.16	-9.19	-8.87	-8.55	-8.20	-7.89	-8.01	-7.35	-6.73	-5.57
18	-11.25	-10.42	-10.96	-18.82	-17.54	-15.84	-13.59	-11.17	-15.42	-12.89	-11.12	-8.67
19	-18.36	-17.00	-16.87	-30.66	-28.65	-24.97	-20.09	-15.69	-24.82	-19.76	-16.28	-12.39
20	-24.79	-23.15	-22.50	-42.07	-38.69	-32.88	-25.33	-19.15	-33.87	-25.97	-20.64	-15.40
21	-33.47	-31.44	-30.15	-57.78	-52.63	-43.90	-32.65	-24.07	-46.64	-34.62	-26.77	-19.45
22	-42.58	-40.12	-38.36	-74.61	-68.33	-56.14	-40.42	-29.08	-60.09	-43.94	-33.39	-23.84
23	-50.32	-47.78	-45.67	-89.83	-82.97	-67.26	-47.37	-33.27	-71.73	-51.78	-39.15	-27.53
24	-62.78	-60.80	-57.02	-116.25	-108.91	-86.33	-58.04	-38.34	-91.95	-65.16	-48.59	-33.39
25	-81.87	-77.97	-72.34	-156.03	-147.66	-113.94	-71.85	-43.71	-122.50	-84.47	-61.38	-40.85

TABLE 9 DISPLACEMENT TRANSDUCER READINGS TAKEN DURING THE TEST ON MODEL 2

FIG. 5. POSITIONAL INFORMATION FOR MODEL 2 DISPLACEMENT TRANSDUCERS

Level	De-Mec Point Strain Readings ($\mu\epsilon$)															
	2	4	6	8	10	12	14	16	18	20	22	24	26	28	30	32
1	0	0	0	0	0	0	0	0	0	0	0	0	0	0	0	0
2	77	32	132	61	79	86	52	70	39	21	44	-17	60	34	48	103
3	75	10	125	59	82	118	34	122	50	29	50	-3	19	-2	20	31
4	51	17	126	43	72	84	23	75	20	30	29	-10	27	9	38	126
5	70	15	156	85	107	138	39	97	29	10	38	-2	25	-2	40	60
6	99	33	229	128	143	331	84	213	106	91	188	10	87	9	63	-231
7	123	33	209	124	122	206	74	178	78	49	107	-7	53	2	64	35
8	91	-31	172	68	55	177	24	125	32	-18	95	-58	-33	-35	19	-51
9	137	-4	200	85	110	289	44	206	79	29	109	-45	19	-28	36	-72
10	84	-8	185	85	101	243	49	152	62	4	108	-50	21	-26	51	-177
11	40	-23	210	73	113	274	57	177	79	32	143	-25	27	4	91	9
13	23	-63	223	86	124	357	38	230	91	33	128	-72	-21	-63	58	-55
15	84	-25	453	435	463	710	143	783	139	59	80	-50	-35	-61	106	-21
16	108	8	533	544	608	886	217	1003	191	88	61	-20	36	93	329	307

17	-68	-128	163	135	199	303	11	446	22	-11	76	-81	-24	-32	116	-6
18	-99	-149	171	146	188	281	-42	349	-150	-133	-173	-182	-117	-85	95	-17

TABLE 10 READINGS FROM TRANSVERSE DE-MEC POINTS AT 3/4 SPAN TAKEN DURING THE TEST ON MODEL 2

Level	De-Mec Point Strain Readings ($\mu\epsilon$)										
	35	37	39	41	43	45	47	49	51	53	55
1	0	0	0	0	0	0	0	0	0	0	0
2	87	33	108	39	83	91	36	53	44	12	83
3	13	14	92	-3	73	139	86	46	60	3	196
4	82	32	103	7	86	125	57	25	36	-7	111
5	79	33	149	34	138	196	84	52	51	3	150
6	146	80	249	73	196	396	224	129	130	63	383
7	142	90	224	79	210	294	178	117	105	52	274
8	78	-1	159	2	111	250	128	42	39	-14	246
9	19	15	186	-2	118	322	197	97	71	3	269
10	23	28	155	-28	85	215	151	37	47	-7	236
11	77	0	198	5	135	297	169	68	59	21	332
13	53	24	239	7	194	473	273	134	121	20	385
15	163	175	581	165	1168	967	652	756	894	190	816

17	68	6	185	-19	408	402	362	356	345	69	520
18	59	29	281	-22	685	467	413	619	527	10	485

TABLE 11 READINGS FROM TRANSVERSE DE-MEC POINTS AT 5/8 SPAN TAKEN DURING THE TEST ON MODEL 2

Level	De-Mec Points Strain Readings ($\mu\epsilon$)															
	58	60	62	64	66	68	70	72	74	76	78	80	82	84	86	88
1	0	0	0	0	0	0	0	0	0	0	0	0	0	0	0	0
2	40	8	66	45	-5	19	-19	40	12	-34	34	-49	-1	-10	-56	-8
3	52	-24	93	118	16	123	134	138	56	46	127	51	34	26	15	3
4	59	-14	92	94	6	72	76	72	18	8	76	30	25	11	38	11
5	67	-25	129	158	11	115	107	114	24	17	99	28	19	11	4	-8
6	96	5	395	142	80	205	276	282	91	67	307	103	110	81	73	28
7	92	3	352	121	71	150	193	194	45	53	213	55	72	55	72	28
8	34	-59	288	13	-9	47	137	113	-31	-34	168	-21	-2	2	33	-49
9	51	-37	479	105	40	161	268	236	24	10	219	24	10	29	13	-22
10	-122	-54	360	52	16	80	175	138	-5	-16	193	-15	35	9	11	-21
11	48	-39	366	32	6	72	178	147	4	-13	255	3	31	20	44	-31
13	24	-42	549	42	55	167	391	351	22	0	378	-13	45	27	40	-51
15	540	686	1428	667	1314	1221	1534	993	385	419	780	495	490	94	636	193
16	992	979	1521	1088	1979	2030	2158	1495	854	1172	1184	775	1249	598	1187	234
17	104	82	266	122	281	279	408	308	66	159	502	157	267	74	189	-45
18	485	448	683	409	826	840	1036	585	130	424	649	348	568	168	464	22

19	1031	984	1926	1688	2744	1445	1541	847	451	958	878	603	1040	447	916	124
20	1334	964	2189	2109	3474	1502	1968	1107	589	1348	852	697	1358	606	1194	154
22	1777	459	3127	4145	7428	1285	3584	1771	917	2895	632	1090	2035	1113	1986	229
24	1813	555	4159	12101	16324	1452	8147	4386	2428	5764	1201	2105	3017	1886	2666	603

TABLE 12 READINGS FROM TRANSVERSE DE-MEC POINTS AT 1/2 SPAN TAKEN DURING THE TEST ON MODEL 2

Level	De-Mec Point Strain Readings ($\mu\epsilon$)										
	91	93	95	97	99	101	103	105	107	109	111
1	0	0	0	0	0	0	0	0	0	0	0
2	1	-9	22	59	4	34	-16	54	18	11	-4
3	-10	-9	-12	97	-5	125	0	255	75	55	-9
4	-4	-8	3	62	-18	52	-36	146	29	7	-3
5	-11	-2	-20	132	-9	85	-22	221	35	24	-1
6	26	41	35	210	43	169	50	513	141	108	0
7	33	38	47	204	45	141	28	393	87	66	3
8	-37	-30	-36	128	-33	39	-61	300	1	-19	32
9	-19	15	19	358	23	143	-2	471	70	30	25
10	-13	5	5	223	5	78	-39	354	30	6	29
11	-20	-9	-9	210	-21	60	-39	357	29	10	25
13	-37	4	118	333	81	155	22	687	34	29	8
15	708	397	1106	1379	643	925	984	1890	336	329	-268

17	14	42	77	255	192	167	226	876	90	141	-211
18	753	359	709	1023	533	688	796	1678	238	404	-387

TABLE 13 READINGS FROM TRANSVERSE DE-MEC POINTS AT 3/8 SPAN TAKEN DURING THE TEST ON MODEL 2

Level	De-Mec Point Strain Readings ($\mu\epsilon$)											
	114	116	120	122	126	128	130	132	134	140	142	144
1	0	0	0	0	0	0	0	0	0	0	0	0
2	-10	16	-12	-8	-36	20	-16	-16	55	-2	-2	33
3	-19	-59	-18	-26	-38	79	12	-15	90	-27	5	55
4	-4	-98	-4	-21	-50	53	-16	-16	79	-6	11	44
5	-20	-63	6	-22	-40	88	-15	-70	91	-41	9	57
6	3	17	69	-6	-12	219	42	10	231	20	50	110
7	48	47	142	33	5	201	48	24	203	-17	54	108
8	-84	-57	-44	-98	-106	114	-71	-90	122	-88	-16	61
9	-55	11	92	-32	-99	236	-22	-34	228	-54	4	80
10	-18	24	87	-28	-73	162	-21	-45	181	-52	19	72
11	-37	27	84	-60	-95	177	-38	-55	212	-74	6	68
13	-40	42	199	92	-129	358	9	-27	300	-87	-4	70
15	83	282	845	1106	22	1665	580	201	1071	210	139	282
16	171	622	1172	1507	387	1717	987	379	1673	695	473	414

17	-127	59	233	274	-15	718	311	-32	568	132	45	93
18	122	421	712	1007	242	1383	779	160	1139	336	170	156

TABLE 14 READINGS FROM TRANSVERSE DE-MEC POINTS AT 1/4 SPAN TAKEN DURING THE TEST ON MODEL 2

Level	De-Mec Point Strain Readings ($\mu\epsilon$)										
	147	149	151	153	155	157	159	161	163	165	167
1	0	0	0	0	0	0	0	0	0	0	0
2	66	43	-2	34	-20	22	10	21	12	5	15
3	-18	26	-28	45	-49	98	17	52	10	33	50
4	24	59	21	89	-31	59	6	35	13	66	11
5	-14	55	-43	58	-73	123	-11	70	1	24	28
6	-12	135	-4	117	-46	204	15	125	39	49	61
7	41	161	21	159	-28	216	39	156	68	104	55
8	-62	103	-67	46	-133	117	-56	39	-51	-38	-35
9	-80	212	-87	115	-126	197	-34	106	-2	16	15
10	-11	205	-32	150	-92	211	-11	143	-4	54	29
11	-75	302	-99	174	-151	182	-36	78	-40	43	10
13	-125	344	-165	197	166	149	-113	134	12	58	17
15	-116	448	179	501	607	607	-36	1110	643	128	506

17	-289	233	-161	307	110	440	306	433	356	-59	158
18	-259	351	105	683	630	1038	799	1068	933	122	471

TABLE 15 READINGS FROM TRANSVERSE DE-MEC POINTS AT 1/8 SPAN TAKEN DURING THE TEST ON MODEL 2

Level	De-Mec Point Strain Readings ($\mu\epsilon$)													
	3	5	9	11	15	17	19	21	23	25	27	29	31	33
1	0	0	0	0	0	0	0	0	0	0	0	0	0	0
2	159	111	134	85	114	120	136	132	115	140	123	144	153	156
3	121	99	116	40	80	108	102	145	130	152	153	172	192	202
4	102	93	156	128	130	112	87	120	106	134	127	130	134	140
5	125	101	119	90	116	129	114	129	118	139	135	150	184	180
6	53	110	124	134	114	116	146	177	159	191	191	261	299	287
7	109	103	157	132	122	123	129	164	153	162	161	174	192	226
8	-47	47	59	91	43	45	61	84	79	108	76	124	177	169
9	55	87	118	109	83	101	132	164	162	168	176	225	255	256
10	-220	57	89	15	47	51	88	109	111	119	106	162	199	201
11	75	94	129	120	70	80	103	130	126	152	139	193	215	228
13	-24	69	102	110	85	102	135	161	165	204	207	249	282	304

TABLE 16 READINGS FROM LONGITUDIANL DE-MEC POINTS AT 3/4 SPAN TAKEN DURING THE TEST ON MODEL 2

Level	De-Mec Point Strain Readings ($\mu\epsilon$)											
	34	36	38	40	42	44	46	48	50	52	54	56
1	0	0	0	0	0	0	0	0	0	0	0	0
2	104	114	147	104	90	103	98	134	105	113	194	151
3	114	143	151	117	118	109	151	180	160	158	209	226
4	101	119	145	105	102	101	114	143	113	125	150	208
5	111	136	154	117	111	120	140	160	116	131	136	174
6	198	197	220	182	179	189	238	232	220	233	266	313
7	170	183	221	164	133	169	193	189	172	182	200	230
8	94	104	120	81	74	87	138	129	143	135	168	192
9	139	179	199	141	155	171	224	226	239	238	266	284
10	113	131	149	104	94	118	150	173	156	163	197	232
11	122	141	161	108	110	126	170	184	181	178	219	249
13	154	182	216	141	168	177	274	269	279	262	305	333

TABLE 17 READINGS FROM LONGITUDINAL DE-MEC POINTS AT 5/8 SPAN TAKEN DURING THE TEST ON MODEL 2

Level	De-Mec Point Strain Readings ($\mu\epsilon$)										
	59	65	67	71	73	75	79	81	83	85	87
1	0	0	0	0	0	0	0	0	0	0	0
2	123	110	150	160	123	138	130	111	124	109	127
3	183	191	236	254	221	211	241	211	194	225	189
4	131	141	160	184	141	130	168	2	134	188	145
5	176	158	159	214	181	158	197	176	159	147	165
6	256	255	308	352	318	326	353	323	302	286	270
7	212	215	218	272	231	234	253	226	212	207	217
8	139	148	181	209	169	170	196	175	161	210	176
9	235	266	305	330	272	271	281	254	234	213	229
10	171	184	216	245	196	202	222	204	185	183	203
11	184	196	233	269	232	236	266	252	224	277	242
13	278	317	351	397	361	350	344	324	286	340	292

TABLE 18 READINGS FROM LONGITUDINAL DE-MEC POINTS AT 1/2 SPAN TAKEN DURING THE TEST ON MODEL 2

Level	De-Mec Point Strain Readings ($\mu\epsilon$)											
	90	92	94	96	98	100	102	104	106	108	110	112
1	0	0	0	0	0	0	0	0	0	0	0	0
2	144	133	134	112	130	118	136	129	116	134	133	103
3	228	213	209	192	207	214	215	194	188	194	179	148
4	155	145	136	117	130	127	137	140	133	150	123	108
5	186	176	171	141	147	159	163	164	165	162	149	121
6	284	270	262	244	272	289	294	294	294	297	267	228
7	231	221	197	165	209	214	228	219	219	225	199	160
8	144	133	125	98	131	128	152	141	143	151	136	101
9	277	264	235	230	245	244	249	231	225	227	202	163
10	180	174	151	142	163	165	182	177	177	180	169	143
11	196	181	163	153	177	182	185	204	207	216	199	161
13	335	317	292	308	301	303	292	270	276	280	241	204

TABLE 19 READINGS FROM LONGITUDINAL DE-MEC POINTS AT 3/8 SPAN TAKEN DURING THE TEST ON MODEL 2

Level	De-Mec Point Strain Readings ($\mu\epsilon$)												
	115	117	121	123	127	129	131	135	137	139	141	143	145
1	0	0	0	0	0	0	0	0	0	0	0	0	0
2	128	115	123	119	99	80	96	93	101	80	78	31	18
3	211	180	207	151	153	107	132	108	110	80	163	45	38
4	145	132	153	123	116	85	109	98	90	89	191	120	35
5	172	158	171	129	138	98	133	113	115	95	193	21	8
6	268	245	276	233	218	182	216	201	188	154	250	103	73
7	216	185	204	176	153	142	173	144	142	92	186	106	76
8	136	109	141	102	106	79	106	105	76	48	148	90	-8
9	249	183	210	169	142	122	158	139	132	83	183	101	2
10	175	147	159	134	113	106	139	118	107	85	145	74	45
11	189	159	172	158	142	124	168	144	128	95	185	111	54
13	280	224	238	181	144	135	171	140	129	84	166	85	47

TABLE 20 READINGS FROM LONGITUDINAL DE-MEC POINTS AT 1/4 SPAN TAKEN DURING THE TEST ON MODEL 2

Level	De-Mec Point Strain Readings ($\mu\epsilon$)											
	146	148	150	152	154	156	158	160	162	164	166	168
1	0	0	0	0	0	0	0	0	0	0	0	0
2	79	84	97	66	86	57	68	51	45	62	64	58
3	104	111	82	64	75	44	76	47	35	40	53	56
4	75	67	75	34	72	36	61	54	41	51	41	57
5	80	68	87	60	59	40	67	39	44	28	60	72
6	140	140	170	95	131	84	104	74	84	71	90	101
7	125	129	130	99	107	77	84	72	77	55	73	81
8	30	47	76	6	51	-3	23	6	9	9	30	38
9	84	105	111	41	72	37	44	22	25	32	49	59
10	81	93	101	52	83	48	59	46	39	34	43	59
11	68	83	116	43	86	48	80	56	53	33	50	65
13	82	110	112	11	48	17	26	13	6	-6	-3	23

TABLE 21 READINGS FROM LONGITUDINAL DE-MEC POINTS AT 1/8 SPAN TAKEN DURING THE TEST ON MODEL 2

FIG. 6. POSITIONAL INFORMATION FOR MODEL 2 DE-MEC POINTS.